Transactions

of the

ASME

Characteristics of Dished-Plate (Belleville) Springs as Measured in Portable Recording Tensiometers . . . . . *J. J. Ryan* 431

The Theory and Design of Long-Deflection Constant-Force Spring Elements . . . . . *F. A. Votta, Jr.* 439

A Contribution to the Problem of Designing Radial Turbomachines . . *O. E. Balje* 451

Some Theoretical Aerodynamic Investigations of Impellers in Radial- and Mixed-Flow Centrifugal Compressors . . . . . *J. D. Stanitz* 473

Single-Stage Radial Turbines for Gaseous Substances With High Rotative and Low Specific Speed . . . . . *W. T. von der Nuell* 499

Research in Exhaust Manifolds . . . . . *P. H. Schweitzer* 517

Operation and Performance of Modern Reheat Boilers . *P. R. Laughlin and H. H. Poor* 529

Some Design Factors Relating to Performance and Operation of Reheat Boilers . . . . . *H. H. Hemenway* 537

A Progress Report of Reheat Boiler Design and Operation . . . . . *W. J. Vogel and E. M. Powell* 545

Reheat Experiences at Port Washington . . . . . *M. K. Drewry* 551

The First Year's Operation of the Dunkirk Steam Station . . . . . *J. N. Ewart* 557

Twenty-Five Years of Reheat Operating Experience on the American Gas and Electric System . . . . . *S. N. Fiala* 561

Operating Experience With Reheat at Edgar Station . . . . . *H. E. Stickle* 569

Station Design With Cyclone-Fired Steam Generators . . . . . *H. C. Schroeder and R. J. Strasser* 573

Effect of Velocity on Tensile Impact Properties of Polymethyl Methacrylate . . . . . *Bryce Maxwell and J. P. Harrington* 579

An Investigation of Electromagnetic Flowmeters . . *H. G. Elrod, Jr., and R. R. Fouse* 589

Analysis of Some Hydraulic Components Used in Regulators and Servomechanisms . . . . . *S. Z. Dushkes and S. L. Cohn* 595

MAY, 1952

VOL. 74, NO. 4

Transactions

of The American Society of Mechanical Engineers

Published on the tenth of every month, except March, June, September, and December

---

Published monthly by The American Society of Mechanical Engineers. Publication office at 20th and Northampton Streets, Easton, Pa. The editorial department is located at the headquarters of the Society, 29 West Thirty-Ninth Street, New York 18, N. Y. Cable address, "Dynamic," New York. Price $1.50 a copy, $12.00 a year for Transactions and the *Journal of Applied Mechanics*; to members and affiliates, $1.00 a copy, $6.00 a year. Changes of address must be received at Society headquarters four weeks before they are to be effective on the mailing list. Please send old as well as new address. . . . By-Laws: The Society shall not be responsible for statements or opinions advanced in papers or . . . printed in its publications (B13, Par. 4). . . . Entered as second-class matter March 2, 1928, at the Post Office at Easton, Pa., under the Act of August 24, 1912. . . .

Characteristics of Dished-Plate (Belleville) Springs as Measured in Portable Recording Tensiometers

By J. J. RYAN,[1] MINNEAPOLIS, MINN.

The development of portable recording tensiometers (force versus time) for maximum tension loads between 5000 and 16,000 lb presented an opportunity for determining the load-deflection characteristics of a series of dished-plate (Belleville) springs of the same size and shape, except for a variation in thickness. Without such an instrument, capable of microscopic measurement, the deflections of these initially coned annular-disk springs of uniform cross section are exceedingly difficult to obtain. This paper describes the tensiometer and compares the theoretical methods of calculation of the spring deflections with the results of the load-deflection tests. Dished-plate (Belleville) springs of the kind discussed here are capable of carrying heavy loads in a small space with near-linear deflections, and an analysis of the design characteristics may encourage their application in other machine elements.

Introduction

THE tensiometer was developed for the purpose of recording large impact loads in units of force and time. The instrument is for portable use, weighing about 6 lb and having an over-all length of 9 in. The application of load deflects very heavy plate springs with subsequent movement of a central post. A scriber on the post marks on a moving film the amplitude of the deflection. A friction governor on a clock motor controls the speed of the film.

The instrument will measure the inertia forces, with respect to time, of falling bodies stopped suddenly while in motion, as in the opening of a parachute. It will record the impact acceleration of instruments and equipment dropped in a supporting carriage as required in Armed Service specifications. It will also measure the live-load forces in structures such as bridges or buildings when placed in series with the tie rods or connectors. It is useful in measuring the suddenly applied loads on towlines attached to ships or barges; on cables used on cranes or hoists to lift heavy weights; or for the measurement of tractive effort and other forces where dynamic conditions of loading exist.

Description of Instrument

The instrument case, of cast magnesium, is made in two sizes to accommodate maximum forces of 8000 lb and 16,000 lb. The internal dimensions of the cases are approximately the same for the five different ranges of springs which were developed. A cut-away drawing, Fig. 1, shows the assembled instrument with all the component parts in position.

The upper pin connector is held by lug projections on the top of the case. The lower connector is attached to a central post. The central post is guided by bearings in the case above and below a stack of dished-plate (Belleville) springs which are compressed by tensile forces applied on the pin connectors.

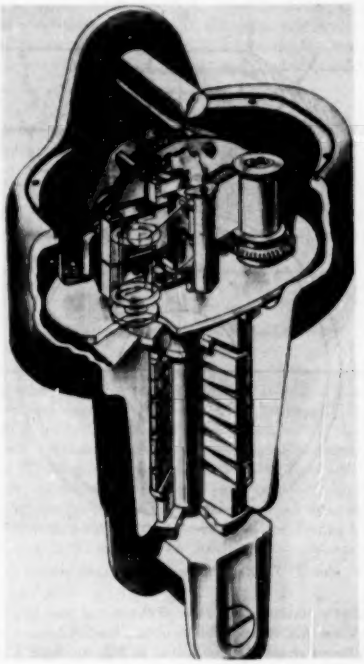

Fig. 1 Ryan Recording Tensiometer

A clockwork mechanism with a governor drives a take-up spool which draws a clear-base film past a scribing surface. About 15 in. of film may be reeled for one winding of the clock in a time from 30 sec to 4 min, depending upon the setting of the governor. Three styli record on the film. These styli consist of scribing needles mounted on flexible parallel cantilever springs. The middle stylus is connected to the central post and records the vertical displacement of the springs. The lower stylus draws a

---

[1] Professor of Mechanical Engineering, University of Minnesota. Mem. ASME.

Contributed by the Machine Design Division and presented at the Fall Meeting, Minneapolis, Minn., September 25–28, 1951, of The American Society of Mechanical Engineers.

Note: Statements and opinions advanced in papers are to be understood as individual expressions of their authors and not those of the Society. Manuscript received at ASME Headquarters, June 12, 1951. Paper No. 51—F-2.

base line. The upper stylus is connected to a spring-mounted mass, which when displaced by a clock-driven cam, produces a timing record as a result of its free vibration.

To prevent binding of the dished-plate springs on the central post and to preserve alignment, flat strips of thin beryllium-copper spring stock are inserted between the post and the plates in the clearance space. The lower nut on the central post is tightened to maintain an initial compression on the plate springs.

The high spring constant, combined with compactness in the axis of loading, makes the Belleville spring applicable for instrument work; however, it was necessary to determine by test if an approximately straight-line relationship of applied load to deflection could be obtained.

Description of Springs

Dished-plate (Belleville) springs consist essentially of annular disks of constant thickness with an initial cone, as shown in Fig. 2.

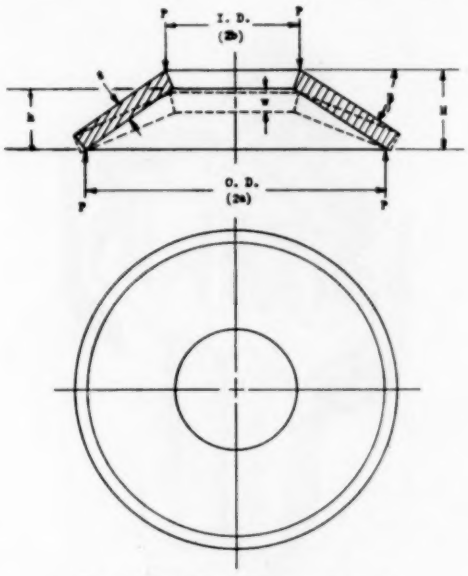

Fig. 2 Dished-Plate (Belleville) Spring

By suitable variation of the ratio of the initial cone height to the disk thickness, h/t, it is possible to obtain load-deflection curves of many different shapes,[2] as indicated in Fig. 3. Such a shape as curve A with $h/t = 2.0$ is desirable when a "snap-acting" device is being designed. When h/t is about 1.5, the springs, known as the "constant-load" type, curve B, show a considerable range of deflection within which the load is practically constant. This characteristic is highly desirable in many applications—for example, the loading of a gasket with a constant force. Curve C is a typical load-deflection curve for the initially flat disk spring. We may consider it as a particular type of Belleville spring, with $h/t = 0$. This load-deflection curve is nearly linear for very small deflections, although the curve is concave upward for larger deflections. An intermediate ratio of cone height to thickness, as

[2] "Mechanical Springs," by A. M. Wahl, Penton Publishing Company, Cleveland, Ohio, 1944, pp. 238–262.

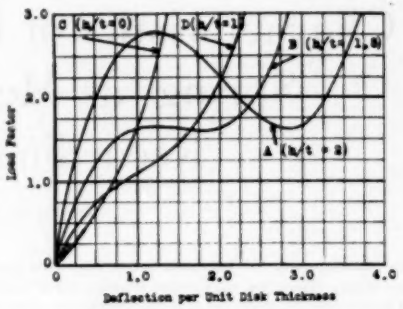

(a) Dished-Plate Springs With Large Deflections

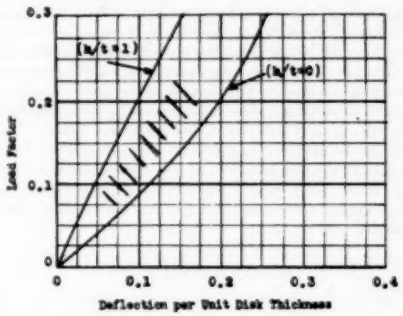

(b) Test Region for Small Deflections

Fig. 3

suggested between curves C and D, $(h/t = 1.0)$, Fig. 3 (*a*), may be expected to give a straight-line load deflection for small deflections in the region shown in Fig. 3 (*b*).

In this paper are described tests of ratios h/t (cone height to thickness) between 0.11 and 0.17, which were found to be satisfactory for the linearity required in instrument work having a high spring constant, combined with compactness in the axis of loading. The deflection curves are linear within normal limits, but tend to be concave upward. Calibration curves are shown for the several cases tested.

Theoretical Methods of Calculation

The application of the mathematical theory of elasticity to dished-plate springs may be approached in several ways. It may be demonstrated that the deflection of initially flat-plate springs is directly proportional to the load when the deflection is small in comparison to the plate thickness.

Poisson's flat-disk formula[3] for small deflections is given by S. Timoshenko as follows

$$P = \frac{wEt^3}{K_1a^2} \qquad [1]$$

where K_1, a constant of the plate dimensions, was calculated by

[3] "Theory of Plates and Shells," by S. Timoshenko, McGraw-Hill Book Company, Inc., New York, N. Y., vol. 1, 1940, p. 64.

TABLE 1 INCHES DEFLECTION PER 1000 LB PER STACK

No.	Max. load, lb	Thickness, in.	No. in stack	Initial cone height, in.	Calculated: 1 Poisson's flat-disk formula	Calculated: 2 Almen and Laszlo formula	Calculated: 3 Circular-ring formula	Test: 4 Stack	Test: 5 Single spring	6 Ratio calculated to test col. 2/col. 4
1	5000	0.1674	9	0.0270	0.04534	0.0439	0.0468	0.040	0.00444	1.10
2	6000	0.1865	9	0.03225	0.0330	0.0313	0.0338	0.030	0.00333	1.04
3	9000	0.21875	7	0.03125	0.0159	0.0150	0.01643	0.0147	0.00210	1.02
4	12000	0.250	7	0.03125	0.0107	0.0101	0.01103	0.010	0.00143	1.01
5	16000	0.281	7	0.03125	0.00750	0.0073	0.00779	0.008	0.00114	0.91

Wahl and Lobo[4] and tabulated in the foregoing reference.[5] The maximum tangential stress at the upper inner edge of the spring disk would be

$$S_1 = K\frac{P}{t^2} \quad \ldots\ldots [2]$$

where K is a similar constant of dimension as before. Since all the dished-plate springs had the same inside and outside radii of 0.755/2 and 1.99/2 in., the ratio $a/b = 2.64$ would have values for K_1 and K of 0.714 and 1.74, respectively. Calculations of deflections using these equations are given in Table 1, column 1.

If the deflections are no longer small in comparison to the thickness, the analysis of problems of this nature must be extended to include the strain of the middle plane of the spring plate. In this case the exact theory is quite complicated, and the deflection is no longer proportional to the load applied.

The exact solutions by the theory of elasticity for the deflections and stresses of dished-plate (Belleville) springs are extremely difficult.[6] However, based upon the assumption of rotation of the radial cross sections without distortion, approximate solutions were derived by Almen and Laszlo.[6] These investigators reported tests which indicated that the assumption was satisfactory for practical use. The final results of the derivations were

$$P = \frac{Ewt}{M(1-\mu^2)a^2}\left[(h-w)\left(h-\frac{w}{2}\right)+t^2\right] \quad \ldots\ldots [3]$$

$$S_1 = \frac{Ew}{M(1-\mu^2)a^2}\left[C_1\left(h-\frac{w}{2}\right)+C_2t\right] \quad \ldots\ldots [4]$$

$$S_2 = \frac{Ew}{M(1-\mu^2)a^2}\left[C_1\left(h-\frac{w}{2}\right)-C_2t\right] \quad \ldots\ldots [5]$$

where the nomenclature is as follows:

- P = load applied uniformly around inner and outer edges of dished-plate (Belleville) spring
- t = thickness of spring
- β = conical angle
- h = conical height
- w = vertical deflection of spring
- a = outside radius of spring
- b = inside radius of spring
- E = Young's modulus
- μ = Poisson's ratio
- S_1 = tangential stress at upper inner edge of spring
- S_2 = tangential stress at lower inner edge of spring

M, C_1, and C_2 are functions of ratio $\alpha = a/b$ as follows

$$M = \frac{6}{\pi \ln \alpha}\cdot\frac{(\alpha-1)^2}{\alpha^2}$$

$$C_1 = \frac{6}{\pi \ln \alpha}\left[\frac{(\alpha-1)}{\ln \alpha}-1\right] \quad \ldots\ldots [6]$$

$$C_2 = \frac{6}{\pi \ln \alpha}\cdot\frac{\alpha-1}{2}$$

Studying Almen and Laszlo's load-deflection formula, Equation [3], it is observed that when the deflection and conical height are small in comparison with the thickness, the first term in the bracket is not large, and if it is neglected, Equation [3] becomes

$$P = \frac{Ewt^3}{M(1-\mu^2)a^2} \quad \ldots\ldots [7]$$

i.e., deflection is directly proportional to the load.

The values of the first term in Equation [3], $(h-w)\left(h-\frac{w}{2}\right)$, are listed in Table 2 for cone height $h = 0$, $0.1t$, and $0.2t$, and the deflection w is varied for 0 to $0.20t$, where t is the plate thickness.

TABLE 2 VALUES OF $(h-w)(h-w/2)$

w	0	$0.05t$	$0.10t$	$0.15t$	$0.20t$
$h = 0$	0	$0.00125t^2$	$0.005t^2$	$0.01125t^2$	$0.02t^2$
$h = 0.1t$	$0.01t^2$	$0.00375t^2$	0	$0.00125t^2$	0
$h = 0.2t$	$0.04t^2$	$0.02625t^2$	$0.015t^2$	$0.00625t^2$	0

As shown by Table 2, the error due to neglecting the first term is a maximum of only 4 per cent when the deflection is minimum and the conical height is 20 per cent of the thickness. The variation from linearity is less for the case with $h = 0.1t$ than in the other cases. Calculations of deflections using the approximate Equation [7] are given in the summary Table 1, column 2.

Another approximate method of analysis may be applied.[7] Considering the spring as a circular ring twisted by couples uniformly distributed along its center line, and neglecting the effect of the change in the angle β, the following formula may be obtained

$$P = \frac{wEb}{(a-b)}\left[\frac{t^3}{12(a-b)}\ln\frac{a}{b}+\beta^2\left(\frac{a+b}{2}-\frac{a-b}{\ln\frac{a}{b}}\right)\right] \quad \ldots\ldots [8]$$

where P, t, w, E, a, b, and β are as defined previously. For large deflections, the angle β changes and the approximation becomes less valid. A summary of values obtained by these equations is given in Table 1, column 3.

Description of Springs Tested

Approximately flat dished-plate (Belleville) springs were used in the recording tensiometer described herein. The deflection of

[4] "Stresses and Deflections in Flat Circular Plates With Central Holes," by A. M. Wahl and G. Lobo, Jr., Trans. ASME, vol. 52, paper APM-52-3, 1930.

[5] Reference 3, p. 475.

[6] "The Uniform-Section Disk Spring," by J. O. Almen and A. Laszlo, Trans. ASME, vol. 58, 1936, pp. 305–314.

[7] "Strength of Materials," by S. Timoshenko, D. Van Nostrand Company, Inc., New York, N. Y., second edition, vol. 2, 1941, pp. 177–183.

each spring was kept within 3/4 of the limiting cone height to obtain an approximately linear load-deflection relation. The springs were stacked in a series of seven or nine, in the manner shown in Fig. 4, to enlarge the deflection recorded by the stylus on the moving film. Tensiometers with five different load capacities were constructed. The springs used had the same inside and outside diameters, and the thickness of the springs was varied to obtain increasing capacities.

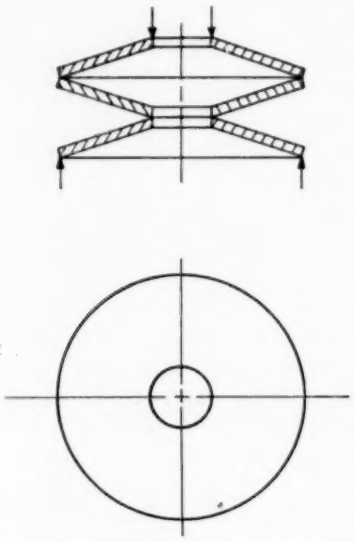

Fig. 4 Dished-Plate (Belleville) Spring Stack

A working drawing of the dished-plate (Belleville) springs is shown in Fig. 5, with the general dimensions and notes on the method of machining and finishing, materials and heat-treatment. Table 3 in Fig. 5 shows the five different spring thicknesses tested, with the individual cone heights and total spring heights. Springs Nos. 1 and 2 were nested in a series of nine, and springs Nos. 3, 4, and 5 in a series of seven.

Each dished-plate spring was compressed to a flat position several times in a press before it was assembled to assure its freedom from cracks and to obtain mechanical stability. The maximum calculated stresses under such conditions usually exceeded 300,000 psi, but only in cases of poor heat-treatment did failure occur in the pressing. After this procedure was initiated, there were few spring failures in the instruments.

Results of Tests

A number of loading tests were made with each of the five spring stacks in tensile-testing machines. As the loads were applied, usually in 1000-lb increments, the tensiometer recording film was moved a short distance by the clock motor. Fig. 6 is an enlargement of a typical record. The amplitudes of displacement were measured on a film reader or with a toolmaker's microscope. In Fig. 7 is plotted the load-deflection calibration chart for a typical stack of springs, specifically, stack No. 3, consisting of seven springs 0.2187 in. thick. This figure represents the average load-deflection curve for a large number of tests, with some representative points plotted and extreme limiting lines shown.

The initial slope of the curve is assumed to determine the spring constant of the stack per 1000 lb load, and thus the equivalent constant for each spring. The friction of the stack is limited to the upper and lower springs. The deflection during the increasing load is always less than the decreasing load, although the slopes are usually the same after the first reduction in load has been applied. Calibration for the increasing load is favored in these curves because of its importance in establishing maximum forces. The deviation from the average is not more than plus or minus 5 per cent for different stacks of the same thickness. This error includes in part the effects of the small edge variations in the

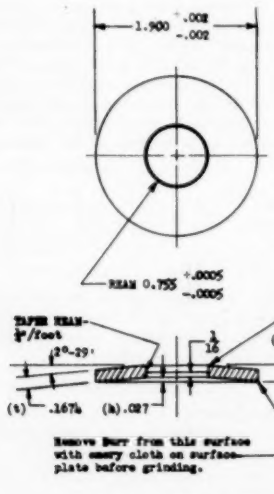

TABLE 3

No.	t	h	H	w/t	h/t
1.	.1674	.027	.194h	.112	.161
2.	.1865	.032	.219	.107	.173
3.	.2187	.031	.250	.091	.143
4.	.250	.031	.281	.080	.125
5.	.281	.031	.312	.071	.111

MATERIAL: X4340 or NE 9442

NOTES:
(1) Heat Treat 1575° F. - Draw to C-42-45.
(2) Nickel Plate .0005 thick.
(3) Relieve Plating Embrittlement-400° F. for 2 hours.

Fig. 5 Working Drawing for Tensiometer Springs

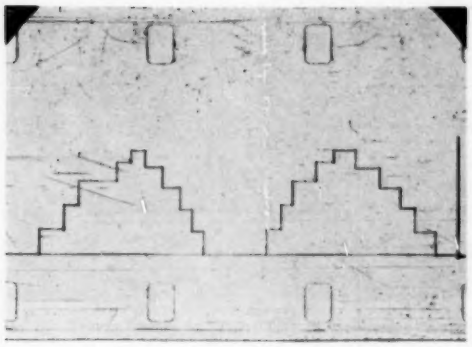

FIG. 6 ENLARGEMENT OF CALIBRATION RECORD

assembly of the stacks, nonuniformity of springs, occasional friction on the center post, and inaccuracies in the testing machines.

A summary of the load-deflection charts for the individual dished-plate springs is given in Fig. 8. The maximum test loads deflected the springs to about two thirds the cone height. The limit of linearity was observed to be approximately one half the cone height. In Fig. 9, a chart compares the deflection constant in inches per 1000 lb of load, as determined from the previous graph, with the inverse cube of the individual spring thickness. A straight line reflects this relationship with considerable accuracy.

COMPARISON OF CALCULATIONS AND TESTS

A tabulation of the calculated deflections of the spring stacks per 1000 lb of load by the three methods outlined in the discussion is presented in Table 1, with the results of each calculation given in their respective columns. The test measurements are listed in column 4. The theory as developed by Almen and Laszlo[4] is considered to be the most accurate, and a comparison of their equation with test is indicated in the ratio of the calculated constant to the test constant as given in column 6. The intermediate column 5 lists the test deflection per 1000 lb of load for the single springs.

The calculations by Almen and Laszlo were 10 per cent higher for the spring with the least thickness and 9 per cent under for the thickest spring. The calculation average for the series of springs is less than 2 per cent over the test values. According to Almen and Laszlo, and Wahl,[2] the deviation of test from calculated values for springs of this kind may be up to 10 per cent. This error appears to be large, but is made up of a number of factors, each of which may be large in itself. The equations are satisfactory as a guide in design. After the plate springs are assembled and held with initial tension, repetition of the calibration tests in the tensiometer have shown no appreciable deviation.

Comparison of Poisson's flat-disk formula and the circular-ring formula with test results indicate slightly higher calculated values, the average ratio of calculated to test constants being 1.07 and 1.10, respectively. Thus the flat-disk formulas and the tables presented by S. Timoshenko,[5,7] by reason of their simplified approach and availability, are usually adequate for the solution of engineering design problems.

RECOMMENDATIONS FOR APPLICATIONS

Dished-plate (Belleville) springs have a number of advantages in their use. They carry high loads in a small space. By stacking in series, large deflections may be obtained. In their displacement, they offer very little friction. In comparison with springs

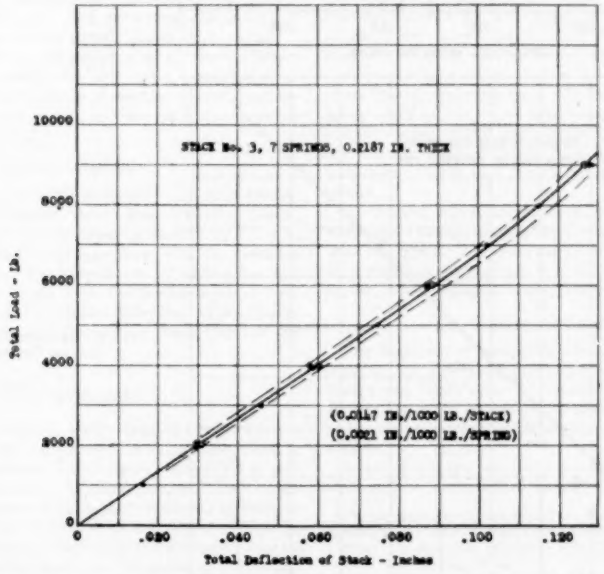

FIG. 7 LOAD-DEFLECTION CALIBRATION CHART FOR A TYPICAL STACK OF SPRINGS
(No. 3, 0.2187 in. thick, 7 springs.)

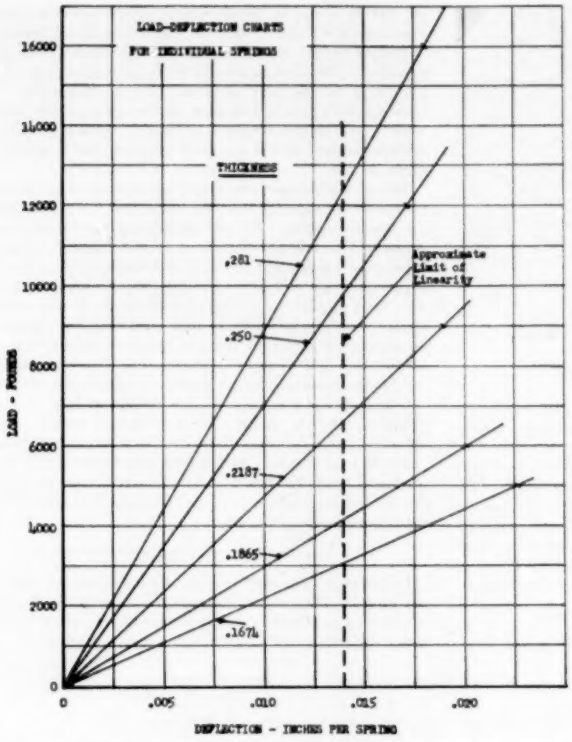

Fig. 8 Load-Deflection Charts for Individual Springs

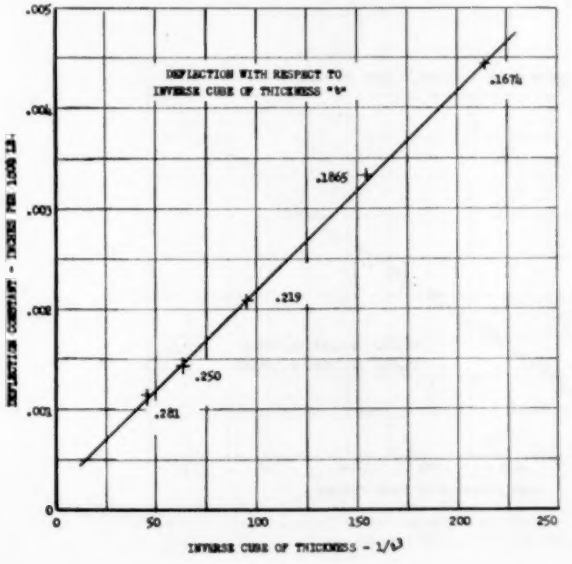

Fig. 9 Deflection With Respect to Inverse Cube of Thickness

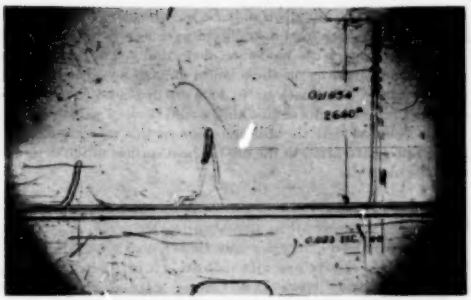

FIG. 10 SAMPLE RECORD OF IMPACT TEST AS RECORDED BY TENSIOMETER

of a similar nature, such as tapered conical springs, built-up springs having internal and external circular inserts, and conical friction springs, they are the cheapest to manufacture and the simplest to maintain. In primer-insert reciprocating presses for the manufacture of .30 caliber ammunition, a pressing and stamping operation, they have exhibited an exceptionally long fatigue life. They are recommended for heavy-duty work.

The greatest use of dished-plate springs has been in instrument applications. A sample record of an impact test as recorded by the tensiometer is shown in Fig. 10. Success in a service that may be calibrated accurately should make their usefulness in other applications more assured.

SUMMARY

The microscopic measurement of the deflections of dished-plate (Belleville) springs under load was made possible by the application in recording tensiometers. The theoretical calculations of the deflections of these initially coned, annular-disk springs of uniform cross section have been investigated by three different methods, and the test results have indicated a reasonable similarity. It is believed the simplicity of calculation and construction of these springs should encourage their application in other machine elements.

ACKNOWLEDGMENTS

The author wishes to express his gratitude to Dr. E. J. Baldes, Physics and Biophysical Section, Mayo Clinic, Rochester, Minn., for suggesting the problem; to his many co-workers for aiding in the investigation; and to Mr. Chang-Kiang Tsai for modifications of the manuscript. The preparation for publication was made possible by grants-in-aid from the Graduate School, and by a Fellowship presented by General Mills Inc., to the Graduate School and the Mechanical Engineering Department of the University of Minnesota.

Discussion

A. M. WAHL.[8] One problem which frequently confronts the spring designer is the choice of allowable working stress, since, in general, it is advantageous to use as high a stress value as permissible consistent with safety. The data given in Table 1 of the paper would seem to indicate that for the tensiometer application described, stresses as high as 300,000 to 350,000 psi (calculated from elastic flat-plate theory, Equation [2] of the paper) may be used at maximum working loads for this material (NE9442). It also should be noted that a presetting operation (consisting of compressing the springs flat several times) was utilized for these springs; residual stresses induced by this presetting operation would of course result in a more favorable stress distribution under load.

Recently a "Manual on Design and Manufacture of Coned Disk Springs or Belleville Springs" was published by the Society of Automotive Engineers.[9] In this manual, prepared by a subcommittee under the direction of the SAE Technical Board Spring Committee, several methods of design including the Almen-Lasslo and elastic flat-plate methods were discussed. It also was suggested that where Belleville springs are statically loaded and are approximately flat when loaded, the following nominal stress formula may be used as an index of load-carrying ability

$$S_n = \frac{3}{\pi}\frac{P}{t^2} \approx 0.96\,\frac{P}{t^2} \qquad [9]$$

where P = load applied at edges and t = spring thickness.

This nominal stress S_n is obtained simply by dividing the external bending moment acting across a diametral section of the spring by the section modulus.[10] This formula is considered to give a better index of the load-carrying ability of the spring without excessive set than the elastic flat-plate formula (Equation [2] of the paper) or the Almen-Lasslo formula (Equation [4]), both of which refer to rather localized stresses at the inside edge of the spring.[11] Using the data given in Table 1 of the paper, nominal stresses were calculated at the maximum loads given using Equation [9] of this discussion. These nominal stresses varied from 165,000 to 193,000 psi. Compared to the values of 300,000 to 350,000 psi, calculated from the elastic-plate theory, these values are more realistic when considering that the yield point of the material is about 180,000 psi for an alloy steel of the hardness utilized in the author's springs.

Incidentally, it should be noted that the use of the elastic-plate formula (Equation [2] of the paper) will yield approximate values for the stress "range" at the inner edge of the spring, where fatigue or repeated loading is involved, and assuming that the load range is taken equal to P in the formula. Test data[12] indicate that for a stress range of 273,000 psi, the life of a Belleville spring made of alloy steel heat-treated to 45–46 Rockwell C, will be between 50,000 and 100,000 cycles, based upon tests of nine springs; where the stress range is 364,000 psi, the life drops to between 15,000 and 38,000 cycles, based on tests of 47 springs.

These stress ranges are maximum values figured at the upper inner edge of the spring using the Almen-Lasslo formula (Equation [4] of the paper). The writer would be interested to know whether the author has obtained any data on expected spring life for repeated loading during the course of his investigation.

AUTHOR'S CLOSURE

The discussion of stresses in dished-plate (Belleville) springs presented by Dr. Wahl and the reference to the "Manual on Design and Manufacture of Coned Disk Springs or Belleville Springs," of which he was one of the principal authors, calls attention to comprehensive design information available on this subject.

Several years ago, when the present work was carried out, it could only be assumed that the high maximum stresses were not

[8] Advisory Engineer, Westinghouse Research Laboratories, East Pittsburgh, Pa. Mem. ASME.

[9] Publication SP-63, available from SAE Special Publications Department, 29 West 39th Street, New York 18, N. Y.

[10] See reference 2 of author's paper for further details concerning derivation of this equation.

[11] See discussion of reference 9 (p. 30) of this discussion for further justification of the writer's Equation [9].

[12] Reference 9, p. 44.

as detrimental to the operation of the springs as was indicated. Application of these springs to many machines has been retarded by this uncertainty. The "Manual" referred to is extremely valuable for its complete analysis of deflections and stresses, allowing the application of the data with assurance.

Stress calculations by the nominal stress method referred to are particularly intriguing. This method allows a common approach to obtain practical design solutions.

The question of the author's experience with these springs under repeated loading can only be answered by the statement that they have been used in stacks in punch-press tools for exerting heavy loads with moderate deflection. They have been loaded many months on three shifts at high speed without excessive failure. No data as to load or displacement could be obtained. Test results of this kind would be very valuable.

It is believed that the dissemination of this information may aid in calling attention to the use of these springs in the design of machine elements.

The Theory and Design of Long-Deflection Constant-Force Spring Elements

By F. A. VOTTA, JR.,[1] LANSDALE, PA.

A thorough study of the "neg'ator," its present and predictable applications and design procedures are discussed in the light of two years' experience in neg'ator development, research, and testing. The neg'ator is characterized by properties which permit it to exert constant or controlled varying force through theoretically infinite deflection. Design formulas and operation of the three major forms of the neg'ator, (1) extension member, (2) A-motor, and (3) B-motor, are discussed and illustrated. The major existing applications of the neg'ator are examined in terms of form, function, field, and type of mechanism and are illustrated by several representative designs.

Nomenclature

The following nomenclature is used in the paper:

- E = modulus of elasticity, psi; carbon spring steel = 30×10^6, stainless = 28×10^6
- F = deflection, in.
- L = length of neg'ator, in.
- N = number of revolutions, coils on output bushing
- P = load, lb
- T = torque, lb-in.
- W = work, ft-lb
- X = over-all length
- Y = over-all width
- Z = over-all height
- b = width of neg'ator material, in.
- $m = \frac{R_i}{R_n}$
- S_f = stress factor
- t = thickness of neg'ator material, in.
- R_n = minimum natural radius of curvature, in.
- R_m = maximum natural radius of curvature, in.
- R_i = expanded radius of curvature of neg'ator due to material build-up, in.
- R_2 = radius of storage bushing, in.
- R_4 = radius of output bushing, in.
- R_4 = radius of output bushing plus neg'ator build-up, in.
- ID = inside diameter of freely coiled neg'ator
- OD = outside diameter of freely coiled neg'ator
- f = fatigue life, cycles

Introduction

Within the last 2 years, experience gained through the development of the neg'ator permits a complete study of neg'ator characteristics, applications—both present and predictable—and design procedures. The solution of a variety of application problems has necessitated an integrated program of research and testing which in turn has increased the data available for the design of neg'ators. Since the neg'ator is capable of exerting constant or controlled varying force through extreme deflections, its characteristics are radically different from those of conventional spring members.

The characteristics of the neg'ator are first discussed and its distinguishing physical and functional properties compared with conventional spiral and extension springs. Design formulas and operation of the three major forms of the neg'ator, (1) extension member, (2) A-motor, and (3) B-motor, are discussed and illustrated.

Some of the more important existing applications of the neg'ator are examined in terms of form, function, field of application, and type of mechanism and are illustrated by representative designs. Additional applications now being evolved through further experience with the neg'ator are also included.

The most common requirements which affect the design of all spring members are force (or torque), deflection (or revolutions), space considerations, and fatigue life. Complete design procedures, based on these application requirements, are given. Tabular and graphical data on the relation of fatigue and stress, dimensions, gradient, force, and deflection, and treatment of other appropriate factors such as spring materials and mounting methods cover the steps of neg'ator design evolving from initial requirements.

Characteristics

The neg'ator is a strip of flat spring material which has been given a curvature by continuous heavy forming so that in its relaxed or unstressed condition the neg'ator is in the form of a tightly wound spiral. In Fig. 1 (*a*) the neg'ator is in its relaxed position and no part of the coiled spring stock is stressed by external causes. The outer end of the neg'ator in Fig. 1(*b*) has been extended by a force P, and the neg'ator, mounted for free rotation, has been partly uncoiled.

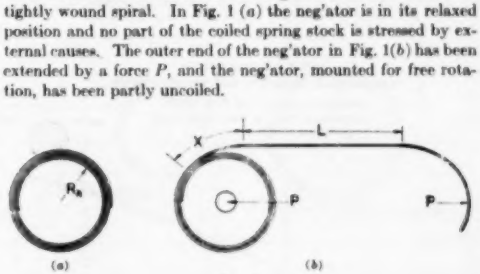

Fig. 1

The force P at any extension is determined only by the work required to straighten the material in zone X from its coiled condition. Force P in Fig. 1(*b*) will then remain constant with extension as long as each incremental length of neg'ator has an equal increase in stress as it is straightened. This condition represents a neg'ator having a zero gradient. The material in zone L has been put under stress, and energy stored in it is proportional to the length of straightened material. The incremental stress increase occurring in zone X can be varied, and a negative, positive, or changing gradient obtained.

[1] Design Engineer, Neg'ator Division, Hunter Spring Company. Jun. ASME.

Contributed by the Machine Design Division and presented at the Fall Meeting, Minneapolis, Minn., September 25–28, 1951, of The American Society of Mechanical Engineers.

Note: Statements and opinions advanced in papers are to be understood as individual expressions of their authors and not those of the Society. Manuscript received at ASME Headquarters, June 11, 1951. Paper No. 51—F-11.

Neg'ator Compared With Spiral and Extension Springs

As an aid in visualizing the unique characteristics of the neg'ator and in evaluating its usefulness as a spring member, the engineer will find a comparison of the neg'ator with a representative spiral spring and extension spring helpful. Table 1 gives eleven characteristics which differentiate a zero-gradient neg'ator from a spiral spring, the most nearly similar conventional spring type.

TABLE 1 CHARACTERISTICS DIFFERENTIATING ZERO-GRADIENT NEG'ATOR FROM SPIRAL SPRING

	Conventional spiral spring	Neg'ator (zero gradient)
1	Cumulative stress limits possible deflection.	Noncumulative stress does not limit deflection.
2	Force equals that required at one point only. Excessive or insufficient force at all other points.	Force substantially constant throughout entire deflection.
3	End of spring is anchored for winding.	Spring is mounted for free rotation of coil.
4	Spiral spring is normally open to allow for winding.	Normally tight wound with each coil in close contact with adjacent turns.
5	Charged by winding to a tight spiral.	Charged by uncoiling outer end of spring.
6	Force developed increases as winding progresses.	Substantially full force at initial deflection.
7	Force delivered (1) angularly; or (2) by means of auxiliary member such as a drum, when it is delivered tangentially.	Force delivered linearly from center of coil to extended end of spring.
8	Spring is stressed as a unit by winding.	Spring is stressed sequentially by increments.
9	Working range is open spiral to tight wound.	Working range from tight spiral to straight or even reverse coiled.
10	Space required for expansion when unwound	Space required for tight spiral only
11	Substantial losses due to intercoil friction during winding and unwinding.	No intercoil friction.

Characteristics 1 and 2 represent the most important differences in operation. Primarily, because stress is noncumulative, a change in deflection of the neg'ator does not affect the stress of the material. Then too, the force delivered by the neg'ator does not depend upon deflection. The other characteristics concern differences in anchoring methods, unstressed condition, method of charging, force development and delivery, stress, working range, space, and intercoil friction.

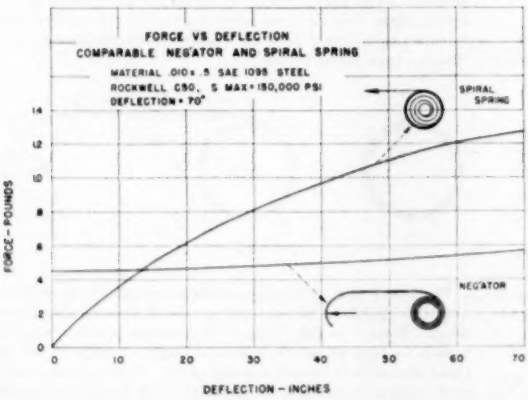

Fig. 2 Force Versus Deflection—Comparable Neg'ator and Spiral Spring

(Each designed for 70 in. deflection and same material. 0.010 × in. 0.5 in. SAE 1095 steel; Rockwell 50; S_{max} = 150,000 psi.)

The curves in Fig. 2 give a graphical comparison of the force-deflection characteristics of the neg'ator and a conventional spiral spring with auxiliary members required to convert its natural torque to lineal force. Both the neg'ator and the spiral spring are made from the same material, with identical dimensions and fatigue life, and both are designed for a 70-in. deflection. Through this deflection the force delivered by the spiral spring increases from zero to 1.25 lb. For the same extension, the force output of the neg'ator increases from 0.465 lb at initial deflection to 0.568 lb at 70-in. deflection. The gradient of the spiral spring is 0.018 lb per in., while the gradient of the neg'ator is 0.00147 lb per in. or approximately $^1/_{12}$ that of a comparable spiral spring.

The most common elastic member which exerts lineal force directly is the simple extension spring. Although the neg'ator and extension spring are not similar in appearance, they are comparable as single-unit spring members which exert a lineal force when deflected from their relaxed position.

The curves in Fig. 3 represent the force-deflection characteristics of a neg'ator with a minimum gradient and an extension spring which has been designed to have the lowest possible positive gradient and to occupy the same linear space as the neg'ator. The extension spring has been designed with an initial tension of 1 lb, and the neg'ator has been designed for an initial force of 1 lb. Both the neg'ator and the extension spring are deflected 10 in. (the limit for the conventional spring). Through this 10-in. deflection the neg'ator force increases from 1 lb to 1.004 lb, which means that the neg'ator has a positive gradient of 0.0004 lb per in. In the same deflection range, a comparable extension spring increases in force from 1 lb to 6.4 lb, a constant positive gradient of 0.540 lb per in. In this comparison the extension spring has a positive gradient which is 1350 times that of the neg'ator.

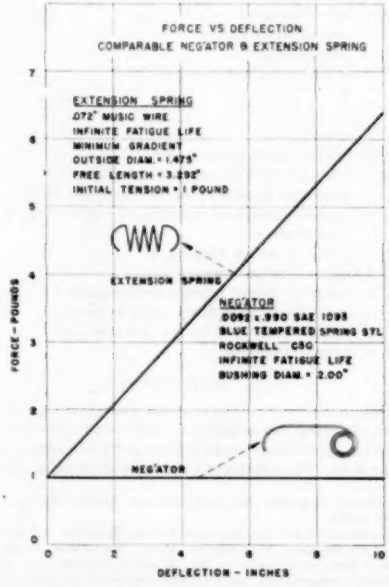

Fig. 3 Force Versus Deflection—Comparable Neg'ator and Extension Spring

Theory and Forms of Neg'ator

The three major forms of the neg'ator, which will be discussed here, are (1) extension member, (2) A-motor, and (3) B-motor. Two other forms, the neg'ator clamp and the neg'ator clip, will not be discussed since their design and function are quite fundamental and are corollary to the basic neg'ator.

Fig. 4 shows the basic neg'ator used as an extension member. The material has been formed in manufacture so that each incremental length of neg'ator has an inherent natural radius of curvature R_n. Actually, only the inside coil of the relaxed neg'ator on the right has its natural curvature; the radii of succeeding coils are greater due to some expansion as the material coils upon itself.

Fig. 4

On the left in Fig. 4 the neg'ator has been mounted upon a freely rotatable bushing of radius R_2 and has been partially deflected. Assuming that the radius R_2 of the mounting bushing is equal to R_n, and that the build-up effect is negligible, the instantaneous force output of the neg'ator is given by the expression

$$P = \frac{Ebt^3}{24R_n^2} \text{ lb} \quad \ldots\ldots\ldots\ldots\ldots\ldots [1]$$

where P is the force in pounds delivered by the neg'ator, b is stock width in inches, t is stock thickness in inches, and E is the modulus of elasticity of the material. Since the neg'ator material may be considered as a thin flat plate, the effect of Poisson's ratio must be incorporated in this formula for a more exact expression. The transverse stress in the material causes a curvature to take place across the width of the material, which produces a slight reduction in force output. Correcting Equation [1] for the effect of Poisson's ratio, we obtain

$$P = \frac{Ebt^3}{24R_n^2} \times 0.91 = \frac{Ebt^3}{26.4R_n^2} \text{ lb} \quad \ldots\ldots\ldots\ldots [2]$$

If R_n, the radius of curvature of the material, remains constant, and if the effect of build-up of succeeding coils is neglected, the force P will remain constant.

The change in curvature from R_n to infinite radius (material pulled out straight) occurs through the short zone X, and, since force P depends only on the work required to deflect the material through zone X from the radius of the outer coil, Equation [2] is not correct when the radius of the outer coil exceeds R_n. Since the material in these outer coils has already been partially straightened by expansion, less work is required to straighten the material through zone X completely. Both Poisson's ratio and coil expansion, produced either by material build-up or a mounting spindle radius greater than R_n are contained in the expression

$$P = \frac{Ebt^3}{26.4}\left[\frac{1}{R_n^2} - \left(\frac{1}{R_n} - \frac{1}{R_1}\right)^2\right] \text{ lb} \quad \ldots\ldots\ldots [3]$$

For a spring material of given width and thickness, force P depends only upon the inherent neg'ator radius R_n and the radius R_1 of the outer coil. Unless there are a large number of coils mounted on the spindle, the effect of material build-up is negligible.

The effect of pre-expansion of the neg'ator material is shown in Fig. 5 where the ratio of R_1/R_n is plotted against the ratio of P_1 (force at expanded radius R_1) to P_n (force at natural radius R_n). From this curve it can be seen that for a small increase in radius over R_n there will be a very small decrease in force. When the neg'ator is used as an extension member, it is not necessary to have a spindle radius greater than 20 per cent more than R_n. While the expansion effect is usually negligible in the design of extension neg'ators, it will be shown that it is quite useful in the design of A-motor and B-motor forms of the neg'ator.

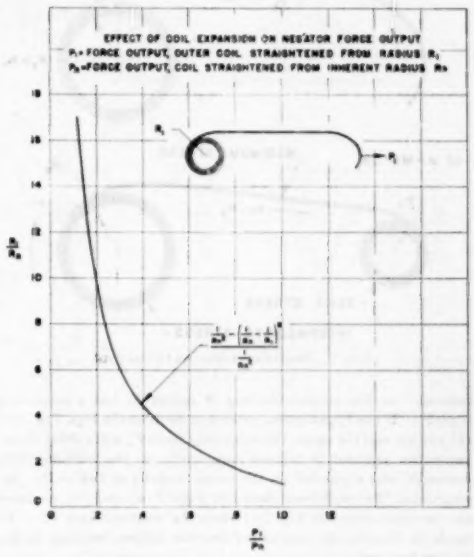

Fig. 5 Effect of Coil Expansion on Neg'ator Force Output (P_1 = force output, outer coil straightened from radius R_1. P_n = force output, coil straightened from inherent radius R_n.)

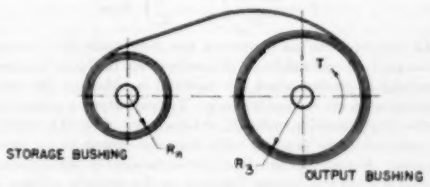

Fig. 6

Fig. 6 shows a partially wound neg'ator A-motor. The energy stored by the neg'ator is delivered by a counterclockwise torque T about the axis of the outer bushing. This torque is delivered as the neg'ator material runs from the large output bushing to the small storage bushing. The radius of the storage bushing is indicated as R_n in Fig. 6.

The action of the A-motor can best be understood by referring to Fig. 7 where the neg'ator is assumed to consist of two extension members mounted, respectively, on the storage and output bushings. The spring material coiling on the storage bushing is shown in Fig. 7(*a*) where the force P_n tends to coil the neg'ator around the bushing of radius R_n. Similarly, in Fig. 7(*b*) the neg'ator

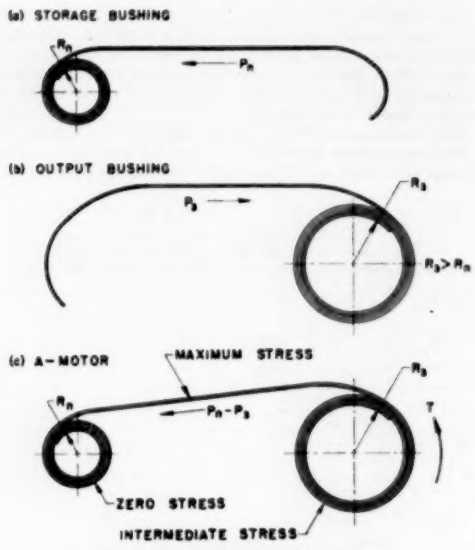

FIG. 7 NEG'ATOR A-MOTOR OPERATION

mounted on the output bushing of radius R_3 has a retracting force P_3. If the hypothetical extension members in Figs. 7(*a*) and (*b*) are one and the same, the retracting force P_n will exceed P_3 because the neg'ator is relaxed completely on the bushing with radius R_n and expanded on the larger bushing of radius R_3. By combining the conditions shown in Figs. 7 (*a*) and (*b*), we have the condition shown in Fig. 7(*c*) where the resultant force $P_n - P_3$ tends to transfer the neg'ator from the output bushing to the storage bushing.

The resultant torque T produced at the output bushing of the A-motor is given by the expression

$$T = \frac{Eb t^3 R_3}{24}\left(\frac{1}{R_n} - \frac{1}{R_3}\right)^2 \text{ lb-in.} \quad [4]$$

In this equation no correction has been made for transverse crowning in the straightened section between bushings because no crowning is present when the material is either on the output bushing or on the storage bushing. Torque output is proportional to the output bushing radius R_3 and is slightly reduced by build-up of material as the neg'ator coils from the output to the storage bushing. In the A-motor the neg'ator material is fully stressed as it passes from the storage bushing to the straight portion and then reduced in stress as it goes from the straightened portion to the output bushing radius. Thus, as the neg'ator material deflects from the output bushing to the storage bushing, it is going from an intermediate stress through maximum stress and then down to zero stress in its relaxed position on the storage bushing.

In appearance the B-motor in Fig. 8 is similar to the A-motor except that the neg'ator has been back-bent around the output bushing so that it is coiled opposite to its inherent curvature. Like the A-motor, the B-motor is charged by winding the neg'ator onto the output bushing and delivers a counterclockwise torque T as the neg'ator runs onto the storage bushing. In the B-motor the neg'ator material goes from maximum stress on the output bushing through an intermediate stress in the straight portion to zero stress on the storage bushing.

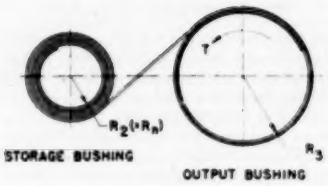

FIG. 8

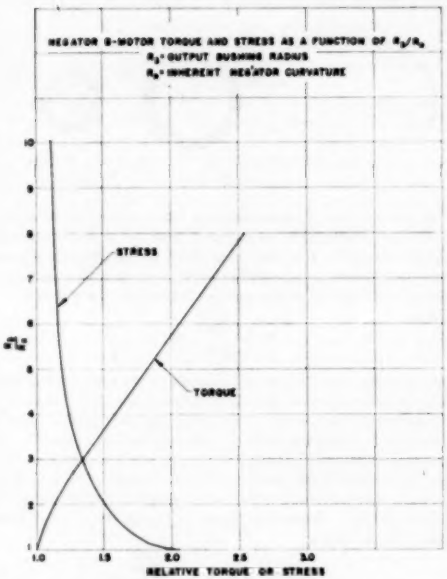

FIG. 9 NEG'ATOR B-MOTOR TORQUE AND STRESS AS A FUNCTION OF R_3/R_n
(R_3 = drive bushing radius; R_n = inherent neg'ator curvature.)

The resultant torque T of the B-motor is given by the expression

$$T = \frac{Eb t^3 R_3}{24}\left(\frac{1}{R_n} + \frac{1}{R_3}\right)^2 \text{ lb-in.} \quad [5]$$

As in the A-motor, no correction has been made for transverse crowning. The torque output is proportional to the radius R_3 of the output bushing. The curves in Fig. 9 show how stress and torque output vary as the ratio R_3/R_n increases. The neg'ator in the form of a B-motor makes maximum utilization of the material because it is used at maximum stress and stored at zero stress.

NEG'ATOR APPLICATIONS

The major fields in which the neg'ator is already being used include machine tools, instruments, appliances, timers and timepieces, electrical machinery, electronic controls, ordnance, aircraft, chemical-processing equipment, cameras, optical equipment, builder's hardware, lighting fixtures, and business ma-

chines. The extension member and the B-motor comprise over 90 per cent of present neg'ator applications.

The principal uses of the neg'ator as an extension member and as a B-motor are given in Table 2. The B-motor uses are generally those in which the output is desired as torque rather than linear force, and the energy is stored (by winding) for controlled release. Often, however, the B-motor is fitted with a drum and cable to deliver linear force. The choice—extension member or B-motor—is governed by the combination of load and deflection requirements and space limitations.

TABLE 2 MAJOR APPLICATIONS OF NEG'ATOR-EXTENSION MEMBER AND B-MOTOR

Function of neg'ator	Type of mechanism
Extension Member	
Motor-brush holder	Electric motors and generators Vacuum cleaner Hand power tool
Power feed	Vacuum-tube machine Stapler Machine tool Vending machine
Counterbalance	Sash balance Oven door Movable lighting fixture High-pressure lubricating equipment Sewing machine Rocket
Retracting and restoring	Slide projector Gasoline pump Typewriter Spring coiler Rotating-beam fatigue tester Cash register Refrigerator door Machine tool
B-Motor	
Drive mechanism	Automatic camera Movie camera Magnetic recorder Clock Gyroscope Phonograph Slide projector Cam Generator Timer
Retracting and restoring	Tape rule Cord reel Seam welder Liquid-level indicator Door closer Ground cable retractor (aircraft) Plastic extruding press
Counterbalance	Movable lighting fixture X-ray machine Liquid-level indicator Door on analytical balance Venetian blinds

The motor-brush assembly in Fig 10 is one of several designs using a neg'ator extension member to press a carbon brush on a commutator with a force that remains constant as the brush wears. It replaces a conventional positive gradient torsion spring assembly, and reduces both commutator wear (resulting from too much force on a new brush) and brush commutator arcing (due to poor contact produced by insufficient force on a well-worn brush). In addition, the low mass of the neg'ator assembly results in shorter excursions of the brush off the commutator and, therefore, improved commutation.

Like the motor-brush spring, the television-tube lift mechanism in Fig. 11 requires a constant force independent of deflection. The force at the extended position (where the glass tip is sealed off) must not be excessive, yet the force at the retracted position must be sufficient to overcome the weight of the television tube and holder to insure full upward travel.

From Table 2 it is evident that the B-motor form of the neg'ator is frequently used as a drive mechanism or prime mover. In the devices listed, the B-motor has usually replaced a conventional power spring motor because it is characterized by constant torque output through more revolutions and lower gear ratios. The curves in Fig. 12 compare the torque output of a power spring motor and a B-motor using the same volume of spring stock. Both motors are designed to drive a movie camera requiring a torque of 2.3 lb-in. Energy in zone 3 is the only portion of the total available energy of the power-spring motor that is actually used to drive the camera. In zone 1 the torque delivered is insufficient, and the energy is wasted; energy in zone 2 released at excessive torque must be dissipated by a governor. With total energy in zones 3 and 4 the same as the power-spring motor, the neg'ator B-motor used all available energy to drive the camera through more revolutions at constant torque.

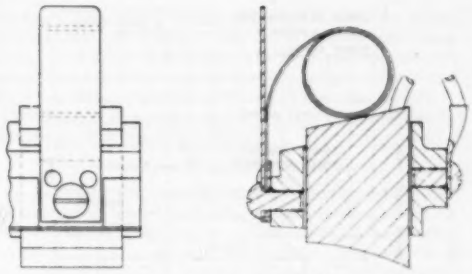

FIG. 10 MOTOR BRUSH ASSEMBLY

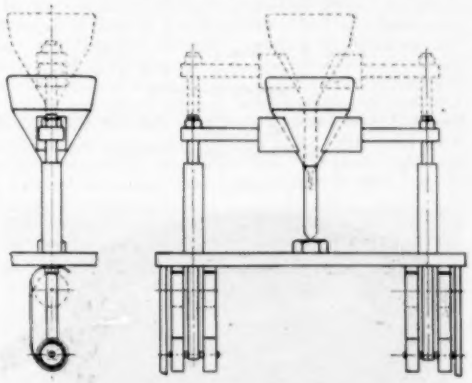

FIG. 11 TELEVISION TUBE LIFT MECHANISM

The B-motor through a planetary drive system retracts a 50-ft steel tape in Fig. 13. The planet gear on the neg'ator bushing at the right engages the sun gear fixed to the center of the housing, and the B-motor drives itself and the tape-drum assembly. Because the load on the drive system increases with extension of the tape, a slightly positive gradient B-motor was specified.

Two B-motors counterbalance the movable fluorescent lighting fixture in Fig. 14. The fixture is supported by two cables from each B-motor which are wound on drums integral with the output bushings. Because the zero gradient B-motors exert the same linear retracting force at any deflection of the cable, the lighting fixture can be lowered for cleaning and servicing.

A wider range of gradients can be obtained with the A-motor. Therefore the A-motor form of neg'ator has been specified in many instrumentation applications where power output is less important than a controlled torque-deflection characteristic

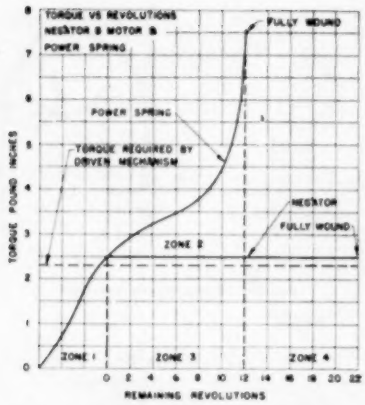

FIG. 12 TORQUE VERSUS REVOLUTIONS—NEG'ATOR B-MOTOR AND POWER SPRING
(Required motor torque = 2.3 in-lb.)

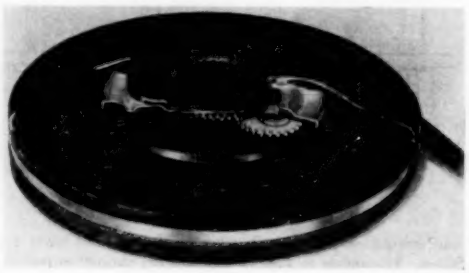

FIG. 13 STEEL TAPE RETRACTED BY B-MOTOR

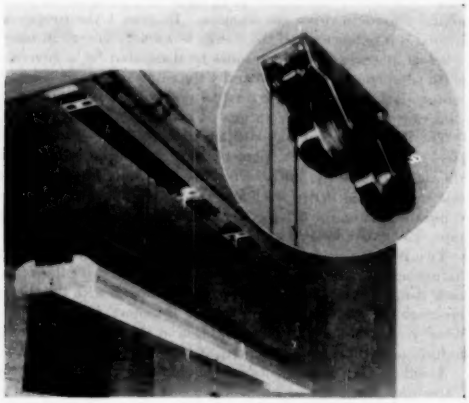

FIG. 14 TWO B-MOTORS COUNTERBALANCE MOVABLE LIGHTING FIXTURE

other than zero. In Fig. 15 the neg'ator A-motor is used as an expanded scale in which the spring material is stored on two bushings of equal radius. Calibration is printed directly on the neg'ator surface. The absence of torque on the metering system, due to balanced tension in the A-motor, provides greater sensitivity and hence improved accuracy. Space requirements of the A-motor expanded scale are less than other systems.

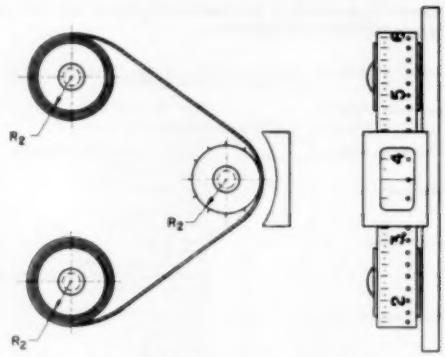

FIG. 15 A-MOTOR USED AS EXPANDED SCALE

NEG'ATOR DESIGN

Practical design procedures for the zero gradient neg'ator extension member, B-motor, and A-motor are based on formulas given in a previous section. Proper design of a particular neg'ator in any of these three forms considers, in addition, the relation of stress and life and certain physical limitations that have been determined both theoretically and empirically.

Consideration which governs the choice of a neg'ator rather than a conventional spring form are as follows: (1) When deflections more than 3 or 4 times the relaxed size are specified, use of the neg'ator is almost mandatory. (2) Constant or near constant force through long deflections is produced only by a neg'ator. Equations [3], [4], and [5] show that the force of each basic form of neg'ator depends upon thickness t, width b, and natural radius R_n. Fatigue life, proportional to stress increase occurring in zone X, depends upon thickness and curvature of the neg'ator material. For a given fatigue life, force is directly proportional to width alone. Only deflection can be varied independently.

In manufacture, a neg'ator is uniformly prestressed so that the radius of curvature R_n is uniform throughout its length and is stress-relieved while in its coiled condition. The natural radii of all coils, except the inside coil, are increased slightly by heat set. The curve in Fig. 16 shows the per cent increase in the radii of outer coils as the ratio of built-up diameter to the relaxed diameter of the inside coil increases.

Increase in natural radii during stress-relieving and larger radii due to build-up result in a neg'ator that will have a slight positive gradient if mounted and used as stress-relieved. However, if the neg'ator is coiled in reverse, with the smallest coil on the outside, the values of stress increase in all coils tend to equalize and force is constant. In designing zero gradient neg'ators with large numbers of coils, where build-up and increase in natural radius after heat-treating cannot be neglected, the neg'ators are always mounted in reverse.

The curve in Fig. 17, obtained from actual fatigue tests on neg'ators, gives the maximum allowable stress factor t/R_n as a

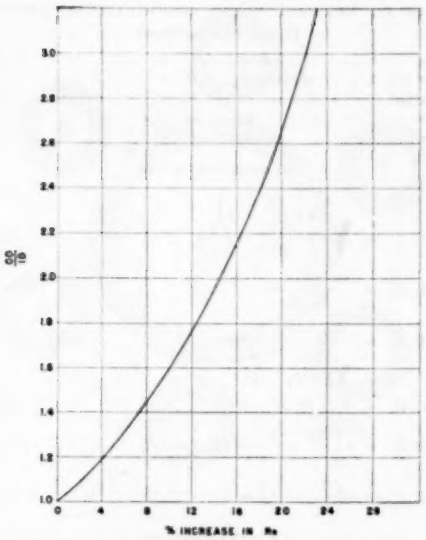

FIG. 16 RADIUS CHANGE OF OUTER COIL AFTER STRESS RELIEF (SAE 1095 steel, stress-relieved 475 F, 30 min.)

function of number of operating cycles. The curve applies to the most common neg'ator material, blue-tempered spring steel, in thicknesses from 0.003 in. to 0.020 in. Stress factors obtained from Fig. 17 are used in the design of neg'ator extension members, A-motors, and B-motors.

There are normally at least three initial requirements, determined by application, which are always assumed constant in neg'ator-design procedure. These are load or torque, deflection or number of turns, and fatigue life. Other factors which are often assumed in design are material (modulus of elasticity E), thickness t, radius R_2 of bushing (storage bushing of motor forms), maximum radius R_1 of output bushing and built-up coils (motor forms). Design procedures based upon the three most common assumptions will be treated specifically; design computations affected by other factors are carried out in a similar manner.

Definitions of all symbols used in the following design procedures are given in the nomenclature.

NEG'ATOR EXTENSION MEMBER

In the design of a neg'ator extension member, it is recommended that the ratio b/t of material width to thickness be between 50 and 200. Neg'ators with proportions outside this range are difficult to handle and physically unstable. The radius R_2 of the mounting bushing is commonly specified as 15 per cent larger than the natural radius R_n.

Design formulas for the neg'ator extension member in Table 3 are separately given for a small number of coils and a large number of coils (mounted reversed). Assuming that initial requirements give load P, deflection F, number of cycles and material, the calculations for a neg'ator with a small number of coils will give thickness t, natural radius R_n, width b, bushing radius R_2, and length L. The maximum stress factor S_f is selected on the curve in Fig. 17 from the specified operating cycles. Note that t and b are designed to next largest nominal sizes. Thickness t is obtained in standard sheet gages while nominal values of width b are in fractional dimensions.

Where there is no initial requirement on width b, the ratio b/t is assumed equal to 100. Substituting in Equation [1] in Table 3, t is given by

$$t = \sqrt{\frac{0.264}{ES_f^2}} \qquad [6]$$

in which E and S_f are known. The next highest nominal values of b and t are then used in Equation [2] to calculate R_n. When R_2 is specified, the maximum thickness t is first calculated as shown in Table 3, Note (b), and b determined in Equation [3]. In such cases the ratio b/t should be checked and if not between 50 and 200 adjustment of b, or t is required. Length L of the neg'ator is determined by Equation [5]. The nomograph in Fig. 18 may be used to approximate t, b, and R_n.

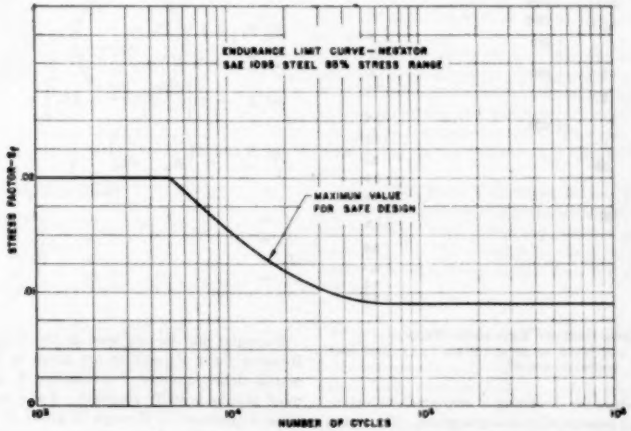

FIG. 17 ENDURANCE-LIMIT CURVE—NEG'ATOR (SAE 1095 steel, 85 per cent stress range.)

TABLE 3 NEG'ATOR DESIGN—ZERO-GRADIENT EXTENSION MEMBER

INITIAL REQUIREMENTS

P =	lb	S_f =	
F =	in.	b =	in.
Material		R_2 =	in.
E =	psi	f =	cycles

10 coils or less	Over 10 coils
[1] $t \geq \dfrac{26.4P}{EbS_f^2}$ = ... in.	[1] $t \geq \dfrac{26.4P}{EbS_f^2}$ = ... in.
[2] $R_n = \sqrt{\dfrac{Ebt^2}{26.4P}}$ = ... in.	[2] $R_m = \sqrt{\dfrac{Ebt^2}{26.4P}}$ = ... in.
[3] $b = \dfrac{26.4P}{EtS_f^2}$ = ... in.	[3] $R_n = \dfrac{R_m}{1.15}$ = ... in.
[4] $R_2 = 1.15\,R_n$ = ... in.	[4] $R_2 = 1.15\,R_m$ = ... in.
[5] $L = F + 10R_2$ = ... in.	[5] $L = F + 10R_2$ = ... in.

NEG'ATOR SPECIFICATIONS

t =	in.	P =	lb
R_n =	in.	F =	in.
R_2 =	in.	Material	
L =	in.	f =	cycles
b =	in.		

NOTES:
(a) Design b and t to next larger nominal size.
(b) When R_2 is an initial requirement calculate t.
Where $R_n = R_2 \div 1.15$, and $t = R_n \times S_f$.
(c) R_n and R_m in Equation [2] are based upon next largest nominal t.

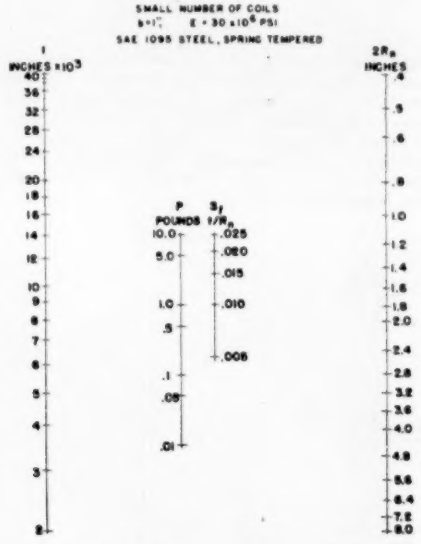

FIG. 18 NEG'ATOR DESIGN—EXTENSION MEMBER
(Small number of coils, b = 1 in., E = 30 × 10^6 psi. SAE 1095 steel, spring-tempered.)

In Table 3 the procedure for designing a zero-gradient extension member with a large number of coils is also given. Maximum and minimum radii of curvature R_m and R_n must both be calculated

TABLE 4 NEG'ATOR DESIGN—ZERO-GRADIENT B-MOTOR

INITIAL REQUIREMENTS

T =	lb-in.	b =	in.
N =	revolutions	R_2 =	in.
Material		R_3 =	in.
E =	psi	m =	
f =	cycles	S_f =	

10 revolutions or less

[1] $t \geq \sqrt{\dfrac{6.6T\left(\dfrac{1}{m}+1\right)}{EbS_f}}$ = ... in.

[2] $R_2 = \dfrac{t(m+1)}{S_f}$ = ... in.

[3] $R_n = \dfrac{1}{\sqrt{\dfrac{24T}{Ebt^2R_2}} - \dfrac{1}{R_2}}$ = ... in.

[4] $R_2 = 1.15\,R_n$ = ... in.

[5] $L = \pi\left[\dfrac{R_3^2 - R_2^2}{t} + 6R_2\right]$ = ... in.

[6] $S_f = t\left(\dfrac{1}{R_n} + \dfrac{1}{R_2}\right)$ = ... in.

Over 10 revolutions

[1] $t = \sqrt{\dfrac{6.6T\left(\dfrac{1}{m}+1\right)}{EbS_f}}$ = ... in

[2] $R_2 = \dfrac{t(m+1)}{S_f}$ = ... in.

[3] $R_2 = R_1 + Nt$ = ... in.

[4] $R_m = \dfrac{1}{\sqrt{\dfrac{24T}{Ebt^2R_2}} - \dfrac{1}{R_2}}$ = ... in.

[5] $R_n = \dfrac{R_m}{1.15}$ = ... in.

[6] $R_2 = 1.15\,R_m$ = ... in.

[7] $R_1 = \sqrt{R_2^2 + R_3^2 - R_2^2}$ = ... in.

[8] $L = \pi\left[\dfrac{R_3^2 - R_2^2}{t} + 6R_2\right]$ = ... in.

[9] $S_f = t\left(\dfrac{1}{R_n} + \dfrac{1}{R_2}\right)$ = ... in

SPECIFICATIONS

t =	in.	Material	
b =	in.	R_2 =	in.
L =	in.	R_3 =	in.
R_n =	in.	N =	revolutions
		T =	lb-in

Formulas and factors used in the design of the zero-gradient B-motor form of neg'ator are given in Table 4. Torque T in pound-inches, number of revolutions N, and fatigue life f are almost always initially specified. For a small number of revolutions, Equations [1] through [5] give t, R_2, R_n, R_2, and L. Equation [6] is used to check previous calculations. To calculate t, b/t is again assumed equal to 100 if not initially specified and S_f is ob-

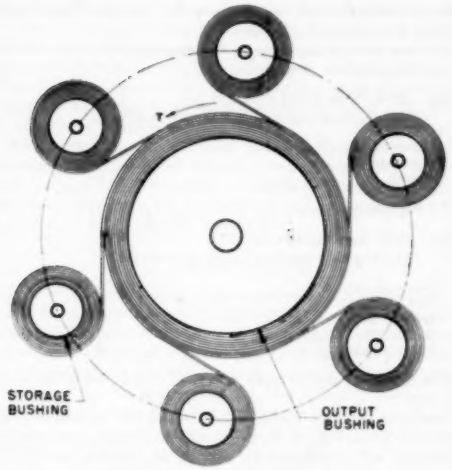

FIG. 19 MULTIPLE NEG'ATOR B-MOTOR

BASED ON BLUE TEMPERED SPRING STEEL, E = 30 × 10⁶ P.S.I.

WORK Ft. Lbs.	t in.	b in.	I.D. in.	D_1 in.	D_2 in.	T Lb.in.	N °	L in.
7.4	.003	.500	.425	9/16	1	.31	46	174
16.7	.004	.625	.590	3/4	1 1/4	.78	41	194
26.4	.005	.750	.720	1	1 5/8	1.20	42	257
50.5	.006	1.000	.880	1 1/8	1 7/8	2.30	42	298
113.0	.008	1.250	1.180	1 1/2	2 1/2	5.15	42	398
172.0	.010	1.500	1.500	2	3	9.15	36	408
280.0	.012	2.000	1.825	2 1/2	3 1/2	17.20	31	410
795.0	.016	2.500	2.360	3 1/4	5	40.00	38	716
1200.0	.020	3.000	3.000	4 1/4	6	72.00	32	784

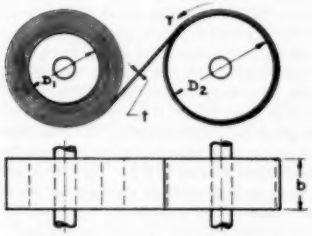

FIG. 20 B-MOTOR DIMENSIONS, MAXIMUM WORK AND CONSTANT TORQUE

tained in Fig. 17. When there are no initial space limitations, m is assumed equal to 2.

Calculations for designing a B-motor with a large number of revolutions are slightly more involved because more intermediate computations are necessary. The final specification values are t in Equation [1], R_2 in Equation [2], R_m in Equation [4], R_n in Equation [5], R_2 in Equation [6], and L in Equation [8] of Table 4

In Fig. 19 the multiple B-motor, consisting of radially arranged storage bushings with the neg'ators connected to a common output bushing, provides more work capacity per unit volume. Consideration must be given to the more rapid increase of R_i which results in a somewhat positive gradient as in a B-motor with a large number of revolutions. The formulas in Table 4 for a large number of coils may be used to design each of the B-motors. The table in Fig. 20 can be used to obtain approximate design values for the B-motor with a large number of revolutions.

Design of the A-motor is based on Equation [4]; however, it is recommended that in actual design the A-motor be considered as two identical extension members mounted on bushings of different radii. The same stress limitations as an extension member apply since the neg'ator operates in the same stress range.

CONCLUSION

The neg'ator offers a means of obtaining a constant force or torque through extreme deflections without the use of auxiliary machine members and thus opens up an entirely new approach to a vast number of design problems. Although in the short span of 2 years the neg'ator has been incorporated in many devices throughout unrelated fields, it is quite apparent that the future will bring many more applications where the unique characteristics of the neg'ator can be employed advantageously.

Discussion

J. H. BILLINGS.[2] The constant load-deflection ratio of the conventional spring is a property which has met the requirements of the designer uniquely for many applications, such as in the development of governors, weighing devices, and indicating instruments. There are many functions, however, calling for the use of springs where the designer finds the property cited nothing short of a nuisance. Examples are counterbalances, most spring motor devices, and all constant-pressure applications. The neg'ator, with its nearly constant load-deflection characteristic, neatly fills a gap which previously existed in the satisfactory utilization of springs.

Referring to Fig. 2 of the paper, it is unnecessary that the force curve for the spiral spring should run to zero. It is possible to design such a spring so that, in the most relaxed position allowed by the design, it will exert any desired portion of its maximum force. This principle is recognized by the author in Fig. 3 where he shows an initial force of 1 lb at zero deflection for the helical spring.

It should be observed that the simplest application of the neg'ator, as an extension spring, involves the use of a bearing, whereas the conventional extension spring does not. With the present relinability and relatively low cost of small bearings this may not be a serious objection. However, the initial cost of the bearing and its maintenance are factors that may not be neglected.

The author states that the endurance-limit curve of Fig. 17 gives stress factors based upon experiments with both the A-motor and B-motor. Presumably the B-motor applications, where the material is used in reversed bending, would require more conservative design-stress values than the other applications described.

H. C. R. CARLSON.[3] Undoubtedly, there are many applications for these new springs in industry, and now that engineering designers have been given formulas for design, and practical examples have been worked out, much time can be saved while

[2] Head, Department of Mechanical Engineering, Drexel Institute of Technology, Philadelphia, Pa. Mem. ASME.

[3] Spring Consultant, The Carlson Company, New York, N. Y. Mem. ASME.

determining whether or not such springs might be suitable for new applications.

It is hoped that more papers of this type will be written covering this spring, particularly to include a comprehensive table showing the characteristics of a large number of such springs so that designers might be able to pick a standard spring from a chart. The table accompanying Fig. 20 shows a few such springs but this table easily could be made more comprehensive and include perhaps a hundred spring sizes.

It might also be well to point out that many designers are interested in knowing how special products are made, and perhaps it would have been interesting to state that these springs can be made on standard spring-coiling machines, available from several manufacturers, by using special feed rolls, special arbors, and special coiling points. It should be pointed out too that this spring and many applications are patented or in the process of having patents issued, and that only two spring-manufacturing companies have been licensed by the patent holder to manufacture these springs.

Spring designers frequently have found that it is possible to use stresses as high as 225,000 psi on flat spiral power springs where the thickness of material is less than 0.040 in., and it might be advisable to point out whether or not such stresses can be used on these constant-force spring elements and still have a fairly long fatigue life.

It is recommended that engineering designers become better acquainted with this type of constant-force spring as, undoubtedly it will be the answer to many design problems which heretofore have not been easily solved, except by using dead weights as counterweight devices.

H. W. Poole.[4] While we have had only limited experience in the application of this new element named the neg'ator, we have found that it meets a requirement not filled by any other known member.

The paper is quite clear to us who are now reasonably acquainted with the neg'ator. However, it seems that its identification as a spring still leaves, in the engineer's mind, the limitations which are usually associated with spring thinking. It would seem that the first requirement for proper conception and appreciation of the neg'ator is to divorce this mechanical element from the realm of the conventional spring.

The neg'ator might better be considered, not as an elastic member or spring, but as the equivalent of an electric motor, hydraulic cylinder, or other work-delivering unit.

If one had the problem of driving a winch to lift 100 lb through 10 ft doing 1000 ft-lb of work, power could be derived from a motor of any given torque if the proper gearing were provided. The problem simply would be to use torque and revolution values, the product of which would equal the total work or total energy required. Obviously, as revolutions are increased, the required torque is decreased—hence a smaller motor could be used. The actual selection would be controlled by the maximum economy, space and costwise, of the combined motor and gear mechanism.

The neg'ator, providing as it does long deflection at constant force, is more nearly analogous to the motor than to a spring. Force or torque is developed, as in the case of the motor, by physical size of the material which in turn determines the size of coil, deflection or revolutions being the other factor to determine the work. Since deflection is simply additional length of material, as in the case of the increased number of revolutions of the motor, the same reasoning results in specifying minimum force acting through the maximum distance. As distance is increased and force reduced, the neg'ator becomes increasingly efficient in the space-work sense.

This can be illustrated simply by assuming that it is required to perform 100 ft-lb of work at:

(*a*) 100-lb force acting over 1 ft
The neg'ator required in this case would be:

Material, in.	0.042 × 4
Diameter, in.	3.66
Length, in.	24
Weight, lb	1.17
Volume coiled, cu in.	55

(*b*) 10-lb force acting over 10 ft
The neg'ator required in this case would be:

Material, in.	0.0166 × 1
Coil diam, in.	1.5
Length, in.	165
Weight, lb	0.8
Volume coiled, cu in.	2¹/₄

The same amount of work would be accomplished by each neg'ator.

This same analogy applies when the neg'ator is used as a B-motor, in which case, a further means of obtaining mechanical advantage will be available by varying the radius of the output means whether it is cable, drive gear, or any other member. Since the optimum number of revolutions for maximum work at constant torque is in the neighborhood of 40 turns, as against 6 to 10 turns of the common clock spring, it is obvious that torque required with the proper modification of gear ratios is in the order of $^1/_4$ to $^1/_7$. It is practical by accepting a rather nominal positive gradient of the motor to build motors delivering 60, 80, or even 100 turns.

When neg'ators, either as extension members or as motors, are used in their most efficient proportions, the space and hence the cost saving is tremendous. To make the most efficient use of such springs, it is necessary for the engineer to depart completely from the thinking which is ordinarily applied to conventional springs and develop some other basic conception such as the motor used in the foregoing illustration.

A. M. Wahl.[6] The writer is at somewhat of a loss to understand the derivation of Equation [2] of the paper which appears to indicate that the load P on a neg'ator spring will be somewhat less if the spring is considered as a thin flat plate than if it is considered as a beam, which is done in deriving Equation [1]. This result does not seem entirely reasonable on the basis of the elastic flat-plate theory since it is known that when a plate is bent in the shape of a cylindrical surface, the stiffness will be about 10 per cent greater than that given by beam theory, assuming the Poisson ratio ν equal to 0.3. Thus for a plate bent to a cylindrical form by a moment M in-lb per in. width and taking $\nu = 0.3$, the expression for curvature $1/r$ is equal to[6]

$$\frac{1}{r} = \frac{12M(1-\nu^2)}{Et^3} = 0.91\left(\frac{12M}{Et^3}\right)$$

This value is 91 per cent of the value obtained on the basis of simple-beam theory.

Using this formula, and considering the neg'ator to act essentially as a plate in bending, the moment necessary to straighten out the strip (i.e., to change the curvature by an amount $1/R_n$) would be greater in the ratio of $1/.91 = 1.10$ than if the strip is

[4] Research and Development, Minneapolis-Honeywell Regulator Company, Brown Instruments Division, Philadelphia, Pa.

[5] Advisory Engineer, Westinghouse Research Laboratories, East Pittsburgh, Pa. Mem. ASME.

[6] See, for example, "Strength of Materials," by S. Timoshenko, part 2, second edition, D. Van Nostrand Company, Inc., New York, N. Y., 1941, p. 120.

considered merely as a beam in bending. If we assume that the load on the spring will be proportional to this moment, it follows that the load obtained by considering the plate effect should be greater by about 10 per cent than if this effect were neglected. In other words, this would seem to indicate that the load given by Equation [2] of the paper should be greater than that given by Equation [1] instead of being less.

Since something may have been overlooked by this method of reasoning, it would be of interest if the author would present details concerning the method of deriving Equation [2]. Any test data tending to support this equation as compared with Equation [1] also would be of interest.

Author's Closure

In answer to Mr. Billings, the comparison illustrated in Fig. 2 is made to show the difference in the force of a conventional spiral spring and neg'ator with the same dimensions. If a minimum initial force is specified, it would then be necessary to pre-extend the spiral spring in order to obtain the required force at zero deflection. Assuming that a minimum load of 0.46 lb must be exerted on a mechanism, the spiral spring must be deflected approximately 12 in. before this force would be realized. The effective deflection of the spiral spring would then be 58 in.—not the available 70 in. The advantages of the neg'ator are further indicated in the additional 12 in. of deflection which are gained.

An actual example of gain in deflection is illustrated in Fig. 12 where torque curves of a neg'ator B-motor and the power spring of a typical motion-picture camera are compared. A minimum torque of 2.3 lb-in. is required. The power spring must be wound through six turns before enough torque is provided to drive the mechanism. Conventional cameras are usually provided with some means of stopping the mechanism when this point is reached so that film will not slow down and cause erratic action. The neg'ator, of course, can be used throughout its full deflection because it develops constant or nearly constant torque. This comparison is explained in detail in the paper.

It is true that in most applications the use of a suitable bearing in the neg'ator bushing is required. However, there are some instances where it has been possible to entirely eliminate both bearing and bushing. The neg'ator is contained within a suitable case and the outer end allowed to protrude through a slot in the case. When the neg'ator is extended, the outer coils roll against the inner surface of the case causing relatively smooth action. An example of such an application is a window sash balance. Although constant force is desirable in a sash balance, the accuracy of this force is not critical so that the friction developed by the rubbing contact between neg'ator and case is not objectionable.

In the case of the straight extension-type neg'ator, stress factor S_f is the ratio $\frac{t}{R_n}$; the B-motor stress factor equals $t\left(\frac{1}{R_n}+\frac{1}{R_1}\right)$. This expression, given in Table 4, accounts for the fact that the material is back-bent on the output bushing of the neg'ator B-motor.

In respect to Mr. Carlson's remarks, once the requirements for a neg'ator have been established, the calculations are quite simple because usually the only variables are material thickness, material width, and bushing radius. Since force or torque is directly proportional to material width, we can design for unit width and then modify this value in order to meet specific load or torque requirements. Compared with the conventional types of springs, the calculations involved are relatively easy, especially for the extension-type neg'ator. After material thickness and fatigue-life requirements have been established, the natural radius of the neg'ator is easily determined in the expression $S_f = \frac{t}{R_n}$. A brief study of the nomograph in Fig. 18 will show that once load and fatigue life have been established, the dimensions of the neg'ator can be fixed.

Standard spring-coiling machines can be used to coil the neg'ator. However, additional special tooling is required in order to form the material properly. Stress calculations and experimental analysis of strain at the surface of the neg'ator have indicated that fiber stresses well over 300,000 psi exist at the surface of the material. These extremely high stress values indicate that the neg'ator contains a high degree of favorable residual stress.

The analogies between the neg'ator and an equivalent electric motor or hydraulic cylinder suggested by Mr. Poole are excellent means of visualizing the most important characteristics of the neg'ator. The comparison between two neg'ators designed to supply 100 ft-lb of work, one providing a force of 100 lb over a distance of 1 ft and the other providing a force of 10 lb over a distance of 10 ft, clearly emphasizes the advantages of making the ratio of deflection to force as large as possible.

It has frequently been found that in discussions with engineers and designers their preconceived ideas on conventional springs serve to make a clear conception of the neg'ator principle rather difficult.

The expression for curvature given by Mr. Wahl is, of course, the correct one for a thin flat plate bent to the cylindrical form. However, in the neg'ator, the material has been initially preformed into a cylindrical section, and force (or moment) is developed when the material is straightened out. As the neg'ator, Fig. 1, is extended by the force P, the material assumes a cross-sectional curvature in the zone L which increases the stiffness of the material in this zone. However, the energy expended in producing this cross-sectional curvature is not in the form of useful work. In this instance it would therefore be necessary to divide by the expression $(1-\nu^2)$ in the formula for curvature.

The original derivation of the basic neg'ator equation was performed by means of elastic energy theory

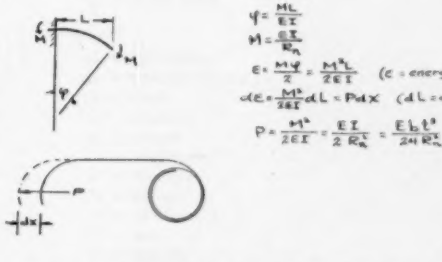

$$\varphi = \frac{ML}{EI}$$

$$M = \frac{EI}{R_n}$$

$$\epsilon = \frac{M\varphi}{2} = \frac{M^2L}{2EI} \quad (\epsilon = \text{energy})$$

$$d\epsilon = \frac{M^2}{2EI}dL = Pdx \quad (dL = dx)$$

$$P = \frac{M^2}{2EI} = \frac{EI}{2R_n^2} = \frac{Eb\,t^3}{24R_n^2}$$

When an attempt was made to verify this equation by actual tests it was noted that the test loads were consistently 10 per cent lower than the calculated loads. It was then suggested that the lower force output was due to the effect of Poisson's ratio and an analysis similar to that suggested by Mr. Wahl was carried out. The discrepancy was at once apparent for, instead of obtaining test results only 10 per cent lower than calculated results, the error increased to approximately 20 per cent.

The reason for the discrepancy was not realized until the cross-sectional curvature of the stressed neg'ator was examined and compared to the curvature developed when a flat strip of identical material was bent into a cylinder of the same radius as the neg'ator. The comparison is shown in Fig. 21.

The analysis indicates that for a thin flat plate bent into a

cylinder the change in cross-sectional shape is negligible and occurs only near the outer edges of the material. In the case of the neg'ator, where the material is coiled to a given natural radius

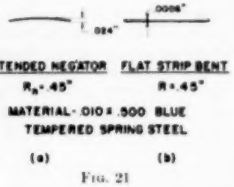

FIG. 21

and then pulled straight, the change in cross-sectional shape is extreme and appears as more of a buckling action under a critical load. If a constant radius is assumed (the curve is approximately circular) it is approximately 1.3 in. Poisson's ratio gives a radius of $3 \times .45 = 1.35$ in.—a close agreement.[7] This relationship does not hold in the case of the flat thin plate bent into a circular shape, Fig. 1(*b*), indicating that the analysis presented by Timoshenko which Mr. Wahl cites does not suffice in this instance.

[7] "Elements of Strength of Materials," by S. Timoshenko and G. H. MacCullough; second edition, D. Van Nostrand Company, Inc., New York, N. Y., 1940, p. 114.

TABLE 5 MATERIAL—SAE 1085 SPRING STEEL
($E = 30 \times 10^6$ psi)

b	t	R_n	P, lb		Per cent error
			Calculated	Test	
.500	.006	.333	1.22	1.11	9.9
.250	.004	.200	.500	.46	8.7
1.000	.012	.607	5.87	5.35	9.7
1.000	.016	.810	7.79	7.00	11.3
.500	.005	.250	1.25	1.14	9.6
.375	.005	.275	.774	.698	10.9
.500	.008	.500	1.28	1.16	10.3
2.000	.024	2.00	8.71	7.79	11.8
1.500	.020	1.50	6.67	6.10	9.3
.750	.014	.70	5.23	4.79	9.2
2.000	.032	1.625	31.0	28.0	10.8

The data contained in Table 5 represent accurate measurements made on neg'ators of different dimensions and show the discrepancy between actual test loads and calculated loads when no modification is made in the basic expression [1]. The data indicate that Equation [1] should give values which are approximately 10 per cent lower. If the effect of Poisson's ratio is considered, as in Equation [2], the calculated load will agree with actual test values. The tabulation includes only a few representative tests. Within the last several years Equation [2] has been verified several thousand times through production inspection.

From an energy standpoint, it might be said that a certain portion of the energy potentially available from the neg'ator is not realized because it is stored as energy required to produce camber in the material.

A Contribution to the Problem of Designing Radial Turbomachines[1]

By O. E. BALJE,[2] FARMINGDALE, L. I., N. Y.

A method is outlined for computing the characteristic values, such as pressure coefficient and efficiency of centrifugal compressors and radial inward-flow turbines, as function of Reynolds number and Mach number, whereby the latter values are defined in such a manner as to represent the weight flow and the pressure ratio of the turbomachine. The influence of blade number, blade angle, speed and diameter ratio of the impeller on the efficiency and pressure coefficient is discussed. The application of this method for computing the characteristic of a particular turbomachine is shown.

Nomenclature

The following nomenclature is used in the paper:

a = characteristic value representing weight flow
A = area, sq ft
b = width, ft
c = absolute velocity, fps
c_p = specific heat at constant pressure, Btu/lb deg F
c_v = specific heat at constant volume, Btu/lb deg F
C = constant
d = diameter, ft
D = outer diameter of impeller, ft
D' = inner diameter of nozzle box, ft
D^* = diameter of flow passage, ft
D_r = outer diameter of annular diffuser, ft
E = constant in viscosity, Equation [12]
g = gravitational constant, fps^2
H = head, ft
J = mechanical equivalent of heat, Btu/ft lb
k^* = average height of surface irregularities, ft
K = ratio of meridional flow velocities
l = length of overlapping section of nozzle blades, ft
L = length of flow channel, ft
m = slip factor
Ma = local Mach number
Ma^* = Mach number of turbomachine
p = pressure, psi
P = power, hp
q = dimensionless coefficient
r = radius, ft
R = gas constant, ft/deg F
Re = local Reynolds number
Re^* = Reynolds number of turbomachine
SFC = Specific fuel consumption, lb per hphr
s = clearance between impeller and casing, ft
S = entropy
$t = l/b_N$ = overlap
T = temperature, deg R
u = peripheral speed, fps
V = volume flow, cfs
w = relative velocity, fps
W = weight flow, lb per sec
z = blade number
α = absolute flow angle
β = relative flow angle; impeller blade angle
$1/\beta^* = 1/\sqrt{1 - Ma^2}$ Prandtl factor
β_W = loss coefficient representing wheel-disk friction
γ = specific weight, lb per cu ft
δ = angle of deflection
Δ = difference
η = efficiency
$\epsilon = D/d$ = diameter ratio of impeller
$\zeta = \lambda L/D^*$ = specific loss coefficient
$\kappa = c_p/c_v$ = ratio of specific heats
λ = general loss coefficient
$\mu = D_r/D$ = diameter ratio of annular diffuser
$\mu' = D'/D$ = diameter ratio of nozzle clearance
ν = kinematic viscosity, ft^2/sec
ρ = degree of reaction
φ = flow factor
$\tau = D^*/b_N$ = characteristic ratio of collector
χ = shock factor

Subscripts:

ad = adiabatic
AD = annular diffuser
b = blade
cl = clearance
cr = critical
C = compressor
d = discharge
D = diffuser
e = effective
H = hub
I = impeller
m = meridional, mean
n = of design
N = nozzle
o = optimum
opt = optimum
P = power
Pr = Prandtl
r = relative eddy
s = sound
sh = shock
st = static
S = supplied
t = total
th = theoretical

---

[1] Clearance for presentation and publication of this paper has been granted by Public Information Office, Wright-Patterson AFB (ECM/ac, B-262, P-2015, 6-4273, June 14, 1950).

[2] Engineering Division, Directorate of Research and Development Headquarters, Air Materiel Command, Dayton, Ohio. Since May, 1951: Stratos Division of the Fairchild Corporation.

Contributed by the Gas Turbine Power Division and presented at the Fall Meeting, Minneapolis, Minn., September 26–28, 1951, of The American Society of Mechanical Engineers.

Note: Statements and opinions advanced in papers are to be understood as individual expressions of their authors and not those of the Society. Manuscript received at ASME Headquarters, May 31, 1951. Paper No. 51—F-12.

t = turbine
u = peripheral
W = wheel disk
x = state at exit of annular diffuser
1 = state before turbomachine
2 = state at outer diameter of impeller
3 = state behind turbomachine

Introduction

In this paper some considerations are presented which deal with a simplified method for computing the efficiency of radial turbomachines and for calculating their characteristics. The simplified method is based upon the following procedure: Each component of the turbomachine is represented by its median flow line, and the effect of each component is expressed by dimensionless coefficients, such as work coefficients and loss coefficients. By applying some generally valid laws of flow mechanics and thermodynamics, these coefficients are presented as functions of some characteristic values such as Reynolds number, diameter ratios, Mach numbers, and flow factors, which refer to the size, the speed, and the shape of the components. By combining the work and loss coefficients of the components, the dimensionless coefficients of the turbomachine, such as efficiency and pressure coefficient, are calculated as functions of the foregoing characteristic values. The latter also have a definite relationship to the design requirements, such as weight flow, inlet pressure, inlet temperature, and pressure ratio so that finally a diagram results showing the efficiency and pressure coefficient as a function of the design requirements. By using this diagram the design data, such as impeller diameter and speed, can be calculated which are required to obtain a particular efficiency.

The losses occurring in the turbomachine are treated by applying the Blasius law to each component of it, since results of special tests conducted on the components of rotating radial turbomachines have indicated the applicability of the Blasius law in the turbulent range. Such tests, however, have not yet advanced far enough to establish definitely the critical Reynolds number for turbomachines. Critical Reynolds numbers shown in the diagram mentioned are determined by applying the well-known relations valid for pipes and ducts. These may not represent true values for all cases, even though the flow passages in the discussed type of turbomachine may closely resemble pipes and ducts.

The diagrams presented have been found to yield a close estimate of the efficiency for a wide range of designs and design conditions. Nevertheless, it is pointed out that the simplified method does not always yield values of extreme exactness, and it is not intended to standardize the efficiencies of radial turbomachines in this paper. Such a task would be premature since the knowledge about flow mechanics in turbomachines is still incomplete in some respects, and special research work will still have to be done before exact relationships can be established.

This paper deals especially with radial turbomachines having impellers of half-shrouded type and blade-tip angles of 90 deg. Turbines of the inward-flow type and compressors of the outward-flow type are discussed. The influence of the Reynolds number on the design of small power plants is demonstrated.

Calculation Principles

(a) *Presentation of Process in T-S Diagram.* A simplified turbine and compressor process is presented in Figs. 1 and 2. In these figures the subscript 1 denotes the state before the turbomachine, subscript 2 the state at the outer diameter of the impeller, subscript 3 the state behind the turbomachine, and subscript "th" a theoretical state. The pressure lines represent the total pressures. The compressor process may be described as follows: Adiabatic compression from the initial state p_1T_1 to the theoretically obtainable state $p_{2-th}\ T_{2-th}$. Fig. 1 shows the resulting increase in the adiabatic pressure head, H_{th}. As a consequence of the flow losses in the impeller, the total pressure behind the impeller p_2 is smaller than its theoretical value p_{2-th}. The distance $p_{2-th}p_2$ in Fig. 1 represents the head loss H_l in the impeller. The temperature remaining constant (no heat conduction or radiation assumed) the state at the end of the impeller is represented by p_2T_{2-th}.

The wheel-disk friction losses cause an increase in total temperature; for representing this loss in the *T-S* diagram it may be

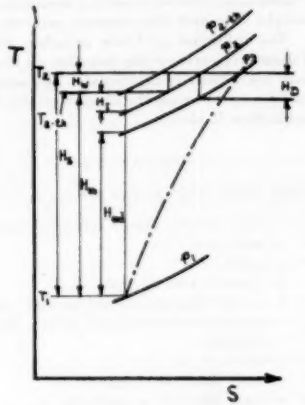

Fig. 1 Simplified Representation of Compressor Process in *T-S* Diagram

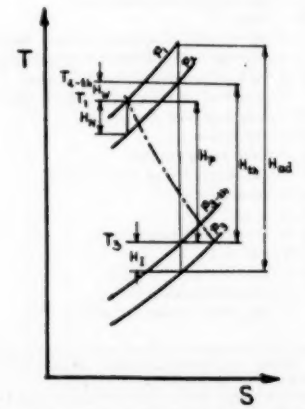

Fig. 2 Simplified Representation of Turbine Process in *T-S* Diagram

assumed that the temperature increase is imparted to the flow directly behind the impeller. This increase in total temperature is represented in Fig. 1 by the distance H_W. The final total temperature T_2 remains constant for the further process because no

energy is added to the process after the impeller. The diffuser losses are represented by the distance H_D in Fig. 1. The final state is represented by $p_3 T_3$, and the actual delivery head of the compressor is represented by the distance H_{sd} in Fig. 1. As long as the divergence of the pressure lines in the T-S diagram[3] can be neglected, the actual pressure head delivered by the compressor can be written in the form $H_{sd} = H_{th} - H_I - H_D$. The adiabatic head to be supplied to the compressor can be represented by $H_S = H_{th} + H_W$. The ratio H_{sd}/H_S represents the adiabatic efficiency η_{sd-c}.

The simplified turbine process, Fig. 2, may be described as follows: Losses in the nozzles (represented by the adiabatic head H_N) decrease the initial pressure p_1 to p_2 at constant temperature T_1. Wheel-disk friction losses H_W increase the initial temperature from T_1 to T_{2-th} at constant pressure p_2. The theoretically obtainable expansion head H_{th} decreases the pressure p_2 to p_{3-th} and the temperature to T_3. The losses in the impeller H_I decrease the pressure p_{3-th} to p_3 at constant temperature T_3. Neglecting again the divergence of the pressure lines, the adiabatic head which must be supplied to the turbine can be expressed by $H_{sd} = H_{th} + H_N + H_I$. The head transformed into shaft power can be expressed as $H_P = H_{th} - H_W$. The ratio H_P/H_{sd} represents the adiabatic efficiency η_{sd-T}.

Since the tip speed of the impeller u_2 is a very significant characteristic value, it is useful to refer the foregoing heads to a fictitious head u_2^2/g. It follows then that $q_{sd-C} = H_{sd-C} g/u_2^2$ represents a pressure coefficent for the compressor, and that $q_{sd-T} = H_{sd-T}\, g/u_2^2$ represents a pressure coefficient for the turbine. Also $q_C = H_{S-C}\, g/u_2^2$ and $q_T = H_{P-T}\, g/u_2^2$ are work coefficients for the compressor and turbine, respectively. In the same manner q_{th} is a coefficient representing the theoretically obtainable work; q_W is a wheel-disk friction coefficient; q_I is an impeller-loss coefficient; q_D is a diffuser-loss coefficient, and q_N is a nozzle-loss coefficient. With these expressions, the relations for the efficiencies can be written $\eta_{sd-C} = q_{sd-C}/q_C$, and $\eta_{sd-T} = q_T/q_{sd-T}$.

(*b*) *Theoretically Obtainable Work.* The work head H_{th} theoretically obtainable, is proportional to the change in moment of momentum of the flow through the impeller and can be expressed by the Euler equation

$$H_{th} = \frac{\Delta(c^2)}{2g} + \frac{\Delta(u^2)}{2g} - \frac{\Delta(w^2)}{2g} \qquad [1]$$

where Δ denotes the differences of the velocity heads between rotor inlet and rotor outlet.

In a blade system designed for converting flow energy into shaft power (turbine), the theoretically obtainable work head is proportional to the algebraic difference of intake moment of momentum and outlet moment of momentum, so that Equation [1] takes the form

$$H_{th-T} = \frac{u_2 c_{u-2}}{g} \pm \frac{u_3 c_{u-3}}{g} \qquad [2]$$

In Equation [2] u denotes the peripheral speed of the impeller and c_u the component of the absolute velocity acting in the peripheral direction. The minus sign in Equation [2] holds for the case, that the outlet moment of momentum acts in the direction of the inlet moment of momentum whereas the plus sign holds when the outlet moment of momentum acts in the opposite direction of the inlet moment of momentum. The peripheral component c_{u-2} at the inlet is mainly dependent upon the nozzle angle; the peripheral component c_{u-3} at the impeller exit is a function of the exit blade angle and the peripheral speed at the outlet. Considering the case where the exit blade angle and the volume flow are kept constant, it is found that a decrease in peripheral velocity produces a decrease in twist running in the same direction as the tip speed (parallel twist), but an increase in the countertwist, Fig. 3.

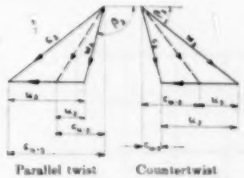

FIG. 3 DISCHARGE TRIANGLES OF TURBINE

Comparing a radial rotor with an axial rotor, it becomes evident that due to the lower peripheral speed at the outlet of a radial rotor, the outlet moment of momentum in a radial rotor generally will be greater than in an axial rotor in the case of countertwist, but will be smaller than in an axial rotor in the case of parallel twist. That means that the work head, theoretically obtainable in a radial rotor, normally will be higher than in an axial rotor, when both blade systems produce the same flow deflection. In the case of countertwist this effect is restricted to certain limits because the moment of momentum is determined by the product of twist component and peripheral speed and, therefore, can be increased also by increasing the peripheral speed. Hence in these cases the theoretically obtainable work of the axial rotor can be superior to that of the radial rotor at equal flow deflection.

The foregoing relationships are explained by the fact that as a consequence of the centrifugal effect in a rotating radial rotor, the static pressure at the outer radius must be higher than at the inner radius. This pressure difference represents a head, the expansion of which gives an additional momentum to the rotor for the case that the flow is directed to the inner radius. This head which mainly determines the degree of reaction is expanded by the decrease in peripheral speed.

To furnish additional relationships, Equation [2] can be transformed. The geometric relations $\cot \alpha_2 = c_{u-2}/c_{m-2}$ and $\cot \beta_2 = w_{u-2}/c_{m-2} = (u_2 + c_{u-2})/c_{m-2}$ can be read from the velocity triangles in Fig. 4. In most cases it is desirable to use the blade angle β_{b-2} instead of the flow angle β_2. These two angles are

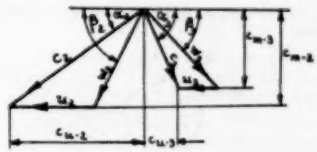

FIG. 4 VELOCITY TRIANGLES OF TURBINE

equal for an infinite blade number. The smaller the number of blades the greater the difference between flow angle and blade angle. This difference can be expressed by introducing the concept of the slip factor (2, 3), which is based upon the assumption that, for producing the desired flow deflection within the rotor, a definite impulse has to be exerted, and that, owing to the limited blade number, this impulse does not coincide with the impulse as

[3] It can be shown that the error resulting from this assumption is smaller than the error resulting from the uncertain knowledge of the losses (1).[4]

[4] Numbers in parentheses refer to the Bibliography at the end of the paper.

given theoretically by the blade angle. With this concept the ratio of the theoretically possible peripheral component of the absolute velocity to its actual value, $c_{u-2-th}/c_{u-2} = m$, is a measure for the influence of the blade number. The value of m is assumed to be a function of the blade number z, the diameter ratio $D/d = \epsilon$ and the blade angle β_{b-2} for compressors, and the blade angle β_{b-1} for turbines, respectively, Fig. 5.[5] Substituting the geometrical relations and the slip factor for the velocities in Equation [2], the relation for the work coefficient becomes

$$q_{th-T} = \left(K_I \cot \alpha_2 + \frac{\cot \beta_{b-2}}{\epsilon_a m}\right)\varphi - \frac{1}{m\epsilon_a^2} \quad \ldots\ldots [3]$$

In Equation [3] φ denotes the flow rate c_{m-2}/u_2, i.e., the ratio of the meridional discharge velocity c_{m-2} to the tip speed u_2 of the impeller. The factor $K_I = c_{m-2}/c_{m-1}$ designates the ratio of the radial component of the inlet and the axial component of the discharge velocity at the impeller, and $\epsilon_a = u_2/u_1 = D/d_a$ the ratio of the peripheral velocities at the inlet and outlet of the impeller, i.e., the effective diameter ratio of the impeller, when d_a represents the diameter at which the median discharge state exists. Equation [3] represents at K_I = const ($\epsilon_a, \alpha_2, \beta_{b-2}$ must be considered as constant for an engine) an equation for a straight line whose inclination with respect to the abscissa φ is determined by the size of the angles α_2 and β_{b-2}, and whose intersection with q_{th} is located at $-1/m\epsilon_a^2$. This means a linear increase of the theoretically obtainable work with the flow rate. The intersection point with the ordinate located at negative q_{th} values indicates that the machine cannot transfer any power at low flow rates but rather absorbs such power, which means that it operates as a compressor.

Equation [3] shows, in addition, that up to a definite flow factor, namely

$$\varphi = \frac{\dfrac{1}{\epsilon_a^2} - 1}{\left(\dfrac{1}{\epsilon_a} - 1\right)\cot \beta_1} \quad \ldots\ldots [4]$$

the theoretically obtainable work is larger in a radial rotor with the flow directed toward the inner radius than in a rotor at purely axial flow ($\epsilon_a = 1$), when both types operate at equal characteristics, i.e., at equal flow deflection and equal acceleration or deceleration of the rotor flow, Fig. 6. Consequently the radial rotor may be superior only up to this particular flow rate.

In a blade system designed for converting shaft power into kinetic or pressure energy (compressor), the theoretically obtainable work head is proportional to the algebraic difference of discharge moment of momentum and inlet moment of momentum so that Equation [1] takes the form

$$H_{th-C} = \frac{u_2 c_{u-2}}{g} \pm \frac{u_1 c_{u-1}}{g} \quad \ldots\ldots [5]$$

The minus sign in Equation [5] applies when the inlet moment of momentum acts in the same direction as the discharge moment of momentum (parallel twist) whereas the plus sign applies for countertwist at the inlet. Using the geometric relation obtained from the velocity triangles, Fig. 7, and th of the slip factor ($m = c_{u-2-th}/c_{u-2}$) the theoretically o ic work can be expressed by the relation

$$q_{th-C} = \left(\frac{\cot \alpha_1}{\epsilon_a} - \frac{K_I \cot}{\epsilon_a}\right)\varphi + \frac{1}{m} \quad \ldots\ldots [6]$$

if the flow factor is determined by $\varphi = c_{m-1}/u_2$ and if the acceleration or deceleration of the meridional rotor flow is expressed by $K_I = c_{m-2}/c_{m-1}$. Equation [6] indicates that the theoretically obtainable work in a compressor is a linear function (for K_I = const) of the flow factor with a slope dependent on the magnitude of the flow deflection in the rotor and the diameter ratio ϵ_a, Fig. 8. An effect of centrifugal forces is not evident from Equation [6] but nevertheless exists, because in the radial rotor with a flow pointing outward a part of the work exists already in static pressure instead of velocity head as mostly in the case of axial rotors.

From the foregoing considerations it becomes evident that the centrifugal forces influence the energy transformation in the radial rotor in such a manner, that for turbine operation at low

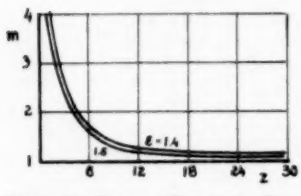

Fig. 5 Slip Factor as Function of Blade Number and Diameter Ratio for β_{b-1} = 90 Deg

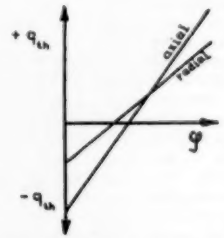

Fig. 6 Coefficient q_{th} as Function of Flow Factor (Turbine)

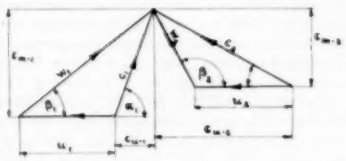

Fig. 7 Velocity Triangles of Compressor

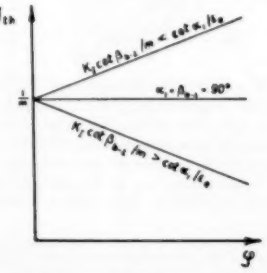

Fig. 8 Coefficient q_{th} as Function of Flow Factor (Compressor)

[5] For α_1 no correction is introduced, so that α_1 denotes the flow angle.

flow rates the theoretically obtainable work (with a flow directed toward the inside radius) is greater than in axial rotors. In compressor operation (with a flow directed outward) a part of the work head is directly transformed into static pressure head. With Equations [3] and [6] a diagram can be plotted, showing the tendency of the theoretically obtainable work of a particular rotor ($\beta_{b-2-c} = \beta_{b-2-T} = 90$ deg; in turbine operation and compressor operation, respectively, Fig. 9. Admitting the flow at the outer diameter with a twist, the rotor produces work, starting at a certain flow rate and increasing with increasing flow rates, line *a*. Driving the rotor, a flow directed outward will be produced and the theoretically obtainable work will be an equidistant function of the flow rate, line *b*. The effect of the centrifugal forces on the theoretically obtainable work, depending upon the direction of the flow, shows especially well the discontinuity point at the flow-rate zero. Such a discontinuity does not occur in an axial rotor, which has no significant centrifugal-force effect as shown by lines *c* and *d* in Fig. 9.

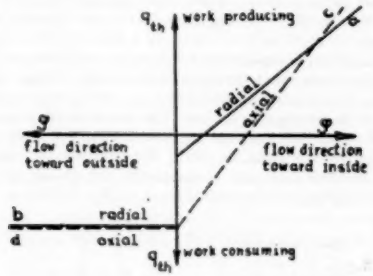

FIG. 9 TURBINE AND COMPRESSOR DIAGRAM OF RADIAL AND AXIAL ROTOR FOR $\beta_{b-2} = 90$ DEG

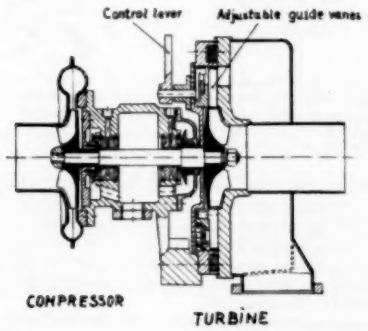

FIG. 10 TURBOSUPERCHARGER DEVELOPED BY DVL IN 1944 ($D = 2.75$ in., $N = 70{,}000$ rpm.)

It may be mentioned that probably the greatest advantages of radial turbomachines are their constructional features which allow a simple arrangement of adjustable guide vanes. This is illustrated in Fig. 10 which shows an exhaust-gas-driven turbosupercharger employing adjustable guide vanes in the nozzle section of the turbine. By controlling the guide vanes, the range of volume flow at constant impeller speed can be increased considerably without appreciably changing the efficiency.

Losses

In order to calculate the actual work capacity of the turbomachines it is necessary to verify the losses. For this purpose the introduction of the Mach number Ma^*, and the Reynolds number Re^*, was believed useful. The Mach number Ma^* is defined as the ratio between the tip speed of the impeller and the velocity of sound as calculated from the inlet flow temperature, i.e., $Ma^*_C = u_2/c_s = Ma^*_T$ with

$$c_s = \sqrt{\frac{2\kappa}{\kappa + 1} g RT_{1-t}} \quad \ldots\ldots [7]$$

These Mach numbers do not represent actual flow velocities and are introduced solely as convenient calculation values representing the tip speed, and yielding, in addition, a direct relation to the pressure ratio, because for the compressor it holds

$$\frac{p_{2-t}}{p_{1-t}} = \left(1 + \frac{\kappa - 1}{\kappa + 1} 2q_{ad} Ma^{*2}_C\right)^{\frac{\kappa}{\kappa - 1}} \quad \ldots\ldots [8]$$

and for turbines

$$\frac{p_{2-t}}{p_{1-t}} = \left(1 - \frac{\kappa - 1}{\kappa + 1} 2q_{ad} Ma^{*2}_T\right)^{\frac{\kappa}{\kappa - 1}} \quad \ldots\ldots [9]$$

The Mach numbers also represent a convenient value for calculating the temperature rise and drop, respectively. For compressors, the relation

$$\frac{T_{2-t}}{T_{1-t}} = 1 + \frac{I2\kappa R}{c_p(\kappa + 1)} q\, Ma^{*}_C{}^2 \quad \ldots\ldots [10]$$

can be derived. The correspondent relation for turbines reads

$$\frac{T_{2-t}}{T_{1-t}} = 1 - \frac{I2\kappa R}{c_p(\kappa + 1)} q Ma^{*}_T{}^2 \quad \ldots\ldots [11]$$

The Reynolds number is defined as the product of impeller tip speed and outer diameter of the impeller, divided by the kinematic viscosity of the flow at the inlet of the turbomachine, i.e., $Re_C^* = Du_2/\nu_1 = Re_T^*$. An approximate relation for the kinematic viscosity of gases can be written in the form

$$\nu = \frac{T^2}{p} E \quad \ldots\ldots [12]$$

The fluid-friction losses can be expressed by the relation

$$H = \lambda \frac{L}{D^*} \frac{c^2}{2g} \quad \ldots\ldots [13]$$

In Equation [13] H denotes the head loss, L a characteristic length of the flow path, D^* a characteristic diameter of the flow passage, c the flow velocity, and λ a loss factor. A theoretical relation for λ is given by von Kármán as $\lambda^{-0.5} = 1.95 \log (Re\sqrt{\lambda}) - 0.55$. This relation for the turbulent range can be represented by the approximation $\lambda = 0.316\, Re^{-0.25}$ (Blasius law), (4) when Re denotes the actual Reynolds number of the flow. With these relations the losses in the turbomachine can be determined. As an example, the derivation of a relation for the losses in an annular diffuser may be presented.

The flow path in this case is approximately a logarithmic spiral, i.e.

$$L = \frac{D(\mu - 1)}{2 \sin \alpha_2} \quad \ldots\ldots [14]$$

when $\mu = D_s/D$ denotes the diameter ratio of the annular diffuser. The characteristic diameter D^* in Equation [13] has to be replaced by $2b_2$ in the case of parallel side walls, b_2 denoting the distance between the walls. This distance can be expressed by the relation ($d_H = 0$)

$$b_2 = \frac{D\gamma_1}{4\epsilon^2 K_1 \gamma_2} \quad \text{[15]}$$

In Equation [13] the expression $\lambda L/D^*$ can be combined to a loss factor ζ by applying Equations [14], [15], and the Blasius law, i.e.

$$\zeta_{AD} = \lambda \frac{L}{D^*} = \frac{0.316\,(\mu - 1)\epsilon^2 K_1 \gamma_2}{\sqrt[4]{Re}\,\sin\alpha_2\,\gamma_1} \quad \text{[16]}$$

In Equation [16] α_2 denotes the angle between the direction of the absolute velocity c_2 and the direction of the rotational speed u_2, i.e.

$$\sin\alpha_2 = \left[1 + \frac{1}{m^2}\left(\frac{1}{\varphi K_1} - \cot\beta_{b-2}\right)^2\right]^{-0.5} \quad \text{[17]}$$

The actual Reynolds number in Equation [16] can be replaced by the Reynolds number of the compressor

$$Re = Re_C^* \frac{\varphi\sqrt{1 + \frac{1}{m^2}\left(\frac{1}{\varphi K_1} - \cot\beta_{b-2}\right)^2}}{4\epsilon_2 T_{2-\infty}/T_{1-\infty}} \quad \text{[18]}$$

For the square of the velocity in Equation [13] the mean velocity head may be taken, i.e., $c^2 = 0.5(c_2^2 + c_x^2)$. The temperature ratio in Equation [18] and the density ratio in Equation [16] can be expressed by the Mach number of the compressor, as demonstrated in Equations [8] and [10], whereby it has to be considered that in Equations [16] and [18] the static temperatures and pressures are required. These differ from the ratio of the total temperatures and pressures (as represented in Equations [8] and [10]), approximately, with the degree of reaction ρ. That means that in Equations [8] and [10] the terms q_{ad} and q will have to be replaced by ρq_{ad} and ρq, respectively. These terms generally are functions mainly of the flow factor, of the angle α_2, of the blade-tip angle β_{b-2}, and of the Reynolds number Re^*. For simplicity reasons the whole expression standing with the Mach number in Equations [8] and [10] may be represented by a factor C, the approximate value of which is quoted in each case. Thus it can be written

$$\frac{T_{2-\infty}}{T_{1-\infty}} = 1 + C_1 Ma^{*}{}_C{}^2 \quad \text{[19]}$$

$$\frac{p_{2-\infty}}{p_{1-\infty}} = (1 + C_2 Ma^{*}{}_C{}^2)^{3.5} \quad \text{[20]}$$

and approximately

$$\frac{\gamma_2}{\gamma_1} = \frac{p_{2-\infty}}{p_{1-\infty}}\frac{T_{1-\infty}}{T_{2-\infty}} = (1 + C_3 Ma^{*}{}_C{}^2)^{2.5} \quad \text{[21]}$$

because the correspondent C_1 and C_3 values differ only slightly in each case.

Introducing Equations [14] to [21] together with the Blasius law into Equation [13] the loss coefficient for the annular diffuser can be written in the form ($d_H = 0$)

$$q_{AD} = \frac{(\mu - 1)(1 + \mu^{-2})K_1{}^{3}\epsilon^{2.5}\varphi^{1.75}\left[1 + \frac{1}{m^2}\left(\frac{1}{\varphi K_1} - \cot\beta_{b-2}\right)^2\right]^{1.375}(1 + C_3 Ma^{*}{}_C{}^2)^{2.5}(1 + C_1 Ma^{*}{}_C{}^2)^{3.5}}{8.95\sqrt[4]{Re_C{}^*}} \quad \text{[22]}$$

Equation [22] shows that the loss coefficient for the annular diffuser can be represented as a function of the Reynolds number Re^*, of the Mach number Ma^*, of the flow factor φ, of the diameter ratios ϵ and μ, of the blade tip angle β_{b-2} and of the factor K_1. For $\beta_{b-2} = 90$ deg the factors C_1 and C_3 nearly become constant (for air $C_1 = 0.14 \div 0.18$, $C_3 = 0.13 \div 0.17$). Equation [22] graphically is represented for $\alpha_1 = \beta_{b-2} = 90$ deg in Fig. 11. This figure shows that the losses in an annular diffuser increase with increasing rates of deceleration (μ) as was to be expected, and with decreasing flow factors. The latter tendency can be explained by the fact that the angle α_2 decreases with decreasing flow factors, see Equation [17]. The smaller the angle the longer the flow path and, consequently, the greater the losses. Similar diagrams can be plotted for $\alpha_1 \neq \beta_{b-2} \neq 90$ deg.

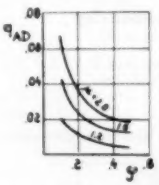

FIG. 11 LOSS COEFFICIENT OF ANNULAR DIFFUSER (Calculated for $Re^* = 2 \times 10^6$, $Ma^* = 0$, $\epsilon = 1.6$, $\beta_{b-2} = 90$ deg, $K_1 = 1$, $m = 1.35$.)

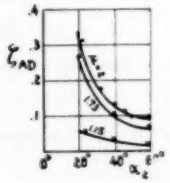

FIG. 12 COMPARISON BETWEEN TEST POINTS AND CALCULATION

It may be added that tests carried through with a radial rotor ($\beta_{b-2} = 90$ deg) in an open annular diffuser furnished a valuable support for the relations stated. According to Equation [16] the loss factor ζ_{AD} is a function of the angle α_2 (as ascertained during the tests by special direction-finding Pitot tubes). For the case treated, Fig. 12 shows that the measured values are satisfactorily represented by Equation [16].

By applying the method outlined, the loss coefficients of the other components can be calculated. For the loss coefficient of a symmetrical scroll with circular cross section, the relation ($d_H = 0$)

$$q_{sc} = \frac{0.35\epsilon^{1.5}K_1{}^{2.5}\left[1 + \frac{1}{m^2}\left(\frac{1}{\varphi K_1} - \cot\beta_{b-2}\right)^2\right]^{0.125}\varphi^{1.75}(1 + C_3 Ma^{*}{}_C{}^2)^{0.625}(1 + C_1 Ma^{*}{}_C{}^2)^{0.875}}{\mu^{1.25}\sqrt[4]{Re_C{}^*}} \left\{1 + \left[\frac{1}{m^2}\left(\frac{1}{\varphi K_1} - \cot\beta_{b-2}\right)^2\right]\left[1 + \left(1 + \frac{1}{2\epsilon}\sqrt{\frac{m}{K_1\mu\left(\frac{1}{\varphi K_1} - \cot\beta_{b-2}\right)(1 + C_1 Ma^{*}{}_C{}^2)^{2.5}}}\right)^{-4}\right]\right\} \quad \text{[23]}$$

has been derived, when the swept angle of the scroll is assumed 420 deg. For $\alpha_1 = \beta_{b-2} = 90$ deg the factors C_2, C_3, and C_4 again become nearly constant ($C_2 = 0.13 \div 0.2$, increasing with increasing μ-values, $C_3 = 0.14 \div 0.16$, $C_4 = 0.21 \div 0.25$). Fig. 13 shows a graphical representation of Equation [23] for $\alpha_1 = \beta_{b-2} = 90$ deg. This figure shows for the loss coefficient of the scroll a

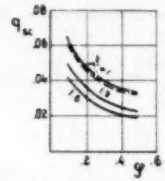

Fig. 13 Losses in a Scroll, Calculated for $Re^* = 2 \times 10^5$, $Ma^* = 1$, $Ma^* = 0.5$—, $\epsilon = 1.6$, $K_I = 1$, $m = 1.25$, $\beta_{b-2} = 90$ Deg, $\alpha_1 = 90$ Deg

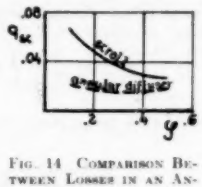

Fig. 14 Comparison Between Losses in an Annular Diffuser and Losses in a Scroll, Calculated for $Re^* = 2 \times 10^5$, $Ma^* = 0.5$, $m = 1.25$, $\epsilon = 1.6$, $K_I = 1$, $\beta_{b-2} = 90$ Deg, $\alpha_1 = 90$ Deg, $\mu = 1$

tendency very similar to that of the loss coefficient of the annular diffuser. This tendency of the losses in the scroll follows from Equation [13] which indicates that the losses increase with decreasing ratios D^*/L. In the scroll the mean length of the flow mainly depends upon the diameter of its inner radius, i.e., $L = D\mu\pi$. The diameter D^* of the scroll is in the first approximation[6] proportional to the diameter d_3 at the end of the scroll. This diameter, according to the relations governing the design of scrolls with circular cross section (2) decreases with decreasing values of α_2, i.e., with decreasing flow factors, as shown by the relation ($d_H = 0$)

$$d_3 = 2D\left[\frac{m(1 + C_4 Ma^{*}{}_{C}{}^{2})^{-2.5}}{4\epsilon^2 K_I\left(\frac{1}{\varphi K_I} - \cot\beta_{b-2}\right)} + \sqrt{\frac{m\mu(1 + C_4 Ma^{*}{}_{C}{}^{2})^{-2.5}}{4\epsilon^2 K_I\left(\frac{1}{\varphi K_I} - \cot\beta_{b-2}\right)}}\right] \quad \ldots\ldots [26]$$

whereby $C_4 = 0.21 \div 0.25$ for $\alpha_1 = \beta_{b-2} = 90$ deg. Therefore the ratio L/D^* and consequently the loss factor decreases with increasing flow factors. Equation [23] reveals also that the losses in the scroll increase with increasing Mach numbers, since the diameter d_3 decreases with increasing Mach numbers as shown in Equation [26].

A comparison between the losses in the scroll and those originating in the annular diffuser, assuming the same degree of deceleration for both, may be of general interest. This comparison is presented in Fig. 14 which shows a superiority of the annular diffuser. It must be pointed out that Equation [23] does not necessarily cover all types of scrolls. Some test results lead to the assumption that the losses in a scroll depend closely upon its shape and that a one-sided scroll has lower losses than a symmetrical scroll, Fig. 15, owing probably to the fact that two

Fig. 15 Symmetrical Scroll One-Sided Scroll

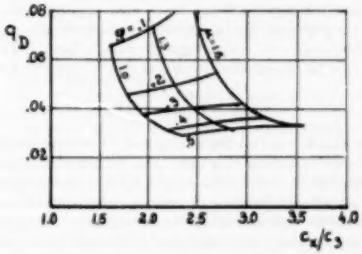

Fig. 16 Diffuser Losses, Calculated for $Re^* = 2 \times 10^5$, $Ma^* = 0.5$, $m = 1.25$, $\epsilon = 1.6$, $Kc = 1$, $\beta_{b-2} = 90$ Deg, $\alpha_1 = 90$ Deg

eddies originate in a symmetrical scroll which interfere with each other, thus causing greater losses than the single eddy in a one-sided scroll. Fig. 16 shows the loss coefficient q_D for a diffuser consisting of an annular space with parallel side walls and adjoining scroll as calculated by applying the relationships presented in Equation [22] and Equation [23].

For judging a complete compressor design it is useful to introduce a characteristic value $K_C = c_{m-3}/c_{m-1}$, representing the ratio between the meridional flow velocities at the outlet and the inlet of the compressor. Presentation of the losses plotted against this characteristic value, Fig. 17, shows that with small flow factors

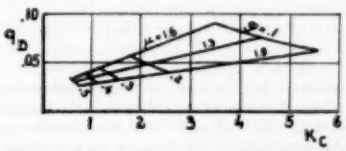

Fig. 17 Diffuser Losses Calculated for $Re^* = 2 \times 10^5$, $Ma^* = 0.5$, $m = 1.25$, $\epsilon = 1.6$, $K_I = 1$, $\beta_{b-2} = 90$ Deg, $\alpha_1 = 90$ Deg

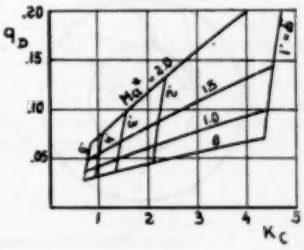

Fig. 18 (*right*) Diffuser Losses Calculated for $Re^* = 2 \times 10^5$, $m = 1.25$, $\epsilon = 1.6$, $\mu = 1.3$, $K_I = 1$, $\beta_{b-2} = 90$ Deg, $\alpha_1 = 90$ Deg

[6] In the derivations D^* denotes the inlet diameter, i.e.

$$D^* = \frac{d_3}{\sqrt{c_z/c_3}\sqrt{\gamma_z/\gamma_3}} \quad \ldots\ldots [24]$$

whereby

$$\frac{c_z}{c_3} = \frac{\sqrt{1 + \frac{1}{m^2}\left(\frac{1}{\varphi K_I} - \cot\beta_{b-2}\right)^2}}{\frac{1}{m}\left(\frac{1}{\varphi K_I} - \cot\beta_{b-2}\right)\left[1 + \sqrt{\frac{m(1 + C_4 Ma^{*}{}_{C}{}^{2})^{-2.5}}{4\epsilon^2 K_I\mu\left(\frac{1}{\varphi K_I} - \cot\beta_{b-2}\right)}}\right]^2} \quad \ldots [25]$$

with $C_4 = 0.21 \div 0.25$ for $\alpha_1 = \beta_{b-2} = 90$ deg.

the exit velocity c_{m-2} is a manifold of the inlet velocity c_{m-1} and that the losses increase considerably with increasing Mach numbers, Fig. 18. If guide vanes are fitted into the annular space it is possible to increase the rate of retardation further without noticeably influencing the losses at the design point.

Another loss originating in the diffuser has to be considered. It was mentioned in the section, Theoretically Obtainable Work, that the flow angle β_2 and the blade angle β_{b-2} have different values. That is true as long as the mean values are considered. Actually, the flow angle at the exit of the impeller varies over the blade passage owing to the relative eddy in the impeller channel. This angle is almost equal to the blade angle at the pressure side of the blade, almost equal to the median flow angle between two blades, and still smaller at the suction side of the blade. These different flow angles cause mixing losses (in a vaneless diffuser) or impulse losses (in a vane-type diffuser) which must be proportional to the difference between blade angle and median flow angle, i.e., proportional to the slip factor. This head loss H_m can be represented by $H_m = [(u_2 - u_2/m)0.5]^2 0.5g^{-1}$, or

$$q_m = 0.125\,(1 - 1/m)^2 \quad [27]$$

Equation [27] is valid for the mixing loss. For the corresponding impulse losses occurring in a vane-type diffuser immediately adjoining the impeller it has to be considered that quite generally the effect of pressure differences, caused by oblique attack on sharp edges, increases with increasing Mach numbers. An appropriate term for representing this influence is the Prandtl factor $1/\beta^*$ with $\beta^* = \sqrt{1 - Ma^2}$, Ma denoting the actual Mach number. Consequently Equation [27] has to be multiplied by the square of the Prandtl factor when impulse losses instead of mixing losses are considered. The foregoing relations would indicate that the impulse losses grow infinite for $Ma = 1$. However, the concept for calculating these losses is based on relations valid for subsonic velocities only and therefore cannot hold for flow velocities approaching the velocity of sound. Unfortunately, for the transition range, no generally valid calculation concept has been found developed.

For computing the flow-friction losses in the impeller, Equation [13] can be used again. By selecting an impeller shape, as illustrated in Fig. 19, the length of the flow passage can be expressed by the relation

$$L = \frac{r_2 - r_1}{\sin \dfrac{\beta_1 + \beta_{b-2}}{2}} \quad [28]$$

when it is assumed that the length of the flow path is equal to the length of a logarithmic spiral extending between the radii r_2 and r_1, with the angle $(\beta_1 + \beta_{b-2})/2$. For the diameter of the flow path, a value may be taken which represents a rectangular channel the one side of which is the width b_2 of the impeller, and the other side of which is the circular arc between two impeller blades, i.e.

$$D^* = \frac{D}{\epsilon}\sqrt{\frac{\gamma_1/\gamma_2}{K_I z}} \quad [29]$$

The mean velocity through the impeller can be represented by the relation

$$c = \frac{w_1 + w_2}{2} = \frac{u_2}{2}\left(\frac{\sqrt{1 + \varphi^2\epsilon^2}}{\epsilon} + \frac{\varphi K_I}{\sin \beta_{b-2}}\right) \quad [30]$$

because for the design point it holds

$$\sin \beta_1 = \frac{\epsilon\varphi}{\sqrt{1 + \varphi^2\epsilon^2}} \quad [31]$$

With these relations the wall-friction losses in the impeller can be determined. However, it must be considered that wall friction alone will be encountered only as long as the impeller blades are straight, i.e., when

$$\cos \beta_{b-2} = \frac{r_1}{r_2}\cos \beta_1 \quad [32]$$

When Equation [32] is not fulfilled, flow-deflection losses have to be considered which mainly depend on the deflection angle δ, i.e.

$$H_{\text{Deflection}} = \frac{\delta c^2}{\sqrt[4]{Re\ 2g}} \times \text{const} \quad [33]$$

where the magnitude of the constant depends on the impeller shape. With these relations the loss coefficient for the impeller can be represented by

$$q_I = \frac{\varphi^{1.75}(1 + K_I)^2}{8}\zeta_I \quad [34]$$

whereby $\zeta_I = \lambda L/D^*$ represents a loss factor of the impeller. This loss factor for compressor impellers can be expressed by the relation

$$\zeta_{I-C} = \frac{\epsilon^{1.25}\sqrt[1.6]{K_I z(1 + C_1 Ma^{*2}_c)^{2.5}}}{\sqrt[4]{Re^*_c}}[f(\varphi, \epsilon, \beta_{b-2}) + f(\delta, \epsilon)] \quad [35]$$

Equations [34] and [35] show that the friction losses of the impeller also can be represented by the characteristic values of the turbomachine, as Reynolds number Re^*, Mach number Ma^*, flow factor φ, diameter ratio ϵ, blade number z, and factor K_I. Fig. 20 shows the values of ζ_{I-C} as calculated for an impeller shape represented in Fig. 19, whereby it is assumed that the inlet blade angle β_1, is "shock-free," i.e.

$$\tan \beta_1 = \varphi\epsilon \quad [36]$$

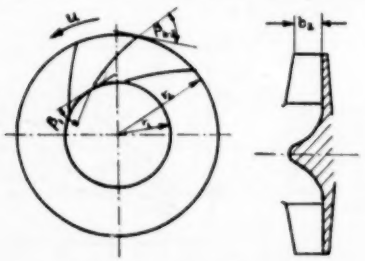

FIG. 19 NOTATIONS AT IMPELLER

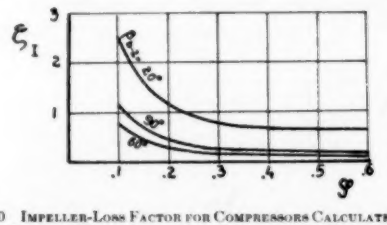

FIG. 20 IMPELLER-LOSS FACTOR FOR COMPRESSORS CALCULATED FOR $Re^* = 2 \times 10^5$, $Ma^* = 0$, $\epsilon = 1.6$, $K_I = 1$, $z = 18$, $\alpha_1 = 90$ DEG

and whereby for simplicity reasons the influence of the compressibility is neglected ($Ma^*_C = 0$).

For calculating the flow-friction losses in a turbine impeller Equation [34] can be used again. With the foregoing concept, for the factor ζ_{I-T}, a relation very similar to Equation [35] can be derived which is graphically represented in Fig. 21, for an im-

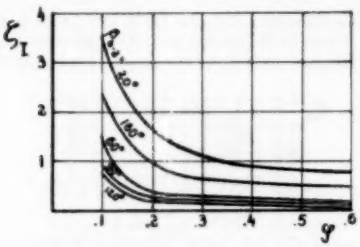

FIG. 21 IMPELLER-LOSS FACTOR FOR TURBINES CALCULATED FOR $Re^* = 2 \times 10^5$, $Ma^* = 0$, $\epsilon = 1.6$, $K_I = 1$, $z = 18$, $\alpha_3 = 90$ DEG

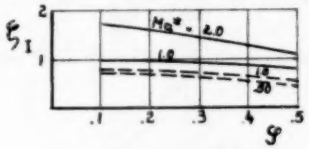

—— Compressor ---- Turbine

FIG. 22 IMPELLER-LOSS FACTOR CALCULATED FOR $Re^* = 2 \times 10^5$, $K_I = 1$, $z = 18$, $\beta_{5-3} = 90$ DEG

peller shape as shown in Fig. 19. For this figure it is assumed that the impeller exit angle is formed according to the relation

$$\tan \beta_{5-3} = \varphi\epsilon, \quad \ldots\ldots\ldots\ldots\ldots\ldots [37]$$

which yields a straight axial direction of the absolute exit velocity, allowing the smallest discharge losses.

For an impeller shape which is preferred when a high stress load (high peripheral speeds) is encountered, Fig. 10, the impeller loss factors, as calculated by a relation very similar to Equation [35] (1) are shown in Fig. 22. In this figure the factor for turbines shows lower values than the corresponding factor for compressors. This difference originates from the fact that in a compressor impeller the deflection in the inducer runner is connected with a retardation of the flow, resulting in greater deflection losses than for a deflection connected with accelerated flow as in the turbine exducer runner.

It may be noted that the relations regarding the losses in compressors are supported in some respect by test results. This may be demonstrated by Fig. 23 which represents some results of special tests performed in the DVL in 1943. Line 1 in Fig. 23 shows the pressure coefficient (related to the total pressures) of the impeller alone (i.e., $q_{th}-q_I$) as a function of the flow rate. Lines 2 and 3 represent the pressure coefficient of a compressor consisting of impeller and annular diffuser with different diameter ratios. Lines 4 and 5 represent the pressure coefficients of a com-

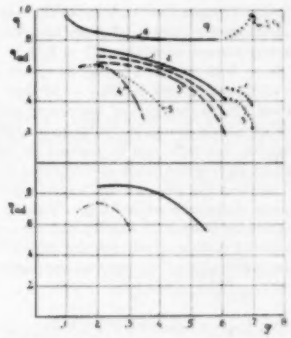

—— Impeller alone
- - - - Impeller with annular diffuser
..... and ——·——Impeller with small annular diffuser and scroll
xxxxxxxx Impeller with $\beta_1 = 90$ deg

FIG. 23 RESULTS OF SPECIAL TESTS WITH A COMPRESSOR: $Ma^* = 0.72$, $\epsilon = 1.74$, $Re^* = 2.2 \times 10^5$ (NOT CONST), $\beta_{5-3} = \alpha_1 = 90$ DEG

pressor, consisting of impeller, a small annular diffuser, and scrolls of different design points. Line 6 in Fig. 23 shows the work coefficient q as a function of the flow factor. These results show clearly that the impeller and the annular diffuser are comparatively insensitive to the volume flow and that mainly the design of the scroll determines the optimum volume flow of the compressor. The derived relationships show a good conformity with the foregoing test results (see also Fig. 12).

A variety of possibilities exists for deriving a relation which represents the nozzle losses in a turbine. If the nozzle design of the turbine is similar to the diffuser design (nozzle-type annular diffuser with adjoining scroll) of a compressor, the calculation principle is similar to the one outlined by deriving relations for the losses in the annular diffuser and the scroll (see Equations [22] and [23]). However, it must be kept in mind that the diffuser design is closely determined by the fact that the admissible pressure gradient per unit flow path is limited in order to avoid flow separation. Therefore the length of the flow path and consequently the losses in a diffuser depend on the rate of deceleration. The danger of flow separation does not exist by accelerating the flow. Therefore the length of the flow path in the nozzles is not determined by flow mechanics but rather by the nozzle construction so that it seems advisable to follow a different approach in deriving a relation for the nozzle losses.

It may be assumed that the nozzle channel is a square. Hence, the length of the flow path in the nozzles becomes $L = b_N(l + 0.5 \cot \alpha_3)$ when $l = l/b_N$ denotes the overlap of the nozzles with l describing the length of the overlapping section of the nozzle blades. By applying Equation [13] the head loss in the nozzle channel becomes $H = (l + 0.5 \cot \alpha_3)\lambda 0.5\, c_3^2 g^{-1}$. In the collector, the head loss becomes $H = 0.5c^3\, \lambda\, 0.5\pi g^{-1}(D/D^*)$. Hence the total loss caused by the nozzles (including collector) can be written in the form $H = \lambda 0.5 c_3^2 g^{-1}\,(l + 0.5 \cot \alpha_3 + 0.5 D\pi/D^*)$. The diameter D^* of the collector can be expressed as a function of the nozzle width, i.e., $D^* = \tau b_N$. Assuming $c_3^2/2$ as the mean velocity head in the nozzle and collector, the nozzle loss coefficient can be expressed by the relation

$$q_N = \left.\frac{\left(l + 0.5 \cot \alpha_3 + \dfrac{2\varepsilon^3 K_I \pi (b_3/b_N)}{\tau(1 - C_3 Ma^{*2}\tau^2)^{2.5}}\right) K_I \varphi^{1.75} \varepsilon^{0.5} (1 - C_3 Ma^{*2}\tau^2)^{0.5}\, 0.159}{\sqrt[4]{Re^*\tau}\, \sin \alpha_3^{1.75}\, \sqrt[4]{1+\tau}\, (1 - C_3 Ma^{*2}\tau^2)^{0.875} (1 - C_3 Ma^{*2}\tau^2)^{0.625} (b_N/b_3)^{2.25}}\right\} \quad \ldots [38]$$

whereby C_1, C_2, and C_3 again are functions of the degree of reaction, and the coefficients q_{ad} and q. For air and $\beta_{b-2} = 90$ deg, these values nearly become constants ($C_1 = 0.16 \div 0.18$, $C_2 = 0.14 \div 0.16$, $C_3 = 0.15 \div 0.17$). Fig. 24 shows a graphical representation of Equation [38] for $\beta_{b-2} = 90$ deg. The ratio b_N/b_2 in Equation [38] is the ratio of the nozzle width and impeller width. This ratio is recommended to be smaller than 1. A suitable relation for this ratio can be derived by the following argument: The jet leaving the nozzle and entering the free space between nozzle and impeller acts as a free jet and expands with an angle of divergence of approximately 7 deg. Therefore the width of the nozzle has to be smaller for exactly this amount when the total energy of the jet shall be effective in the impeller. With this concept and simple geometrical relations, an appropriate equation for the ratio can be written in the form

$$\frac{b_N}{b_2} = 1 - \frac{0.375\varepsilon^2(\mu' - 1)K_I}{\sin \alpha_2 \, (1 - C_3 Ma^{*2}_T)^{0.5}} \quad \ldots\ldots\ldots [39]$$

whereby $\mu' = D'/D$ with D' representing the inner diameter of the nozzle box. Equation [39] graphically is represented in Fig. 25

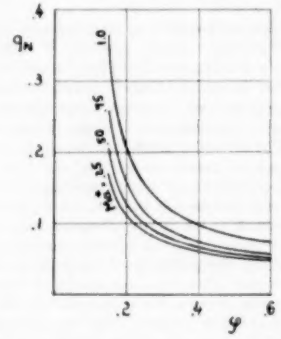

FIG. 24 NOZZLE-LOSS COEFFICIENT CALCULATED FOR $Re^* = 2 \times 10^6$, $\varepsilon = 1.6$, $\tau = 3$, $t = 1.5$, $\mu' = 1.02$, $K_I = 1$, $\beta_{b-2} = 90$ DEG

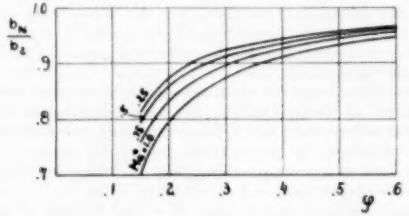

FIG. 25 RATIO OF IMPELLER WIDTH AND NOZZLE WIDTH, CALCULATED FOR $\mu' = 1.02$, $\beta_{b-2} = 90$ DEG

Another loss which has to be considered in turbomachines is the wheel-disk friction. This loss originates in the space between impeller and casing. The medium enclosed in this space rotates around the axis of the impeller owing to the drag exercised by the outer walls of the impeller, but only with a fraction of the impeller speed due to the friction at the stationary walls of the casing. Theoretical considerations show that these losses are proportional to the cube of the impeller-tip speed, proportional to the square of the impeller diameter, proportional to the mean specific weight of the enclosed medium, and proportional to a loss factor β_W which mainly depends upon the Reynolds number. Customarily, these losses are represented by referring to the horsepower lost therewith and are written in the form

$$P_W = u_2^3 D^2 \gamma_m \beta_W \text{ const} \quad \ldots\ldots\ldots [40]$$

whereby the constant in Equation [40] is 10^{-6} for the metric system [5]. Values for the loss factor β_W of a plain disk, as found by different investigators (6, 7, 8, 9) are presented in Fig. 26, whereby

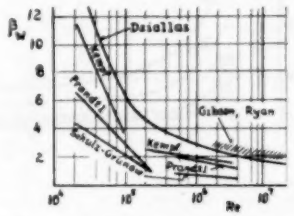

FIG. 26 DISK-FRICTION LOSS FACTOR β_W, AS FOUND BY DIFFERENT INVESTIGATORS

for the turbulent range the Prandtl relation can be written in the form

$$\beta_{W-Pr} = \frac{28.55}{\sqrt[5]{Re}} \quad \ldots\ldots\ldots [41]$$

Test results on radial compressors (10) indicated that for impellers of turbomachines the wheel-disk friction is greater than given by Equation [41], owing probably to a certain amount of reverse flow directed from the outer rim of the impeller to the axis, as caused by the higher pressure differences between outer rim and axis. The literature (10) indicates that $\beta_W = 3\beta_{W-Pr}$ for double-shrouded wheels, $\beta_W = 4\beta_{W-Pr}$ for half-shrouded wheels, and $\beta_W = 5\beta_{W-Pr}$ for unshrouded wheels can be regarded appropriate.

With Equations [40] and [41] the loss coefficient q_{W-C} representing the wheel-disk friction losses of a half-shrouded compressor wheel can be written in the form ($d_H = 0$)

$$q_{W-C} = \frac{0.0535\varepsilon^2(1 + \gamma_2/\gamma_1)}{\varphi \sqrt[5]{Re^*_C}} \quad \ldots\ldots\ldots [42]$$

The corresponding loss coefficient for turbines takes the form[7] ($d_H = 0$)

$$q_{W-T} = \frac{0.0535\varepsilon^2(1 + \gamma_2/\gamma_3)}{\varphi \sqrt[5]{Re^*_T}} \cdot \frac{(1 - 0.333 q_{ad} Ma^{*2}_T)^{0.4}}{(1 - 0.333 q_{ad} Ma^{*2}_T)^{0.7}} \quad [43]$$

Both relations are graphically presented in Fig. 27. Equations [42] and [43] show that these losses are proportional to the square of the diameter ratio and the reciprocal value of the flow factor, and that they increase with increasing Mach numbers.

A closer examination of the wheel-disk friction losses reveals that the losses depend also on the distance s, between impeller and casing. This may be demonstrated in a simplified consideration. As mentioned before, the medium enclosed in this space rotates with a fraction of the impeller speed, i.e., $u_{sl} = yu_2$. This peripheral speed has a twofold effect. Due to the centrifugal forces, a

[7] The difference between Equations [42] and [43] is caused by the different reference points of the Reynolds numbers Re^*_C and Re^*_T.

part of the medium (particles close to the impeller) flows from the axis to the outer rim whereas the other part (particles close to the casing) flows from the rim to the axis owing to the pressure difference created by the peripheral speed. Hence a relative eddy

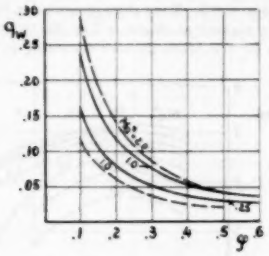

——— Turbine - - - - Compressor

FIG. 27 COEFFICIENT FOR WHEEL-DISK FRICTION LOSSES CALCULATED FOR $Re^* = 2 \times 10^5$, $\epsilon = 1.6$, $\beta_{b-2} = 90$ DEG

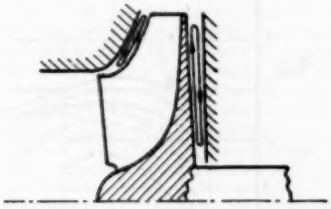

FIG. 28 RELATIVE EDDY BETWEEN IMPELLER AND CASING

originates in the space between impeller and casing, Fig. 28. The velocity of this relative eddy w_r is proportional to the pressure difference, i.e., $w_r = yu \times$ const, and the mass flow $W = D\,s\,y\,u\,\gamma_r \times$ const. Hence the power absorbed by the relative eddy is $P_r \approx W\,H = y^3\,u^3\,sD\,\gamma_r \times$ const, the head H being proportional to the square of the peripheral speed yu. Comparing the foregoing equation with Equation [40], it follows that

$$\frac{P_r}{P_W} = \frac{\gamma_r y^2 s}{\gamma_m \beta_W D} \text{ const} \quad \ldots\ldots [44]$$

In Equation [44] the factor y is a function of the distance s. Equation [41] is the relation for the minimum value of the loss factor β_W. Since the power absorbed by the relative eddy represents the wheel-disk friction, it follows from Equation [44] that β_W is a function of the ratio s/D, and that Equation [41] must be supplemented by a relation for the optimum value s_o/D. In the literature (7), values for s_o/D are given as function of the Reynolds number for the case that a plane disk is considered. For impellers of turbomachines, no definite relations for the optimum clearance have been found in the available literature. Some test results on compressors lead to the assumption that the optimum clearance is smaller than the optimum clearance for plane disks. These tests suggest the equation

$$\left(\frac{s_o}{D}\right)_C = \frac{(1 + 0.25 Ma^{*2}_C)}{(1 + 0.5 Ma^{*2}_C)} \frac{0.07}{\sqrt[5]{Re^*_C}} \quad \ldots\ldots [45]$$

for compressor wheels. The corresponding relation for turbine wheels takes the form[7]

$$\left(\frac{s_o}{D}\right)_T = \frac{(1 - 0.5\,Ma^{*2}_T)}{(1 - 0.25 Ma^{*2}_T)} \frac{0.07}{\sqrt[5]{Re^*_T}} \frac{(1 - 0.333 q_M Ma^{*2}_T)^{0.4}}{(1 - 0.333 q_{ad}\,Ma^{*2}_T)^{0.7}} \quad \ldots\ldots [46]$$

CHARACTERISTICS

(a) *Compressors.* The relationships derived in the previous section provide sufficient means to calculate some basic performance diagrams which yield valuable relations for the design of radial turbomachines. For this task the pressure coefficient

$$q_{ad-C} = q_{th} - q_I - q_{AD} - q_{se} - q_m \quad \ldots\ldots [47]$$

and the efficiency

$$\eta_{ad-C} = \frac{q_{ad-C}}{q_C} = \frac{q_{ad-C}}{q_{th} + q_W} \quad \ldots\ldots [48]$$

have been calculated for different conditions and are presented as function of the flow factor φ. Fig. 29 shows such a diagram as calculated for different blade-tip angles β_{b-2}, thus demonstrating the effect of β_{b-2} on pressure coefficient and efficiency. As it was to be expected from Equation [6] (see also Fig. 8), the pressure coefficient decreases with decreasing angles β_{b-2} and increasing flow factors. Optima efficiencies are to be expected for slightly backward-curved impeller blades, i.e., $\beta_{b-2} < 90$ deg.[8] This phenomenon can be explained by the fact that the degree of reaction increases with decreasing blade-tip angles. With increasing degree of reaction, an increasing part of the kinetic energy is transformed into pressure energy within the impeller. This process achieves a better efficiency in a rotating impeller than in a stationary diffuser because the boundary layer is always activated by the centrifugal forces and therefore grows at a slower rate than in a stationary diffuser. By exaggerating the backward curvature, i.e., by selecting very small tip angles β_{b-2}, the length of the impeller channels, and consequently the friction losses, increase considerably and finally compensate the beneficial effect of the centrifugal forces, so that the obtainable efficiency decreases again.

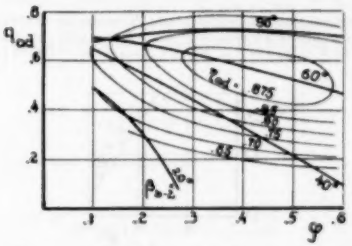

FIG. 29 CHARACTERISTIC COMPRESSOR VALUES, CALCULATED FOR $Re^* = 2 \times 10^5$, $Ma^* = 0$, $K_I = 1$, $z = 18$, $\epsilon = 1.6$, $\mu = 1.3$, $\alpha_{1C} = 90$ DEG
(No discharge losses assumed.)

Although an impeller with 90-deg blade-tip angle has slightly inferior efficiencies, this impeller type stresswise is superior when a design as shown in Fig. 10 is used and therefore allows higher peripheral speeds, i.e., higher pressure ratios. Before representing numerical values for this type, some limits due to the influence of the sound velocity may be discussed.

[8] It must be mentioned that the sharp drop in efficiency for $\beta_{b-2} = 20$ deg is true only for the assumed 18 blades. By taking fewer blades, the efficiency obtainable with $\beta_{b-2} = 20$ deg will be slightly higher.

As is well known, it is desired in many cases that no actual velocity exceed the value $0.9c_r$. A critical point is the relative inlet velocity w_1.[9] Its relation to the characteristic values of the compressor can be written in the form

$$\frac{w_1}{c_r} = Ma_{1\text{-}c} = Ma^*_c \sqrt{\frac{1}{\epsilon^2} + \varphi^2} \quad \ldots\ldots [49]$$

for shock-free inlet conditions, Fig. 30. This figure indicates that

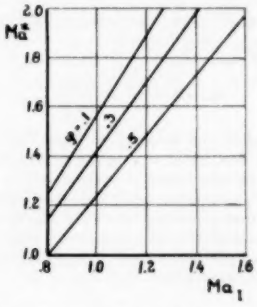

FIG. 30 RELATION BETWEEN MACH NUMBER AT INLET OF COMPRESSOR AND MACH NUMBER Ma^* OF COMPRESSOR, CALCULATED FOR $m = 1.25$, $\epsilon = 1.6$, $K_I = 1$, $\beta_{3\text{-}1} = \alpha_1 = 90$ DEG

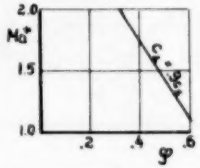

FIG. 31 LIMITS FOR APPLICATION OF PREROTATION AT COMPRESSOR INLET CALCULATED FOR $Ma^* = 0.9$, $\epsilon = 1.6$

the Mach number of the compressor may exceed the value $Ma^*_C = 1$; however, it should not exceed the value $Ma^*_C = 1.3$ (for $\varphi = 0.3$) when w_1 shall remain within the desired limits. By imparting prerotation of a positive direction to the flow at the impeller inlet ($\alpha_1 > 90$ deg), it is possible considerably to extend these limits, because by this means the velocity w_1 decreases. At the same time, however, the velocity c_1 increases, so that $c_1 = 0.9\,c_r$ represents the limit for the application of prerotation, Fig. 31. As a consequence of the prerotation, the theoretically obtainable work decreases with the degree of prerotation (see Equation [6]), so that it seems to be favorable to apply prerotation only on those points of the impeller where the velocity w_1 would exceed the critical value, i.e., one will apply prerotation first at the outer diameter of the inlet down to that point where no prerotation is necessary.[10]

By using the relations derived previously, and by considering the restrictions just indicated, the basic performance diagram of radial compressors, having impeller blade-tip angles of 90 deg, assumes the form as presented in Fig. 32. This figure shows that the pressure coefficient drops only a little with increasing flow factors and that optima efficiencies are to be expected for flow factors close to $\varphi = 0.3$. The values presented in Fig. 32 also can be plotted in a manner as shown in Fig. 33, by substituting the pressure ratio for the Mach number according to Equation [8].

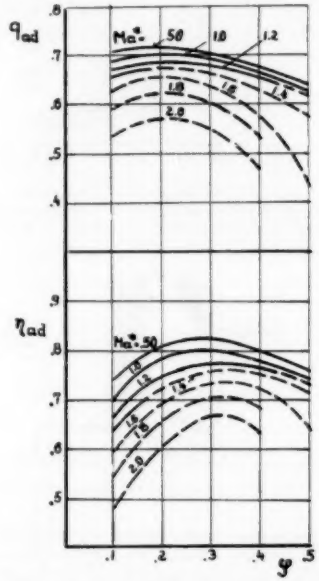

FIG. 32 CHARACTERISTIC VALUES OF COMPRESSORS WITH $\beta_{3\text{-}1} = 90$ DEG, CALCULATED FOR $Re^* = 2 \times 10^6$, $\epsilon = 1.6$, $m = 1.25$, $K_I = 1$, $\mu = 1.3$
(No discharge losses assumed.)

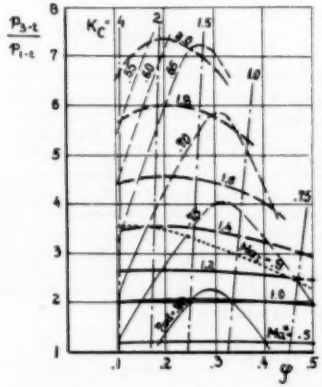

FIG. 33 RELATIONS FOR DESIGN OF COMPRESSOR WITH $\beta_{3\text{-}1} = 90$ DEG, CALCULATED FOR $Re^* = 2 \times 10^6$, $K_I = 1$, $\epsilon = 1.6$, $m = 1.25$ $\mu = 1.3$, $\varkappa = 1.4$

[9] It must be mentioned that the impeller-discharge velocity c_2 also approaches sound velocity at high values of Ma^*. However, by providing an annular diffuser without guide vanes directly behind the impeller, the influence of the sound velocity probably will be unimportant.

[10] With this arrangement the inlet momentum becomes nonuniform, so that the change of impulse within the rotor is different for different flow lines. For the calculations a mean state is assumed without accounting for a mutual interference of the flow lines.

Fig. 33 shows additionally the characteristic value K_C and indicates that this value decreases with increasing flow factors. The value K_C is of special importance when the static discharge pressure p_{3-s} is considered instead of the total discharge pressure p_{3-t} indicated in the diagram. These two discharge pressures differ for the amount of the pressure head $H_d = c_{3-s}^2/2g$, which in a dimensionless form also can be represented by a corresponding loss coefficient

$$q_d = \frac{H_d}{u_2^2/g} = 0.5 K_C^2 \varphi^2 \quad \ldots\ldots [50]$$

Consequently, in cases where the static discharge pressure is considered, the pressure coefficient becomes for the amount of q_d smaller than indicated. The corresponding compressor efficiency is

$$\eta_{ad-s} = \frac{q_{ad} - q_d}{q} = \eta_{ad}\left(1 - \frac{q_d}{q_{ad}}\right) \quad \ldots\ldots [51]$$

It will be noted that in Figs. 32 and 33 the lines are partly solid and partly dashed. The dashed part of the lines indicate the range where prerotation is applied.

Figs. 32 and 33 at the same time represent in a very rough and optimistic form the characteristic of a compressor with adjustable guide vanes. Actual tests, Fig. 34,[11] showed that the range of flow factors (range of volume flow at constant speed) where the efficiency is constant, is about 60 to 70 per cent of the range indicated in Figs. 32 and 33. This difference originates from the fact that by calculating Figs. 32 and 33 no shock losses at the inducer and in the collector (scroll) had to be assumed, which, however, occur when the characteristic of a particular compressor is concerned.

It might be mentioned that the concept presented in this paper also can be adapted for calculating the characteristic of a particular compressor. Thereby it has to be considered that the dimensions of the turbomachine are now fixed by the design, i.e., by using, for example, Fig. 32 or 33. That means that the impeller width b_2 (Equation [15]), the inducer angle β_1 (Equation [36], and the scroll diameter d_4 (Equation [26]) are now constant and not variable as it was supposed by deriving some of the equations for the loss coefficients (Equations [22], [23], [35]). Hence these equations have to be modified slightly and must be presented in the form

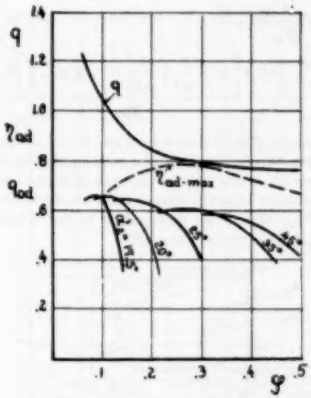

FIG. 34 TEST RESULTS OF COMPRESSOR WITH ADJUSTABLE GUIDE VANES (DVL) $Ma^* = 0.6$, $\varkappa = 1.54$, $z = 8$, $Re^* = 10^5$ (NOT CONST), α_3' = NOZZLE POSITION, NOT EQUAL TO FLOW ANGLE α_3

ducer blades and oblique attack of the tongue of the scroll. These losses can be calculated by well-known methods (11), and can be presented in the form of dimensionless loss coefficients such as

$$q_{sh-I} = \frac{\chi}{2\varepsilon_s \varkappa (1 - Ma_I^2)} \left(\frac{\varphi_n}{\varphi_o} - 1\right)^2 \quad \ldots\ldots [55]$$

for the shock loss at the inducer and

$$q_{sh-sc} = \frac{\chi}{m^2 2\mu^2 \varkappa (1 - Ma_{sc}^2)} \left(\frac{K_{I-n}\varphi_n}{K_{I-o}\varphi_o} - 1\right)^2 \quad \ldots\ldots [56]$$

for the shock loss at the tongue of the scroll. The factor χ in Equations [55] and [56] denotes a shock coefficient, the magnitude of which is 1 for an infinite number of inducer blades and about 0.5 for a sharp tongue. With decreasing number of inducer blades and decreasing sharpness of the scroll tongue, the value of the shock coefficient decreases. For calculating the change of the factor K_I it holds the equation

$$K_{I-C} = \frac{A_1}{A_2}\frac{\gamma_1}{\gamma_2} \quad \ldots\ldots [57]$$

The change of density in Equation [57] can be determined by using Equations [8] and [10] whereby, however, the factors q_{ad} and q have to be replaced by ρq_{ad} and ρq, and whereby in each case the proper values of ρ, q_{ad}, and q have to be used, ρ denoting the degree of reaction

$$q_{AD-n} = q_{AD-o} \frac{K_{I-n}^2 \varphi_n^{1.75}\left[1 + \frac{1}{m^2}\left(\frac{1}{\varphi_n K_{I-n}} - \cot\beta_{1-2}\right)^2\right]^{1.75} \sqrt[4]{Re^*_n}}{K_{I-o}^2 \varphi_o^{1.75}\left[1 + \frac{1}{m^2}\left(\frac{1}{\varphi_o K_{I-o}} - \cot\beta_{1-2}\right)^2\right]^{1.75} \sqrt[4]{Re^*_o}} \quad \ldots\ldots [52]$$

$$q_{sc-n} = q_{sc-o} \frac{\left[1 + \frac{1}{m^2}\left(\frac{1}{\varphi_n K_{I-n}} - \cot\beta_{1-2}\right)^2\right]\left(\frac{1}{\varphi_n K_{I-n}} - \cot\beta_{1-2}\right)^2 \sqrt[4]{Re^*_n}}{\left[1 + \frac{1}{m^2}\left(\frac{1}{\varphi_o K_{I-o}} - \cot\beta_{1-2}\right)^2\right]\left(\frac{1}{\varphi_o K_{I-o}} - \cot\beta_{1-2}\right)^2 \sqrt[4]{Re^*_o}} \quad \ldots\ldots [53]$$

$$q_{I-n} = q_{I-o} \frac{\varphi_n^{1.75}(1 + K_{I-n})^2 \sqrt[4]{Re^*_o}}{\varphi_o^{1.75}(1 + K_{I-o})^2 \sqrt[4]{Re^*_n}} \quad \ldots\ldots [54]$$

whereby index o denotes the design point, and index n any point besides the design point. Additionally, shock losses (sometimes referred to as impulse losses) occur by oblique attack of the in-

[11] These results cannot claim to represent optimal values because the arrangement of the guide vanes was very unfavorable (straight vanes with turning point in the middle of the guide vanes).

$$\rho = \frac{H_{ad} - c_3^2/2g - H_l}{H_{ad}} = 1 - \frac{\varphi^2 K_I^2 \left[1 + \frac{1}{m^2}\left(\frac{1}{\varphi K_I} - \cot \beta_{b-2}\right)^2\right] - 2q_l}{2q_{ad}} \quad [58]$$

As an example, Fig. 35 shows some calculated values for K_I and indicates that this factor decreases with increasing Mach numbers. Generally, it can be said that the characteristic of a particular compressor is much steeper than the basic characteristic shown in Figs. 32 and 33, due mainly to the shock losses, especially the shock losses at the scroll.

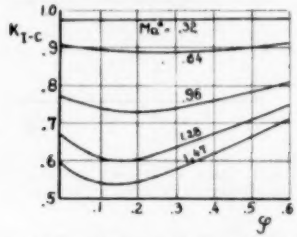

FIG. 35 FACTOR K_{I-C} AS FUNCTION OF FLOW FACTOR, CALCULATED FOR $m = 1.25$, $\epsilon = 1.6$, $A_1/A_2 = 1$, $\beta_{b-2} = \alpha_1 = 90$ DEG

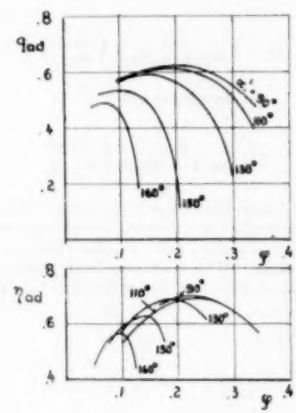

FIG. 36 TEST RESULTS ON COMPRESSOR WITH VARIABLE GUIDE VANES BEFORE IMPELLER
($Ma^* = 1.12$, $\epsilon = 1.68$, $z = 16$, $Re^* = 3.5 \times 10^5$, not constant.)

In some cases prerotation of the flow at the inlet of the impeller is used for controlling purposes by providing adjustable guide vanes before the compressor wheel (12). The effect of prerotation is similar to the effect produced by a change in blade-tip angle β_{b-2} (see Fig. 8). The pressure coefficient q_{ad} is changed without considerable drop in efficiency. Fig. 36 shows actual test results (13). The change of the pressure coefficient originates mainly from the change of the theoretical work coefficient q_{th} (Equation [6]). This controlling device is applied when the pressure ratio of the compressor shall be varied at constant impeller speed and when at the same time the efficiency drop shall be kept as low as possible (12).

(b) Turbine. In order to show some basic relations for turbines, a procedure similar to the one employed in the preceding section can be applied. The pressure coefficient can be calculated by

$$q_{ad-T} = q_{th} + q_l + q_N \quad [59]$$

and the efficiency by

$$\eta_{ad-T} = \frac{q_{th} - q_N}{q_{ad-T}} \quad [60]$$

Introducing Equations [3], [34], [38], and [43] into Equations [59] and [60], the dependency of the pressure coefficient and efficiency on the characteristic turbine values φ, β_{b-2}, Re^*, and Ma^* can be calculated. This procedure results in a multitude of curves from which only very few are significant. Obviously, it is sufficient to select values which promise optima efficiencies for different possible combinations. Optima efficiencies are to be expected at points where no shock losses occur at the impeller inlet, and when at the same time the absolute exit velocity c_3 of the impeller is straight axially. That means that in Fig. 4 the relative flow angle β_2 must be equal to the blade-tip angle β_{b-2}, i.e.

$$\cot \beta_{b-2} = \cot \alpha_2 - \frac{1}{K_I \varphi} \quad [61]$$

Furthermore, the absolute flow angle α_3 in Fig. 4 must be 90 deg, i.e.

$$\cot \beta_3 = \frac{1}{\varphi \epsilon_s} \quad [62]$$

Introducing Equations [61] and [62] into Equation [3], the following theoretical work coefficient results

$$q_{th-T} = 1 + \varphi K_I \cot \beta_{b-2} \quad [63]$$

By using Equations [59], [60], and [63], the pressure coefficient and efficiency have been calculated for different blade angles β_{b-2}. These values are presented in Figs. 37 and 38 as functions of the flow factor. The difference between these diagrams is that in Fig. 38 additionally the exit velocity c_3 is considered lost, i.e., pressure coefficient and efficiency are related to the static exit pressure p_{3-st}. That means that Equation [59] takes the form $q_{ad-T} = q_{th} + q_l + q_N + q_d$ whereby q_d denotes the discharge loss coefficient

$$q_d = \frac{1}{2}\left[\varphi^2 + \left(\varphi \frac{\cot \beta_{b-2}}{m} - \frac{1}{m \epsilon_s}\right)^2\right] \quad [64]$$

as derived from the velocity triangle, Fig. 4. For $\alpha_3 = 90$ deg (straight axial exit velocity), Equation [64] becomes $q_d = 0.5\varphi^2$. Figs. 37 and 38 show that the radial inward-flow turbine with an impeller shape as shown in Fig. 19, has its highest efficiencies with blade angles β_{b-2} of 60 deg to 100 deg.[13] That means that a blade-tip angle of 90 deg yields efficiencies very close to the maximum obtainable efficiency. When, with this blade-tip angle, an impeller shape as shown in Fig. 10, is used, considerably higher peripheral speeds and consequently the expansion of greater heads can be handled. This type will be investigated in more detail in the following.

For $\beta_{b-2} = 90$ deg, it results from Equation [63] that $q_{th} = 1$ for optima efficiencies. This is a good approximation which,

[13] It must be noted that the sharp drop in efficiency at $\beta_{b-2} = 160$ deg is true only for the assumed blade number $z = 18$. The optimum blade number for $\beta_{b-2} = 160$ deg is smaller than 18, so that for $\beta_{b-2} = 160$ deg and $z < 18$, slightly higher efficiencies are to be expected.

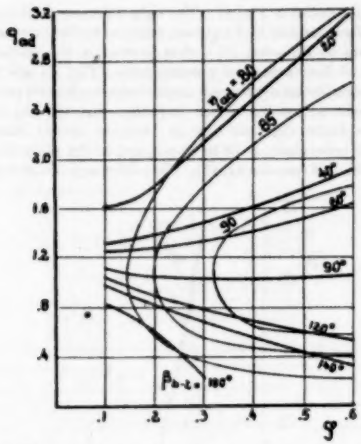

FIG. 37 CHARACTERISTIC TURBINE VALUES, CALCULATED FOR $Re^* = 2 \times 10^6$, $Ma^* = 0$, $K_I = 1$, $z = 18$, $\epsilon = 1.6$, $\tau = 3$, $i = 1.5$ $\mu' = 1.02$
(No discharge losses assumed.)

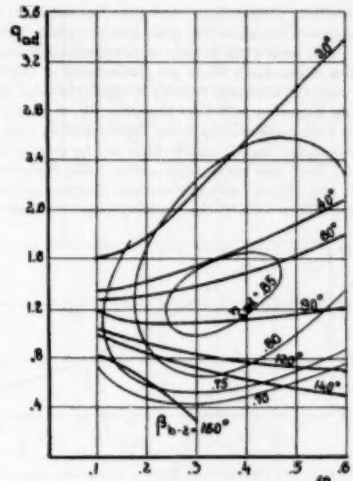

FIG. 38 CHARACTERISTIC TURBINE VALUES CALCULATED FOR $Re^* = 2 \times 10^6$, $Ma^* = 0$, $K_I = 1$, $z = 18$, $\epsilon = 1.6$, $\tau = 3$, $i = 1.5$, $\mu' = 1.02$
(Discharge losses included.)

however, cannot always be correct since the assumption which led to Equation [63] is an approximation only. In order to determine the exact design conditions, Equations [61], [62], and [63] must be disregarded, and Equation [59] must be written in the form

$$q_{ad-\tau} = q_{sh} + q_I + q_N + q_d + q_{ch} \quad \ldots\ldots [65]$$

The factor q_{sh} denotes a coefficient for the shock losses at the impeller inlet which, according to well-known relation for shock-losses (11) can be expressed by

$$q_{sh} = \frac{\chi}{2\beta^{*2}} (K_I \varphi \cot \alpha_2 - 1)^2 \quad \ldots\ldots [66]$$

With Equation [65] the relation for the efficiency can be written in the form

$$\eta_{ad-\tau} = \frac{q_{sh} - q_W}{q_{ad-\tau}} = 1 - \frac{q_W + q_I + q_N + q_d + q_{ch}}{q_{sh} + q_I + q_N + q_d + q_{ch}} \quad [67]$$

The efficiency becomes a maximum where the quotient in Equation [67] becomes a minimum. Hence, by differentiating the quotient in Equation [67] in terms of φ, an equation for the optimum φ-value results. Unfortunately, by introducing in the foregoing quotient the original equations (Equations [3], [34], [38], [43], [64], [66]) for the loss and work coefficients, a very complex equation of high degree results which cannot be solved for φ. In order to simplify the problem, the nozzle-loss coefficient q_N may be regarded constant by choosing τ and φ-values correspondingly. With this assumption the differentiation yields an equation of the fourth degree which can be solved by the approximation

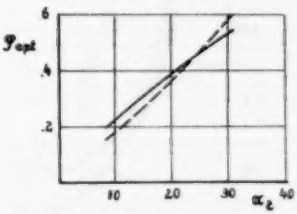

FIG. 39 OPTIMUM FLOW FACTOR FOR TURBINES AS FUNCTION OF FLOW ANGLE α_2
According to Equation [61]—, and according to Equation [68] ——.)

It is of general interest to compare the φ_{opt} values, resulting from Equation [68] with the φ_{opt} values resulting from Equation [61] ($\varphi_{opt} = \tan \alpha_2 K_I^{-1}$ for $\beta_{b-2} = 90$ deg), in order to show the difference between the more exact solution and the first simplifying assumption. This comparison is carried through with the simplifying assumption that

$$\tan \beta_2 = \tan \alpha_2 \frac{\epsilon_z}{K_I} \quad \ldots\ldots [69]$$

Equation [69] results by equalizing Equations [61] and [62] after both have been solved for φ. Fig. 39 shows both φ_{opt} values as function of the angle α_2, and indicates that only for $\alpha_2 = 24$ deg both values are equal. For smaller α_2-values the more exact Equa-

$$\varphi_{opt}^2 = \frac{\left(\frac{\chi}{2\beta^{*2}} + \frac{1}{2m^2\epsilon_z^2} + 0.1\right)\left(1 + \sqrt{1 + \frac{0.4\left(\frac{\chi K_I^2 \cot^2 \alpha_2}{2\beta^{*2}} + \frac{1}{2} + \frac{\cot^2 \beta_2}{2m^2} + \zeta_I\right)}{\left(K_I \cot \alpha_2 + \frac{\cot \beta_2}{\epsilon_z m}\right)\left(\frac{\chi}{2\beta^{*2}} + \frac{1}{2m^2\epsilon_z^2} + 0.1\right)^2}}\right)}{2\left(\frac{\chi K_I^2 \cot^2 \alpha_2}{2\beta^{*2}} + \frac{1}{2} + \frac{\cot^2 \beta_2}{2m^2} + \zeta_I\right)} \quad \ldots [68]$$

tion [68] results in greater φ_{opt} values than Equation [61] and, for greater α_2-values, Equation [68] gives smaller values than Equation [61]. This means that in most cases optimum efficiency is obtained when slight shock losses are encountered at the impeller inlet and when the discharge velocity is slightly of axial direction. Introducing Equation [68] into Equation [3], it results in the theoretical work coefficient q_{th} being slightly greater than one for small φ-values and slightly smaller than one for greater values of φ, Fig. 40. With this relationship and by using Equations [34], [38], [39], and [43], a basic performance diagram for radial inward-flow turbines with 90-deg blade-tip angle is calculated and

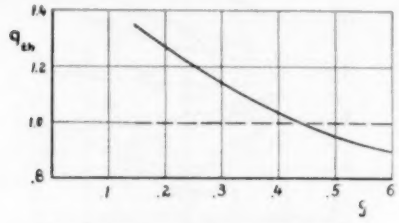

FIG. 40 OPTIMUM q_{th} VALUE FOR TURBINES
(According to Equation [61] ---, and according to Equation [68] ——)

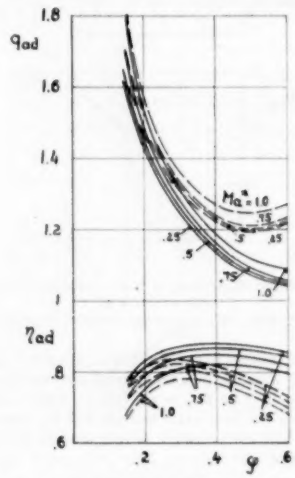

FIG. 41 CHARACTERISTIC VALUES OF TURBINES WITH $\beta_{b-2} = 90$ DEG, CALCULATED FOR $Re^* = 2 \times 10^5$, $K_I = 1$, $\epsilon = 1.6$, $m = 1.25$, $\tau = 3$, $l = 1.5$, $\mu' = 1.02$
(—— Discharge losses included.)

presented in Fig. 41.[12] This diagram gives valuable information for the design and shows that only for a limited range of the flow factor high efficiencies can be expected when discharge losses have to be considered. Fig. 42[13] shows basically the same relations as already presented in Fig. 41. The only difference is that in Fig. 42 the Mach number Ma^* has been replaced by the pressure ratio (according to Equation [9]), thus presenting the efficiency as function of flow factor and pressure ratio. Figs. 41 and 42 also can be regarded as very rough and optimistic characteristics of a turbine with adjustable vanes. In reality, Fig. 43,[13] the range of the flow factor (volume flow at constant speed) where the efficiency is constant, is 70 to 80 per cent of the range shown in Figs. 41 and 42 (see also 14, 15). This difference can be explained

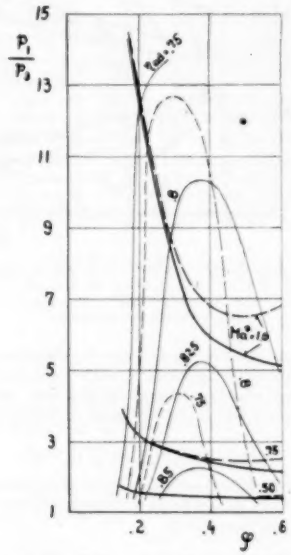

FIG. 42 RELATIONS FOR DESIGN OF TURBINES WITH $\beta_{b-2} = 90$ DEG, CALCULATED FOR $Re^* = 2 \times 10^5$, $K_I = 1$, $\epsilon = 1.6$, $m = 1.25$, $\tau = 3$, $l = 1.5$, $\mu' = 1.02$, $\kappa = 1.4$
(Discharge losses included ---.)

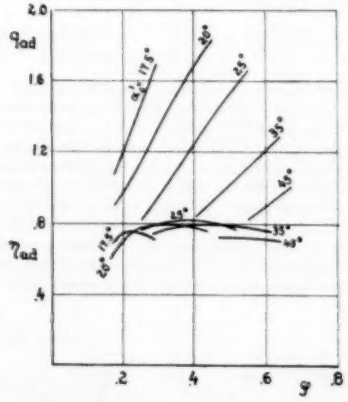

FIG. 43 TEST RESULTS OF A TURBINE WITH ADJUSTABLE GUIDE VANES (DVL) $Ma^* = 1.6$, $\epsilon = 1.54$, $z = 8$, $^1Re^* = 6.4 \times 10^5$ (NOT CONSTANT) α'_2 = NOZZLE POSITION, NOT EQUAL TO FLOW ANGLE α_2

[12] This diagram shows a considerable drop of the efficiency at small flow factors. This results from the assumption of a constant value for τ as justified for some turbine designs with adjustable guide vanes covering a wide range of φ. If fixed guide vanes are considered the factor τ can increase with decreasing flow factors, so that for small values of φ better efficiencies will result than are represented in this diagram.

by the fact that in calculating Figs. 41 and 43, the direction of the discharge velocity has been chosen in such a manner as to obtain maximum efficiency for every flow factor. This cannot be achieved when a particular impeller is considered.

The derived equations can also be used for calculating the characteristic of a particular turbine. Hence it must be considered that now the dimensions of the turbine are fixed and not variable as assumed when deriving some equations for the loss coefficients. Therefore these equations have to be presented in a different manner and take the form

$$q_{I-n} = q_{I-o} \frac{\varphi_n^{1.75}(1 + K_{I-n})^2 \sqrt[4]{Re^*_o}}{\varphi_o^{1.75}(1 + K_{I-o})^2 \sqrt[4]{Re^*_n}} \quad \ldots\ldots [70]$$

$$q_{N-n} = q_{N-o} \frac{\varphi_n^{1.75} K_{I-n}^{1.75} \sqrt[4]{Re^*_o}}{\varphi_o^{1.75} K_{I-o}^{1.75} \sqrt[4]{Re^*_n}} \quad \ldots\ldots [71]$$

in which index o denotes the design point, and index n any point besides the design point. For the theoretical work the original Equation [3] has to be used, and shock losses at the impeller inlet (Equation [66]) have to be considered. Particular attention has to be paid to the influence of the factor K_I which changes according to the relation

$$K_{I-T} = \frac{A_3 \gamma_3}{A_2 \gamma_2} \quad \ldots\ldots [72]$$

The area ratio in Equation [72] is determined by the chosen design. The density ratio in Equation [72] can be calculated by using Equations [9] and [11] whereby, however, the factor q_{ad} and q have to be replaced by ρq_{ad} and ρq, and whereby in each case the proper values for q_{ad} and q have to be used, ρ denoting the degree of reaction

$$\rho = \frac{H_{ad} - H_N - c_2^2/2g}{H_{ad}} = 1 - \frac{\left(\frac{b_2}{b_N}\right)^2 \varphi^2 K_I^2 \sin \alpha_2^{-2} - 2q_N}{2q_{ad}} \quad \ldots\ldots [73]$$

Fig. 44 shows as an example the factor K_I as a function of the flow factor and Mach number. This figure indicates that K_I decreases considerably with increasing flow factors. Consequently, the theoretical work coefficient is not a linear function of the flow factor any more (see Equation [3]), but becomes a function of higher degree as shown in Fig. 45. This figure at the same time represents the calculated characteristic of a radial turbine. Comparison between a calculated characteristic and test points is shown in Fig. 46 which demonstrates that the method presented yields fairly accurate values (16).

The absolute velocity c_2 at the nozzle end can be expressed in terms of the sound velocity

$$\frac{c_2}{c_s} = Ma_{II-T} = Ma^*_T \frac{\varphi K_I b_2}{\sin \alpha_2 b_N} \quad \ldots\ldots [74]$$

This relation is graphically shown in Fig. 47. It must be mentioned that $Ma_{II-T} = 1$ does not represent a definite limit. It merely indicates the point where sound velocity exists at the end of the nozzle, and special attention has to be paid to the nozzle design, because for $Ma_{II-T} > 1$ the flow after expands behind the nozzle and changes its direction.

Design Charts

In the foregoing considerations it has been shown that only for a limited range of flow factors maximum efficiencies can be expected, and that for compressors as well as for turbines the value $\varphi = 0.3$ is about the center point of this range. In the following,

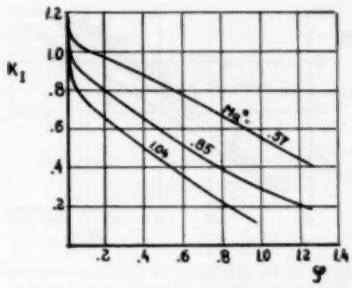

Fig. 44 Factor K_{I-T} as Function of Flow Factor, Calculated for $\alpha_2 = 18$ Deg, $\beta_{b-2} = 90$ Deg, $m = 1.25$, $A_3/A_2 = 1.18$

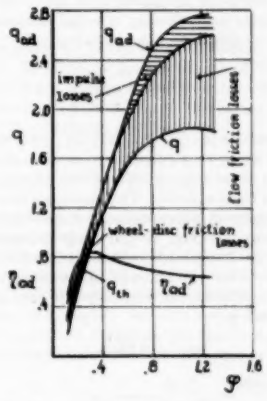

Fig. 45 Calculated Turbine Characteristic

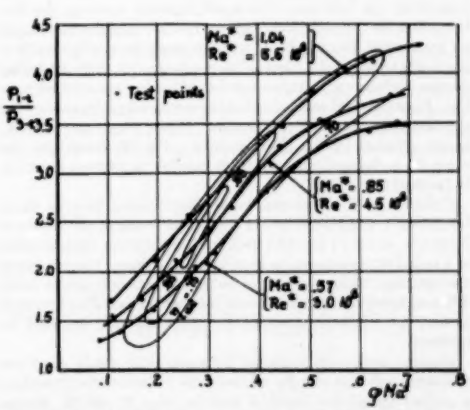

Fig. 46 Comparison Between Calculated Turbine Characteristic and Test Points
($\alpha_2 = 18$ deg, $m = 1.25$, $A_3/A_2 = 1.18$, $\beta_{b-2} = 90$ deg, $\kappa = 1.4$.)

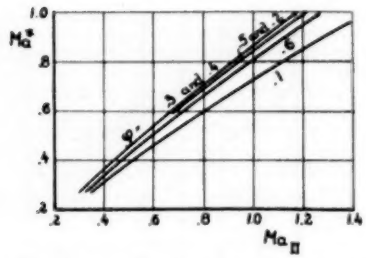

FIG. 47 RATIO OF MACH NUMBER AT EXIT OF NOZZLES AND MACH NUMBER Ma^* OF TURBINE, CALCULATED FOR $K_I = 1$, $\mu' = 1.02$, $\beta_{0-1} = 90$ DEG

for this value some more detailed considerations are presented.

Of special interest is the influence of the blade number z on pressure coefficient and efficiency of radial compressors. By introducing for the slip factor the approximation[14]

$$m = 1 + \frac{6.2}{z\sqrt{\epsilon}} \quad \ldots\ldots\ldots\ldots\ldots\ldots [75]$$

and using Equations [6], [22], [23], [27], [34], [35], [36], [42], Fig. 48 can be plotted which shows that the pressure coefficient increases with increasing blade number whereas the efficiency has a maximum at certain blade numbers. This maximum is very flat so that an optimum number of blades cannot be stated, but merely a range of blade numbers. In Fig. 49 this range is represented by its median value z_m. It must be emphasized that the blade number can be made $z = (0.9 \div 1.1)z_m$ without any change in efficiency. The pressure coefficient, however, depends very closely on the blade number and is

$$q_{ad} = 0.94 q_{ad-z_m} \quad \ldots\ldots\ldots\ldots\ldots\ldots [76]$$

for $z = 0.9\, z_m$ and

$$q_{ad} = 1.03 q_{ad-z_m} \quad \ldots\ldots\ldots\ldots\ldots\ldots [77]$$

for $z = 1.1 z_m$. The tendency of the optimum blade number is explained by the fact that with small Reynolds number the friction losses are comparatively high so that the friction surface must be kept small, i.e., the blade number must be small. For high Reynolds numbers the friction losses are smaller, so that a higher friction surface, i.e., a higher number of blades, becomes admissible. Equation [26] indicates that the scroll design depends on the slip factor, i.e., on the blade number. Consequently the value K_C is also affected by the blade number. Fig. 50 shows how the value K_C is changed when the blade number is different from $z = 18$ (as used in Fig. 33).

Unfortunately, no relation for the dependency between shock coefficient χ and blade number z has been found in the available literature, so that a consideration for the optimum blade number of a radial turbine has to be kept for a later time. Very probably the optimum blade number for radial turbines will not be much different from the optimum blade number for radial compressors so that the relations presented in Fig. 49 also may be used for turbines.

General design diagrams for turbomachines result when the pressure coefficient and the efficiency for different Mach numbers is plotted against the Reynolds number, Figs. 51 and 52. Such a diagram has general validity for all gases with κ-values from 1.2

[14] For more exact relations see (2, 3).

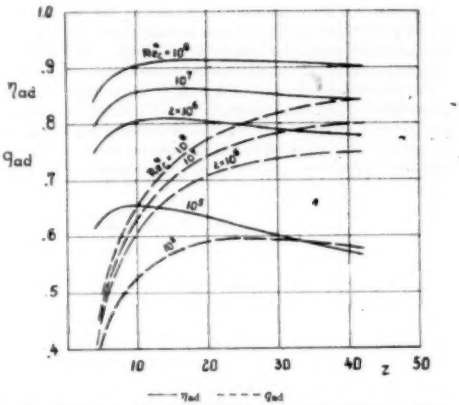

FIG. 48 PRESSURE COEFFICIENT q_{ad} AND EFFICIENCY OF COMPRESSORS AS FUNCTION OF BLADE NUMBER z, CALCULATED FOR $Ma^* = 1$, $\epsilon = 1.6$, $K_I = 1$, $\mu = 1.3$, $\varphi = 0.3$.
(No discharge losses assumed.)

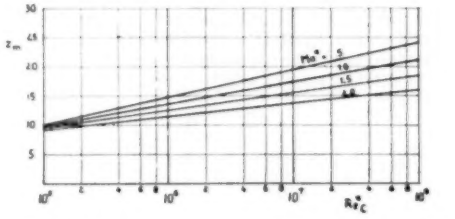

FIG. 49 MEDIAN VALUE OF OPTIMUM BLADE NUMBER FOR COMPRESSORS, CALCULATED FOR $\epsilon = 1.6$, $\mu = 1.3$, $K_I = 1$, $\varphi = 0.3$.

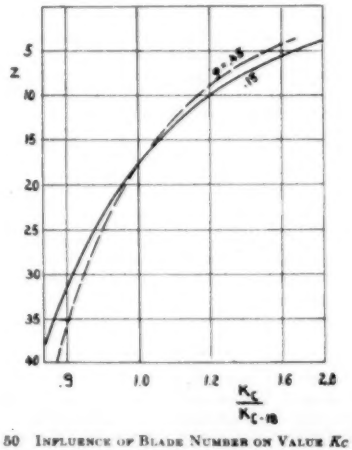

FIG. 50 INFLUENCE OF BLADE NUMBER ON VALUE K_C

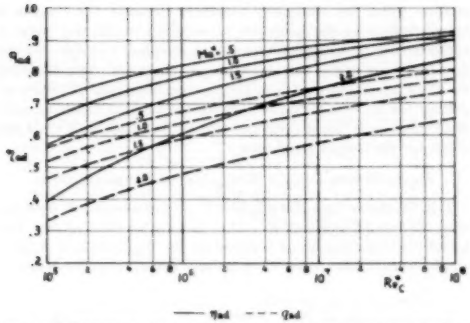

—— η_{ad} - - - q_{ad}

FIG. 51 PRESSURE COEFFICIENT q_{ad} AND EFFICIENCY OF COMPRESSORS AS FUNCTION OF THE REYNOLDS NUMBER Re^* FOR $\varphi = 0.3$, $\epsilon = 1.6$
(No discharge losses assumed.)

to 1.5,[15] and with viscosity values which follow Equation [12]. The procedure by which this diagram may be used is a trial-and-error method.

Compressors. Given values: Compression ratio p_2/p_1, weight flow W, inlet temperature T_1, and inlet pressure p_1. By first assuming a pressure coefficient q_{ad}, the Mach number Ma^* is calculated by using Equation [8]. With the same value of q_{ad}, the peripheral speed is calculated by the relation $u_2 = \sqrt{gH_{ad}q_{ad}}$, H_{ad} denoting the pressure head corresponding to p_2/p_1 and T_1. The inlet velocity is found by $c_{m-1} = \varphi u_2$, and the inlet area by $A_1 = V_1/c_{m-1}$, V_1 denoting the inlet volume with

$$V_1 = \frac{WT_1R}{p_1\ 144}$$

with R as gas constant. The inlet diameter is $d = \sqrt{4A_1/\pi}$,[16] and the outer diameter becomes $D = d\epsilon$. With Equation [12] the dynamic viscosity is determined and the Reynolds number $Re^* = Du_2/\nu_1$. For this Reynolds number and the initially calculated Mach number Ma^*, the pressure coefficient q_{ad} has to be read from Fig. 51 and compared with the first assumed value of q_{ad}.

This procedure has to be repeated until both q_{ad} values are equal. From Fig. 51 the efficiency also is found. By using Fig. 51, the influence of the blade number, as indicated by Equations [76] and [77] has to be taken into account. From Equations [15] and [26] the width b_2 of the impeller and the diameter d_3 of the scroll are found. The diameter of the annular diffuser is $D_z = \mu D$ and the angle β_1 of the impeller results from Equation [36]. The optimum clearance s_o between impeller and casing is calculated by Equation [45]. For cases where this clearance must be greater for constructional reasons it follows from Equations [44] and [45] that a drop in efficiency has to be expected which amounts to approximately

$$\frac{\eta}{\eta_o} = \frac{1 + \dfrac{2(1 + 0.5\ Ma^{*2})s_o/D}{\varphi/\epsilon^3}}{1 + \dfrac{2(1 + 0.5Ma^{*2})s/D}{\varphi/\epsilon^3}} \quad \ldots\ldots [78]$$

Turbines. When for the turbine the same values are given as listed for compressors, the procedure is essentially the same as described for compressors. The following differences, however, must be considered. Equation [9] applies instead of Equation [8] for calculating the Mach number. The discharge velocity c_{m-2} and area A_2 are calculated instead of inlet velocity c_{m-1} and area A_1. Consequently the discharge volume

$$V_2 = \frac{WT_2R}{p_2\ 144}\frac{\gamma_2}{\gamma_3}$$

has to be used instead of V_1, whereby the density ratio γ_2/γ_3 can be calculated by Equations [9] and [11], wherein $q = \eta_{ad}\ q_{ad}$.

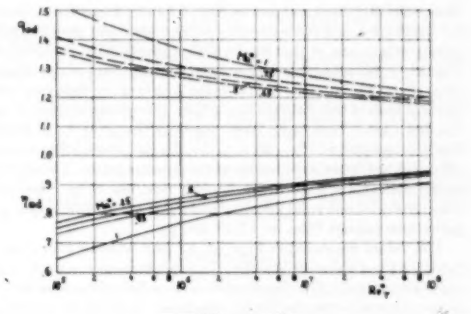

—— η_{ad} - - - q_{ad}

FIG. 52 PRESSURE COEFFICIENT q_{ad} AND EFFICIENCY OF TURBINES AS FUNCTION OF REYNOLDS NUMBER Re^* FOR $\varphi = 0.3$, $\epsilon = 1.6$
(No discharge losses assumed.)

Fig. 52 has to be used instead of Fig. 51, and the influence of the blade number (Equations [76] and [77]) has to be disregarded. The relation $b_3 = 0.25De^{-2}K_f^{-1}\gamma_3/\gamma_2$[16] applies for calculating the impeller width, and Fig. 25 for computing the nozzle width. Equation [46] instead of Equation [45] applies for the optimum clearance. For greater clearances an efficiency drop of

$$\frac{\eta}{\eta_o} = \frac{1 - \dfrac{2s/D}{(1 - 0.5Ma^{*2}_T)\varphi/\epsilon^3}}{1 - \dfrac{2s_oD}{(1 - 0.5Ma^{*2}_T)\varphi/\epsilon^3}} \quad \ldots\ldots [79]$$

has to be expected.

The trial-and-error procedure can be avoided when, in Figs. 51 and 52, the Mach number is replaced by the pressure ratio according to Equations [8] and [9]. Such a diagram, however, can be valid for a definite κ-value only. In order to simplify the procedure further, the Reynolds number can be expressed by a new characteristic value a, which for compressors can be written in the form[16]

$$\text{const}\ \frac{\sqrt{p_1W}}{T_1^{1.35}} = \frac{Re^*_c\sqrt{\varphi}\ E}{\sqrt{Ma^*_c}\ \epsilon\ 1.34}\sqrt[4]{\frac{R(\kappa+1)}{\kappa g}} = a_c \quad [80]$$

For turbines this characteristic value takes the form[16]

$$\text{const}\ \frac{\sqrt{p_1W}}{T_1^{1.35}} = \frac{Re^*_T\sqrt{\varphi}\ (1 - 0.333q_{ad}Ma^{*2}_T)^{1.75}\ E}{\sqrt{Ma^*_T}\ \epsilon\ (1 - 0.333qMa^{*2}_T)^{3.5}\ 1.34}\sqrt[4]{\frac{R(\kappa+1)}{\kappa g}} = a_T \quad \ldots\ldots [81]$$

The constant in the equation depends on the dimensional system used (const = 1 for metric system), and the value E is the constant in the viscosity Equation [12] ($E = 7.3\ 10^{-9}$ for air).

[15] This restriction results from Equations [8] and [10], because only for this range the rise of the κ-value does not seriously affect the change of density.

[16] No hub assumed, i.e., $d_N = 0$.

Hence the Reynolds number in Figs. 51 and 52 can be replaced by the value a, and the value a by weight flow, inlet pressure, and inlet temperature, so that finally a diagram results as presented in Fig. 53.[17] By using this diagram the starting point is the weight flow W in Fig. 53(b). The a-value is found by following the vertical lines in this diagram to the lines $p_1 = \text{const}$, and following the horizontal lines from this point to the lines $t_1 = \text{const}$. For this a-value in Figs. 53(a) or (c), the pressure coefficient and efficiency are found as functions of the pressure ratio. The shaded range indicates a zone where laminar flow has to be expected, when the relations valid for pipes and ducts are applied to the impeller flow passage ($Re_r = 1.7 \times 10^4/\varphi$).

The values presented in Figs. 51, 52, and 53 have been calculated for fixed values of φ and ϵ. In order to present a more complete survey over the characteristics of radial turbomachines it is necessary to compute similar diagrams for different values of φ and ϵ. Figs. 32 and 41 indicate by which proportions the flow factor φ changes the characteristic values q_{ad} and η_{ad} of compressors and turbines. Hence, by using these figures in addition to Figs. 51, 52, or 53, the influence of the flow factor can be accounted for. In regard to the influence of the diameter ratio ϵ it can be said by considering Equations [22], [23], [35], [38], [42], [43] that, generally, by applying a greater diameter ratio, the efficiency will be decreased slightly. Smaller diameter ratios very often yield slightly higher efficiencies. Test results on compressor wheels with a diameter ratio of $\epsilon = 1.35$ supported the foregoing conclusion in some respects.

It must be pointed out that by using the Blasius law in calculating the efficiencies, an assumption regarding the maximum admissible roughness already has been made. This becomes evident when the relation for the flow resistance in rough channels is considered. This relation can be written in the form

$$\lambda = \left(\frac{k^*}{D^*}\right)^{0.214} 0.17 \qquad [82]$$

when k^* denotes the average height of surface irregularities. The result of comparing Equation [82] with Equation [13] and the Blasius law is that the calculated efficiencies can be true only as long as the relation

$$k^* \leq \frac{D^* 6.65}{Re^{0.9}} \qquad [83]$$

is fulfilled. That means that the maximum admissible roughness is

$$k^*_{max} = \frac{D^* 6.65}{Re^{0.9}} \qquad [84]$$

Substituting the characteristic diameter D^* and the individual Reynolds number Re in Equation [84] by the impeller diameter D and the characteristic value a, the maximum admissible roughness for obtaining the efficiencies cited in Fig. 53 is

$$\frac{k^*_{max}}{D} = \frac{y}{a^{0.5} Ma^{*0.4} 10^7} \qquad [85]$$

where $y = 2$ for the annular diffuser, $y = 2.8$ for the scroll, and $y = 1.23\,(1 - 0.165 Ma^{*2}_T)^{3.5}/(1 - 0.33 Ma^{*2}_T)$ for the nozzles. For the impeller no relation can be given because investigations regarding the influence of the surface roughness on rotating parts have not yet progressed far enough. Probably the roughness in rotating parts is of minor influence—maybe close to $y = 3.5$ instead of $y = 2.4$ for compressors and $y = 2.4(1 - 0.165 Ma^{*2}_T)^{0.1}/(1 - 0.11 Ma^{*2}_T)^{0.35}$ for turbines, as resulting when applying the relation valid for stationary channels—because the roughness mainly influences the boundary layer which in rotating parts is activated by centrifugal forces and, consequently, influences the flow to a lesser degree than in stationary channels. The efficiency for $k^* > k^*_{max}$ can be read from Fig. 53 when taking the efficiency resulting for $a = a_s(k^*_{max}/k^*)^{1.35}$ for the original Mach number Ma^* when a_s is the a-value for the design point, and k^* is the value for the actual roughness.

[17] For further simplifications see reference (17).

Small Power Plants With Radial Turbomachines

Fig. 53 shows that the efficiencies of turbomachines decrease with decreasing weight flows and increasing pressure ratios. Detailed investigations as established by Dr. E. Naumann demonstrated that this tendency has a decisive influence on the design of

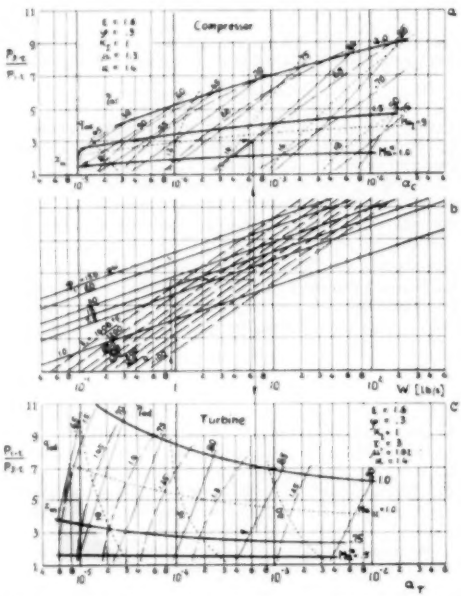

Fig. 53 Design Chart for Compressors and Turbines ($\beta_{3-2} = 90$ Deg, $d\mu = 0$)
(No discharge losses assumed.)

small power plants consisting of compressor, combustor, and turbine. As is well known, the over-all efficiency of such power plants increases with increasing pressure ratios and increasing gas temperatures as long as the efficiency of compressor and turbine can be assumed constant. When, however, for the turbomachines efficiencies as indicated in Fig. 53 (and when additionally different φ- and ϵ-values are considered for matching the speeds of compressor and turbine) are assumed, the over-all efficiency of the power plant becomes dependent upon the pressure ratio and on the weight flow, i.e., net power, in such a manner that for each amount of net power and each gas temperature an optimum pressure ratio results.

As an example, some of these relationships are presented in Fig. 54. This diagram shows the optimum pressure ratio and the lowest obtainable specific fuel consumption as function of the net power for different gas temperatures. This diagram also shows that the required rotational speeds increase with decreasing net

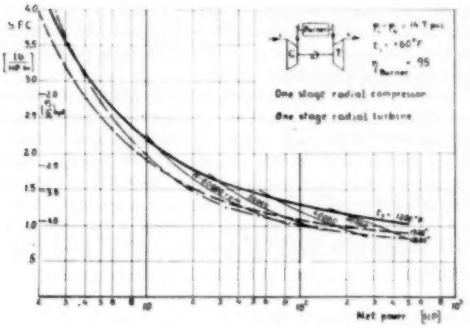

FIG. 54 MINIMUM SPECIFIC FUEL CONSUMPTION OF SMALL POWER PLANTS AS FUNCTION OF NET POWER

power. It is interesting to note that for extremely small net power the application of especially high gas temperatures increases the fuel consumption.

It may be mentioned that the investigations also revealed that lower fuel consumptions (up to 15 per cent) than indicated in Fig. 54 can be obtained when two turbines are used (one turbine driving the compressor and a power turbine), because thus the speeds of compressor and turbine are closer to the optimum speed of each unit. With this arrangement the speed of the unit must be increased (up to 40 per cent).

ACKNOWLEDGMENTS

The author expresses his gratitude to Prof. F. L. Schwartz, University of Michigan, for his interest and support in submitting this paper. Special acknowledgment is due to Dr. F. J Neugebauer, General Electric Company, and Dr. M. Schilhansl, Brown University, for valuable advice in discussing the essential phases of this paper.

BIBLIOGRAPHY

1 "A Contribution to the Precalculation of Radial Compressors," by O. E. Balje, Technical Report, GS-USAF-Wright-Patterson Air Force, No. 97.

2 "Die Kreiselpumpen für Flüssigkeiten und Gase," by C. Pfleiderer, Julius Springer Verlag, Berlin, Germany, Göttingen; Heidelberg, Germany, 1949.

3 "Das Förderhöhenverhältniss radialer Kreiselpumpen mit logarithmisch-spiraligen Schaufeln," by A. Busemann, *Zeitschrift für angewandte Mathematik und Mechanik*, vol. 8, 1928, pp. 372–384.

4 "Huette I (Engineers Handbook)," twenty-sixth edition, Wilhelm Ernst and Sohn, Berlin, Germany, 1931.

5 "Steam Turbines," by A. Stodola, Julius Springer, Berlin, Germany, 1905.

6 "Der Reibungswiderstand rotierender Scheiben in Gehäusen," by F. Schultz-Grunow, *Zeitschrift für angewandte Mathematik und Mechanik*, vol. 15, 1935, pp. 191–204.

7 "Über Verluste und Wirkungsgrade bei Kreiselpumpen," by R. Dziallas, *Wasserkraft und Wärmewirtschaft*, 1943, p. 106.

8 "The Resistance to Rotation of Disks in Water at High Speeds," by A. H. Gibson and A. Ryan, Proceedings of The Institution of Civil Engineers, vol. 179, 1909–1910, part 1, pp. 313–331.

9 "Guide to the Flow Theory," by L. Prandtl, translated from the German, June, 1949, published by Central Air Documents Office, Wright-Patterson Air Force Base, Dayton, Ohio.

10 "Lader und Aufladung von Flugmotoren," by W. I. Dimitrijewsky and K. W. Cholschtschewnikoff, Moscow, 1939, translated from the Russian by ZWB, 1943.

11 "Technische Stroemungslehre," by B. Eck, Julius Springer Verlag, Berlin, Germany, 1941.

12 "Regelung der Foerderhoehe von Flugmotorenladern durch regelbaren Eintrittsdrall," by H. Pfau, ZWB Bericht No. FB 1302, Berlin-Adlershof, 1940.

13 "Beschreibung und Untersuchung der Lader der russischen Flugmotoren, AM 35 and AM 38," by N. Dietrich, ZWB Bericht No. UM 1166, Berlin-Adlershof, 1944.

14 "The Radial Turbine," by W. T. von der Nuell, Technical Data Digest, vol. 12, 1947, pp. 5–31; Central Air Documents Office, Dayton, Ohio.

15 "The Radial Flow Turbine in Comparison to the Axial Flow Turbine," by E. Knoernschild, Technical Report (Preprint), No. F-TR-1198 IA GS-USAF-Wright-Pat-No. 160.

16 "Untersuchungen an Radialturbinen," by O. E. Balje, Dissertation der Technischen Hochschule, Munich, Germany, 1945.

17 "A Contribution to the Design of Radial-Turbomachines," by O. E. Balje, *Technical Data Digest*, vol. 15, 1950, pp. 21–35, Central Air Document Office, Dayton, Ohio.

Discussion

W. T. VON DER NUELL.[18] The author has presented a chart demonstrating his opinion with regard to the influence of the Reynolds number on the efficiency of turbomachines. An increase of 10 points in efficiency is co-ordinated with an increase in Reynolds number from approximately 3×10^5 to 2×10^6.

This subject can safely be called a controversial one. And cases are known where, in spite of rather accurate testing both with variation in size of the machines tested and in flowing substances, only minor if any Reynolds-number influence could be detected, although also, surface roughness conditions were observed as closely as engineering (as contrasted with the physicist's work) would permit.

It would be quite interesting to hear whether those who know are in agreement with the author or care to present their experience.

AUTHOR'S CLOSURE

The influence of the Reynolds number on the efficiency of turbomachines has been studied in several places and has also been treated in the literature.[19] As an example, a pertinent

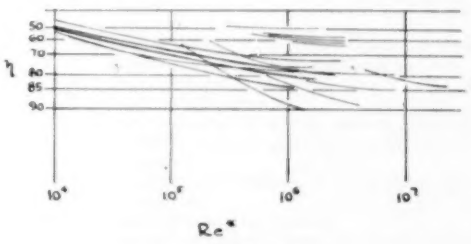

FIG. 55

diagram[20] presenting test results regarding the influence of the Reynolds number on the efficiencies of turbomachines is shown in Fig. 55 which shows the same tendency and in very many cases the same absolute values as shown in Figs. 51 and 52. This seems to prove that the concepts used in the precalculations give sufficient consideration to the main influences, usually experienced in turbomachines. One aspect, however, which cannot yet be covered adequately is the influence of the degree of turbulence on the characteristics of turbomachines.

The influence of the degree of turbulence was first encountered as measurements on the same airfoil gave different results

[18] AiResearch Manufacturing Company, a Division of the Garrett Corporation, Los Angeles, Calif.

[19] "The Influence of Reynolds Number on the Performance of Turbomachinery," by Hunt Davis, Harry Kottas, and A. M. G. Moody, Trans. ASME, vol. 73, 1951, pp. 499–509.

[20] Diagram of Fig. 55 taken from footnote 19.

when tested in wind tunnels of different sizes and design. This difference is explained by the fact that the degree of turbulence of the wind tunnel flow varies with design and tunnel size. By determining a turbulence factor[21] (defined as the ratio of the critical Reynolds number of a sphere in a nonturbulent air stream to the critical Reynolds number in the tunnel), the different results can be correlated. This turbulence factor and its characteristics has been investigated in wind-tunnels and it seems to be standard practice for wind-tunnel tests to refer the test results to a specified standard turbulence.

In the field of turbomachines, the degree of turbulence very probably has some influence also and occasionally may compensate the influence of the Reynolds number. However, the knowledge of the turbulence factor in turbomachines does not seem to have progressed far enough to establish definite relationships for its influence in radial turbomachines.

In view of these considerations, it seems justified to assume that the precalculated values are fairly correct, as long as they are referred to the same degree of turbulence (for example, to the turbulence of the free atmosphere). If, therefore, cases are known where only a minor, if any, Reynolds number influence could be detected, it would be quite interesting to know the details of machines size and test setup in those cases, in order to learn more about the turbulence factor in radial turbomachines.

[21] "Turbulence Factors of N.A.C.A. Wind Tunnels as Determined by Sphere Tests," by Robert C. Platt, NACA Report No. 558.

Some Theoretical Aerodynamic Investigations of Impellers in Radial- and Mixed-Flow Centrifugal Compressors

By J. D. STANITZ,[1] CLEVELAND, OHIO

The purpose of this paper is to present the numerical results of several theoretical, aerodynamic investigations of impellers in radial and mixed-flow centrifugal compressors and to discuss the significance of these results with respect to improved compressor performance. The solutions are not intended to supply specific design information but rather to help create a general understanding and awareness of the flow conditions in impellers of centrifugal compressors. The paper is given in two parts. In Part 1 two-dimensional relaxation solutions for compressible and incompressible fluids are presented for flow with axial symmetry (two solutions) and for flow between blades on surfaces of revolution about the axis of the impeller (eight solutions). The effects of variations in the following design and operating conditions of the impeller are investigated: (*a*) Compressor flow rate, (*b*) impeller-tip speed, (*c*) number of blades, and (*d*) blade curvature on flow surfaces of revolution. The numerical results are presented in plots of the streamlines, constant-velocity or Mach number lines, and constant static-pressure lines. In Part 2 three approximate methods of solution are presented which can be used for relatively rapid analysis of compressible flow between blades on flow surfaces of revolution.

Nomenclature

The following nomenclature is used:

- A = ratio, Equation [17*a*]
- A, B, C = coefficients, Equation [C-13], Appendix C
- a = annulus area normal to flow surface of revolution
- b = number of blades
- c = speed of sound
- exp = exponential [$\exp(x) = e^x$]
- F = body force, or "distributed blade force," per unit weight of fluid (dimensionless)
- F_R, F_θ, F_Z = components of F in R, θ, Z-direction (positive in direction of increasing R, θ, Z)
- g = acceleration due to gravity
- H = channel height ratio, h/h_T, Fig. 8
- h = channel height normal to flow surface of revolution
- M_T = impeller-tip speed (impeller-tip Mach number), Equation [2]
- P = pressure ratio, p/p_o
- p = static (stream) pressure
- Q = velocity relative to impeller (dimensionless: Q expressed as a ratio of c_o)
- Q_M = meridional velocity, Equation [3], Fig. 3
- Q_R, Q_θ, Q_Z = components of relative velocity Q in R, θ, Z-directions (positive in the directions of increasing R, θ, Z)
- R, θ, Z = cylindrical co-ordinates relative to impeller (dimensionless: R and Z expressed as ratios of r_T, θ positive counterclockwise), Fig. 3
- R = gas constant
- R_x = largest radius at which fluid is assumed to be perfectly guided by blades on flow surface of revolution (in approximate circulation method)
- r_T = impeller-tip radius
- S = distance along blade surface (dimensionless: S expressed as a ratio of r_T)
- T = static (stream) temperature
- t = time
- W = total flow through annulus area a
- α, β, ϵ = directions defined by Equations [4], [5], and [6], Fig. 3
- β_b = blade angle on flow surface of revolution (thin blades only), Equation [16]
- Γ = absolute circulation
- γ = ratio of specific heats
- δ = ratio of passage width to blade spacing on flow surface of revolution at constant R and Z
- δ = boundary-layer thickness
- λ = whirl ratio, Equation [8]
- μ = slip factor, ratio of average absolute tangential velocity of fluid at impeller tip to tip speed of impeller
- ξ, η = transformed co-ordinates, Equations [B-4] (Appendix B)
- ρ = static (stream) weight density
- σ = angular blade spacing, measured on conic surface of revolution, Equation [15]
- φ = flow coefficient, Equation [14]
- ψ = stream function, defined by Equation [A-9] (Appendix A) for meridional plane and by Equation [B-3] for flow surfaces of revolution
- ω = angular velocity of impeller (counterclockwise)

Subscripts:

- abs = component of absolute velocity along blade surface
- avg = average value across passage between blades on flow surface of revolution
- b = blade
- d = driving face of blade (face in direction of rotation)
- o = stagnation condition upstream from impeller
- s = standard solution
- T = impeller tip
- t = trailing face of blade (face opposed to direction of rotation)

---

[1] Head, Applied Compressor and Turbine Analysis Section, Lewis Flight Propulsion Laboratory, National Advisory Committee for Aeronautics. Jun. ASME.

Contributed by the Gas Turbine Power Division and presented at the Fall Meeting, Minneapolis, Minn., September 26–28, 1951, of The American Society of Mechanical Engineers.

Note: Statements and opinions advanced in papers are to be understood as individual expressions of their authors and not those of the Society. Manuscript received at ASME Headquarters, October 1, 1950. Paper No. 51—F-13.

$1'$ = upstream from impeller
x = largest radius at which fluid is considered to be perfectly guided by blades (in approximate, circulation method)

Superscripts:

$'$ value estimated by correlation equations

PART I RELAXATION SOLUTIONS

Introduction

The design of centrifugal compressors is largely an art based upon experience obtained from cut-and-try methods. If detailed knowledge of flow conditions within centrifugal compressors existed, rational design methods based on this knowledge might be developed for centrifugal compressors with improved performance. For example, boundary-layer separation, which decreases compressor efficiency, could be controlled by aerodynamic design methods based on knowledge of the velocity gradients that result from various design configurations. Knowledge of the flow conditions within centrifugal compressors can be determined by theoretical and/or experimental aerodynamic investigations. Some theoretical investigations are considered in this paper.

In the past, several methods of analysis that apply to centrifugal compressors (references 1 to 6,[2] for example) have been developed, but few numerical solutions have been reported in detail (references 1, 4, 5, and 6, for example). The purpose of this paper is to present the numerical results of several theoretical, aerodynamic investigations of impellers in radial and mixed-flow centrifugal compressors and to discuss the significance of these results with respect to improved compressor performance. The solutions presented are not intended to supply specific design information but rather to help create a general understanding and awareness of the flow conditions in impellers of centrifugal-type compressors.

For given operating conditions, the flow within compressors depends on the compressor geometry (three-dimensional-flow effects) and on the fluid properties (compressibility and viscosity). The effect of compressibility is considered in this paper and some three-dimensional-flow effects are indicated by the combination of two-dimensional solutions. The effects of viscosity are neglected.

In Part I of this paper, two-dimensional relaxation solutions are presented for flow with axial symmetry and for flow between blades on surfaces of revolution about the axis of the impeller. The effect of variations in the following design and operating conditions of the impeller are investigated: (*a*) compressor flow rate, (*b*) impeller-tip speed, (*c*) number of blades, and (*d*) blade curvature on flow surfaces of revolution.

The work presented in this paper was conducted at the Lewis Flight Propulsion Laboratory of the NACA and is partially reported in references (7 to 10).

Preliminary Considerations

Consider the flow of an ideal fluid through a typical impeller passage such as shown in Fig. 1. The fluid is free to follow whatever path the pressure and inertia forces require of it. If, however, the number of blades in the impeller approaches infinity, the space between blades approaches zero, and the path of the fluid is limited to the curved mean surface of the blade. (The blades become infinitely thin so that the two surfaces of each blade approach a mean surface.) The fluid motion is thus reduced from a general three-dimensional motion to a two-dimensional motion restricted to the mean blade surface. The streamlines of this two-dimensional motion can be projected on the meridional plane

[2] Numbers in parentheses refer to the Bibliography at the end of the paper.

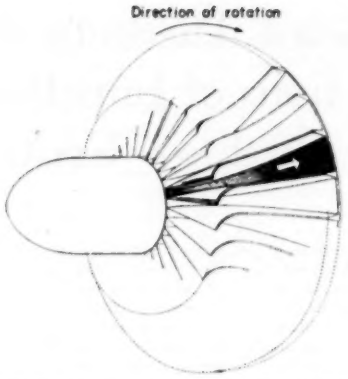

Fig. 1 Passage in Impeller of Typical Centrifugal Compressor

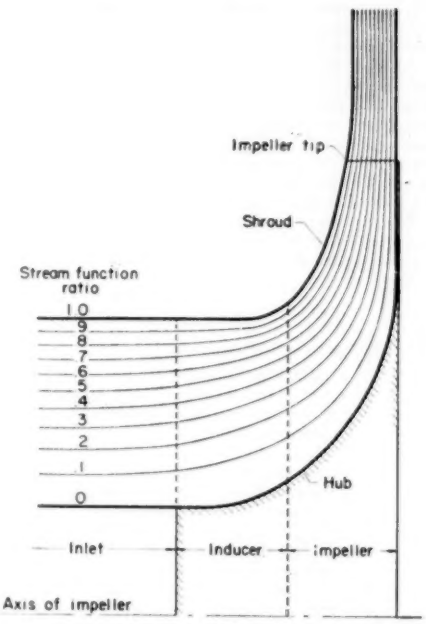

Fig. 2 Streamlines in Meridional Plane for Axial-Symmetry Solution of Impeller With Inducer Vanes Described in Fig. 4 (Streamline designation indicates percentage of flow through compressor between streamline and impeller hub. Incompressible flow; Qz/M_T equal to 0.3429 far upstream from impeller.)

(axial-radial plane) as shown in Fig. 2. The solutions are axially symmetrical because the infinite number of blades prevent the fluid properties from varying about the axis of the compressor. Ruden (11) has shown that, provided the blades are not too widely spaced in the compressor, axial-symmetry solutions give a good conception of the mean flow between blades. Solutions of this type are presented in this paper.

For finite blade spacing, flow conditions vary between blades

(circumferentially about the axis of the impeller), as well as from hub to shroud. To investigate the variation between blades, it is assumed that the flow is limited to surfaces of revolution generated by rotating the center line of the channel between adjacent streamlines in the meridional plane (axial-symmetry solution, Fig. 2) about the axis of the compressor. For sufficiently close streamline spacing in the meridional plane, flow conditions are considered uniform normal to these surfaces of revolution. Thus the flow is limited to two-dimensional motion on flow surfaces of revolution. Blade-to-blade solutions of this type are presented in this paper.

Blade-to-blade solutions can be obtained for every flow surface of revolution generated by the center lines between adjacent streamlines in the meridional plane. Therefore flow conditions can be determined approximately throughout the passage. The resulting quasi-three-dimensional solution is obtained by the combination of two types of two-dimensional solutions (axial-symmetry solution and blade-to-blade solutions). Such a combination of solutions prohibits the possibility of a corkscrew path which the fluid might follow in a true three-dimensional solution, but it does give a better idea of the flow than does any two-dimensional solution alone.

The cylindrical co-ordinates R, θ, Z shown in Fig. 3 are convenient to use in theoretical studies of the flow in impellers of centrifugal compressors. These co-ordinates are dimensionless, the linear co-ordinates R and Z having been divided by the impeller tip radius r_T (so that R equals 1.0 at the impeller tip, for example). The co-ordinate system rotates with the impeller about the Z-axis. The angular velocity ω is always positive and in the counterclockwise direction as shown in Fig. 3.

The velocity Q, relative to the rotating co-ordinate system, has components Q_R, Q_θ, and Q_Z in the R, θ, Z-directions, respectively (Fig. 3). These velocities are dimensionless, having been divided by the stagnation speed of sound c_o upstream from the impeller, where

$$c_o^2 = \gamma g R T_o \quad \ldots\ldots [1]$$

in which R is the gas constant.

The impeller-tip speed is likewise dimensionless and equal to the impeller-tip Mach number M_T which is defined by

$$M_T = \frac{\omega r_T}{c_o} \quad \ldots\ldots [2]$$

Thus the tangential velocity of the impeller at any radius R is equal to RM_T and the absolute tangential velocity of the fluid is equal to $(RM_T + Q_\theta)$.

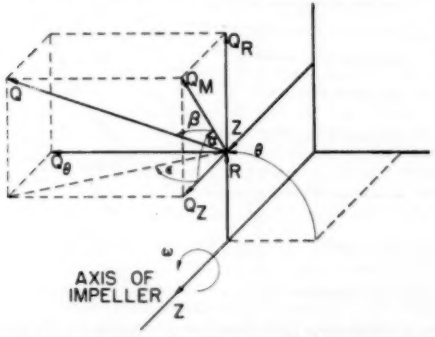

FIG. 3 CYLINDRICAL CO-ORDINATES AND VELOCITY COMPONENTS RELATIVE TO ROTATING IMPELLER

(All quantities are dimensionless. Linear co-ordinates are measured in units of impeller-tip radius; velocity components are measured in units of stagnation speed of sound upstream from impeller.)

In addition to the three components of the relative velocity Q_R, Q_θ, and Q_Z it is convenient to define a fourth velocity component, lying in the meridional plane (RZ-plane) and defined as the meridional velocity Q_M where from Fig. 3

$$Q_M^2 = Q_R^2 + Q_Z^2 \quad \ldots\ldots [3]$$

The meridional velocity Q_M helps define two angles α and β, shown in Fig. 3, from which figure

$$\left.\begin{aligned} Q_R &= Q_M \sin\alpha \\ Q_Z &= Q_M \cos\alpha \end{aligned}\right\} \quad \ldots\ldots [4]$$

and

$$\left.\begin{aligned} Q_M &= Q\cos\beta \\ Q_\theta &= Q\sin\beta \end{aligned}\right\} \quad \ldots\ldots [5]$$

The angle ϵ also shown in Fig. 3, is defined by

$$\tan\epsilon = \frac{Q_\theta}{Q_Z} \quad \ldots\ldots [6]$$

From the general energy equation it can be shown that the static (stream) temperature T is related to the relative velocity Q by (reference 8)

$$\frac{T}{T_o} = 1 + \frac{\gamma - 1}{2}\left[(RM_T)^2 - Q^2 - 2M_T\lambda_U\right] \quad \ldots\ldots [7]$$

where λ is the whirl ratio (absolute moment of momentum divided by $r_T c_o$) given by

$$\lambda = R(RM_T + Q_\theta) \quad \ldots\ldots [8]$$

The pressure ratio P and the density ratio ρ/ρ_o are likewise related to the relative velocity Q by

$$P = \frac{p}{p_o} = \left(\frac{T}{T_o}\right)^{\frac{\gamma}{\gamma-1}} = \left\{1 + \frac{\gamma-1}{2}\left[(RM_T)^2 - Q^2 - 2M_T\lambda_U\right]\right\}^{\frac{\gamma}{\gamma-1}} \quad \ldots\ldots [9]$$

and

$$\frac{\rho}{\rho_o} = \left(\frac{T}{T_o}\right)^{\frac{1}{\gamma-1}} = \left\{1 + \frac{\gamma-1}{2}\left[(RM_T)^2 - Q^2 - 2M_T\lambda_U\right]\right\}^{\frac{1}{\gamma-1}} \quad \ldots\ldots [10]$$

AXIAL-SYMMETRY SOLUTIONS

The distribution of streamlines and lines of constant relative velocity in the meridional plane are considered in this section. Two incompressible solutions are presented for the same impeller with straight impeller blades. In the first solution the inducer vanes are immediately ahead of the impeller; in the second solution the vanes are removed, and the straight impeller blades are extended indefinitely upstream parallel to the axis of the impeller. (A description of the impeller and inducer vanes is given later.) Comparison of these solutions gives an indication of the influence of inducer vanes on the flow in impellers.

Basic Idea. The basic idea of a "distributed blade force," required for rational solutions with axial symmetry in compressors and turbines, is clearly shown by a simple development starting with the general equations for three-dimensional motion without viscosity. In terms of the relative velocity and co-ordinate ratios used in this paper, the equations of motion become (assuming the flow is steady relative to the rotating blades)

$$Q_R \frac{\partial Q_R}{\partial R} + \frac{Q_\theta}{R}\frac{\partial Q_R}{\partial \theta} + Q_Z \frac{\partial Q_R}{\partial Z} - \frac{(Q_\theta + RM_T)^2}{R} = -\frac{gp_o}{\rho c_o^2}\frac{\partial P}{\partial R} + \frac{gr_T F_R}{c_o^2} \quad [11a]$$

$$Q_R \frac{\partial Q_\theta}{\partial R} + \frac{Q_\theta}{R}\frac{\partial Q_\theta}{\partial \theta} + Q_Z \frac{\partial Q_\theta}{\partial Z} + 2Q_R M_T + \frac{Q_R Q_\theta}{R} = -\frac{gp_o}{\rho c_o^2}\frac{\partial P}{R\partial \theta} + \frac{gr_T F_\theta}{c_o^2} \quad [11b]$$

$$Q_R \frac{\partial Q_Z}{\partial R} + \frac{Q_\theta}{R}\frac{\partial Q_Z}{\partial \theta} + Q_Z \frac{\partial Q_Z}{\partial Z} = -\frac{gp_o}{\rho c_o^2}\frac{\partial P}{\partial Z} + \frac{gr_T F_Z}{c_o^2} \quad [11c]$$

where F is the body force (resulting from an arbitrary force field) per unit weight of fluid at any point in the flow field. (For example, F is equal to unity in the gravitational force field.) If axial symmetry is assumed, then the partial derivatives with respect to θ in Equations [11] become zero and in particular Equation [11b] becomes

$$Q_R \frac{\partial Q_\theta}{\partial R} + Q_Z \frac{\partial Q_\theta}{\partial Z} + 2Q_R M_T + \frac{Q_R Q_\theta}{R} = \frac{gr_T F_\theta}{c_o^2}$$

which from Equation [8] is equivalent to

$$\frac{d\lambda}{dt} = \frac{gRF_\theta}{c_o} \quad [12]$$

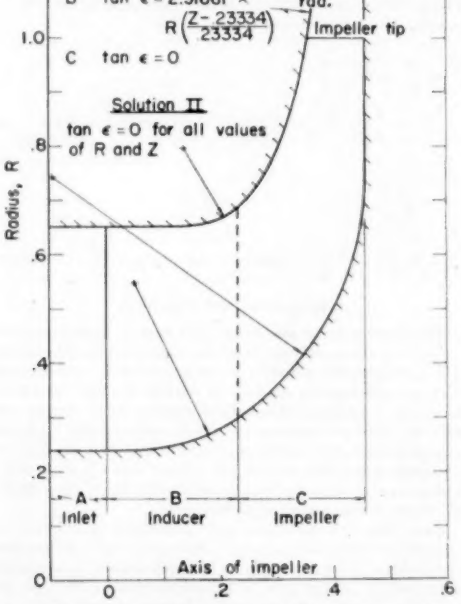

FIG. 4 DIMENSIONS OF COMPRESSOR FOR AXIAL-SYMMETRY SOLUTIONS I AND II
(Zero impeller blade thickness; vaneless diffuser.)

The left side of Equation [12] is the rate of change of moment of momentum (in dimensionless form). If the blades exert a guiding action on the fluid, $(d\lambda)/(dt)$ is not equal to zero and, therefore, from Equation [12], the body force F cannot equal zero. In impellers with a finite number of blades $(d\lambda)/(dt)$ results from pressure differences on the two surfaces of each blade. The blade forces resulting from these pressure differences approach zero as the number of blades approach infinity, but the weight of fluid contained between blades also approaches zero, and the ratio of blade force to weight of fluid approaches a value which is the body force or the distributed blade force F, at any point (R, Z) in the meridional plane.

The distributed blade force F must be normal to the mean blade surface, because F results from pressures which act normal to the blade surfaces. For axial symmetry, the relative velocity Q lies on the mean blade surface so that the condition for F being normal to the mean blade surface is given by

$$F_R Q_R + F_\theta Q_\theta + F_Z Q_Z = 0 \quad [13]$$

The concept of a distributed blade force which acts normal to the blade surface was introduced by Lorenz (14) in 1907.

Method of Axialysis. A differential equation for the stream function ψ in the meridional plane is developed in Appendix for constant λ_U and for impellers with radial blade elements, that is, for impellers with the mean blade surface generated by radial lines normal to the axis of rotation. The geometry of the impeller is arbitrary in all other respects. The differential Equation [A-10] or [A-11] (Appendix A) is solved by relaxation methods to

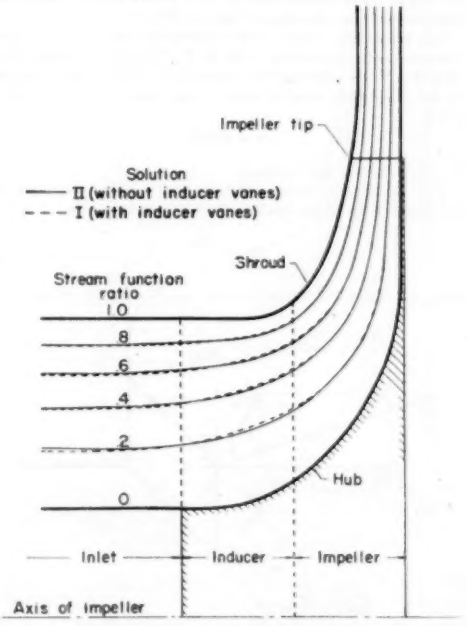

FIG. 5 COMPARISON OF STREAMLINES IN MERIDIONAL PLANE FOR AXIAL-SYMMETRY SOLUTIONS OF IMPELLERS DESCRIBED IN FIG. 4, WITH AND WITHOUT INDUCER VANES
(Streamline designation indicates percentage of flow through compressor between streamline and impeller hub. Incompressible flow; Qz/Mr equal to 0.3429 far upstream from impeller.)

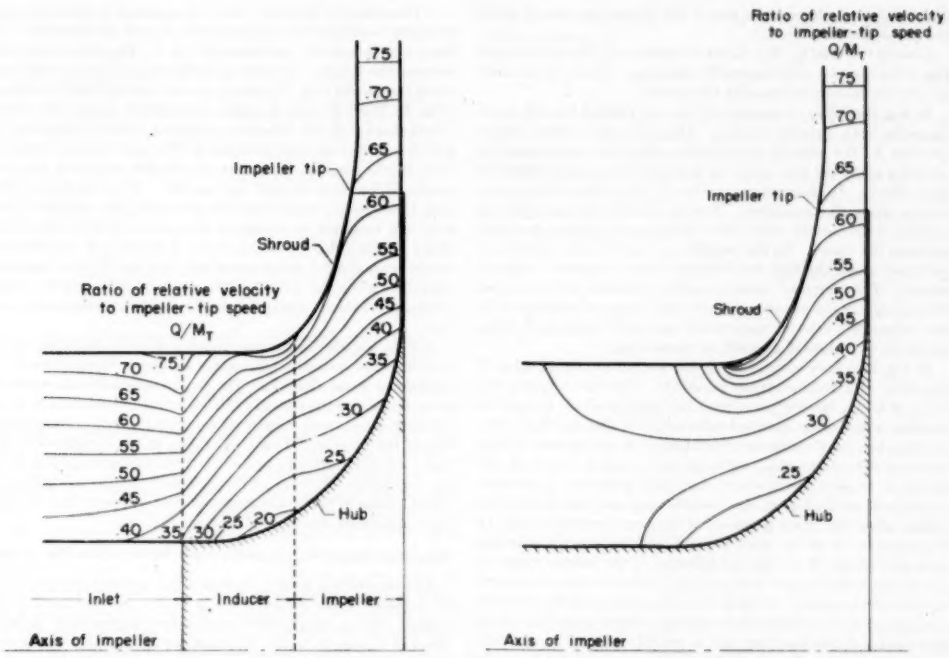

(a) Solution I: Impeller with inducer vanes

(b) Solution II: Impeller with inducer vanes removed and straight impeller blades extended upstream parallel to axis of compressor

FIG. 6 LINES OF CONSTANT RELATIVE VELOCITY IN MERIDIONAL PLANE FOR AXIAL-SYMMETRY SOLUTION OF IMPELLER DESCRIBED IN FIG. 4

(Incompressible flow; Q_Z/M_T equal to 0.3429 far upstream from impeller.)

obtain the distribution of ψ for given boundary conditions. Lines of constant ψ are streamlines, and the velocity distribution is determined from the distribution of ψ. A completely general method of analysis is given in reference (6).

Description of Impeller. Two axial-symmetry solutions have been obtained for the same impeller with straight (β and ϵ equal zero) blades of zero thickness. Dimensions of the impeller profile in the meridional plane are indicated in Fig. 4. For solution I the inducer vanes (region B in Fig. 4) are located immediately ahead of the impeller (region C). To simplify the numerical procedure, the inducer vanes are continued through the inlet region A (Fig. 4), at the ideal angles for no vane loading. For solution II, the inducer vanes were removed and the straight impeller blades were extended indefinitely upstream parallel to the axis of the compressor. (Thus for solution II, $\tan \epsilon$ and $\tan \beta$ equal zero everywhere up to the impeller tip.) A vaneless diffuser was assumed in both solutions.

Conditions of Solution. Both solutions are for incompressible flow and for the same ratio of impeller-tip speed to volume flow rate. This ratio of tip speed to flow rate corresponds to a value of Q_Z/M_T equal to 0.34286 upstream from the impeller. For incompressible flow, the stagnation speed of sound c_o contained in the definitions of Q and M_T is a fictitious quantity which cancels because Q and M_T appear as ratios of one another.

Streamlines. Streamlines for the two axial-symmetry solutions are shown in Figs. 2 and 5. The streamlines are designated by a stream-function ratio such that the value of the streamline indicates the percentage of flow through the compressor between the streamline and the impeller hub. At a given radius, the streamline spacing is indicative of the meridional velocity Q_M with close spacing indicating high velocities and wide spacing indicating low velocities.

In Fig. 2 streamlines are shown for solution I (the impeller with inducer vanes) and, in Fig. 5 the streamlines of solution I are compared with the streamlines for solution II (the impeller with inducer vanes removed). The streamline distribution is nearly the same for both solutions, indicating that, at least for thin blades ($\delta = 1.0$) and incompressible flow, blade curvature about the axis of the compressor has only a small effect upon the stream-function distribution in axial-symmetry solutions.

Also, it is interesting to note that for solution II, in which $\tan \epsilon$ equals zero, the differential Equation [A-11] (Appendix A) for the distribution of ψ becomes

$$\frac{\partial^2 \psi}{\partial R^2} - \frac{1}{R}\frac{\partial \psi}{\partial R} + \frac{\partial^2 \psi}{\partial Z^2} = 0$$

which is identical to the differential equation for the distribution of ψ in axial-symmetry problems with no impeller blades at all.[9] Thus for incompressible flow the stream-function distribution in the meridional plane is the same with or without thin blades.

[9] Reference (15), p. 126.

(Approximately the same is true if the blades are curved about the axis of the compressor.)

Lines of Constant Q/M_T. Lines of constant Q/M_T are shown in Fig. 6 for the two axial-symmetry solutions. (Q/M_T is the ratio of relative velocity to impeller tip speed.)

In Fig. 6(a) lines of constant Q/M_T are plotted for solution I (impeller with inducer vanes). Ahead of the inducer vanes (section A) the velocity accelerates along the shroud and decelerates along the hub (much as it might when approaching any duct elbow). In the inducer (section B) the relative velocity decreases along all streamlines. This deceleration results from the turning of the inducer vanes which increases the relative flow area between the blades. In the impeller (section C) the velocity accelerated along the hub but remains about constant along the shroud. The "relative" velocity rapidly becomes uniform across the passage in the vaneless diffuser and increases indefinitely as the "absolute" velocity approaches zero with increasing radius (required by constant moment of momentum).

In Fig. 6(b) lines of constant Q/M_T are plotted for solution II (impeller with inducer vanes removed). For this solution, the value of Q/M_T far upstream from the impeller elbow is equal to 0.34286 (which is the specified value of Q_Z/M_T far upstream from the impeller, see Conditions of Solution). A comparison of Figs. 6(a) and 6(b) shows that, although the velocities are quite different in those regions where the blade geometry is different (sections A and B, Fig. 4), the velocities are much the same in the region where the blade geometry is the same (section C, Fig. 4). Therefore, at least for incompressible axial-symmetry solutions with thin blades ($\delta = 1.0$), the influence of the inducer vanes on the velocity distribution, and so forth, probably does not extend far into the impeller. If, however, the axial-symmetry solution for an impeller with finite blade spacing is based upon some mean flow surface (extending from hub to shroud) rather than upon the mean blade surface, the effect of the inducer-vane curvature on the flow in the impeller depends upon the effect of the vane curvature upon the deviation of the mean flow surface from the mean blade surface.

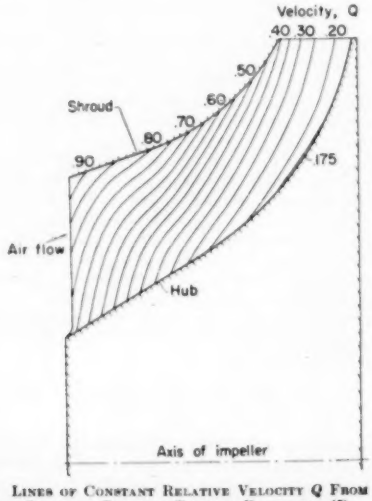

FIG. 7 LINES OF CONSTANT RELATIVE VELOCITY Q FROM AXIAL-SYMMETRY SOLUTION GIVEN IN REFERENCE (5)
(Equivalent impeller-tip speed, 1331 fps; equivalent compressor weight flow, 8.74 lb per sec; impeller-tip radius, 6 in.)

A Compressible Solution. Lines of constant Q, from the axial-symmetry solution for compressible flow given by Hamrick, Ginsburg, and Osborn (5), are shown in Fig. 7. For this compressible solution the velocity decelerates continuously, and at a high rate, along the shroud (Fig. 7) whereas for the incompressible solutions (Fig. 6) there is only a slight deceleration along the shroud. This behavior of the velocities along the shroud in the two impellers can be explained as follows: The annulus cross-sectional area of the impeller in the incompressible solutions decreases nearly 50 per cent through the impeller. This reduction in flow area tends to accelerate the velocities along the shroud. However, the tendency to accelerate is opposed by the rather sharp elbow profile (Fig. 4), which, if the flow area did not decrease, would cause a rapid deceleration following the point of maximum curvature along the shroud. The resultant effect is only a slight decrease in velocity along the shroud for the incompressible solution.

For the impeller in the compressible solution, the annulus flow area does not decrease, but neither is there a sharp elbow in the meridional plane (Fig. 7). The major reason for the rapid deceleration along the shroud in the compressible solution is the increasing density and, therefore, decreasing velocity, from inlet to exit of the impeller. This deceleration in the compressible solution probably results in boundary-layer separation, which lowers the compressor efficiency and is one reason that centrifugal pumps (incompressible fluids) are generally more efficient than centrifugal compressors (compressible fluids).

BLADE-TO-BLADE SOLUTIONS ON FLOW SURFACES OF REVOLUTION

The distribution of flow characteristics (velocity, pressure, etc.) on surfaces of revolution between blades is considered in this section. Seven compressible solutions are presented to show the effect of variations in the following parameters: (a) Compressor flow rate, (b) impeller-tip speed, (c) number of blades, and (d) blade curvature on flow surfaces of revolution. An eighth solution for incompressible flow is presented.

Basic Idea. In the preceding section, streamlines were obtained in the meridional plane from solutions based upon axial symmetry. Consider any two meridional streamlines (Fig. 2, for example), sufficiently close together so that flow conditions can be considered uniform along the normal between streamlines. As discussed previously, the center line of the channel between these streamlines generates a surface of revolution when rotated about the axis of the compressor. Variations in the flow between blades on the flow surface of revolution are presented in this section.

Method of Analysis. In references (7) and (8) a general method of analysis is developed for two-dimensional, compressible, nonviscous flow in centrifugal compressors with arbitrary blade shape (on the flow surface of revolution), varying height of channel between streamlines in the meridional plane and with "conic" flow surfaces of revolution (generated by "straight" center lines of the channel between adjacent streamlines in the meridional plane). In Appendix B this analysis is extended to include curved flow surfaces of revolution such as result, in general, from curved streamlines in the meridional plane (Fig. 2, for example).

Flow Field Investigated. The solutions presented in this section were obtained in a region of the compressors (including the impeller tip, Fig. 8) that was considered to be unaffected by the inlet configuration of the impeller or by the diffuser vanes; that is, the impeller-inlet and the diffuser vanes (if any) must be far enough removed from the region investigated not to affect the flow appreciably in that region. (For the two incompressible, axial-symmetry solutions already presented, the influence of the inducer vanes was found not to extend very far into the impeller.)

The solutions presented are not related to any particular blade

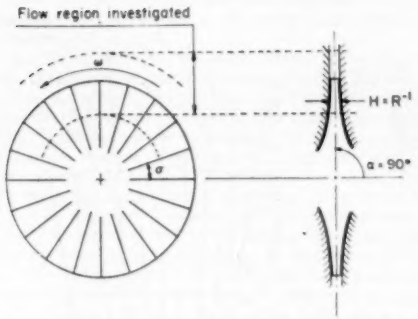

FIG. 8 SOME COMPRESSOR DESIGN CHARACTERISTICS USED IN RELAXATION SOLUTIONS FOR VARIATION IN FLOW FROM BLADE TO BLADE

(Straight blades are shown although logarithmic-spiral blades were also investigated.)

profile in the meridional plane; the center line of the channel between streamlines has been arbitrarily specified as a straight line; the height H (Fig. 8) of the channel between streamlines in the meridional plane has been specified to be such that the annulus flow area normal to the flow surface is constant. The solutions are for radial-flow impellers (α equals 90 deg, Fig. 8) with thin blades. The same solutions also apply (8) to certain mixed-flow impellers with conic flow surfaces of revolution (α less than 90 deg), with fewer blades, but with the same angular blade-spacing σ (Fig. 8) measured on the conic flow surface of revolution.

Design and Operating Parameters. The following parameters are defined in order to describe the design and operating conditions of the radial-flow impellers being investigated:

(*a*) The impeller-tip Mach number M_T is defined by Equation [2].

(*b*) The flow coefficient φ is defined by

$$\varphi = \frac{W}{\rho_e a_T c_e} \quad \ldots\ldots\ldots\ldots\ldots\ldots [14]$$

where W is the total flow rate through the channel generated by adjacent streamlines in the meridional plane and where a_T is the annulus flow area normal to this channel at the impeller tip. If the adjacent streamlines that form the channel in the meridional plane are taken to be the impeller hub and shroud, W becomes the total compressor flow rate, and φ is directly proportional to the standard "equivalent flow rate" (defined in reference 16).

(*c*) The angular blade-spacing σ (Fig. 8) measured on a radial or conic surface of revolution is defined by

$$\sigma = \frac{2\pi}{b} \sin \alpha \quad \ldots\ldots\ldots\ldots\ldots\ldots [15]$$

where b is the number of blades.

(*d*) The blade angle β_b for thin blades is defined by Equation [5] along the blade surface. In terms of the co-ordinates, the definition becomes

$$\beta_b = \tan^{-1}\left(\sin \alpha \frac{Rd\theta}{dR}\right) \quad \ldots\ldots\ldots\ldots [16]$$

(For all solutions presented β_b is constant, that is, independent of radius. For straight blades β_b is zero, and for backward-curved, logarithmic-spiral blades β_b is less than zero.)

Of the eight numerical solutions to be presented, one has been selected as "standard," and for each of the remaining solutions one parameter (or at most two) is varied from the standard conditions as shown in Table 1.

TABLE 1 PARAMETERS FOR NUMERICAL SOLUTIONS

Solution	φ	M_T	σ (deg)	β_b	Type of flow
Standard	0.5	1.5	12	0	Compressible (γ = 1.4)
1	0.7	1.5	12	0	Compressible (γ = 1.4)
2	0.9	1.5	12	0	Compressible (γ = 1.4)
3	0.5	2.0	12	0	Compressible (γ = 1.4)
4	0.5	1.5	18	0	Compressible (γ = 1.4)
5	0.5	1.5	18	0	Incompressible
6	0.5	1.5	18	$\tan^{-1}(-0.5)$	Compressible (γ = 1.4)
7	0.5	1.5	18	$\tan^{-1}(-1.0)$	Compressible (γ = 1.4)

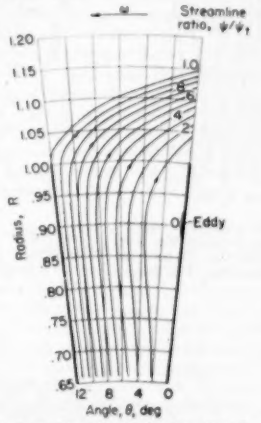

(*a*) Standard solution: Straight blades (β_b, 0); flow coefficient φ 0.5; impeller-tip Mach number M_T, 1.5; constant flow area; angular blade-spacing σ, 12 deg; compressible flow (γ, 1.4)

FIG. 9 RELATIVE STREAMLINES FOR FLOW THROUGH CENTRIFUGAL COMPRESSOR

(Streamline designation indicates percentage of flow through passage between streamline and driving face of blade—right side of passage. Solutions, Figs. 9*b* to 9*h*, inclusive, follow.)

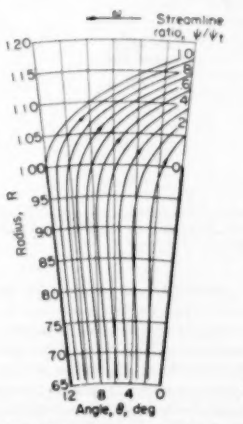

FIG. 9(*b*) SOLUTION 1: FLOW COEFFICIENT φ, 0.7; OTHER PARAMETERS SAME AS STANDARD SOLUTION, FIG. 9(*a*)

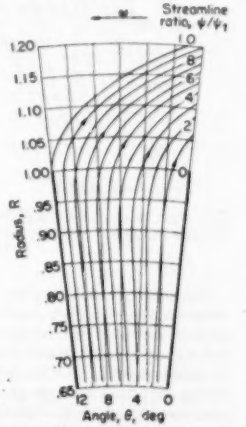

FIG. 9(*c*) SOLUTION 2: FLOW COEFFICIENT φ, 0.9; OTHER PARAMETERS SAME AS STANDARD SOLUTION, FIG., 9(*a*)

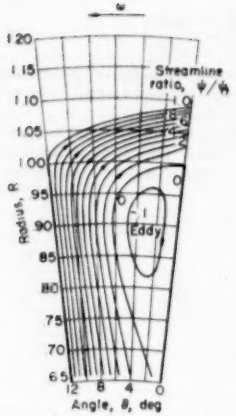

FIG. 9(d) SOLUTION 3: IMPELLER-TIP MACH NUMBER M_T, 2.0; OTHER PARAMETERS SAME AS STANDARD SOLUTION, FIG. 9(a)

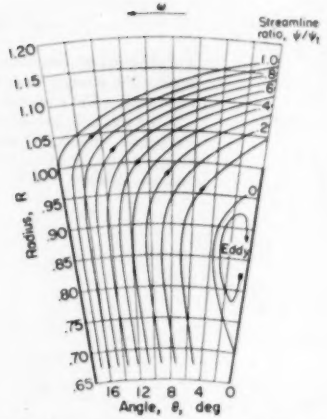

FIG. 9(e) SOLUTION 4: ANGULAR BLADE-SPACING σ, 18 DEG; OTHER PARAMETERS SAME AS STANDARD SOLUTION, FIG. 9(a)

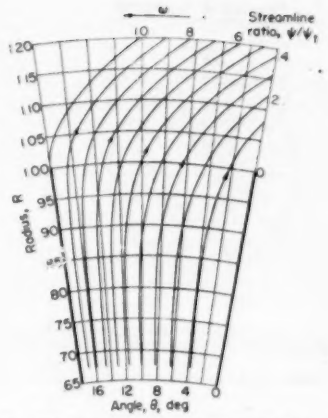

FIG. 9(f) SOLUTION 5: INCOMPRESSIBLE FLUID; OTHER PARAMETERS SAME AS SOLUTION 4, FIG. 9(e)

(Note that φ and M_T are based upon c_0, the magnitude of which is assumed equal to speed of sound at inlet conditions for compressible solutions.)

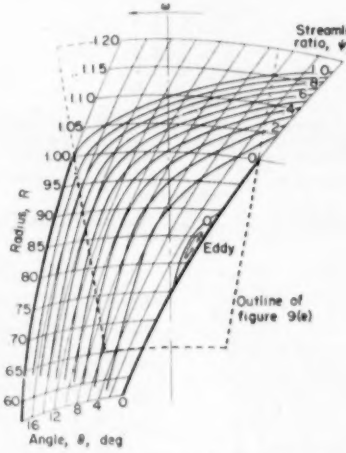

FIG. 9(g) SOLUTION 6: BACKWARD-CURVED, LOGARITHMIC-SPIRAL BLADES [β_b, TAN^{-1} (—0.5)]; OTHER PARAMETERS SAME AS SOLUTION 4, FIG. 9(e)

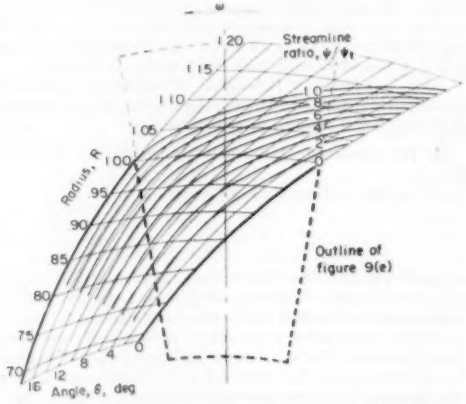

FIG. 9(h) SOLUTION 7: BACKWARD-CURVED, LOGARITHMIC-SPIRAL BLADES [β_b, TAN^{-1} (—1.0)]; OTHER PARAMETERS SAME AS SOLUTION 4, FIG. 9(e)

The incompressible solution (solution 5) was obtained for the same impeller-tip Mach number M_T and for the same flow coefficient φ used in the corresponding compressible solution (solution 4), but with the density ρ constant and equal to ρ_o of the compressible solution. For incompressible flow, M_T and φ are fictitious quantities (because the speed of sound is infinite for incompressible fluids), the definitions of which contain a constant, finite speed of sound equal to c_o for the compressible solution. Therefore the same values of the impeller-tip speed and of the compressor flow rate result from the same values of M_T and φ for the compressible and incompressible solutions.

The numerical results are presented in plots of the streamlines, constant Mach number lines, and (for certain solutions only) constant static-pressure-ratio lines.

Streamlines. The streamline configurations (relative to the impeller) for the eight solutions are shown in Fig. 9. The streamlines are designated by a stream-function ratio ψ/ψ_t such that the values of a streamline indicates the percentage of flow through the passage between the streamline and the driving face of the blade (the blade surface in the direction of rotation). For a given density ratio and channel height, the streamline spacing is indicative of the velocity relative to the impeller with close spacing indicating high velocities and wide spacing indicating low velocities. To assist in the proper geometrical orientation of the backward-curved-blade solutions (Figs. 9*g* and 9*h*) a dashed outline of the

flow field of the corresponding straight-blade solution (Fig. 9e) is superimposed on the flow field of the curved-blade solutions in Figs. 9(g) and 9(h).

As a result of absolute irrotational motion in the vaneless diffuser, the absolute tangential velocity of the fluid decreases as the radius R increases. The relative tangential velocity therefore takes on large negative values, and the relative streamlines in the vaneless diffuser are steeply sloped in the direction opposite to the impeller rotation. The higher the impeller-tip speed and the lower the volume flow rate, the greater is the slope.

The streamlines for the standard solution are given in Fig. 9(a). For the design and operating conditions of this solution, an eddy has just begun to form on the driving face of the blade. The eddy is attached to the blade, and the fluid in the eddy rotates relative to the impeller with an angular velocity equal and opposite to that of the impeller so that the absolute motion of the fluid is irrotational. Along the blade surface in the region of the eddy, the velocities are directed inward.

An expanded view of the eddy obtained in solution 4 is shown in Fig. 10. The flow rate within the eddy amounts to less than 2

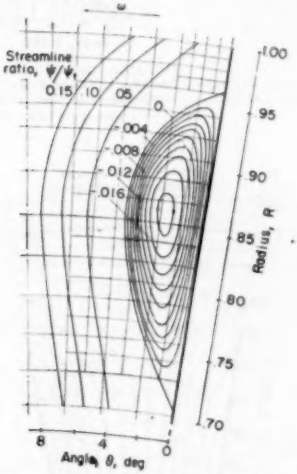

FIG. 10 RELATIVE EDDY ON DRIVING FACE OF BLADE IN SOLUTION 4 (Streamline designation indicates percentage of flow through passage between streamline and driving face of blade; right side of passage. Flow coefficient φ, 0.5; impeller-tip Mach number M_T, 1.5; constant flow area; angular blade-spacing σ, 18 deg; compressible flow, γ, 1.4.)

per cent of the flow rate through the impeller (as indicated by the designation of the streamlines). This low flow rate indicates low relative velocities within the eddy. The relative velocity at the center of the eddy is zero.

In actual practice, large eddies are probably unstable and it is desirable to avoid these eddies by proper design and operating conditions of the impeller. From an inspection of Fig. 9 it appears that the eddy can be reduced or eliminated by increasing the flow coefficient φ (compare Fig. 9a with Figs. 9b and 9c) decreasing the impeller-tip Mach number M_T (compare Figs. 9a and 9d) decreasing the angular blade spacing σ (compare Figs. 9a and 9e) using incompressible fluids (compare Figs. 9e and 9f) and by curving the blades backward (compare Fig. 9e with Figs. 9g and 9h). (It will be shown in Part 2 that the eddy is also reduced or eliminated by curving the blades forward.)

For a given impeller geometry, the size of the eddy depends upon the relative magnitudes of the volume flow rate per unit flow area (that is, the average meridional velocity Q_M) and the impeller-tip speed. If the volume flow rate is zero, the eddy occupies the entire passage between blades, and its "rotational speed" increases directly with the impeller-tip speed. As the volume flow rate increases (for a fixed impeller-tip speed), the eddy decreases in size until it finally disappears. The flow rate at which the eddy disappears increases as the impeller-tip speed increases. This same trend is characteristic of compressor surge, and instability of the eddy flow is suggested as a possible exciting force for surge in centrifugal-type compressors. At high impeller-tip speeds, large eddies can occur even for sizable values of the flow rate. For example, in Fig. 9(d) (standard flow rate but impeller-tip Mach number of 2.0), the eddy occupies more than one half of the available flow area at a radius of 0.90. In actual practice, however, boundary-layer phenomena can be expected to reduce the effective flow area of the passage, thus increasing the volume flow rate per unit area through the effective flow area and thereby reducing the size of the eddy considerably. The eddy does not exist in the incompressible-flow solution (Fig. 9f) because, although the corresponding compressible-flow solution has a rather large eddy (Fig. 9e) the volume flow rate is higher for incompressible flow as a result of the lower fluid density ρ_0 in the region of the impeller tip.

For a given impeller-tip speed and compressor flow rate, the eddy is reduced or eliminated by curving the impeller blades backward (Figs. 9g and 9h) or forward, because the effective flow area across the passage along a normal between blades is reduced, thus increasing the volume flow rate per unit area and thereby reducing the size of the eddy. Also, for a given impeller-tip speed and compressor flow rate, the eddy is reduced or eliminated by increasing the number of blades (that is, decreasing σ) because the decreased blade loading causes the velocity Q_d along the driving face of the blade to become more nearly equal to the mean channel velocity, thus increasing Q_d and thereby reducing or eliminating the eddy which is characterized by negative velocities along the blade surface.

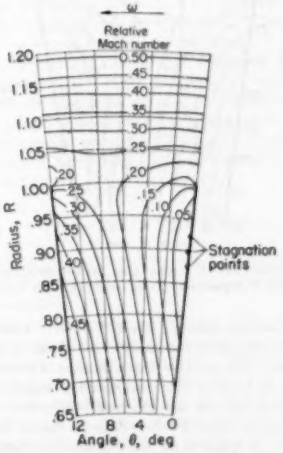

(a) Standard solution: Straight blades (β_b, 0); flow coefficient φ 0.5; impeller-tip Mach number M_T, 1.5; constant flow area; angular blade-spacing σ, 12 deg; compressible flow (γ, 1.4)

FIG. 11 LINES OF CONSTANT MACH NUMBER RELATIVE TO IMPELLER (Solutions, Figs. 11b to 11h, follow.)

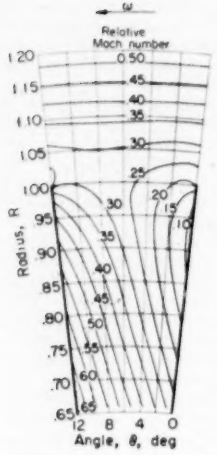

FIG. 11(*b*) SOLUTION 1: FLOW COEFFICIENT φ, 0.7; OTHER PARAMETERS SAME AS STANDARD SOLUTION, FIG. 11(*a*)

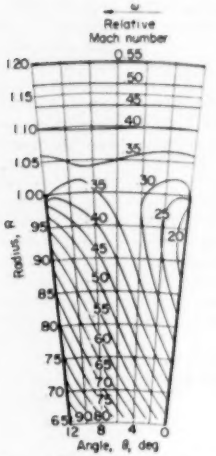

FIG. 11(*c*) SOLUTION 2: FLOW COEFFICIENT φ, 0.9; OTHER PARAMETERS SAME AS STANDARD SOLUTION, FIG. 11(*a*)

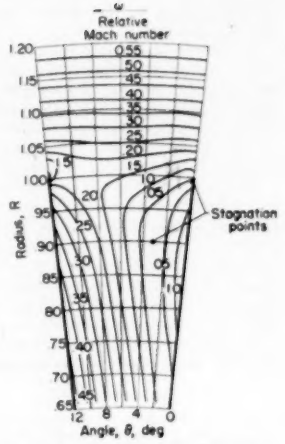

FIG. 11(*d*) SOLUTION 3: IMPELLER-TIP MACH NUMBER M_T, 2.0; OTHER PARAMETERS SAME AS STANDARD SOLUTION, FIG. 11(*a*)

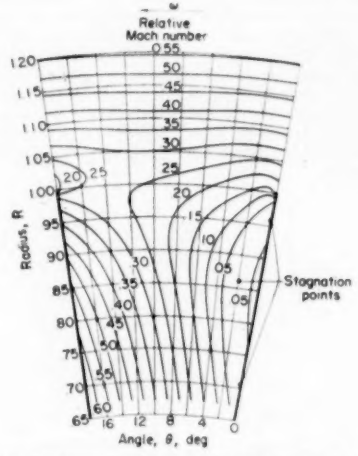

FIG. 11(*e*) SOLUTION 4: ANGULAR BLADE-SPACING σ, 18 DEG; OTHER PARAMETERS SAME AS STANDARD SOLUTION

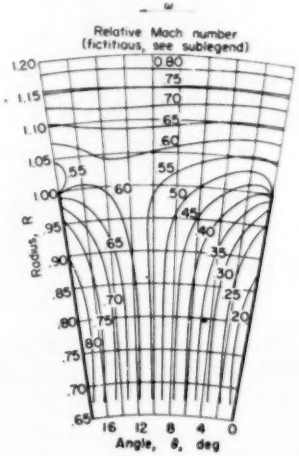

FIG. 11(*f*) SOLUTION 5: INCOMPRESSIBLE FLUID; OTHER PARAMETERS SAME AS SOLUTION 4, FIG. 11(*e*)

(Note that φ and M_T are based upon same constant c_o, the magnitude of which is equal to speed of sound at inlet conditions for compressible solutions. For incompressible fluids, relative Mach number becomes fictitious and is equal to the relative velocity Q measured in units of c_o.)

Lines of Constant Relative Mach Number. Lines of constant Mach number relative to the impeller are shown in Fig. 11 for the eight solutions. The relative Mach number is defined as the relative velocity divided by the local speed of sound c. The Mach number plotted for the incompressible solution (Fig. 11*f*) is a fictitious quantity equal to the relative velocity Q in which the denominator c_o is equal to the inlet stagnation speed of sound for the compressible solutions. As already mentioned, this inlet stagnation speed of sound is also contained in the denominators of φ and M_T so that for incompressible solutions, in which Q, φ, and M_T always appear as ratios, the results are independent of the assigned value of c_o.

The standard solution is given in Fig. 11(*a*). The general characteristics of these plots are similar. The velocities (as indicated by the Mach number lines) along the driving face of the blade are low; the velocities along the trailing face (blade surface opposed to the direction of rotation) are high; and the velocities become equal on both the driving and trailing faces at the blade tip (as required by the Joukowski condition). At the stagnation points indicated in the figures, the relative Mach number is zero. These stagnation points result from the relative eddies discussed in the

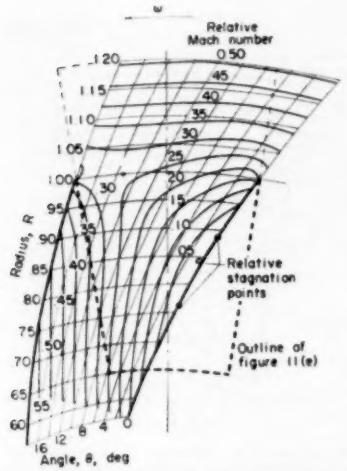

FIG. 11(*g*) SOLUTION 6: BACKWARD-CURVED, LOGARITHMIC-SPIRAL BLADES [β_b, TAN^{-1} (—0.5)]; OTHER PARAMETERS SAME AS SOLUTION 4, FIG. 11(*e*)

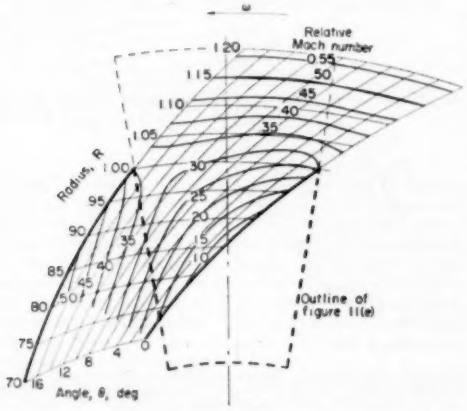

FIG. 11(*h*) SOLUTION 7: BACKWARD-CURVED, LOGARITHMIC-SPIRAL BLADES [β_b, TAN^{-1} (—1.0)]; OTHER PARAMETERS SAME AS SOLUTION 4, FIG. 11(*e*)

section on streamlines. The maximum Mach number occurs on the trailing face of the blade at a radius well within the impeller, and the flow decelerates along the face of the blade from this point to the blade tip. This deceleration, which becomes rapid near the blade tip, is conducive to boundary-layer separation, which lowers the compressor efficiency. The deceleration is seen to decrease as the blades become more backward-curved. (Compare Figs. 11*e*, 11*g*, and 11*h*.)

If boundary-layer effects are neglected, the nonuniformity of the velocities at the impeller tip becomes negligible at a radius of approximately 1.10 for σ equal to 12 deg (Figs. 11*a* to 11*d*) and at a radius of approximately 1.15 for σ equal to 18 deg (Figs. 11*e* to 11*h*). Flow conditions in the vaneless portion of the diffuser immediately following the impeller, therefore, become essentially uniform at a ratio of $(\ln R)/\sigma$ approximately equal to 0.45. This rapid adjustment of the flow indicates that, provided the absolute velocity is subsonic and provided the boundary layer can be neglected or mixes rapidly in the diffuser, vaned diffusers can be located quite close ($\ln R/\sigma = 0.45$) to the impeller tip without appreciable losses resulting from poor (unsteady) velocity distribution relative to the stationary diffuser vanes. However, in the event of boundary-layer separation on the impeller-blade surfaces, the velocity distribution should be considerably more irregular than obtained in these solutions.

The average relative Mach number at the impeller tip is low (even for large values of φ and for backward-curved blades) because of the high impeller-tip Mach numbers, which result in high fluid densities and therefore low velocities. In practice, however, separated boundary layers, resulting from large velocity decelerations along the blade surfaces, reduce the effective flow area of the impeller passage and thereby increase the average relative Mach number at the impeller tip.

From an inspection of Fig. 11 it appears that the maximum relative Mach number (on the trailing face of the blade) is increased by increasing the flow coefficient φ (compare Fig. 11*a* with Figs. 11*b* and 11*c*), is apparently not much affected by increasing the impeller-tip Mach number M_T (compare Figs. 11*a* and 11*d*), is increased by increasing the angular blade-spacing σ (compare Figs. 11*a* and 11*e*), or by changing to an incompressible fluid (compare Figs. 11*e* and 11*f*), and is not much affected (for the range investigated) by curving the blades backward (compare Fig. 11*e* with Figs. 11*g* and 11*h*). Some reasons for the foregoing behavior will be given in Part 2.

Lines of Constant Static-Pressure Ratio. Lines of constant static-pressure ratio (local static pressure divided by the absolute inlet stagnation pressure) are shown in Fig. 12 for four of the solutions. The standard solution is given in Fig. 12(*a*). The general characteristics of these plots are the same (and for this reason plots are not included for all of the solutions). At a given radius, the pressure ratio is higher on the driving face of the blade than on the trailing face except at the blade tip where the pressure ratios are equal (the blade unloads). This difference in pressure ratio accounts for the impeller torque.

From Figs. 12(*b*), 12(*c*), and 12(*d*) it is interesting to note that as the logarithmic-spiral blades become more backward-curved, the static-pressure ratio at the impeller tip remains essentially unchanged, although of course the work input and, therefore, the absolute total pressure decreases. The reason for this small effect of blade curvature on the static-pressure ratio at the impeller tip is evident from

$$\frac{p}{p_o} = \left\{1 + \frac{\gamma - 1}{2}\left[(RM_T)^2 - Q^2 - 2M_T\lambda_U\right]\right\}^{\frac{\gamma}{\gamma-1}} \quad \ldots [9]$$

which shows that, if $(RM_T)^2 \gg Q^2$ at the impeller tip, p/p_o is only slightly affected by the increase in Q that results when the blades are curved backward.

The absolute kinetic energy of the fluid at the discharge from the impeller is proportional to the difference between the absolute total pressure and the static pressure. Therefore this kinetic energy decreases and becomes a smaller per cent of the total energy input as the blades become more backward-curved (because, if $M_T^2 >> Q^2$, the static pressure ratio remains essentially constant whereas the absolute total pressure decreases). If impellers are more efficient than diffusers, as is generally the case, compressors with backward-curved impeller blades are more efficient than compressors with straight impeller blades, not so much because the impeller is more efficient (as it might be, because of the lower blade loading), but rather because the kinetic

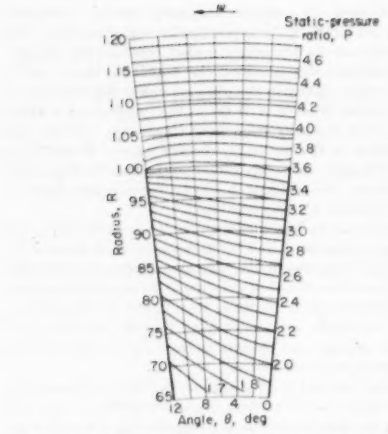

(a) Standard Solution: Straight blades (β_b, 0); flow coefficient φ 0.5; impeller-tip Mach number M_T, 1.5; constant flow area; angular blade-spacing σ, 12 deg; compressible flow (γ, 1.4)

FIG. 12 LINES OF CONSTANT STATIC-PRESSURE RATIO
(Solutions Figs. 12b to 12d, follow.)

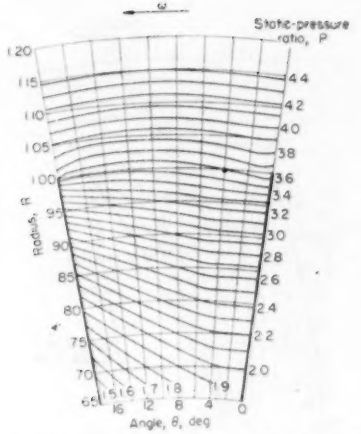

FIG. 12(b) SOLUTION 4: ANGULAR BLADE-SPACING σ, 18 DEG; OTHER PARAMETERS SAME AS STANDARD SOLUTION, FIG. 12(a)

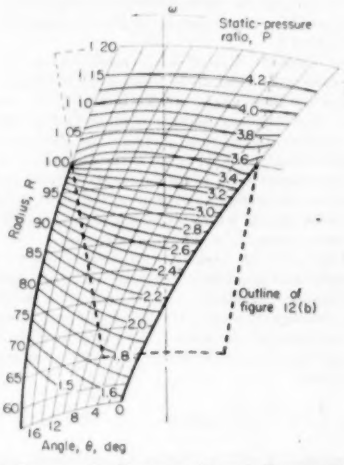

FIG. 12(c) SOLUTION 6: BACKWARD-CURVED, LOGARITHMIC-SPIRAL BLADES [β_b, TAN^{-1} (−0.5)]; OTHER PARAMETERS SAME AS SOLUTION 4, FIG. 12(b)

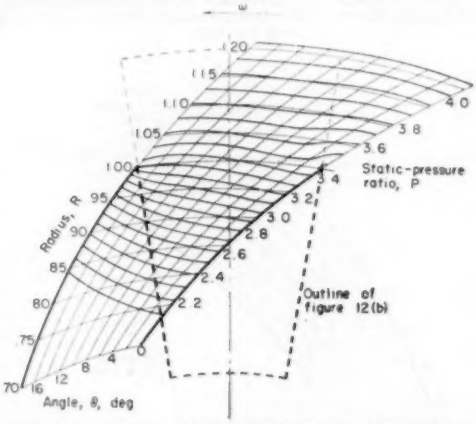

FIG. 12(d) SOLUTION 7: BACKWARD-CURVED, LOGARITHMIC-SPIRAL BLADES [β_b, TAN^{-1} (−1.0)]; OTHER PARAMETERS SAME AS SOLUTION 4, FIG. 12(b)

energy that must be converted to static pressure in the diffuser is a smaller per cent of the total energy input. In a similar manner it can be concluded that compressors with forward-curved impeller blades are less efficient (than compressors with straight impeller blades) because the absolute kinetic energy at the impeller discharge is a greater per cent of the total energy input.

Velocity Distribution Along Blade Surfaces. The relative velocity distribution along the driving and trailing faces of the blades, Q_d and Q_t, are of special interest because of boundary-layer considerations. These velocities are plotted in Fig. 13 for the eight blade-to-blade solutions as a function of the radius R.

For the simple geometric blade shapes investigated (straight and logarithmic spiral) the velocity decelerates rapidly in all eight solutions along the trailing face of the blade near the impeller tip.

Negative values of Q along the driving face of the blade indicate the presence of a relative eddy. Detailed examinations of the effect of φ, M_T, σ, and β_b on Q_d and Q_t will be given in Part 2.

A measure of the tendency for boundary-layer separation (or its equivalent in a rotating channel) from the blade surfaces is given by the term

$$\frac{\delta}{Q}\frac{dQ}{dS}$$

where δ is the boundary-layer thickness in units of the tip radius r_T, and S is distance along the blade surface, likewise in units of the tip radius. For a given value of δ the more negative the value of

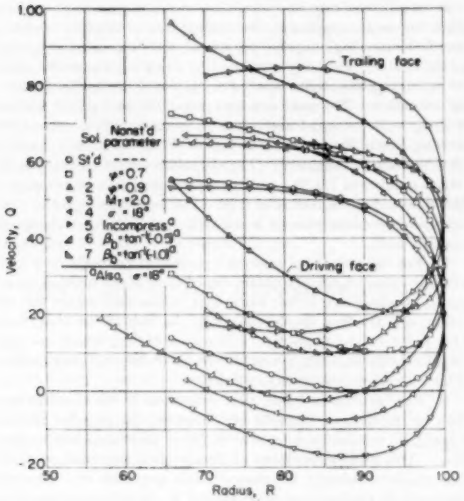

FIG. 13 DISTRIBUTION OF VELOCITIES Q_d AND Q_t ALONG DRIVING AND TRAILING FACES OF BLADE FROM RELAXATION SOLUTIONS

$$\frac{1}{Q}\frac{dQ}{dS}$$

the more likely is separation of the boundary layer. In Fig. 14

$$\frac{1}{Q}\frac{dQ}{dS}$$

is shown as a function of R at the critical region along the trailing face of the blade near the impeller tip for the two backward-curved, logarithmic-spiral blades (solutions 6 and 7, Table 1) and for the corresponding straight blade (solution 4). It is evident that for the same impeller-tip speed, etc., adverse velocity gradients at the critical region along the trailing face of the blade near the tip are less for backward-curved, logarithmic-spiral blades than for straight blades. This same situation was found to exist when M_T was adjusted so that the work input was the same for the three impellers considered in Fig. 14.

From the standpoint of velocity gradients along blade surfaces, the mixed-flow centrifugal impeller possesses some distinct advantages over the radial-flow type. Any solution obtained for flow between blades in a two-dimensional radial-flow impeller also applies (8) to certain equivalent mixed-flow impellers with a smaller number of geometrically similar passages lying on a conic flow surface. Such an equivalent mixed-flow impeller has the same velocity distribution as a function of the radius ratio R along the blade surfaces. However, the velocity gradient in terms of the distance S along the blade surface becomes

$$\frac{dQ}{dS} = \frac{dQ}{dR}\frac{dR}{dS} = \frac{dQ}{dR}\sin\alpha$$

where $(dQ)/(dR)$ is the same for equivalent radial and mixed-flow impellers. Thus the velocity gradient in mixed-flow impellers with conic flow surfaces is less than the velocity gradient in radial-flow impellers by a ratio equal to $\sin\alpha$. The same conclusion is expected to apply qualitatively to any mixed-flow impeller with arbitrary profile in the meridional plane, provided the passages between blades are geometrically similar for both the radial and mixed-flow impellers. Furthermore, if the number of blades in the mixed-flow impeller is increased to the same number in the radial-flow impeller, a further reduction in the velocity gradients should result from the decrease in σ (in Fig. 13, compare solution 4 with the standard solution). Therefore, in general, mixed-flow centrifugal compressors should be more efficient than the radial-flow type.

Slip Factor. The impeller slip factor μ is defined as the ratio of the average absolute tangential velocity at the impeller tip to the tip speed of the impeller. The slip factors have been computed for each of the eight blade-to-blade solutions and are given in Table 2.

TABLE 2 IMPELLER SLIP FACTORS

Solution	Nonstandard parameter	Slip factor
Standard	.....	0.934
1	$\varphi = 0.7$	0.937
2	$\varphi = 0.9$	0.938
3	$M_T = 2.0$	0.935
4	$\sigma = 18°$	0.909
5	Incompressible[a]	0.892
6	$\beta_b = \tan^{-1}(-0.5)$[a]	0.834
7	$\beta_b = \tan^{-1}(-1.0)$[a]	0.768

[a] Also, $\sigma = 18$ deg.

It appears that σ and β_b are the only variables investigated that affect the computed slip factor. In particular, it will be noted that the slip factor is approximately the same for compressible and incompressible flow (compare solutions 4 and 5) although the streamline configurations for the two examples are very different (compare Figs. 9*e* and 9*f*). The angular blade-spacing σ affects the slip factor because, as the blades are spaced farther apart they

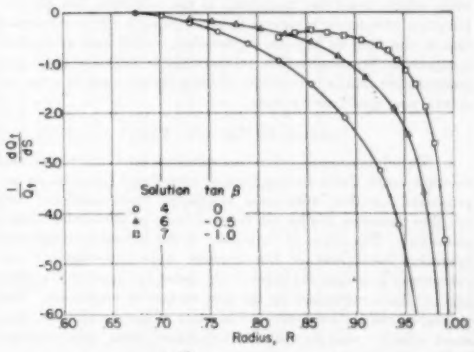

FIG. 14 VARIATION IN $\frac{1}{Q}\frac{dQ}{dS}$ WITH RADIUS ALONG TRAILING FACE OF BLADE FOR THREE VALUES OF BLADE ANGLE β_b

(Flow coefficient φ, 0.5; impeller-tip Mach number M_T, 1.5; constant flow area; angular blade-spacing σ, 18 deg; compressible flow, γ, 1.4.)

exert less influence on the average flow direction at the impeller tip so that the slip factor decreases. For an infinite number ($\sigma = 0$) of straight blades the fluid is perfectly guided in the radial direction at the impeller tip and the slip factor μ is unity.

Based on the numerical results of the six relaxation solutions for $\beta_b = 0$ the following expression has been derived (9) for the slip factor of impellers with straight blades

$$\mu = 1 - 0.315\sigma$$

Stodola's expression for the slip factor of impellers with straight blades is

$$\mu = 1 - 0.500\sigma$$

Thus both equations agree that for straight blades the slip factor depends only on the angle σ. Stodola's equation, however, indicates a somewhat smaller slip factor than was obtained by the relaxation solutions.

As would be expected, the slip factor is less for backward-curved blades than for straight blades (in Table 2 compare solutions 6 and 7 with 4) because for backward-curved blades the tangential component of the relative velocity is opposed to the direction of rotation, thus reducing the absolute tangential velocity. If the slip factor is corrected by adding this tangential component of the relative flow, assuming the fluid is perfectly guided by the blades, the corrected slip factors become

Solution	β_b	$\mu_{corrected}$
4	$\tan^{-1}(0)$	0.899
6	$\tan^{-1}(-0.5)$	0.901
7	$\tan^{-1}(-1.0)$	0.904

These corrected values of μ are approximately equal and it is concluded, therefore, that the slip velocity (which is defined as the actual average absolute tangential velocity of the fluid at the impeller tip minus the ideal absolute tangential velocity, assuming perfect guiding of the fluid by the blades) is the same for the range of negative blade angle β_b investigated. This conclusion is not in agreement with the well-known Stodola correction which assumes the slip velocity varies directly with $\cos \beta_b$.[4]

Compressibility Effects. The large effect of compressibility upon the streamline configuration (and, therefore, upon the other flow conditions) is shown by a comparison of Figs. 9(*e*) and 9(*f*). The large eddy that exists for compressible flow completely disappears for incompressible flow. Fig. 11 shows large compressibility effects upon the magnitude of the velocities, but the distribution of velocity is similar in some respects. It is concluded that if the fluid in high-speed, rotating, radial and mixed-flow compressors is compressible, incompressible solutions give poor quantitative results (exception, the slip factor) and, in some respects, poor qualitative results.

Summary of Results—Part I

1 Two-dimensional, relaxation solutions for compressible and incompressible fluids in impellers of centrifugal compressors are presented for flow with axial symmetry (two solutions) and for flow between blades on flow surfaces of revolution (eight solutions). The effect of variations in the following design and operating conditions of the impeller were investigated: (*a*) compressor flow rate, (*b*) impeller-tip speed, (*c*) number of blades, and (*d*) blade curvature on the flow surface of revolution. The numerical results are presented in plots of the streamlines, constant relative velocity (or Mach-number) lines, and constant static-pressure lines.

2 For incompressible flow, streamlines in the meridional plane (axial-symmetry solution) are the same with or without thin, straight blades that lie on meridional planes. (The streamlines are almost the same with or without thin blades that are curved about the axis of the impeller.)

3 Just ahead of the inducer the velocity accelerates along the shroud and decelerates along the hub.

4 For incompressible, axial-symmetry solutions based on the mean blade surface, the influence of the curved inducer vanes on the velocity distribution does not extend far into the impeller.

5 The rapid deceleration of the flow along the shroud in the compressible, axial-symmetry solution results from the compressibility of the fluid and is probably one reason that centrifugal pumps (incompressible fluids) are generally more efficient than centrifugal compressors (compressible fluids).

[4] Reference (1), p. 1259.

6 A relative eddy, the instability of which may be an exciting force for surge, appears on the driving face of impeller blades at low flow rates, high impeller-tip speeds, and large angular spacing of the blades. The eddy is reduced by using incompressible fluids or by curving the blades forward or backward on the flow surfaces of revolution. The eddy rotates relative to the impeller with an angular velocity equal and opposite to the impeller. Along the driving face of the blade in the region of the eddy, the velocity is directed inward (negative). For the solution with an impeller-tip Mach number of 2.0, the eddy occupies more than 50 per cent of the flow area at a radius of 0.90. For zero flow rate the eddy occupies the entire passage at all radii for all impeller-tip speeds (except zero).

7 For the numerical examples presented (straight and logarithmic-spiral blades) the maximum relative Mach number occurs on the trailing face of the blade at a radius well within the impeller, and the flow decelerates along the face of the blade from this point to the blade tip. This deceleration, which becomes rapid near the blade tip, is conducive to boundary-layer separation, which lowers the compressor efficiency.

8 For nonviscous fluids, flow conditions in the vaneless portion of the diffuser immediately following the impeller become essentially uniform at a ratio of $(\ln R)/\sigma$ approximately equal to 0.45. This rapid adjustment of the flow indicates that, provided the absolute velocity is subsonic, and provided the boundary layer can be neglected or mixes rapidly in the vaneless part of the diffuser, vaned diffusers can be located quite close ($\ln R = 0.45\sigma$) to the impeller tip without appreciable losses resulting from poor (unsteady) velocity distribution relative to the stationary diffuser vanes.

9 For high impeller-tip Mach numbers (and if the boundary layer is neglected) the average relative Mach number at the impeller tip is low (even for the large values of flow rate and for the range of backward-curved blades investigated).

10 At a given radius the velocity is lower on the driving face of the blade than on the trailing face, except at the impeller tip where both velocities are equal. Therefore the static pressure is higher on the driving face of the blade than on the trailing face, except at the impeller tip where both pressures are equal. This difference in pressure accounts for the impeller torque.

11 If the impeller-tip speed is large compared to the average relative velocity at the impeller tip, the static pressure at the impeller tip is essentially the same for impellers with straight blades and for impellers with backward or forward-curved blades, although the work input and, therefore, the absolute total pressure, is less for backward-curved blades and greater for forward-curved blades.

12 If impellers are more efficient than diffusers, and if the impeller-tip speed is large compared to the average relative velocity at the impeller tip, compressors with backward-curved impeller blades are, in general, more efficient than compressors with straight impeller blades, not so much because the impeller is more efficient (as it might be, because of the lower blade loading) but rather because less kinetic energy (in per cent of the total energy input) must be converted to static pressure in the diffuser—a process which is relatively inefficient.

13 For the same impeller-tip speed, compressor flow rate, and so forth, adverse velocity gradients at the critical region along the trailing face of the blade near the tip are less for backward-curved, logarithmic-spiral blades than for straight blades.

14 Mixed-flow impellers should be more efficient than radial-flow impellers, because, for the same number of similarly shaped blades, the velocity gradients are considerably less in mixed-flow impellers.

15 The computed impeller slip factor is independent of the

impeller-tip speed, the compressor flow rate, and the compressibility of the fluid. The slip factor is a function only of the blade spacing (number of blades) and the blade curvature on flow surfaces of revolution.

16 The slip factor is less for backward-curved blades than for straight blades but, if the slip factor is corrected for the average relative tangential velocity at the impeller tip, assuming perfect guiding of the fluid by the blades, this "corrected" slip factor is a function of the blade spacing only (for the range of impeller-blade discharge angle investigated).

17 Compressibility has a large effect upon the streamline configuration and on the magnitude of the relative velocity. Compressibility does not affect the slip factor.

PART 2 APPROXIMATE METHODS OF ANALYSIS

Introduction

The relaxation solutions presented in Part 1 of this paper required a large amount of computing. Therefore it would be advantageous to have quicker means, even if less accurate, of estimating the flow conditions within impellers. In Part 2 of this paper three approximate methods of analysis are considered for blade-to-blade solutions on flow surfaces of revolution. The three methods apply to different regions of the passage between impeller blades and to different impeller configurations.

Correlation Equations for Straight Blades on Conic Flow Surfaces of Revolution

The first, and most accurate, of the three approximate methods of analysis is limited to impellers with thin, straight blades on conic flow surfaces; that is, the blade angle β_b on a conic flow surface of revolution is zero. For this method of analysis correlation equations were developed (9) whereby the flow conditions (Q_θ, Q_M, and ψ/ψ_t) in any impeller with straight blades on a conic flow surface can be determined (in the region between blades near the impeller tip) for all operating conditions from the known flow conditions of the "standard" solution presented in Part 1. These known flow conditions of the standard solution are given in Tables 3, 4, and 5. The correlation equations were developed in terms of $(\ln R)/\sigma$ and $(\theta \sin \alpha)/\sigma$ (where θ is zero along the driving face), that is, the flow conditions at a point $[(\ln R)/\sigma, (\theta \sin \alpha)/\sigma]$ of a given impeller are obtained from the flow conditions of the standard solution at the same value of $(\ln R)/\sigma$ and $(\theta \sin \alpha)/\sigma$. The method of analysis is developed in reference (9). Only the final equations and their application are considered herein.

Stream-Function Ratio ψ/ψ_t. The stream-function ratio ψ/ψ_t varies across the impeller passage from 0 along the driving face of

TABLE 3 STREAM-FUNCTION RATIO ψ/ψ_t FOR STANDARD SOLUTION OF PART 1

[Conditions for standard example: $(\varphi)_s = 0.5$; $(Mr)_s = 1.5$; constant flow area; $\sigma_s = 0.20944$ radians; $(\gamma)_s = 1.4$]

		$\ln \frac{R}{\sigma}$	$\frac{\theta \sin \alpha}{\sigma}$										
$[(Q_M)_{s=1}]_c$	R_c		0	0.1	0.2	0.3	0.4	0.5	0.6	0.7	0.8	0.9	1
0.3168	0.70	−1.7030	0	0.040	0.095	0.165	0.244	0.341	0.451	0.570	0.702	0.848	1.0
0.2941	0.75	−1.3736	0	0.031	0.078	0.143	0.220	0.316	0.427	0.549	0.686	0.840	1.0
0.2735	0.80	−1.0654	0	0.022	0.061	0.120	0.197	0.291	0.401	0.529	0.671	0.831	1.0
0.2536	0.85	−0.7760	0	0.014	0.047	0.101	0.177	0.270	0.383	0.509	0.655	0.824	1.0
0.2348	0.90	−0.5031	0	0.011	0.042	0.097	0.171	0.265	0.377	0.503	0.650	0.819	1.0
0.2275	0.92	−0.3981	0	0.012	0.046	0.102	0.177	0.270	0.382	0.506	0.651	0.816	1.0
0.2202	0.94	−0.2954	0	0.016	0.054	0.113	0.189	0.283	0.392	0.517	0.660	0.820	1.0
0.2133	0.96	−0.1949	0	0.023	0.069	0.132	0.212	0.305	0.413	0.536	0.675	0.828	1.0
0.2100	0.97	−0.1454	0	0.029	0.080	0.146	0.228	0.321	0.429	0.550	0.684	0.832	1.0
0.2067	0.98	−0.0965	0	0.038	0.093	0.163	0.247	0.341	0.447	0.566	0.697	0.839	1.0
0.2034	0.99	−0.0480	0	0.048	0.111	0.185	0.270	0.366	0.472	0.586	0.713	0.850	1.0
0.2002	1.00	0	0	0.062	0.133	0.210	0.297	0.393	0.499	0.611	0.734	0.862	1.0

TABLE 4 MERIDIONAL VELOCITY Q_M FOR STANDARD SOLUTION OF PART 1

[Conditions for standard example: $(\varphi)_s = 0.5$; $(Mr)_s = 1.5$; constant flow area; $\sigma_s = 0.20944$ radians; $(\gamma)_s = 1.4$]

		$\ln \frac{R}{\sigma}$	$\frac{\theta \sin \alpha}{\sigma}$										
$[(Q_M)_{s=1}]_c$	R_c		0	0.1	0.2	0.3	0.4	0.5	0.6	0.7	0.8	0.9	1.0
0.3168	0.70	−1.7030	0.103	0.146	0.190	0.234	0.278	0.323	0.368	0.412	0.456	0.501	0.549
0.2941	0.75	−1.3736	0.065	0.112	0.159	0.206	0.253	0.301	0.348	0.396	0.443	0.492	0.543
0.2735	0.80	−1.0654	0.033	0.082	0.133	0.181	0.230	0.280	0.329	0.378	0.428	0.479	0.533
0.2536	0.85	−0.7760	0.008	0.059	0.110	0.160	0.210	0.259	0.309	0.357	0.408	0.460	0.515
0.2348	0.90	−0.5031	−0.001	0.049	0.099	0.148	0.194	0.239	0.285	0.330	0.378	0.430	0.483
0.2275	0.92	−0.3981	0.002	0.051	0.100	0.146	0.189	0.231	0.273	0.316	0.363	0.413	0.463
0.2202	0.94	−0.2954	0.010	0.058	0.105	0.148	0.186	0.224	0.261	0.299	0.342	0.390	0.438
0.2133	0.96	−0.1949	0.025	0.072	0.115	0.151	0.184	0.216	0.248	0.280	0.316	0.360	0.407
0.2100	0.97	−0.1454	0.037	0.082	0.122	0.155	0.184	0.213	0.241	0.270	0.301	0.342	0.388
0.2067	0.98	−0.0965	0.055	0.095	0.131	0.158	0.184	0.209	0.234	0.259	0.286	0.321	0.362
0.2034	0.99	−0.0480	0.091	0.115	0.139	0.161	0.184	0.205	0.227	0.249	0.271	0.293	0.316
0.2002	1.00	0	0.199	0.131	0.148	0.166	0.184	0.202	0.220	0.238	0.254	0.271	0.199

TABLE 5 RELATIVE TANGENTIAL-VELOCITY Q_θ FOR STANDARD SOLUTION OF PART 1

[Conditions for standard example: $(Mr)_s = 1.5$; $\sigma_s = 0.20944$ radians]

	$\ln \frac{R}{\sigma}$	$\frac{\theta \sin \alpha}{\sigma}$										
R_c		0	0.1	0.2	0.3	0.4	0.5	0.6	0.7	0.8	0.9	1.0
0.70	−1.7030	0	0.008	0.015	0.020	0.023	0.024	0.023	0.020	0.015	0.008	0
0.75	−1.3736	0	0.008	0.015	0.020	0.023	0.024	0.023	0.020	0.015	0.008	0
0.80	−1.0654	0	0.008	0.014	0.018	0.021	0.022	0.021	0.019	0.015	0.008	0
0.85	−0.7760	0	0.005	0.009	0.011	0.012	0.013	0.013	0.012	0.010	0.006	0
0.90	−0.5031	0	−0.002	−0.004	−0.007	−0.008	−0.008	−0.007	−0.005	−0.003	−0.001	0
0.92	−0.3981	0	−0.007	−0.013	−0.018	−0.021	−0.022	−0.021	−0.016	−0.011	−0.005	0
0.94	−0.2954	0	−0.013	−0.024	−0.033	−0.038	−0.039	−0.037	−0.031	−0.022	−0.012	0
0.96	−0.1949	0	−0.023	−0.041	−0.054	−0.061	−0.062	−0.060	−0.052	−0.039	−0.021	0
0.97	−0.1454	0	−0.030	−0.053	−0.068	−0.076	−0.077	−0.074	−0.066	−0.050	−0.029	0
0.98	−0.0965	0	−0.040	−0.067	−0.083	−0.091	−0.094	−0.091	−0.081	−0.065	−0.039	0
0.99	−0.0480	0	−0.053	−0.083	−0.100	−0.109	−0.112	−0.108	−0.099	−0.082	−0.052	0
1.00	0	0	−0.072	−0.102	−0.119	−0.128	−0.131	−0.127	−0.118	−0.100	−0.070	0

one blade to 1.0 along the trailing face of the next blade. At a given point $[(\ln R)/\sigma, (\theta \sin \alpha)/\sigma]$ on the conic flow surface of revolution, the value of the stream-function ratio for any impeller with straight blades and for any operating condition can be estimated by the following correlation equation (reference 9)

$$\frac{\psi'}{\psi_t} = \frac{\theta \sin \alpha}{\sigma} + \frac{A}{(Q_M)_{avg}} \left(\left[(Q_M)_{avg} \left(\frac{\psi}{\psi_t} - \frac{\theta \sin \alpha}{\sigma} \right) \right]_s + \frac{\theta \sin \alpha}{\sigma} \left(\frac{\theta \sin \alpha}{\sigma} - 1 \right) \times \left\{ \frac{(Q_\theta)_s}{2} [\sigma - \sigma_s] + (R - R_s)(M_T \sigma)_s \right\} \right) \quad [17]$$

where the prime indicates estimated value of flow condition (stream-function ratio in this case) at a given point $[(\ln R)/\sigma, (\theta \sin \alpha)/\sigma]$ and the subscript s indicates standard value (from standard solution) of flow condition at the same values of $(\ln R)/\sigma$ and $(\theta \sin \alpha)/\sigma$. Also

$$A = \frac{M_T \sigma}{(M_T \sigma)_s} \quad [17a]$$

$$(Q_M)_{avg} = \frac{\varphi}{\frac{\rho_{avg}}{\rho_o} RH}$$

where, from Equation [10], of Part 1

$$\frac{\rho_{avg}}{\rho_o} = \left\{ 1 + \frac{\gamma - 1}{2} \left[(RM_T)^2 - \left(\frac{\varphi}{\frac{\rho_{avg}}{\rho_o} RH} \right)^2 - 2M_T \lambda_U \right] \right\}^{\frac{1}{\gamma - 1}}$$

where the subscript (avg) indicates the average value at the radius R corresponding to a given value of $(\ln R)/\sigma$.

Relative Velocities Q_M and Q_θ. The meridional velocity Q_M can be estimated by the following correlation equation (reference 9)

$$Q_M' = (Q_M)_{avg} + A[Q_M - (Q_M)_{avg}]_s + A \left[2 \left(\frac{\theta \sin \alpha}{\sigma} \right) - 1 \right] \times \left\{ \frac{(Q_\theta)_s}{2} [\sigma - \sigma_s] + (R - R_s)(M_T \sigma)_s \right\} \quad [18]$$

The relative tangential velocity Q_θ is always zero along the blade surfaces (necessary condition for straight blades) and is maximum halfway between blades. At a given point $[(\ln R)/\sigma, (\theta \sin \alpha)/\sigma]$, Q_θ can be estimated by the following correlation equation (reference 9)

$$Q_\theta' = A(Q_\theta)_s \quad [19]$$

The estimated values of ψ/ψ_t, Q_M, and Q_θ given by Equations [17, 18, 19] have been compared in reference (9) with the values obtained from the six relaxation solutions presented in Part 1 of this paper for $\beta_b = 0$. The agreement was excellent in all cases. As an example of this agreement, the velocity distributions along the driving and trailing faces of the blade obtained from the relaxation solutions are compared in Figs. 15 and 16 with the distributions given by the correlation Equation [18]. The design and operating parameters of the relaxation solutions are given in Table 1, Part 1 of this paper.

An important application of Equation [18] is the determination of velocities along the driving and trailing faces of the blades, because these velocities affect the behavior of the boundary layer on the blades. The velocities have been computed over a wide range of impeller-tip Mach number M_T, flow coefficient φ, and angular blade spacing σ, and the computations are presented in Figs. 17, 18, and 19.

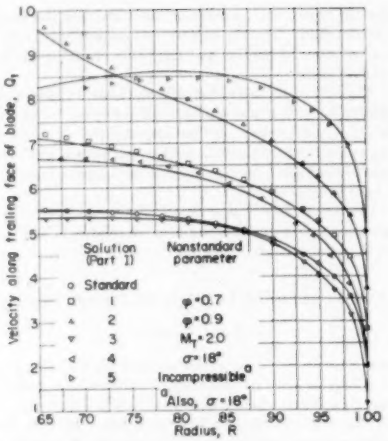

FIG. 15 COMPARISON BETWEEN RELAXATION VALUES AND ESTIMATED VALUES—CORRELATION EQUATION [18]—OF VELOCITY ALONG TRAILING FACE OF STRAIGHT BLADE

(Solid lines obtained from correlation equation; plotted points obtained from relaxation solutions of Part 1.)

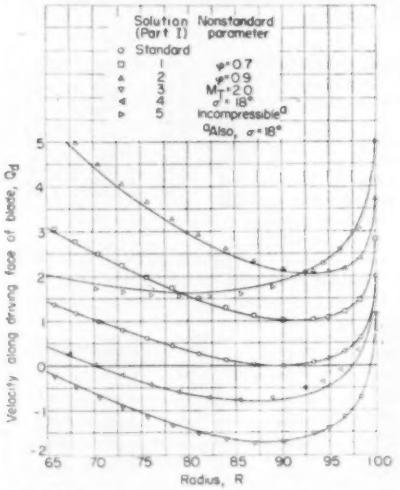

FIG. 16 COMPARISON BETWEEN RELAXATION VALUES AND ESTIMATED VALUES—CORRELATION EQUATION [18]—OF VELOCITY ALONG DRIVING FACE OF STRAIGHT BLADE

(Solid lines obtained from correlation equation; plotted points obtained from relaxation solutions of Part 1.)

Effect of M_T on Q_d and Q_t. The effect of M_T upon the velocities along the driving and trailing faces of a straight blade is shown in Fig. 17. In this figure all design and operating conditions (other than M_T) were maintained constant at the values used for the standard solution in Part 1. For M_T equal to zero the velocities are equal on both faces of the blade. For all other values of M_T the relative velocities are higher on the trailing face than on the driving face (except at the tip) and as the impeller-tip speed

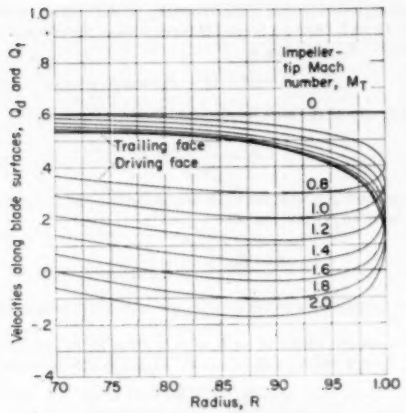

FIG. 17 EFFECT OF IMPELLER-TIP MACH NUMBER UPON VELOCITY ALONG DRIVING AND TRAILING FACES OF STRAIGHT BLADE
(Correlation Equation [18]; flow coefficient φ, 0.5; constant flow area; angular blade spacing σ, 12 deg; compressible flow, γ, 1.4.)

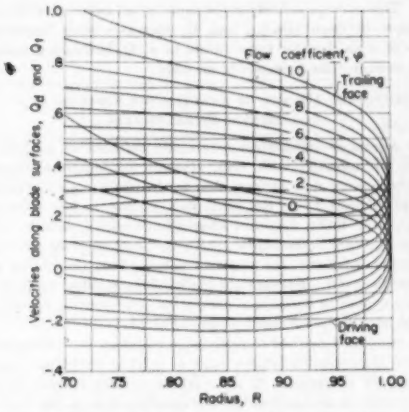

FIG. 18 EFFECT OF FLOW COEFFICIENT UPON VELOCITY ALONG DRIVING AND TRAILING FACES OF STRAIGHT BLADE
(Correlation Equation [18]; impeller-tip Mach number M_T, 1.5; constant flow area; angular blade spacing σ, 12 deg; compressible flow, γ, 1.4.)

increases the difference in velocities along the two faces increases. Except near the tip, this increase in velocity difference results primarily from a decrease in velocity along the driving face, and for high values of M_T this velocity becomes negative, which indicates the presence of an eddy (see Part 1). The small effect of M_T upon Q_t was also evident in Fig. 13 of Part 1, and results from a combination of effects. At higher values of M_T, the difference between Q_t and $(Q_M)_{avg}$ increases (as evidenced by the fact that the difference between Q_t and Q_d increases), but $(Q_M)_{avg}$ itself decreases, because of the increased density, so that the net result is only a small change in Q_t with changes in M_T. At the blade tip the velocities become equal on both surfaces (Joukowski condition), and this velocity decreases with increasing M_T because of the higher gas density.

Effect of φ on Q_d and Q_t. The effect of flow coefficient φ upon the velocities along the driving and trailing faces of a straight blade is shown in Fig. 18. In this figure all design and operating conditions (other than φ) were maintained constant at the standard values. At each radius the difference between Q_t and Q_d is independent of φ (that is, remains constant). The average meridional velocity $(Q_M)_{avg}$, however, decreases with decreasing flow coefficient, so that for low flow coefficients Q_d becomes negative, which indicates the presence of an eddy.

The continued, rapid increase in Q_d and Q_t with decreasing R for the higher values of φ indicates that, for these higher flow rates, choke conditions are being approached at some lower value of R where the average density is lower and $(Q_M)_{avg}$ therefore higher. This condition was also evident in solution 2 (see Fig. 13 of Part 1).

At the blade tip, the velocity becomes equal on both surfaces and this velocity increases with increasing flow coefficient because of the increased average meridional velocity $(Q_M)_{avg}$. For φ equal to zero, that is, for zero flow rate through the impeller, the velocities are equal on both surfaces of the blade (but opposite in sign). As a result, from Equation [9] of Part 1 the pressures on both blade surfaces are equal, and no work is done by the impeller. The entire flow within the passage is an eddy.

Effect of σ on Q_d and Q_t. The effect of the angular blade spacing σ, upon the velocities along the driving and trailing faces of a straight blade is shown in Fig. 19. In this figure all design and

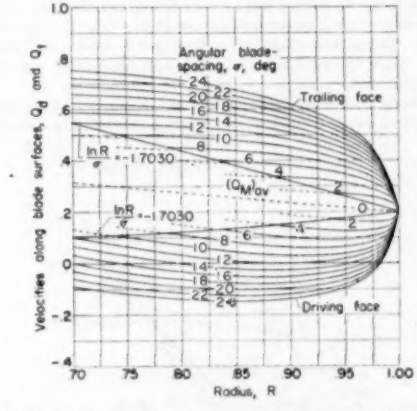

FIG. 19 EFFECT OF ANGULAR BLADE SPACING UPON VELOCITY ALONG DRIVING AND TRAILING FACES OF STRAIGHT BLADE
(Correlation Equation [18]; dashed lines obtained from simplified analysis, Equation [20a]; flow coefficient φ, 0.5; impeller-tip Mach number M_T, 1.5; constant flow area; compressible flow, γ, 1.4.)

operating conditions (other than σ) were maintained constant at the standard values. Increased values of σ indicate fewer blades (for the same cone angle α). The minimum value of $(\ln R)/\sigma$ for which standard values of Q_M are given in Table 4 is —1.7030, which for values of σ less than standard (σ = 12 deg) corresponds to values of R greater than 0.7, as shown in Fig. 19. However, for values of R less than those resulting from $(\ln R)/\sigma$ equal to —1.7030, the simplified method of analysis (to be presented next) may be used to extrapolate the curves to all lesser values of R (provided the inlet configuration to the impeller can be ignored at these lesser values of R). This simplified method of analysis has been used to extrapolate the curves for σ less than 12 deg in Fig. 19 (dashed lines).

For σ equal to zero, the velocities are the same on both surfaces of the blade and are equal to the average velocity $(Q_M)_{avg}$ (dashed

line). This average velocity is the same for all values of σ but the difference between $(Q_M)_{av_8}$ and Q_d increases with increasing values of σ so that for large values of σ, Q_d becomes negative, which indicates the presence of an eddy.

Simplified Method of Analysis for Straight and Logarithmic-Spiral Blades

The second of the three approximate methods of analysis is limited to impellers with thin, straight, or logarithmic-spiral blades on a conic flow surface, that is, the blade angle β_b (Equation [16] of Part 1) on the conic flow surface is zero (straight blades) or a finite constant (logarithmic-spiral blades). For positive values of β_b the blades are forward-curved in the direction of impeller rotation; for negative values of β_b the blades are backward-curved. For straight blades this simplified method of analysis applies to surfaces of revolution generated by curved or straight lines in the medional (axial-radial) plane.

The simplified method of analysis is based on the assumption that for high solidity blades, such as exist in centrifugal compressors, the component of the relative velocity normal to the blade is zero at all radii within the impeller, that is, the fluid is perfectly guided by the blades. This assumption allows an important simplification of the equation for absolute irrotational motion which can then be integrated to give the velocity distribution across the passage along a normal to the blade surfaces. As will be seen, the method can be used to estimate the flow conditions within the impeller everywhere except near the tip (and inlet). The method of analysis is developed in references (7) and (10). Only the final equations and their application are considered herein.

Velocity Distribution Between Blades. Expressed in terms of the cylindrical co-ordinate θ, the equation developed in reference

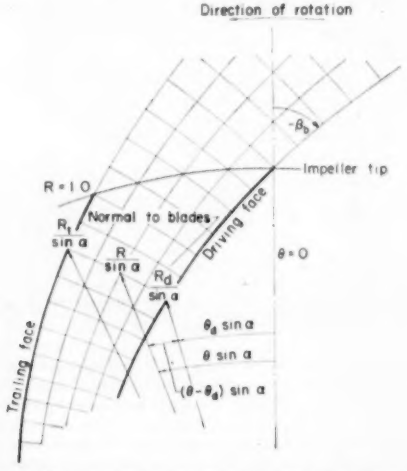

Fig. 20 Nomenclature for Logarithmic-Spiral Blade on Developed Cone Surface

(10) for the distribution of velocity Q along a normal between logarithmic-spiral blades (Fig. 20), becomes

$$Q = Q_d \exp[(\theta - \theta_d) \tan \beta_b \sin \alpha] + \frac{2R_d M_T}{\sin \beta_b} \sinh[(\theta - \theta_d) \tan \beta_b \sin \alpha] \quad [20]$$

where Q_d is determined from continuity considerations (to be discussed later). Along a normal between blades, the radius R varies with $(\theta - \theta_d)$ according to

$$R = R_d \exp[-(\theta - \theta_d) \tan \beta_b \sin \alpha] \quad [21]$$

If θ_d is zero at the impeller tip, then θ_d is related to R_d by

$$\theta_d = \frac{\tan \beta_b}{\sin \alpha} \ln R_d \quad [22]$$

At the trailing face of the blade across the passage along the normal between blades (Fig. 20)

$$(\theta - \theta_d)_t = \frac{\sigma}{\sec^2 \beta_b \sin \alpha} \quad [23]$$

Thus, from Equations [20] to [23], Q is a known function of R and θ.

For straight blades $\beta_b \to 0$ so that, from Equations [21] and [22], $\theta_d \to 0$ and $R \to R_d = \text{const}$. Equation [20] becomes

$$Q = Q_d + 2RM_T \theta \sin \alpha \quad [20a]$$

which agrees with the expression derived in reference (7) (note the different definition of θ in reference 7).

Stream-Function Distribution Between Blades. The distribution of the stream function ψ (defined by Equation [B-3] (Appendix B) along a normal between blades is given by reference (10)

$$\psi = \frac{\sin \alpha}{\cos \beta_b} \int_0^{\theta - \theta_d} \frac{\rho}{\rho_o} HRQ \, d(\theta - \theta_d) \quad [24]$$

where H is a known function of R, R is a function of $(\theta - \theta_d)$, given by Equation [21], Q is a function of $(\theta - \theta_d)$, given by Equation [20], and ρ/ρ_o is a function of Q, given by Equation [10] of Part 1. To determine Q_d in Equation [20], Equation [24] is integrated numerically across the passage along the normal to give

$$\psi_t = \frac{\sin \alpha}{\cos \beta_b} \int_0^{\left(\frac{\sigma}{\sec^2 \beta_b \sin \alpha}\right)} \frac{\rho}{\rho_o} HRQ \, d(\theta - \theta_d) \quad [25]$$

where from reference (10)

$$\psi_t = \varphi\sigma$$

Equation [25] is satisfied when the proper value of Q_d (determined by trial and error) is contained in the expression for Q (Equation [20]). After the value of Q_d is determined, the variation in ψ with $(\theta - \theta_d)$ along the normal between blades is determined by the numerical solution of Equation [24].

If $\beta_b = 0$ (straight blades), then HR is independent of θ and Equation [24] with Equation [20a] and with Equation [10] of Part 1 integrates to give (reference 7)

$$\psi = \frac{H}{2\gamma M_T}(P_d - P) \quad [26]$$

where the static-pressure ratio P is given by Equation [9] of Part 1 in which Q is given by Equation [20a]. When the proper value of Q_d has been obtained as indicated previously, Equation [26] determines the distribution of ψ across the passage for impellers with straight blades. Equations [24] and [26] were used to determine the distribution of ψ along the upstream boundary between blades for the eight blade-to-blade relaxation solutions in Part 1.

Comparisons With Relaxation Solutions. Some comparisons between results of the simplified method of analysis and the relaxation solutions are given in Figs. 21 and 22. In Fig. 21 the velocity

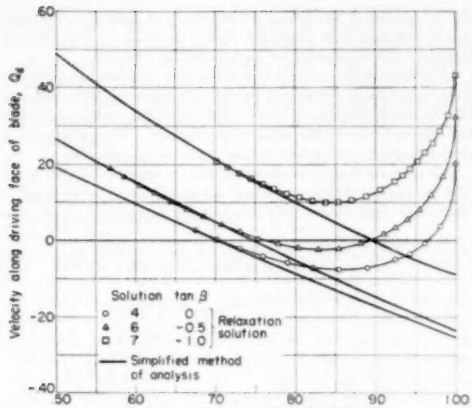

FIG. 21 COMPARISON OF VARIATION IN Q_d WITH R AS OBTAINED BY RELAXATION METHODS—PART 1—AND BY SIMPLIFIED METHOD OF ANALYSIS FOR THREE VALUES OF BLADE ANGLE

(Flow coefficient φ, 0.5; impeller-tip Mach number M_T, 1.5; constant flow area; angular blade-spacing σ, 18 deg; compressible flow, γ, 1.4.)

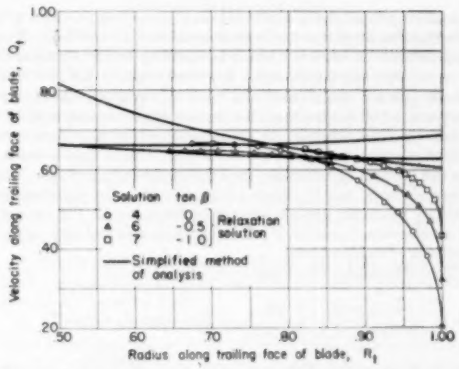

FIG. 22 COMPARISON OF VARIATION IN Q_t WITH R AS OBTAINED BY RELAXATION METHODS—PART 1—AND BY SIMPLIFIED METHOD OF ANALYSIS FOR THREE VALUES OF BLADE ANGLE β_b

(Flow coefficient φ, 0.5; impeller-tip Mach number M_T, 1.5; constant flow area; angular blade-spacing σ, 18 deg; compressible flow, γ, 1.4.)

Q_d is plotted against radius R_d for three values of β_b; in Fig. 22, the velocity Q_t is plotted against R_t for the same values of β_b. The agreement is considered satisfactory away from the impeller tip, and excellent agreement exists for all values of R less than the values shown on these plots.

A Particular Set of Solutions. For backward-curved, logarithmic-spiral blades in general, Equation [24] must be integrated by numerical methods. If, however, the fluid is incompressible ($\rho/\rho_o = 1$) and if the flow area normal to the flow surface of revolution is constant ($HR = 1$) Equation [24] integrates to give (reference 10)

$$\frac{Q_d}{M_T} = \frac{\sin\beta_b}{\exp\left[\dfrac{\sigma\tan\beta_b}{\sec^2\beta_b}\right] - 1} \times \left\{\frac{\varphi}{M_T}\sigma - \frac{2R_d}{\sin^2\beta_b}\left[\cosh\left(\frac{\sigma\tan\beta_b}{\sec^2\beta_b}\right) - 1\right]\right\} \quad \ldots\ldots [27]$$

and, from Equation [20] with

$$(\theta - \theta_d) = (\theta - \theta_d)_i = \frac{\sigma}{\sec^2\beta_b \sin\alpha}$$

$$\frac{Q_t}{M_T} = \exp\left[\frac{\sigma\tan\beta_b}{\sec^2\beta_b}\right]\left\{\frac{Q_d}{M_T} + \frac{2R_t}{\sin\beta_b}\sinh\left(\frac{\sigma\tan\beta_b}{\sec^2\beta_b}\right)\right\} \quad \ldots [28]$$

Equations [27] and [28] give the variation in Q_d/M_T and Q_t/M_T with R, β_b, σ, and φ/M_T. For incompressible flow the speed of sound contained in the denominators of Q, M_T, and φ has no physical significance and may have any arbitrary value since these quantities appear as ratios in Equations [27] and [28]. Q/M_T is the ratio of the relative velocity to the tip speed of the impeller and φ/M_T is proportional to the ratio of the flow rate through the impeller to the tip speed of the impeller.

In order to obtain a qualitative idea of the effect of β_b upon the values of Q_d and Q_t, the variation in Q_d/M_T and Q_t/M_T with β_b for various values of R is plotted in Fig. 23, for σ equal to 0.31416 and φ/M_T equal to 0.25. The minimum value of Q_d/M_T occurs in the immediate neighborhood of β_b equal to 0. Relative eddy

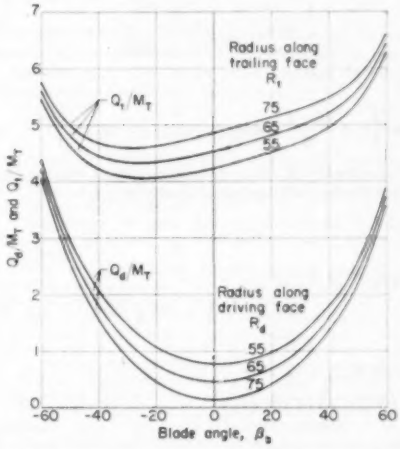

FIG. 23 VARIATION IN VELOCITY ALONG DRIVING AND TRAILING FACES OF BLADE WITH BLADE ANGLE β_b FOR SEVERAL VALUES OF R

(Angular blade spacing σ, 18 deg; constant flow area; ratio φ/M_T, 0.250; incompressible flow.)

flows on the driving face of the blade are characterized by negative velocities along the blade surface. Thus, for the same impeller-tip speed, etc., forward-curved blades ($\beta_b > 0$) and backward-curved blades ($\beta_b < 0$) have less tendency than straight blades ($\beta_b = 0$) for the formation of undesirable relative eddy flows on the driving face. In Fig. 13 of Part 1 the variation (with β_b) in the relative velocities Q_d and Q_t on the driving and trailing faces of the blade at a radius ratio of 0.75 (for example) agrees with the trend shown in Fig. 23. In particular, the value of Q_t is somewhat lower in both figures for β_b equals $\tan^{-1}(-0.5)$ than for $\tan^{-1}(0)$ and $\tan^{-1}(-1.0)$.

APPROXIMATE CIRCULATION METHOD FOR ARBITRARY BLADE SHAPES ON CURVED FLOW SURFACES OF REVOLUTION

The last of the three approximate methods of analysis applies to

impellers with arbitrary blade shapes (with varying thickness and blade angle) on arbitrary, curved flow surfaces of revolution. The approximate circulation method is based upon the condition of zero absolute circulation about any closed path in the flow field which does not enclose part of a blade. In addition, the fluid is assumed to be perfectly guided by the blades except near the blade tip (and possibly the blade inlet) where a correction is added to account for the blade unloading. The method of analysis can be used to determine the velocities everywhere along the blade surfaces, but no information concerning the variation in velocity across the passage between blades is given. The method is developed in Appendix C. The final equations and their application are considered here.

From Equations [C-1] and [C-6] (Appendix C)

$$Q_t = \frac{\cos\beta_d \cos\beta_t}{\cos\beta_t + \cos\beta_d}\left\{\frac{2Q_{avg}}{\cos\beta_d} + RM_T(\tan\beta_d - \tan\beta_t) + \sin\alpha\frac{d}{dR}\left[(RM_T + Q_{avg}\sin\beta_{avg})\frac{R2\pi\delta}{b}\right]\right\} \quad [29]$$

and

$$Q_d = 2Q_{avg} - Q_t \quad [30]$$

where

$$Q_{avg} = \frac{\varphi}{\frac{\rho_{avg}}{\rho_o}\cos\beta_{avg}HR\delta} \quad [C\text{-}7]$$

where

$$\frac{\rho_{avg}}{\rho_o} = \left\{1 + \frac{\gamma-1}{2}\left[(RM_T)^2 - Q_{avg}^2 - 2M_T\lambda_U\right]\right\}^{\frac{1}{\gamma-1}} \quad [C\text{-}8]$$

and where, for $R \leqslant R_s$ (R_s is the largest radius at which the fluid is considered to be perfectly guided by the blades)

$$\beta_{avg} = \frac{\beta_d + \beta_t}{2} \quad [C\text{-}2a]$$

or, for $R_s \leqslant R \leqslant 1.0$

$$\sin\beta_{avg} = A + BR + CR^2 \quad [C\text{-}2b]$$

where

$$\left.\begin{aligned} A &= (\sin\beta_{avg})_T - B - C \\ B &= \left(\frac{1+R_s}{1-R_s}\right)\left(\frac{d\sin\beta_{avg}}{dR}\right)_s - \frac{2R_s}{(1-R_s)^2}\left[(\sin\beta_{avg})_T - (\sin\beta_{avg})_s\right] \\ C &= \frac{(\sin\beta_{avg})_T - (\sin\beta_{avg})_s - (1-R_s)\left(\frac{d\sin\beta_{avg}}{dR}\right)_s}{(1-R_s)^2} \end{aligned}\right\} \quad [C\text{-}13]$$

where

$$(\sin\beta_{avg})_T = \frac{M_T(\mu-1)}{(Q_{avg})_T} \quad [C\text{-}11]$$

in which

$$(Q_{avg})_T = \frac{\varphi}{\frac{\rho_{avg}}{\rho_o}\delta\sqrt{1 - \left[\frac{M_T(\mu-1)}{(Q_{avg})_T}\right]^2}} \quad [C\text{-}12]$$

The last term in Equation [29] is determined from the slope of

$$(RM_T + Q_{avg}\sin\beta_{avg})\frac{R2\pi\delta}{b}$$

plotted against R where Q_{avg} is obtained from Equation [C-7] and β_{avg} is obtained from Equation [C-2a] or [C-2b]. Therefore Q_t and Q_d can be determined by Equations [29] and [30].

This approximate circulation method of analysis has been applied to the same design and operating conditions of the 4th and 7th relaxation solutions (Table 1) and the results are compared in Figs. 24 and 25 with the relaxation solutions. The agreement is good considering the approximate nature of the analysis.

This method of analysis also applies in the region of the blade inlet if the relative velocity approaches approximately tangent to the blade. (In some cases it may be necessary to apply a correction to

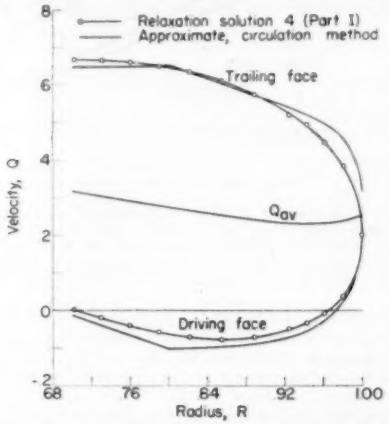

FIG. 24 COMPARISON OF VARIATION IN VELOCITY WITH RADIUS ALONG DRIVING AND TRAILING FACES OF A STRAIGHT BLADE AS OBTAINED BY RELAXATION METHODS—SOLUTION 4, PART 1—AND BY APPROXIMATE, CIRCULATION METHOD

(Flow coefficient φ, 0.5; impeller-tip Mach number M_T, 1.5; constant flow area; angular blade spacing σ, 18 deg; compressible flow, γ, 1.4.)

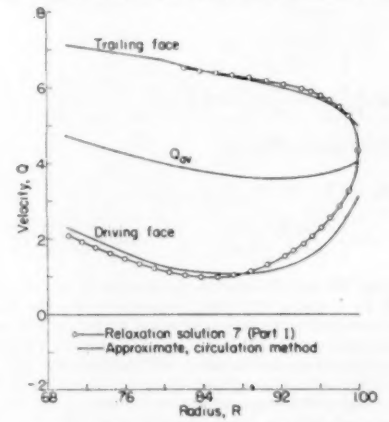

FIG. 25 COMPARISON OF VARIATION IN VELOCITY WITH RADIUS ALONG DRIVING AND TRAILING FACES OF A BACKWARD-CURVED, LOGARITHMIC-SPIRAL BLADE [β_b, $\tan^{-1}(-1.0)$], AS OBTAINED BY RELAXATION METHODS—SOLUTION 7, PART 1—AND BY APPROXIMATE, CIRCULATION METHOD

(Flow coefficient φ, 0.5; impeller-tip Mach number M_T, 1.5; constant flow area; angular blade-spacing σ, 18 deg; compressible flow, γ, 1.4.)

β_{w_2} similar to that developed for the blade tip, Appendix C, although if the blade inlet is designed for gradual loading this correction may not be required.) For large angles of attack at the inducer inlet, however, a stagnation point exists well up on the blade surface from the leading edge, and the flow reverses itself upstream from this point. Under these extreme conditions the approximate circulation method will not apply in the vicinity of the blade inlet.

Discussion

Several points related to the results presented in Parts 1 and 2 of this paper are now considered.

Viscous Effects. The solutions presented in Parts 1 and 2 of this paper assume that the fluid viscosity is zero. If the viscosity is not zero, a boundary layer develops on the flow surfaces, and if the velocity gradients are sufficiently negative, this boundary layer may separate, which alters the shape of the flow field and thus changes the velocity distribution, and so forth. If the boundary layer is thick or has separated, then the solutions presented in this paper must be corrected for the boundary-layer thickness, which can be considered to change the effective shape and flow area of the impeller passage. Outside of the boundary layer the fluid can be considered nonviscous. The solutions, as presented in this paper, can be used to estimate (approximately) if, and where, boundary-layer separation might occur as a result of the computed velocity gradients, and may also be used to determine the proper location for boundary-layer suction to prevent flow separation.

Future Design Methods. Losses in centrifugal compressors result from the viscosity of the fluid. In the impeller these losses are largely contained in the boundary layer. The larger the boundary layer the greater the losses and the lower the compressor efficiency. The size of the boundary layer is governed by the velocity gradients. In particular, if these gradients are negative and sufficiently large, the boundary layer may separate, causing large losses. For the simple blade shapes analyzed in this paper large, negative gradients always occur on the trailing face of the blade near the tip (Fig. 13 of Part 1, and Figs. 17, 18, and 19 of Part 2). Therefore, boundary-layer separation (or its equivalent in a rotating channel) probably occurs in all impellers with these simple blade shapes, and the compressor efficiency is thereby reduced. For efficient centrifugal compressors it is important to develop impeller-design methods by which blade shapes (including the hub and shroud contours) can be computed for prescribed velocities that do not decelerate excessively along the flow surfaces. Impellers designed by such methods will be characterized by curved blades of varying thickness with no distinction between impeller blades and inducer vanes. For structural reasons (as well as aerodynamic reasons) the impellers will probably be mixed-flow type.

Diffusers. Although the investigations presented in this paper are limited to the impeller of centrifugal compressors, a major portion of the losses in centrifugal compressors probably occurs in the diffuser. However, a large part of these losses in the diffuser have their origin in the thick (or separated) boundary layer at the impeller tip. As a result of this boundary layer, mixing losses occur in the diffuser, and the diffuser vanes operate under nonsteady flow conditions with rapidly varying angle of attack. When these adverse conditions, resulting from the large boundary layer at the impeller tip, have been eliminated by proper impeller design, then theoretical and experimental research on diffusers can be expected to result in centrifugal compressors with high efficiency.

Summary of Results—Part 2

1 In Part 2 of this paper three approximate methods of solution are presented which can be used for rapid analysis of compressible flow between blades on flow surfaces of revolution.

2 For straight blades and compressible fluids the impeller-tip Mach number has only a small effect upon the velocity along the trailing face of the blade (except in the immediate vicinity of the impeller tip).

3 For straight blades the difference between velocities on the trailing and driving faces of the blades increases with increasing tip Mach number and blade spacing, but is independent of the compressor flow rate.

4 A large part of the losses in diffusers have their origin in the thick (or separated) boundary layer at the impeller tip of most present-day impeller designs.

5 For efficient centrifugal compressors, it is important to develop impeller-design methods by which blade shapes (including the hub and shroud contours) can be computed for prescribed velocities that do not decelerate excessively along the flow surfaces. Impellers designed by such methods probably will be characterized by curved blades of varying thickness with no distinction between impeller blades and inducer vanes.

Acknowledgments

The author wishes to express his appreciation for the valuable suggestions and assistance received from his associates, especially from Mr. Gaylord O. Ellis, under whose direction the relaxation solutions reported herein were carried out.

BIBLIOGRAPHY

1 "Steam and Gas Turbines," by A. Stodola, McGraw-Hill Book Company, Inc., New York, N. Y., vol. 2, sixth edition, 1927.

2 "Potential Flow Through Centrifugal Pumps and Turbines," by E. Sörensen, NACA TM 973, 1941.

3 "The Theory of Flow Through Centrifugal Pumps," by William Bollay, Theodore von Kármán Anniversary volume, CIT, May 11, 1941.

4 "D-C Network-Analyzer Determination of Fluid-Flow Pattern in a Centrifugal Impeller," by C. Concordia and G. K. Carter, *Journal of Applied Mechanics*, Trans. ASME, vol. 14, 1947.

5 "Method of Analysis for Compressible Flow Through Mixed-Flow Centrifugal Impellers of Arbitrary Design," by J. T. Hamrick, A. Ginsburg, and W. M. Osborn, NACA TN 2165, August, 1950.

6 "A General Theory of Three-Dimensional Subsonic and Supersonic Flow in Turbomachines Having Arbitrary Hub and Casing Wall Shapes," by Chung-H. Wu, ASME Preprint 50—A-79, 1950.

7 "Two-Dimensional Compressible Flow in Conical Mixed-Flow Compressors," by J. D. Stanitz, NACA TN 1744, 1948.

8 "Two-Dimensional Compressible Flow in Turbomachines With Conic Flow Surfaces," by J. D. Stanitz, NACA Rep. 935, 1949.

9 "Two-Dimensional Compressible Flow in Centrifugal Compressors With Straight Blades," by J. D. Stanitz and G. O. Ellis, NACA Rep. 954, 1950. (Formerly NACA TN 1932.)

10 "Two-Dimensional Compressible Flow in Centrifugal Compressors With Logarithmic-Spiral Blades," by G. O. Ellis and J. D. Stanitz, NACA TN 2255, 1951.

11 "Investigation of Single Stage Axial Fans," by P. Ruden, NACA TM 1062, 1944.

12 "Relaxation Methods in Theoretical Physics," by R. V. Southwell, Clarendon Press, Oxford, England, 1946.

13 "The Numerical Solution of Compressible Fluid Flow Problems," by H. W. Emmons, NACA TN 932, 1944.

14 "Zur neuen Theorie der Kreiselrader," by H. Lorenz, *Zeitschrift für das Gesamte Turbinenwesen*, Heft 4 und 6, 1907.

15 "Hydrodynamics," by Horace Lamb, Dover Publications, New York, N. Y., sixth edition, 1945.

16 "Standard Procedures for Rating and Testing Multistage Axial-Flow Compressors," by NACA Subcommittee on Compressors, NACA TN 1138, 1946.

Appendix A

Method of Analysis for Flow With Axial Symmetry in Compressors and Turbines With Radial Blade Elements

The equation of motion in the radial direction, Equation [11a], with partial derivatives with respect to θ equal to zero for axial symmetry and with F_R equal to zero for radial blade elements, becomes

$$Q_R \frac{\partial Q_R}{\partial R} + Q_Z \frac{\partial Q_R}{\partial Z} - \frac{(M_T R + Q_\theta)^2}{R} = -\frac{g p_o}{\rho c_o^2} \frac{\partial P}{\partial R} \quad [A\text{-}1]$$

Also, from Equations [9] and [10] with λ_U assumed constant from streamline to streamline

$$\frac{\partial P}{\partial R} = \gamma \frac{p}{p_o} \left[R M_T^2 - Q_R \frac{\partial Q_R}{\partial R} - Q_\theta \frac{\partial Q_\theta}{\partial R} - Q_Z \frac{\partial Q_Z}{\partial R} \right] \quad [A\text{-}2]$$

Therefore, combining Equations [A-1], [A-2], and [1], and noting that

$$p_o = \rho_o R T_o$$

the following equation is obtained

$$Q_Z \left(\frac{\partial Q_Z}{\partial R} - \frac{\partial Q_R}{\partial Z} \right) + Q_\theta \frac{\partial Q_\theta}{\partial R} + \frac{Q_\theta^2}{R} + 2 Q_\theta M_T = 0 \quad [A\text{-}3]$$

(Note that an identical equation can be developed from Equations [11c] and [9] and from Equation [13] with F_R equal to zero.) From Equation [6]

$$\frac{\partial Q_\theta}{\partial R} = \tan \epsilon \frac{\partial Q_Z}{\partial R} + Q_Z \sec^2 \epsilon \frac{\partial \epsilon}{\partial R} \quad [A\text{-}4]$$

and for radial blade elements

$$\frac{\tan \epsilon}{R} = f(Z)$$

so that

$$\sec^2 \epsilon \frac{\partial \epsilon}{\partial R} = \frac{\tan \epsilon}{R} \quad [A\text{-}5]$$

Therefore, from Equations [A-3], [A-4], [A-5], and [6]

$$(1 + \tan^2 \epsilon) \frac{\partial Q_Z}{\partial R} - \frac{\partial Q_R}{\partial Z} + 2 \tan^2 \epsilon \frac{Q_Z}{R} + 2 M_T \tan \epsilon = 0 \quad [A\text{-}6]$$

For axial symmetry, the continuity equation becomes

$$\frac{\partial}{\partial R} \left(R \frac{\rho}{\rho_o} Q_R \right) + \frac{\partial}{\partial Z} \left(R \frac{\rho}{\rho_o} Q_Z \right) = 0 \quad [A\text{-}7]$$

If the blade thickness of the impeller being investigated (finite number of blades) varies with R and Z, the ratio δ of passage width between blade surfaces to blade spacing in the circumferential direction can be introduced into Equation [A-7] to give

$$\frac{\partial}{\partial R} \left(\delta R \frac{\rho}{\rho_o} Q_R \right) + \frac{\partial}{\partial Z} \left(\delta R \frac{\rho}{\rho_o} Q_Z \right) = 0 \quad [A\text{-}8]$$

(Although for axial symmetry the blades become infinitely thin, the space between blades also becomes infinitely small and the ratio δ of these quantities has a finite value equal to that of the impeller with a finite number of blades.) The continuity Equation [A-8] is satisfied by a stream function ψ which is defined by

$$\left.\begin{aligned} \frac{\partial \psi}{\partial R} &= \delta R \frac{\rho}{\rho_o} Q_Z \\ \frac{\partial \psi}{\partial Z} &= -\delta R \frac{\rho}{\rho_o} Q_R \end{aligned}\right\} \quad [A\text{-}9]$$

Equations [A-6] and [A-9] combine to give

$$(1 + \tan^2 \epsilon) \frac{\partial^2 \psi}{\partial R^2} + \frac{\partial^2 \psi}{\partial Z^2} - (1 + \tan^2 \epsilon) \frac{\partial \psi}{\partial R} \frac{\partial \ln \left(\delta R \frac{\rho}{\rho_o} \right)}{\partial R} - \frac{\partial \psi}{\partial Z} \frac{\partial \ln \left(\delta R \frac{\rho}{\rho_o} \right)}{\partial Z} + \frac{2 \tan^2 \epsilon}{R} \frac{\partial \psi}{\partial R} + 2 \delta R \frac{\rho}{\rho_o} M_T \tan \epsilon = 0 \quad [A\text{-}10]$$

In this equation the density ratio ρ/ρ_o is related to the velocity components Q_R, Q_θ, and Q_Z by Equation [10] and the velocity components are related to the stream function ψ by Equations [A-9] and [6]. This system of Equations [6], [10], [A-9], and [A-10] can be solved for given boundary conditions by relaxation methods (references 12 and 13), to give the distribution of ψ in the meridional plane, from which the distribution of Q can be determined directly from Equations [A-9] and [6]. In some cases it may be advantageous to transform co-ordinates before solving the equations.

If the fluid is incompressible ($\rho/\rho_o = 1$), and if the ratio of blade thickness to blade spacing is zero ($\delta = 1$), Equation [A-10] becomes

$$(1 + \tan^2 \epsilon) \frac{\partial^2 \psi}{\partial R^2} + \frac{\partial^2 \psi}{\partial Z^2} + \frac{(\tan^2 \epsilon - 1)}{R} \frac{\partial \psi}{\partial R} + 2 R M_T \tan \epsilon = 0 \quad [A\text{-}11]$$

Equation [A-11] was solved by relaxation methods to obtain the solutions presented in Figs. 4, 5, and 6.

Appendix B

Method of Analysis for Two-Dimensional Compressible Flow Between Blades of Arbitrary Shape on Flow Surfaces of Revolution

The center line of a channel between adjacent streamlines that were obtained from an axial-symmetry solution in the meridional plane (Fig. 4, for example) is shown in Fig. 26, together with the co-ordinates, velocities, and the like, at a point on the center line. A tangent at this point to the center line in the meridional plane

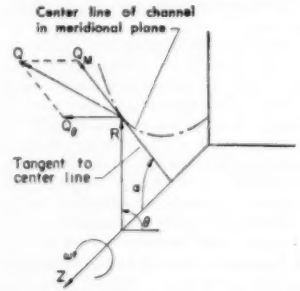

Fig. 26 Co-Ordinates, Velocities, and the Like, at a Point on Center Line of a Channel Between Adjacent Streamlines in Meridional Plane; Axial-Symmetry Solution

intersects the axis of the compressor with the angle α as indicated. If this tangent line is rotated about the axis it generates the surface of a cone which is tangent to the flow surface of revolution obtained by rotating the center line (Fig. 26). At the circumferential line of tangency a fluid particle on the flow surface of revolution is also on the conic flow surface. This fluid particle is shown in Fig. 27 on a developed view of the cone surface.

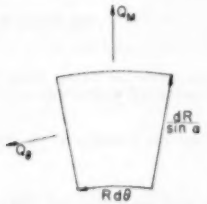

FIG. 27 FLUID PARTICLE ON DEVELOPED SURFACE OF CONE AT POINT WHICH IS TANGENT TO FLOW SURFACE OF REVOLUTION

Absolute Irrotational Motion. In the absence of shock, viscous effects, and so forth, the absolute motion of the fluid on the surface of revolution is irrotational so that the absolute circulation Γ is zero and from Fig. 27

$$d\Gamma = 0 = \frac{\partial}{\partial R}\left[(RM_T + Q_\theta)R\,d\theta\right]dR - \frac{\partial}{\partial\theta}\left[\frac{Q_M dR}{\sin\alpha}\right]d\theta \quad \text{[B-1]}$$

from which

$$0 = 2RM_T \sin\alpha + Q_\theta \sin\alpha + R\sin\alpha\,\frac{\partial Q_\theta}{\partial R} - \frac{\partial Q_M}{\partial\theta}$$

where by $\partial/\partial R$ is meant variations with respect to R along the surface of revolution.

Continuity. From continuity considerations for the fluid particle in Fig. 27

$$\frac{\partial}{\partial R}\left(\frac{\rho}{\rho_o}\,Q_M\,HR\right) + \frac{\partial}{\partial\theta}\left(\frac{\rho}{\rho_o}\,Q_\theta\,\frac{H}{\sin\alpha}\right) = 0 \quad \text{[B-2]}$$

where H, the channel-height ratio, is defined by

$$H = \frac{h}{h_T} = f(R)$$

where h_T is the channel height at the impeller tip. A stream function ψ satisfies the continuity Equation [B-2] if defined as

$$\left.\begin{aligned}\frac{\partial\psi}{\partial\theta} &= \frac{\rho}{\rho_o}\,Q_M\,HR\\ \frac{\partial\psi}{\partial R} &= -\frac{\rho}{\rho_o}\,Q_\theta\,\frac{H}{\sin\alpha}\end{aligned}\right\} \quad \text{[B-3]}$$

Transformation of Co-Ordinates. For convenience in the relaxation solution the following transformation of co-ordinates is introduced

$$d\xi = \frac{1}{\sin\alpha}\,\frac{dR}{R} \quad \text{[B-4a]}$$

and

$$d\eta = d\theta \quad \text{[B-4b]}$$

Equation [B-4a] integrates to give ξ as a function of R with ξ arbitrarily equal to zero when R equals 1, and Equation [B-4b] integrates to give η equal to θ. By this transformation, which is conformal, the curved flow surface of revolution becomes a flat plane ($\xi\eta$-plane). Lines of constant ξ and η, corresponding to co-ordinates of the $\xi\eta$-plane, are shown on a flow surface of revolution in Fig. 28. The problem is solved in the $\xi\eta$-plane and transformed back to the curved flow surface of revolution.

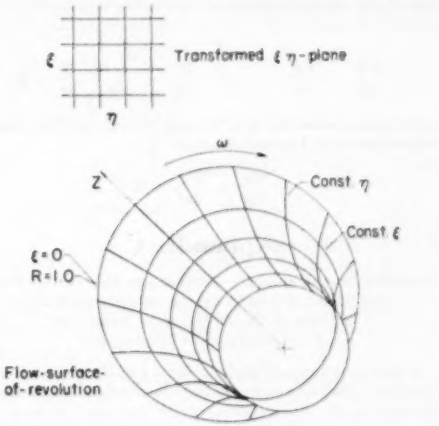

FIG. 28 LINES OF CONSTANT ξ AND η, I.E., CO-ORDINATES OF TRANSFORMED $\xi\eta$-PLANE, ON A FLOW SURFACE OF REVOLUTION

General Differential Equation for Stream-Function Distribution. In terms of the transformed co-ordinates, Equation [B-1] for absolute irrotational motion becomes

$$0 = 2RM_T \sin\alpha + Q_\theta \sin\alpha + \frac{\partial Q_\theta}{\partial\xi} - \frac{\partial Q_M}{\partial\eta} \quad \text{[B-5]}$$

and Equation [B-3] for the stream function becomes

$$\left.\begin{aligned}\frac{\partial\psi}{\partial\eta} &= \frac{\rho}{\rho_o}\,Q_M\,HR\\ \frac{\partial\psi}{\partial\xi} &= -\frac{\rho}{\rho_o}\,Q_\theta\,HR\end{aligned}\right\} \quad \text{[B-6]}$$

Equations [B-5] and [B-6] combine to give (note that H and R are independent of η)

$$\frac{\partial^2\psi}{\partial\xi^2} + \frac{\partial^2\psi}{\partial\eta^2} - \frac{\partial \ln H}{\partial\xi}\,\frac{\partial\psi}{\partial\xi} - \frac{\partial \ln\frac{\rho}{\rho_o}}{\partial\xi}\,\frac{\partial\psi}{\partial\xi} - \frac{\partial \ln\frac{\rho}{\rho_o}}{\partial\eta}\,\frac{\partial\psi}{\partial\eta} - 2\,\frac{\rho}{\rho_o}\,HR^2 M_T \sin\alpha = 0 \quad \text{[B-7]}$$

In this equation the density ratio ρ/ρ_o is related to the velocity components Q_M and Q_θ by Equation [10] where $Q^2 = Q_M^2 + Q_\theta^2$, and the velocity components as related to the stream function ψ by Equation [B-6]. This system of Equations [10, B-6, B-7] can be solved for given boundary conditions by relaxation methods (references 8, 12, and 13) to give the distribution of ψ for two-dimensional flow past arbitrary blade shapes on the flow surface of revolution. The velocity components, and, therefore, the pressure, density, and so forth, can be obtained from the distribution of ψ by means of Equation [B-6].

For flow through an axial-flow compressor $\sin\alpha$ can be zero so that Equation [B-7] becomes

$$\frac{\partial^2\psi}{\partial\xi^2} + \frac{\partial^2\psi}{\partial\eta^2} - \frac{\partial \ln H}{\partial\xi}\frac{\partial\psi}{\partial\xi} - \frac{\partial \ln \frac{\rho}{\rho_o}}{\partial\xi}\frac{\partial\psi}{\partial\xi} - \frac{\partial \ln \frac{\rho}{\rho_o}}{\partial\eta}\frac{\partial\psi}{\partial\eta} = 0$$

For a plane, two-dimensional cascade H is equal to unity and the differential equation reduces to

$$\frac{\partial^2\psi}{\partial\xi^2} + \frac{\partial^2\psi}{\partial\eta^2} - \frac{\partial \ln \frac{\rho}{\rho_o}}{\partial\xi}\frac{\partial\psi}{\partial\xi} - \frac{\partial \ln \frac{\rho}{\rho_o}}{\partial\eta}\frac{\partial\psi}{\partial\eta} = 0$$

For incompressible flow ρ/ρ_o is equal to unity, and the equation finally reduces to Laplace's equation

$$\frac{\partial^2\psi}{\partial\xi^2} + \frac{\partial^2\psi}{\partial\eta^2} = 0$$

Appendix C

Approximate Circulation Method for Estimating Velocities Along Blade Surfaces of Impellers With Arbitrary Blade Shape on Arbitrary Flow Surfaces of Revolution

A fluid strip between blades along a line of constant R on an arbitrary curved flow surface of revolution is shown in a developed view in Fig. 29. The velocities at the blade surfaces are Q_d and Q_t, as indicated in the figure, and the velocity between blades along lines of constant R is assumed constant and equal to Q_{avg}, where

$$Q_{avg} = \frac{Q_d + Q_t}{2} \quad \text{[C-1]}$$

Also, the flow direction in the passage between blades is assumed constant and equal to β_{avg} where for $R \leq R_x$

$$\beta_{avg} = \frac{\beta_d + \beta_t}{2} \quad \text{[C-2a]}$$

and for $R_x \leq R \leq 1.0$

$$\sin \beta_{avg} = A + BR + CR^3 \quad \text{[C-2b]}$$

where A, B, and C are coefficients to be determined, and where R_x is the largest radius at which the fluid is considered to be perfectly guided by the blades, that is, the radius at which the simplified method of analysis breaks down. From an inspection of Fig. [21] the value of R_x for σ equal to $\pi/10$ radians (18 deg) is about 0.800. For other values of σ, the value of R_x can be estimated from

$$\frac{\ln R_x}{\sigma} = \frac{\ln 0.8}{\pi/10} = -\frac{2.23}{\pi} \quad \text{[C-3]}$$

(If the blades were designed to unload at the tip, the guiding of the fluid by the blades may be effective at a radius somewhat greater than the value for R_x given by Equation [C-3].)

In the absence of shock, viscous effects, and the like, the absolute circulation around the fluid strip in Fig. 29 is zero so that

$$0 = \left(Q_{abs}\frac{dR}{\sin\alpha\cos\beta}\right)_d - \left(Q_{abs}\frac{dR}{\sin\alpha\cos\beta}\right)_t + \frac{d}{dR}\left[(RM_T + Q_{avg}\sin\beta_{avg})\frac{R2\pi\,\delta}{b}\right]dR \quad \text{[C-4]}$$

where the subscript "abs" indicates component of absolute velocity along blade surface. But from considerations of zero absolute circulation about the triangles at the driving and trailing faces in Fig. 29

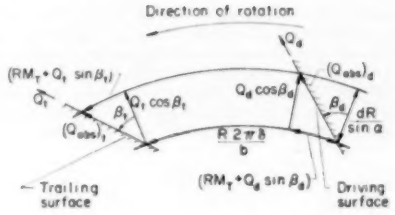

Fig. 29 Developed View of Fluid Strip Between Blades Along Line of Constant R on Flow Surface of Revolution

$$\left(Q_{abs}\frac{dR}{\sin\alpha\cos\beta}\right)_d = Q_d\cos\beta_d\frac{dR}{\sin\alpha} + (RM_T + Q_d\sin\beta_d) \times \frac{dR}{\sin\alpha}\tan\beta_d \quad \text{[C-5a]}$$

and

$$\left(Q_{abs}\frac{dR}{\sin\alpha\cos\beta}\right)_t = Q_t\cos\beta_t\frac{dR}{\sin\alpha} + (RM_T + Q_t\sin\beta_t) \times \frac{dR}{\sin\alpha}\tan\beta_t \quad \text{[C-5b]}$$

From Equations [C-4] and [C-5]

$$\frac{Q_d}{\cos\beta_d} - \frac{Q_t}{\cos\beta_t} + RM_T(\tan\beta_d - \tan\beta_t) + \sin\alpha\frac{d}{dR}\left[(RM_t + Q_{avg}\sin\beta_{avg})\frac{R2\pi\,\delta}{b}\right] = 0 \quad \text{[C-6]}$$

If Q_{avg} and β_{avg} are known, Q_d and Q_t can be determined from Equations [C-1] and [C-6].

The following approximate equation results from continuity considerations at radius R

$$\frac{W}{\rho_o a_T c_o} = \varphi = \frac{\rho_{avg}}{\rho_o}Q_{avg}\cos\beta_{avg}\,HR\delta$$

from which

$$Q_{avg} = \frac{\varphi}{\frac{\rho_{avg}}{\rho_o}\cos\beta_{avg}\,HR\delta} \quad \text{[C-7]}$$

where from Equation [10] of Part 1

$$\frac{\rho_{avg}}{\rho_o} = \left\{1 + \frac{\gamma-1}{2}[(RM_T)^2 - Q_{avg}^2 - 2M_T\lambda_U]\right\}^{\frac{1}{\gamma-1}} \quad \text{[C-8]}$$

Thus, if β_{avg} is known, Q_{avg} can be computed from Equations [C-7] and [C-8] by trial and error.

To determine β_{avg} for $R_x \leq R \leq 1.0$ the constants A, B, and C in Equation [C-2b] must be determined from the following three conditions:

1 At R_x where β_d and β_t are known from the blade geometry

$$(\sin\beta_{avg})_x = \sin\left(\frac{\beta_d + \beta_t}{2}\right) \quad \text{[C-9]}$$

2 At R_s where $\frac{d\beta_d}{dR}$ and $\frac{d\beta_i}{dR}$ are known from the blade geometry

$$\frac{d(\sin \beta_{avg})_s}{dR} = \cos\left(\frac{\beta_d + \beta_i}{2}\right)_s \frac{d}{dR}\left(\frac{\beta_d + \beta_i}{2}\right) \quad [C\text{-}10]$$

3 At R equals 1.0

$$\sin \beta_{avg} = (\sin \beta_{avg})_T$$

where $(\sin \beta_{avg})_T$ is determined from the slip factor μ, which is defined by (reference 7)

$$\mu = 1 + \frac{(Q_{avg} \sin \beta_{avg})_T}{M_T}$$

so that

$$(\sin \beta_{avg})_T = \frac{M_T(\mu - 1)}{(Q_{avg})_T} \quad [C\text{-}11]$$

The slip factor μ is assumed to be known, or can be estimated, as a result of the work presented in Part 1 of this paper. (If the blades were designed to unload at the tip, the guiding of the fluid by the blades may be more effective so that the slip factor μ may be more nearly equal to the theoretical value obtained assuming perfect guiding of the fluid.) The velocity $(Q_{avg})_T$ in Equation [C-11] is obtained from Equation [C-7] if $\cos \beta_{avg}$ is replaced by $\sqrt{1 - \sin^2 \beta_{avg}}$

$$(Q_{avg})_T = \frac{\varphi}{\frac{\rho_{avg}}{\rho_e} \delta \sqrt{1 - \left[\frac{M_T(\mu - 1)}{(Q_{avg})_T}\right]^2}} \quad [C\text{-}12]$$

Equation [C-12] is solved for $(Q_{avg})_T$ by trial and error.

From the three conditions given by Equations [C-9], [C-10], and [C-11], the constants A, B, and C in Equation [C-2b] become

$$\left.\begin{aligned} A &= (\sin \beta_{avg})_T - B - C \\ B &= \left(\frac{1 + R_s}{1 - R_s}\right)\left(\frac{d \sin \beta_{avg}}{dR}\right)_s \\ &\quad - \frac{2R_s}{(1 - R_s)^2}\left[(\sin \beta_{avg})_T - (\sin \beta_{avg})_s\right] \\ C &= \frac{1}{(1 - R_s)^2}\left[(\sin \beta_{avg})_T - (\sin \beta_{avg})_s \right. \\ &\quad \left. - (1 - R_s)\left(\frac{d \sin \beta_{avg}}{dR}\right)_s\right] \end{aligned}\right\} \quad [C\text{-}13]$$

Therefore Q_d and Q_i can be determined as functions of R along the blade surfaces from Equations [C-1] and [C-6] in which the fourth term of Equation [C-6] is determined by the slope of $(RM_T + Q_{avg} \sin \beta_{avg}) \frac{R\sigma\delta}{\sin \alpha}$ plotted against R where Q_{avg} and $\sin \beta_{avg}$ are determined by Equations [C-7], [C-2], and [C-13].

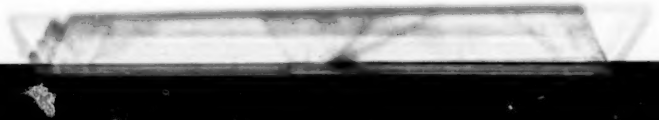

Single-Stage Radial Turbines for Gaseous Substances With High Rotative and Low Specific Speed

By W. T. VON DER NUELL,[1] LOS ANGELES, CALIF.

The turbine with radial inward flow, long known and in use as a water-power plant (1),[2] is rapidly gaining interest for gaseous energy carriers. Single-stage versions with wheels of shapes well known from aircraft-engine superchargers are now generally accepted in gas and air turbines when, relatively speaking, low mass flow in conjunction with high energy content per weight unit of the working substance characterize the available energy supply. Combining efficiency of 80 per cent and upward with attractive simplicity, this turbine type is bound to conquer its field. At present, aircraft auxiliary-power units represent its predominant application.

Nomenclature

The following nomenclature is used in the paper:

r = radius
D = diameter
b = blade or vane depth
v = tip speed
c = gas velocity
α = nozzle angle
β = blade angle
R_a = reaction
A = area
J = mechanical equivalent of heat
R = gas constant
ρ = density
κ = ratio of specific heats
H_{ad} = head (ft lb/lb) isentropic
φ_{ad} = head coefficient
Q = volume flow per unit of time
W = weight flow per unit of time
p = pressure
T = temperature
g = gravitational acceleration
P = power

Subscripts:

m = meridional
t = tangential
ex = exit
in = inlet
no = nozzle
turb = turbine

Introduction

Before presenting a few design considerations for radial air, gas, and steam turbines a brief historical background may well be of interest. After having demonstrated, in 1936, efficiencies of aircraft superchargers not materialized theretofore, the author decided to study these machines when operated as air turbines, of course, with reversal of the direction of both flow and rotation. Considering the flow dynamics in these turbines, efficiencies equally as high and higher than those observed on compressors were anticipated Not only this prospect, however, made the subject attractive; the additional significance of simple turbines for low specific speeds contributed to forming the opinion that real progress, not to say advancement of the art, was to be gained from the radial-type turbine for compressible fluids. The combination of high efficiency, low specific speed, and great simplicity was the objective. Being mainly interested in lightweight turbomachinery, early studies[3] and experiments were greatly restricted to single-stage units with 90-deg wheels. Of course, the author never considered the radial-type turbine as anything but a good unit for low specific speeds, nor has he thought of the 90-deg wheel as the only desirable configuration.

Some compressor results referred to were published (2) in 1937, showing better than 75 per cent total efficiency of single-stage units with pressure ratios above 2:1. A closer study soon revealed relatively high losses in the diffusing system and, somewhat later, the good performance characteristics of the impellers, Figs. 1 (*a*) and (*b*). With this in mind and knowing that a nozzle ring and nozzle box for a turbine could hardly have losses as great as those experienced in the diffusing members of the compressors, there was little, if any, doubt that efficiencies better than 80 per cent, possibly up to 90 per cent, were obtainable even in very small turbines, provided the specific-speed conditions were observed properly. Out of the early tests conducted to check the matter experimentally, hardly anything remained in the author's possession because of war consequences. Figs. 2 (*a*) and (*b*) show a Daimler-Benz aircraft supercharger which, when run as a turbine, produced performance values shown in Fig. 3. Similarly high, and even higher, values were obtained with units designed as turbines. Before going further it seems in order to explain briefly the specific speed and its importance.

Specific Speed

There exist several different definitions of the specific speed; yet, these differences are not consequential as long as a uniform basis of comparison is maintained for both the radial and the axial configuration. The specific speed is a measure of the similarity

[1] Project Engineer, heading the Gas Turbines Project of AiResearch Manufacturing Company, a division of the Garrett Corporation.

[2] Numbers in parentheses refer to the Bibliography at the end of the paper.

Contributed by the Gas Turbine Power Division and presented at the Fall Meeting, Minneapolis, Minn., September 26–28, 1951, of The American Society of Mechanical Engineers.

Note: Statements and opinions advanced in papers are to be understood as individual expressions of their authors and not those of the Society. Manuscript received at ASME Headquarters, July 11, 1951. Paper No. 51—F-16.

[3] As Chief Director of the DVL Institute for Turbomachinery and Professor for aircraft turbomachinery at Berlin. The doctor dissertations "Die Festigkeit hochbeanspruchter rein radial beschaufelter Kreiselverdichter-Laufräder" in Jahrbuch der Deutschen Luftfahrtforschung 1944 (The Strength of Highly Stressed Impellers of the Straight Radial Type), by K. J. Mueller and "Untersuchungen an Radialturbinen" (Investigations on Radial Turbines), by O. E. Balje, originated from this research work at DVL.

characteristics of turbomachinery and its particular operating conditions.

The specific-speed characteristic, probably first introduced for water turbines by Kamerer several decades ago, is slowly but certainly finding its way into being recognized as a valuable, if not the most valuable, means for identifying the basic capabilities of rotating-blade systems.

Derivable from the simplified Euler equation

$gH = qv^2$, with q being called the head coefficient, and from v/c = const, for geometrically similar conditions (3) is the well-known expression

$$\vartheta = \frac{N\sqrt{Q}}{(gH)^{3/4}}$$

If

D = wheel diameter
b = blade depth at D
$c_s = \sqrt{2gH_{ad}}$ = head velocity
α = nozzle angle
v/c_s = velocity ratio = ν
v = tip speed
N = rpm
R_s = wheel reaction
$Y = b/D$ depth diameter ratio
$Q = \pi Dbc_m$ = volume flow

for the radial wheel there results

$$\vartheta_{rad} = 0.9488\, Y\nu \sqrt{\sin\alpha}\, \sqrt[4]{1-R_s}$$

For $Y = 0.03$ and $\alpha = 5$ deg, and with $R_s = 0.5$, one finds $\vartheta_{rad} = 0.026$, whereas $\vartheta_{rad} = 0.13$ with $Y = 0.11$; $\alpha = 35°$, $R_s = 0.5$. A turbine wheel whose specific speed falls within

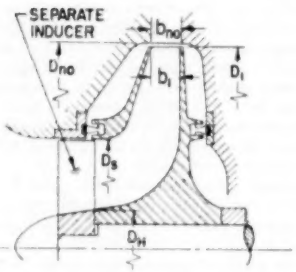

FIG. 1(a) FULLY SHROUDED IMPELLER, THRUST BALANCED AND WITH SEPARATE INDUCER

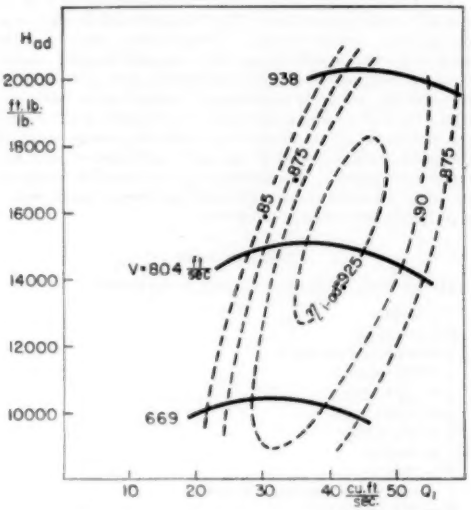

FIG. 1(b) PERFORMANCE CHART OF IMPELLER ALONE AS SHOWN IN FIG. 1(a)

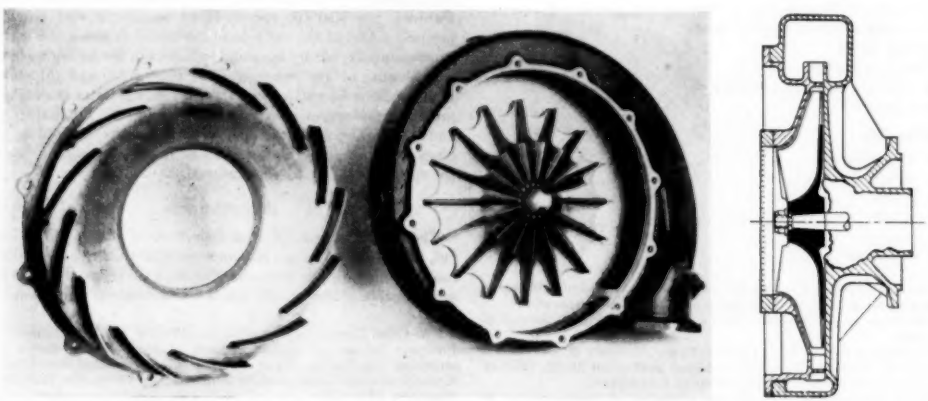

(a) (b)

FIG. 2 SUPERCHARGER OF GERMAN AIRCRAFT ENGINE DB 600

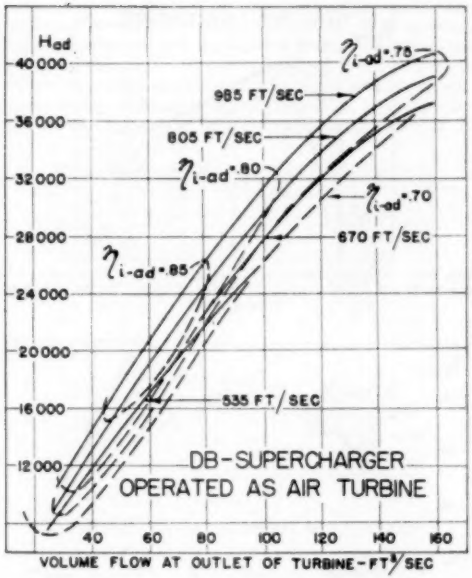

FIG. 3 PERFORMANCE CHART OF UNIT SHOWN IN FIG. 2, OPERATED AS AN AIR TURBINE

approximately this range between 0.026 and 0.13 is, in general, advantageously of the radial type, whereas, for higher ϑ-values, an axial wheel is usually preferable.

Whereas, in the foregoing, the wheel inlet area was introduced as the characteristic value, in a previous report (4), the wheel-discharge condition was referred to. Arguments can be presented for and against either case.[4] The basic facts remain unchanged. Radial-type wheels are the correct answer for low specific-speed conditions. A chart like the one shown in Fig. 4, based on generally accepted characteristics, indicates the range difference of specific speed for the two types considered over a wide blade-to-jet velocity variation. The advantage to be expected or obtained with the most suitable wheel configuration is one of efficiency, which is a feature normally ranking high in the comparative evaluation of merits. Moreover, for reasons of economy and ease of manufacture, the choice in favor of the radial wheel appears advantageous wherever the specific speed justifies it.

For those engineers who are unfamiliar with the merit of the specific speed or even doubtful, the following train of thought, seemingly wholly different, leads to the same conclusions and, moreover, is presented here in lieu of design calculations.

The equation for the turbine output desired

$$P = \frac{WH_{ad}}{550}\eta$$

permits the calculation of the weight flow W of gas per time unit after having assumed the efficiency η and determined

$$H_{ad} = \frac{\kappa}{\kappa - 1} RT_{in}\left[1 - \left(\frac{p_{ex}}{p_{in}}\right)^{\frac{\kappa-1}{\kappa}}\right] \text{ in ft-lb/lb}$$

[4] When dealing with incompressible fluids, this difference does not exist. Cavitation problems, however, require attention.

The nozzle throat area A results from

$$A_{no} = \frac{W\sqrt{RT_{in}}}{\psi\mu P_{in}}$$

with ψ as found in the literature (5) and μ the contraction coefficient. The pressure ratio $(p/p)_{no}$ across the nozzle can be figured from the head

$$H_{ad\,no} = (1 - R_s)H_{ad}$$

converted into velocity in the nozzles with R_s representing the reaction of the wheel. With an ID of the nozzle D_{no}, a depth b_{no}, and a nozzle angle α, the continuity requires

$$\pi D_{no} b_{no} \sin\alpha_{no}\,\tau = \frac{W\sqrt{RT_{in}}}{\psi\mu P_{in}}$$

with τ accounting for finite vane thickness.

Let all dimensions, see Fig. 1(*a*), be expressed as fractions or multiples of the wheel diameter D_1 (outlet diameter of the wheel D_s and hub diameter D_h in the plane of D_s) by

$$D_{no} = uD_1$$
$$b_{no} = aD_1$$
$$D_s = vD_1$$
$$D_h = wD_s = vwD_1$$

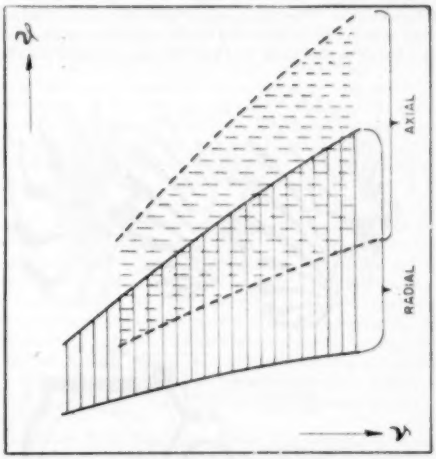

FIG. 4 SIMPLIFIED CHART FOR SPECIFIC SPEED PLOTTED VERSUS VELOCITY RATIO

Introducing the exit velocity c_{ex} from the impeller as

$$c_{ex} = z\sqrt{2gH_{ad}}$$

the simplified Euler equation

$$H_{ad} = \eta_{ad}\frac{v^2}{g} \quad (\eta_{ad} = \text{head coefficient})$$

with

$$v = \frac{\pi D_1 N}{720};$$

and remembering that $Q_{ex} = \frac{WRT_{ex}}{p_{ex}}$

with

$$T_{ex} = T_{in} - \eta_{isd}\Delta T_{ad}$$

simple algebraic transformations result in

$$\sin \alpha_{ex} = \frac{p_{ex}}{p_{in}} \sqrt{\frac{T_{in}}{R}} \left(\frac{1}{\psi\mu}\right) \left(\frac{v^2(1-w^2)g}{4us}\right) \left(\frac{\sqrt{2g_{ad}w^2}}{T_{in} - \eta_{isd}\frac{g_{ad}w^2}{gc_{pl}}}\right)$$

This equation or any other arrangement thereof tells practically the same story as does the specific-speed equation. If, for example, all "arbitrary" values on the right-hand side of the equation have been selected, and the numerical evaluation then results in an unacceptable nozzle angle, then, this clearly evidences that either the "arbitrary" values assumed have to be changed or that an acceptable combination of all numerical values which, in other words, means a desirable wheel configuration cannot be found. This result, then, is just another way of saying that the problem statement requires a different wheel, that is, a wheel configuration of a different specific speed like an axial wheel, provided it is properly suited for the purpose.

Wheel Configurations and Related Problems

A semi-radial turbine wheel also referred to as a diagonal wheel in several publications is shown in Fig. 5 representing an exhaust turbosupercharger with a two-stage compressor and a turbine of the Birman type. The turbine wheel with fully curved blades has a very small ratio of inlet over outlet diameter (approximately 1.2). As can be seen easily and has been demonstrated elsewhere,

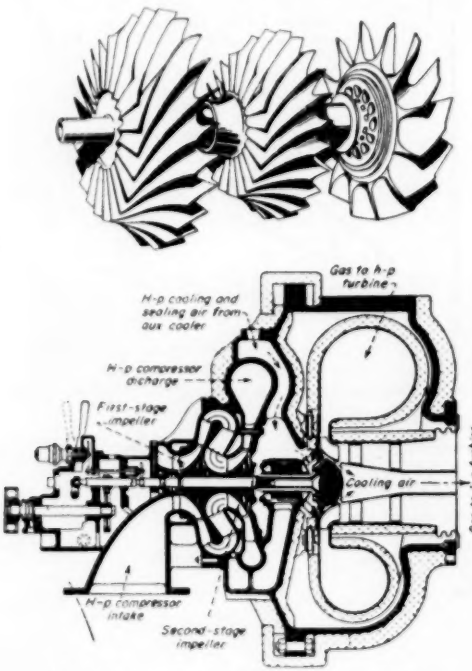

Fig. 5 Turbosupercharger of Birmann Bladed Type (De Laval Steam Turbine Company from *Power*.)

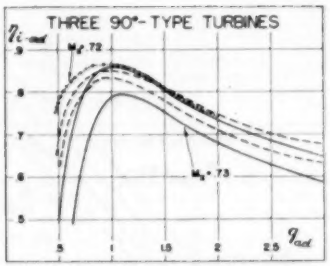

Fig. 6(a) Efficiencies as a Function of Head Coefficient for Single-Stage Centripetal Turbines, Tested Up to Pressure Ratios of 6:1

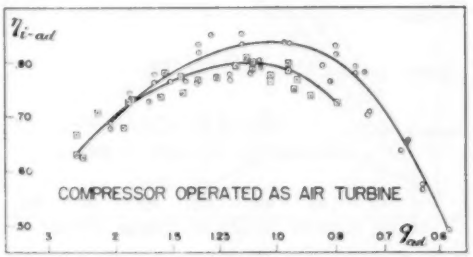

Fig. 6(b) Efficiency as Function of Head Coefficient, Plotted in Reverse as Compared to Fig. 6(a), Obtained With a Compressor Impeller With Backward Curved Blades—When Operated as Air Turbine

this very fact characterizes this wheel as one of moderate rather than low specific speed not utilizing the blade loading resulting from the greater difference of circumferential tip speed between inlet and outlet characteristic for larger diameter ratios. Shaping the blades on the practically unshrouded wheel such that all elements are located on straight lines through the center of rotation, a wheel of this type can be built for high tip speeds; it tends, however, toward heavy disk or hub portions. Experimental data to which access could be obtained do not show efficiencies approaching those demonstrated in Figs. 3 and 6 (*a*) and (*b*) but have given efficiency curves very similar in shape and almost equidistant, however, some 7 to 12 per cent lower at comparable conditions of operation (6).

A similar wheel configuration with a somewhat greater diameter ratio, thus, more like Francis wheels of water turbines, has been used by Dr. von Ohain (E. Heinkel Aircraft Company) during his turbojet development some 15 years ago.

As outlined previously, purpose and intent of the author's work were mainly toward simpler wheel configuration and lower specific speed in turbines, as it had been with compressors for a good many years.

The three best known configurations for 90-deg wheels with straight blades in the radial portion used during the past 3 or 4 decades for high-speed, lightweight compressors, especially for aircraft superchargers, are shown in Fig. 7 (7). Considerations similar to those for the compressor are applicable to the use of these wheels in radial turbines. The unshrouded impeller *a* (called "Rateau Star") is the most simple and oldest configuration. The main aerodynamical disadvantage of this wheel results from the fact that an energy exchange, necessarily representing a loss, occurs between the two faces of the blades on both sides of

the impeller requiring a finite clearance between the rotating blades and the stationary walls of the housing. High tip speeds have been obtained with this impeller type. With a steel impeller manufactured in 1932, tests up to tip speeds of 2000 fps without destruction or permanent deformation were performed.

The energy exchange losses on one side of the blades are eliminated in the so-called semi-shrouded impeller per *b* (Fig. 7).

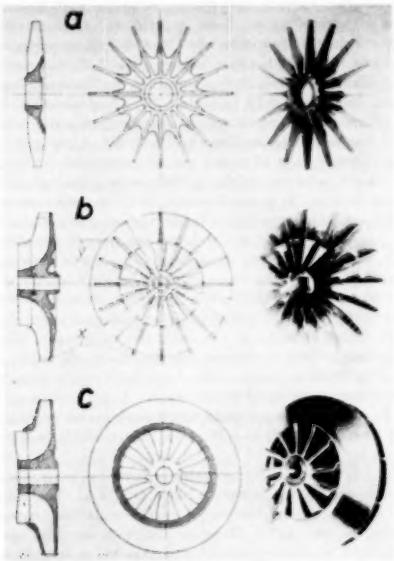

FIG. 7 THREE MAIN PHASES OF DEVELOPMENT OF AIRCRAFT SUPERCHARGER IMPELLERS

This impeller type, produced by the tens of thousands for aircraft purposes, is still simple as far as manufacturing is concerned and is, efficiencywise, superior to the Rateau type. Instead of bending the axial portion of the blades, a method used predominantly, a separate inducer similar to the ones shown in *b* and *c*, Fig. 7, can be used to provide for suitable blade angles.

Stationary turbocompressors are normally equipped with fully shrouded impellers built up from three parts, namely, the back shroud, the blades, the front shroud, the latter one being a one-piece design or consisting of a heavy ring forming the inlet eye of the impeller with a shroud attached to this ring. Numerous variations of this type of impeller are on the market. The separate elements are usually connected by riveting, and in some instances by welding or brazing. The maximum tip speeds for which this design approach has been used successfully are around 1200 fps, which value does not necessarily represent the maximum obtainable. It can, however, be stated that this built-up type is probably not the most attractive design for very high tip speeds. The explanation for the great interest in fully shrouded impellers in spite of the structural problems involved is simply the fact that they can offer improved efficiency as well as elimination of critical tolerance problems, especially in multistage machines.

In an attempt to improve the strength of fully shrouded, lightweight compressor impellers, 15 years ago the author suggested the configuration *c*, Fig. 7. The advantages of this type have been demonstrated and the production difficulties, originally considered to be prohibitive, have been overcome to such an extent that a German aircraft manufacturer accepted this wheel for production engines (Fig. 28). In an effort to maintain the aerodynamical advantages of the fully shrouded impeller and, at the same time, to keep the manufacturing reasonably simple, the author also suggested a split of the impeller into two parts along a plane perpendicular to the shaft, the location of which within the depth of the impeller was determined by a stress analysis of the front portion of the impeller consisting of a part of the hub, the front shroud with the rim, and a part of the radial blades. Tip speeds up to 1400 fps, obtained successfully with this configuration, were considered satisfactorily high some 12 years ago. The all-in-one-piece impeller of this configuration was apparently superior and the problem of producing it from preshaped forgings or as precision castings using modern techniques can hardly be considered impracticable, at least for highly critical machinery.

The experience gathered with compressors is to quite an extent directly applicable to turbines, especially as long as similar maximum temperatures are considered as exist in compressors with pressure ratios up to 4 and 5 per stage. The event of the utilization of radial wheels in high-temperature gas turbines called for extended stress study.

Whereas the stress analysis for impellers of the *b* and *c* type, Fig. 7, is sufficiently difficult, even though thermal stresses were mostly disregarded, their application to gas turbines with high temperatures makes it mandatory to take the thermal stresses into account, a problem not solved mathematically as yet. In the calculation of the stresses in a semi-shrouded compressor impeller two simplifying assumptions are usually made: (*a*) The mass of the blades is distributed evenly over the disk, and (*b*) the nonsymmetry of the disk is neglected. Methods for a more accurate stress analysis have been developed by considering blades and disk separately and then superimposing forces as dictated by the compatibility requirement. The presentation of further details of these methods would exceed the limits of this paper. Experimental checks demonstrated satisfactory coincidence of calculated and measured deformation (8). The fully shrouded all-in-one-piece wheel, *c* in Fig. 7 presents an even more complicated stress problem which, to the best of the author's knowledge, has not been solved analytically. The manner, now in use, of determining the acceptability of a wheel through whirl testing can hardly be considered desirable, and is expensive when attempting to approach temperature conditions as they exist during the starting, operation, and shutdown of a gas turbine. This work suffers, at present, also greatly from the fact that very little is known about the true temperature distribution in these wheels.

No attempt to go into any details on this subject can be made here. However, a simple consideration, though disputable as to its merits, but still indicating limitations, which to overcome seems rather unlikely at present, may be of interest. Six simple elements, Fig. 8, namely, two disks of uniform strength, a disk of constant thickness, two blades of uniform strength and constant cross section, respectively, and a free rotating ring have been compared under the following assumptions: (*a*) The temperature of the body, plotted as the abscissa in the chart, is constant; (*b*) the maximum stress equals the strength of the material assumed. (Below 1000 F the yield strength and about 1000 F the thousand-hour rupture strength were selected.) The result of this consideration can only be indicative of limits, especially since the disks and the blades are treated as separate elements without taking into account compatibility requirements, and because the temperature gradients which normally exist in a turbine wheel have been neglected altogether in spite of the fact that they can very easily be a most critical factor. Considering a disk of uni-

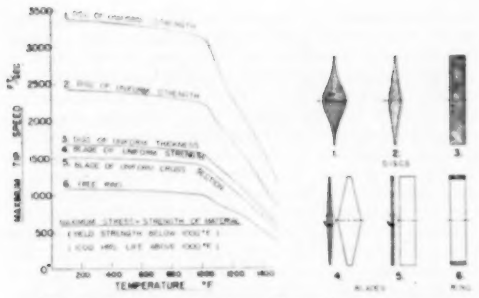

FIG. 8 RESULTS OF SIMPLIFIED STRESS CONSIDERATIONS

form thickness and a blade of uniform strength showing up as the same curve in this plot under the assumptions made, a tip speed of around 1500 fps appears possible up to 800 or 1000 F metal temperature. Radial-type gas-turbine wheels with average temperatures around 1000 F and tip speeds above 1500 fps have actually been run over hundreds of hours. In these cases the temperature gradient in the wheels was probably rather great owing to configuration and conditions of operation. It seems possible, even though difficult, to so design a turbine that the axial temperature gradient, i.e., at a constant radius of the turbine wheel, is kept within acceptable limits, and that the radial temperature gradient is such that with present-day materials and methods tip speeds in excess of 1600 fps and at rather high gas-turbine-cycle temperatures become acceptable for radial gas turbines. Here, as in many other cases, joint efforts of the aerodynamicist (who may hardly like the shape of a blade of uniform strength) and the stress analyst (who may well prefer just this shape) are absolutely necessary to develop radial wheels, permitting higher tip speeds. Efficient single-stage radial-type gas turbines with pressure ratios between 4 and 6, and cycle temperatures between 1400 and 1800 F most certainly appear worthy of all efforts. Such units will attain recognition, for instance, in the automotive field in general or for special applications.

With increasing emphasis on weight reduction materials are stressed closer to their ultimate strengths. Therefore, a thorough investigation of the dynamic stresses becomes all the more important. Even though the shape of a 90-deg wheel seems, and generally is, rather simple the problem of blade vibration occasionally has caused considerable difficulties.

During World War II, serious accidents resulting from impeller blades breaking from vibration in the supercharger of a German aircraft engine have occurred. All records covering the rather extensive studies conducted did not survive the war. The best known later publications on this subject are probably the ones by R. G. Voysey (9). Conditions of a similar nature can exist in a turbine, and it appears that attention has to be given to this matter. The opinion has been expressed that as long as no gearing is attached to the turbine shaft, the torsional modes of the wheel can be neglected. However, even a simple method for precalculating the three-dimensional bending problem existing in the different modes of vibration is not available yet, thus leaving this problem pretty much to an experimental evaluation and development. In his paper Voysey offers an approximate solution by "scale effect."

No final or comprehensive statement with respect to the most favorable number of blades in the wheels can be offered. In the first place, any such statement would require a special definition of what is favorable. When maximum efficiencies are more important than minimum difficulties and cost of manufacture, the answer is likely to be somewhat different from cases where simplicity and ease of manufacture are the decisive factors. As a matter of fact, the two extremes mentioned are somewhat representative of the conditions in gas turbines on one and exhaust turbosuperchargers on the other side.

For compressor impellers the problem of blade number has been dealt with quite extensively. Some results were published more than 10 years ago (10). At that time compressor impellers with blade numbers varying from thirty-two to one were tested in impellers of approximately 7 in. and 10 in., respectively, with diameter ratios of approximately 1.75 and 1.66, respectively. In both cases the variation in efficiency as well as in (pressure or) head coefficient was relatively small when the blade numbers were changed from around 12 to around 20. A remarkable drop in both efficiency and pressure coefficient occurred with blade numbers of 4 or less in the smaller wheel and of 8 or less in the larger wheel. These results, of course, are not universally applicable because of the influence of the special configuration of inlet and diffusing system. It seems, however, that the basic observations outlined are largely applicable to the turbine wheel of the 90-deg type. A wheel similar to the larger compressor impeller mentioned, which was tested in one turbine, showed only a small change in efficiency with blade numbers between 19 and 11; and even a decrease to 7 blades represented a drop in over-all efficiency of only approximately 5 per cent of the maximum value obtained at that time. In some of the cases the variation in efficiency actually might have been even less had the blade angles of the exducer or inducer, respectively, been individually matched to each and every new wheel configuration. In the unit presented in Figs. 2 (*a*) and (*b*) and 3, good turbine efficiencies were obtained with a 12-blade wheel, in spite of an objectionable curvature of the bent blades.

It appears that recently promising progress has been made with respect to calculating favorable blade numbers. The results of these studies, partly analytical, partly empirical, cannot be published as yet. Let it, therefore, suffice to say, that the basis for this work originates from a transformation of cascade results, combined with a balancing between decreased influence of the finite number with increasing blade number and a simultaneous increase in wetted area, that is, surface friction. The relationship between diameter ratio, blade number, and blade loading enters these—shall we say—speculations, of course. So far, a surprising verification of the predicted results is, however, notable.

NOZZLES AND SCROLLS

The calculation of the flow areas required and the design of the blading system offer no real problem as long as the pressure ratio across the turbine is not more than—let us say—the square of the critical pressure ratio and as long as not more than about 80 per cent temperature-drop efficiency is demanded. For higher pressure ratios the jet deflection (Prandtl-Meyer effect) and other mostly known features of supersonic flow require further careful consideration.

Euler's and Bernoulli's equations, the continuity compliance, equations for isentropic, polytropic, or isothermal change of state, approximative calculations regarding the influence of finite blade numbers and heat-transfer problems cover the most important "tools."

Detailed discussion of these matters presented in publications (4, 5, 11) will, therefore, be omitted in favor of additional information.

Whereas the nozzle vanes in the DB supercharger, Fig. 2, tested as a turbine, were of a shape and number quite common for compressors and very similar to those used in some radial inward flow turbines, some manufacturers seem to favor straight nozzle vanes similar to those shown in Figs. 9 (*a*) to (*d*). To pass judgment

on the superiority of one or the other approach seems unjustified as yet for two main reasons: (*a*) Insufficient basic work has been done to permit a clear comparison, and (*b*) the difference in "efficiency" may not be sufficiently significant, thus leaving the decision up to structural considerations and those of manufacturing. Known recommendations for the design of turbine nozzles (5) can be followed rather easily, and relatively low diameter ratios of the nozzle ring have been found to be as good as greater ones resulting from "long" nozzle channels. Some of the basic design considerations concerning nozzles used for flow measurements should be kept in mind.

In the case of a radial turbine, the question can be asked whether nozzle vanes are essential or not. Compressors and pumps with so-called vaneless diffusers and/or volute-type scrolls as diffusing means are well known. They offer certain advantages such as a flat head-volume curve and less tendency for pulsation. A reversal of the flow in this compressor configuration represents, of course, a turbine without nozzle vanes. The calculation of such a turbine offers no special difficulties.

For reasons of simplicity, the flowing medium will be considered to be a perfect nonviscous gas and the sidewalls of the vaneless ring assumed to be parallel with the axial distance or channel depth b. The tools at disposal are

(1) $p v^{\kappa} = \dfrac{p}{\rho^{\kappa}} = \text{const}$ (isentrope)

(2) $r c_t = \text{const} = k$ (free vortex)

(3) $\rho A c = \text{const}$ (continuity)

(4) $\Delta H_{sd} = \Delta \dfrac{c^2}{2_g} = c_p \Delta T$ (constant energy)

Following this sequence, and with x and y representing two radii of the vaneless ring considered, and with c_m and c_t characterizing the meridional and the tangential components of the velocity c

$$\frac{p_x}{\rho_x^{\kappa}} = \frac{p_y}{\rho_y^{\kappa}}; \quad r_x c_{tx} = r_y c_{ty}$$

$$\rho_x b_x r_x c_{mx} = \rho_y b_y r_y c_{my}$$

$$(c_{mx}^2 + c_{tx}^2) - (c_{my}^2 + c_{ty}^2) = 2gJc_p(T_y - T_x)$$

Combining these equations leads to

$$\frac{c_{mx}^2 - c_{my}^2}{2g} + \frac{c_{ty}^2}{2g}\left[\left(\frac{r_y}{r_x}\right)^2 - 1\right] + \frac{\kappa}{\kappa - 1}\frac{p_y}{\rho_y}\left\{\left(\frac{r_y c_{my}}{r_x c_{mx}}\right)^{\kappa - 1} - 1\right\} = 0$$

Per definition of the nozzle angle α, there is

$$\tan \alpha = \frac{c_m}{c_t}$$

with

$$c_t = \frac{k}{r}$$

and

$$c_m = f(r)$$

or

$$\tan \alpha = \frac{r f(r)}{k}$$

If two radii from the center of the ring to two points representing the beginning and the end of a flow filament include the angle Φ, there is per geometry

$$\tan \alpha = \frac{dr}{r d\Phi}$$

or transformed

$$d\Phi = \frac{k dr}{r^2 f(r)}$$

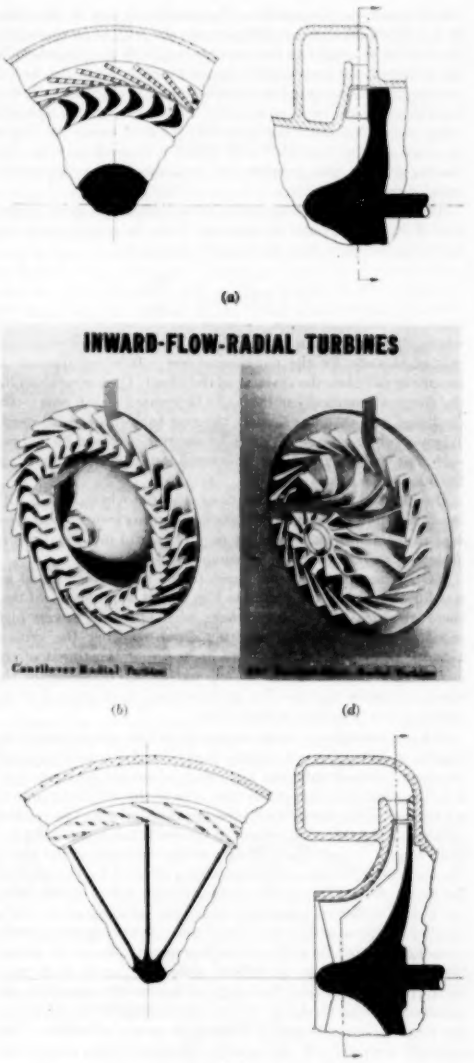

FIG. 9 SCHEMATIC CROSS SECTIONS AND THREE-QUARTER VIEWS OF SINGLE-STAGE CENTRIPETAL TURBINES

which represents the answer to the question of how to determine Φ as a function of r or, in other words, the path of an element of the flowing substance in the vaneless ring with parallel sidewalls. As is known, for nonviscous, noncompressible fluid, the flow of constant angular momentum between parallel sidewalls follows a logarithmic spiral (sink or source). Considering a sink flow of a compressible substance one finds that the fluid leaves the ring at an angle smaller than that with which it entered the ring (12). Taking friction into account the deviation from a logarithmic spiral decreases somewhat.

The calculation of the geometric conditions for a given weight flow W, pressure p, and temperature T can be approached in the following manner: The determining throat area

$$A = \pi 2rb \sin \alpha = \frac{W}{\rho c}$$

where the density can be calculated on the basis of isentropic change of state for the nonviscous flow. It is not unusual to assume or calculate the reaction of the wheel (4), thus establishing the thermodynamical conditions to be created at the nozzle-ring discharge, and then to calculate the ring backward—so to speak. When a volute-type scroll precedes the ring it should be laid out such that the dimensioning of the scroll results in a flow match at the inlet to the nozzle ring.

Over and above the deliberations essential when dealing with incompressible fluids, the limitations resulting from critical pressure ratios and critical velocity require careful investigations in designing turbomachinery for compressible fluids.

Restricting the discussion again to the single-stage radial inward-flow-type turbine similar to Fig. 9(*c*), it is quite evident that there are at least three places where, when operating at very high pressure ratios, choking resulting from reaching the critical velocity can occur. These three areas are at the throat of the nozzles, at the inlet of the wheel, and at the discharge of the wheel, assuming that the flow path between these areas is so designed as not to impose a restriction.

It is not too difficult to determine the proper throat area of the nozzles, based upon test results or published recommendations. However, without sufficient knowledge about the reaction of the wheel the dimensioning of the inlet area to the wheel can present a problem when the over-all pressure ratio permits the relative velocity at the OD of the wheel to approach the critical velocity. With respect to a similar difficulty at the discharge of the wheel, the knowledge of the energy extraction effected by the wheel is essential. In this respect the turbine design suffers equally from the lack of sufficient knowledge about the influence of the finite number of blades, as does the compressor. Not being in possession of enough test results with very high pressure ratios of, let us say, from 5 to 10 per stage, no definite statement can be made here, except that it is felt that the danger of incorrectly estimating the conditions at the discharge of the wheel seems to be somewhat less than the one with regard to the inlet area of the wheel. The standard approach via the velocity triangles at the points considered at the impeller and, thus, establishing a basis for a calculation of the thermodynamical state of the flowing substance at those points is, for the time being, probably as good as any other approach in so far as the designer is concerned. Space does not permit a detailed presentation of this procedure.

Without going into an extensive and partly speculative analysis, it is rather difficult to determine as a function of nozzle angle the change in magnitude of the blade to jet velocity ratio or head coefficient at which maximum efficiency will be obtained. Experimental data gained from one radial turbine with pivoted nozzle vanes indicates that the head coefficient at which maximum efficiency occurs increases slightly with decreasing nozzle angles (compare Fig. 20). However, this observation does not as yet justify the quotation of numerical values. It appears to be in contradiction with values resulting from a simplified one-dimensional analysis, the assumptions in which, do, however, not exist when one and the same turbine is operated at different nozzle angles.

Shaft and Seal Matters

No complete analysis of these two problems can be attempted in this paper. Therefore, only a few remarks will be presented on the assumption that they indicate some of the difficulties encountered, not necessarily commonly known.

In the design of extremely small high-speed turbomachinery with wheel diameters of, let us say, from 2 to 4 in. and at or around speeds of rotation of 100,000 rpm, the problems of critical shaft speed and bearing type, arrangement and losses are, some times, difficult ones. During the development of a small exhaust turbosupercharger, mentioned elsewhere in this paper, with 3-in. wheels and 70 to 80 $\times 10^3$ rpm, quite a variety of reasons forced the use of journal bearings as well as so-called stiff shaft, thus resulting in a shaft diameter of approx 0.4 in. Using oil taken from the sump of the reciprocating engine to be supercharged, a loss of about 2 hp was experienced from the two journal bearings with an l/d ratio of 1, whereas two ball bearings only consumed about $^1/_2$ hp, all at 80,000 rpm. In small turbines produced for airplane-cabin refrigeration, ball bearings with mist lubrication have been proved to offer a good service and reasonably low friction losses. In very small gas turbines, however, one frequently faces the necessity of using an abundant amount of lubricant for cooling reasons, that is, for preventing an excessively large flow of heat from the turbine wheel through the shaft. In antifriction bearings, large amounts of lubricant generally contribute to increased power loss (10). Where weight and space are not at a premium, so-called outboard-bearing arrangements offer the advantage of decreased heat flow to the bearing. Brown-Boveri's small exhaust turbosupercharger (Fig. 10) has a back-to-back radial-type rotor

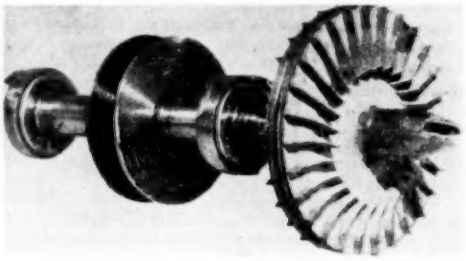

Fig. 10 Rotor of Small Exhaust Turbosupercharger (Brown, Boveri Cie, Switzerland.)

cantilever mounted, thus eliminating the "hot" turbine bearing altogether.

Of course, wherever possible, operating the rotor above the critical speed, or designing for high critical speed of the rotor can diminish both the size and the friction losses of the bearings. For very small turbomachinery, one cannot but acknowledge a definite need for a new approach regarding the bearing problems. The features mostly desired are reduction to elimination of liquid lubricants and, where this approach seems impossible due to heat-flow conditions, lubricants and bearings, capable of operating at considerably higher temperatures than are permissible at present, should be developed. Furthermore, because of very

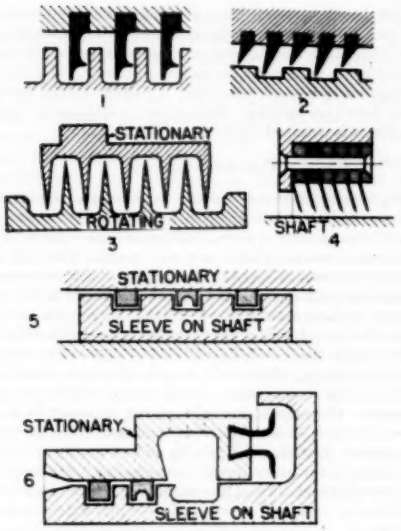

FIG. 11 SEALS FOR TURBOMACHINERY FOR COMPRESSIBLE FLUIDS

small clearances frequently required between stationary and rotary elements, correspondingly small clearances or "looseness" are desired of the bearings. It appears that thoughts of this kind can hardly be called utopian. As far as need for thrust bearings is concerned it can be said that these normally do not present a serious problem, because the impeller or wheel thrust, in general, can be kept to a small value by means of properly pressure balancing the disk surfaces producing thrust.

One of the factors usually influencing the efficiency of turbomachinery is seal leakage. Numerous seal configurations have been developed. Some of these can almost be considered more or less accepted standards, for instance, in steam turbines. Examples 1 and 2 in Fig. 11 show two well-known arrangements. For lightweight, high-speed turbomachinery, requirements are somewhat different from heavy stationary steam turbines, and modified configurations have been developed, for instance, for the aircraft superchargers. In example No. 3 a seal type also based on the labyrinth effect is shown, which was used probably as early as 30 years ago. Another solution which offers certain advantages in so far as mass production and replacement are concerned is shown in example No. 4. This configuration has been used successfully and is easily adaptable to different conditions regarding pressure difference and temperature. Example No. 5 shows an entirely different approach, namely, the so-called piston-ring seal which also has been made to work satisfactorily in mass-produced aircraft machinery. The opinions about the merit of this design are widely split, mainly with respect to the question of lubrication. Presence of oil in the compressed air is totally not permissible, for instance, in air-conditioning systems. Example No. 6, which the author suggested for the first five-stage, high-altitude supercharger of the radial type, shows a combination of double thin edge seal combined with a piston-ring seal separated by a ventilated or pressurized chamber. This seal, somewhat space-consuming, operated satisfactorily. When discussing the importance of seals, it must be kept in mind that they are not only essential for efficiency reasons, because whenever thrust control or thrust equalization on wheel types dealt with in this paper are of importance, some kind of seal problem also exists. Fig. 1(*a*) shows the application of the thin edge portion of example No. 6 to a turbine and/or compressor wheel. This configuration has been used successfully after proper fabrication and centering techniques had been learned.

PERFORMANCE CHARTS

During the past two decades it has become commonly accepted practice to present the performance characteristics of turbocompressors in dimensionless or semidimensionless ordinates. Because of its known influence the velocity of sound has been introduced as the denominator for dimensionless characteristic values, like the wheel Mach number, defined as the quotient of wheel-tip speed and sonic velocity. The volume flow divided by a typical flow area (e.g., the square of the wheel diameter) times sonic velocity, or the inlet velocity divided by sonic velocity (called the inlet Mach number) are values frequently plotted as abscissa with the pressure ratio as ordinate and wheel Mach number and efficiency as parameters.

These characteristic values and others derived therefrom naturally can also be used for turbines. Somewhat varied expressions, dependent upon the intended usage of the performance chart, can offer additional advantages. One example is shown in Fig. 12 which can be considered to be self-explanatory. This chart is comparable to the well-known compressor charts of similar appearance. Once a turbine has been built and tested and the results have been plotted in this manner, the performance to be expected under varied operational conditions is known for the turbine tested as well as others built geometrically similar, provided the "extrapolation" does not reach out too far with respect to Mach number and pressure ratio.

Another rather useful and general chart can be obtained by plotting weight flow times the square root of the inlet temperature, divided by the product of inlet pressure and nozzle throat area versus the pressure ratio applied to the unit. When torque considerations are important, a dimensionless torque characteristic, defined as the quotient of the turbine torque measured and the product of pressure applied, nozzle area and wheel diameter, offers advantages and can be plotted versus wheel Mach number

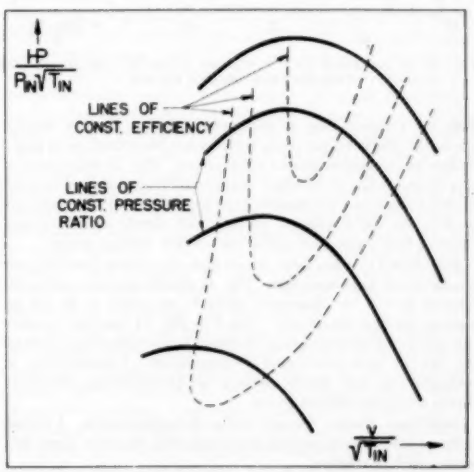

FIG. 12 PERFORMANCE PLOT OF AN AIR TURBINE

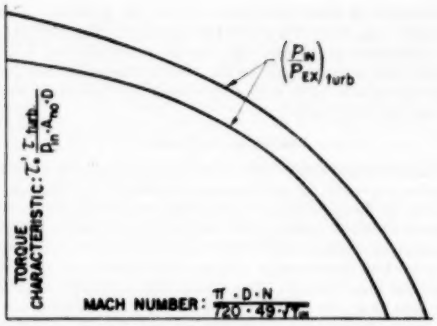

FIG. 13 TURBINE TORQUE VERSUS TURBINE WHEEL MACH NUMBER

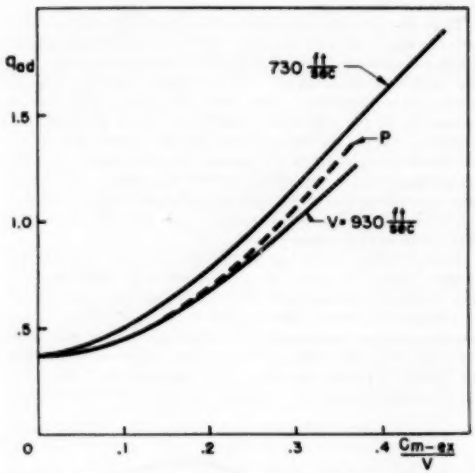

FIG. 14 COMPARISON OF CALCULATED (LINE P) AND MEASURED TURBINE PERFORMANCE VALUES

with the pressure ratio as parameter. Such a chart is helpful where the whole torque characteristics are important, as in automotive or pneumatic starter applications. Fig. 13 shows such a plot for one radial inward-flow turbine exhibiting a shape basically known from some automotive-type torque converters which go back to the old Foettinger patents with closely coupled radial outward-flow pump and radial inward-flow turbine rotors.

Elsewhere (4) it has been shown how other type charts can be precalculated approximately. Fig. 14 proves that the approach referred to can be considered valuable especially as an aid to analyze the flow conditions. Line *P* in Fig. 14 had been precalculated, based on assumptions believed to be reasonable, whereas the two full lines were found by experiment. Unfortunately, a corresponding and simple method for precalculating efficiency curves cannot be offered as yet.

Additional charts, demonstrating the performance of radial turbines with special control provisions, will be given when discussing such provisions.

This paper is not the place to discuss the merits of or justifications for the different definitions of turbine efficiency observed to be in use. Whenever efficiencies are mentioned in this paper, the energy available is calculated from total conditions at the turbine inlet and static pressure at the turbine discharge. Moreover, no discharge configurations recovering a portion of the discharge velocity have been included. It is felt that a satisfactory basis for comparisons is obtained when using this definition.

CONTROL METHODS

Going back in the literature about water turbines some 50 to 60 years one finds treatises in books explaining that a very important factor in favor of the radial-type turbine is the simplicity of economical load adaptation over wide ranges. The early axial water turbines were adapted to the varying output requirements by throttling or by changing the degree of admission to the wheel, and these methods are still in use on axial steam turbines. With the introduction of high-efficiency radial-type turbines for compressible fluids, the considerable advantage of changing the mass flow of the working substance by varying the nozzle throat areas all around the circumference of the turbine wheel was again recognized. The nozzle parts to be moved are naturally located between two parallel plain walls perpendicular to the center line of the turbine, thus almost suggesting quite a number of mechanisms changing the nozzle throat area according to almost any desired rate of change. The following basic characteristics can be regarded as a measure for the quality of the different control methods:

(*a*) The less the turbine efficiency changes with varied throat area the better the system is.

(*b*) The simpler the parts and the mechanism, the more reliable the mechanism, and the simpler the problem of maintenance is, the better the system.

(*c*) A system of low inertia and small motion of the control mechanism is desirable.

(*d*) The system and its parts should be as little sensitive to impurities in the working medium as possible.

With these thoughts in mind, the different control methods,

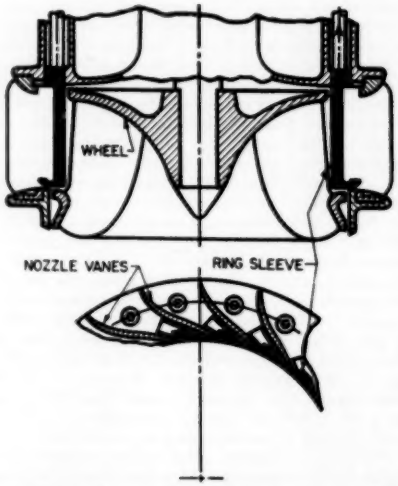

FIG. 15 WATER TURBINE WITH ADMISSION CONTROL THROUGH RING SLEEVE

that is, methods to adapt the turbine output to the load requirement, will be discussed in the following:

The method of controlling the output by "throttling" is widely known and used, so are its features and simplicity; the analysis does not present problems. Throttling means losing or wasting energy. Therefore, the system efficiency is the lower the more the demand and the supply of energy differ.

Both in the field of water turbines (1) and water pumps, a "ring sleeve," as shown in Fig. 15, in the closed position, is well-known and was used late in the 19th century by American turbine companies in water turbines at Niagara Falls. Swiss and French manufacturers have also used this method. The cylindrical sleeve between nozzle outlet and turbine wheel can be moved parallel to the axis of the turbine. As has been pointed out in literature, the design of the ring should be such that, independent of its position, the fluid flow is well guided in order to prevent flow patterns detrimental to maintaining good efficiencies over a wide range of nozzle-area change. Reasonable freedom regarding the relationship between axial location of the sleeve and effective nozzle throat area can be secured; for instance, by twisting the nozzle vane such that with a linear decrease in actuation a more than linear decrease in effective nozzle area can be obtained. The sleeve control may have a certain disadvantage in common with the throttling control when the operational conditions require maximum efficiency at part load (compare in contrast the characteristics of a variable area nozzle as in Fig. 21). However, performance charts demonstrating the relationship between part load and efficiency have apparently not been published. Aside from design problems, the sleeve seems to offer two attractive features, namely, a moderate sacrifice in efficiency at part load, and the possibility of being used as a shut-off means.

"Partial admission" is another known way for output control. There are quite a number of configurations like subdivided nozzle boxes or turbine inlet housings with control valves at each housing section, or special mechanisms with blocks that can be moved into some or all nozzle throats to vary the degree of admission. Efficiency curves covering this system were not at hand except those shown in Fig. 16 calculated from published (13) and unpublished test results. The value c_s used in the dimensionless abscissa is somewhat arbitrarily selected and defined as inlet volume flow divided by πDb, which represents the meridional inlet area of the wheel. A statement as to the general applicability of these results cannot be offered at present. The decrease in efficiency shown can hardly be called great over a range from 100 per cent down to 35 per cent admission. Some of the more interesting constructions for partial admission in water turbines are—in a simplified form—shown in Figs. 17 (*a*) and (*b*), because they may inspire the designer of radial turbines for compressible fluids.

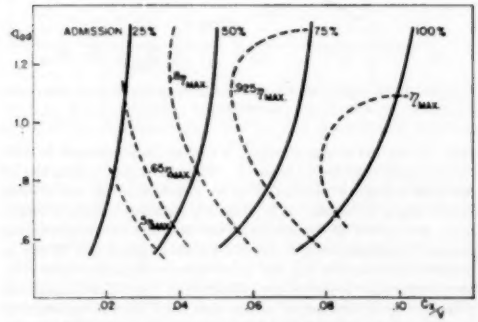

FIG. 16 INFLUENCE OF PARTIAL ADMISSION ON EFFICIENCY OF RADIAL-TYPE AIR TURBINES
(Approximative results from different investigations.)

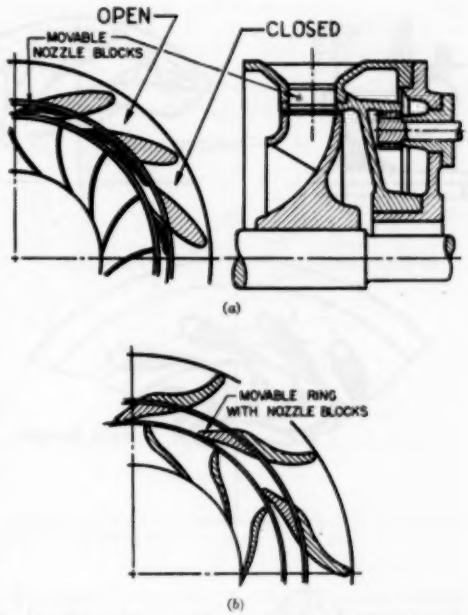

FIG. 17 PARTIAL ADMISSION CONTROL AS USED IN WATER TURBINES

The method widely used for varying the throat area in radial-type turbines is the one introduced around the turn of the century and frequently referred to as the "Fink control system." A wide variation, see Figs. 18 (*a*), (*b*), and (*c*), of vane patterns and mechanisms have been developed successfully. This method of control has rightfully been called the superior method and has demonstrated its reliability at least in water turbines over long periods. Some important design requirements are (*a*) small leakage losses or, in other words, minimum clearance between vanes and side walls; (*b*) low friction forces; (*c*) favorable flow conditions in all vane positions (14); and (*d*) small forces resulting from the pressure distribution around each vane. In many cases it is also desirable to design for total shut-off of the through-flow in the fully closed position of the nozzle vanes. It would go too far to describe design details here since considerable information is available in the literature. One of the 11,000-hp water turbines of the Ontario Power Company at Niagara Falls delivered around the turn of the century by the German Machine Works J. M. Voith, for instance, is equipped with this system.

The author has used this method successfully in experimental air turbines before World War II and in a very small exhaust turbosupercharger previously mentioned. The air turbines were mainly built as stop-gap equipment for special cooling and refrigeration purposes. Construction difficulties experienced with these units were actually only of a minor nature. During this development one unit was equipped with flexible nozzle vanes fabricated from thin spring-leaf steel, so arranged that the variation of the throat areas was obtained by deforming the flexible vanes

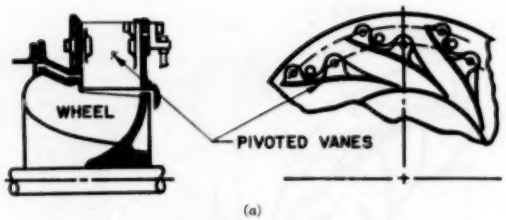

(a)

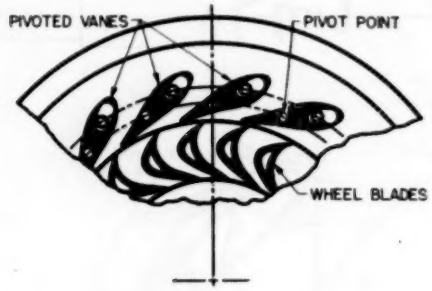

(b)

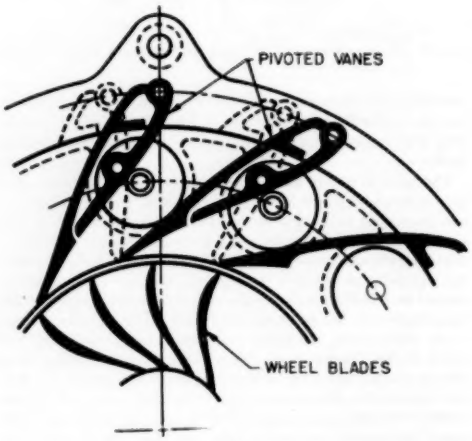

(c)

FIG. 18 VARIABLE-AREA NOZZLE ARRANGEMENTS WITH PIVOTED VANES AS USED IN WATER TURBINES

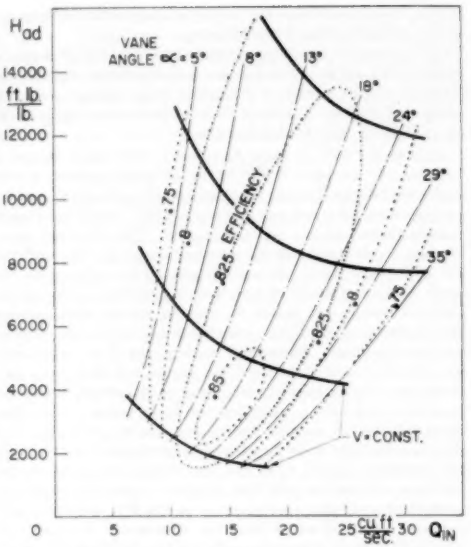

FIG. 19 TEST RESULTS OBTAINED WITH SINGLE-STAGE CENTRIPETAL AIR TURBINE OF THE 90-DEG TYPE
(Load controlled by a variable-area nozzle ring with pivoted vanes. First machine of this type built.)

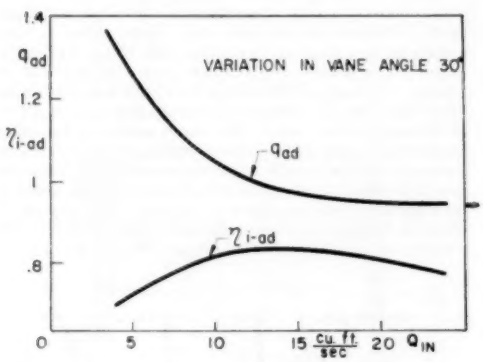

FIG. 20 SAME AS FIG. 19, EXCEPT FOR DIFFERENT NOZZLE ARRANGEMENT

such that good nozzle shapes, the importance of which may have been overestimated at that time, were always maintained.

What few test results survived the occupation by the Russian Army are shown in Figs. 19 and 20. Fig. 19 represents a full performance chart of an air turbine with head plotted versus inlet-volume flow with curves of constant tip speed, of constant vane angle, and of constant shaft efficiency as parameters (4). The lines of constant nozzle angle and of constant efficiency coincide very well and approach quadratic parabolas rather closely. At the time of the experiments on this unit it was felt that, by certain design changes, a further improvement in efficiency could have been obtained. The load range within the 75 per cent efficiency plateau, that is, between 5-deg and 35-deg nozzle angle, is roughly 1:2. Fig. 20, obtained with a different unit, also serves to demonstrate how flat the curve connecting points of maximum efficiencies stays with a variation of 30 deg in nozzle angle; and in Fig. 21, based upon still another unit (15), two important features are illustrated: (*a*) The change in efficiency as a function of nozzle area, and (*b*) the influence of doubling the specific blade loading of the same unit. The design point is so selected that sizable load variations downward and upward, accompanied by very gradual efficiency decrease, are

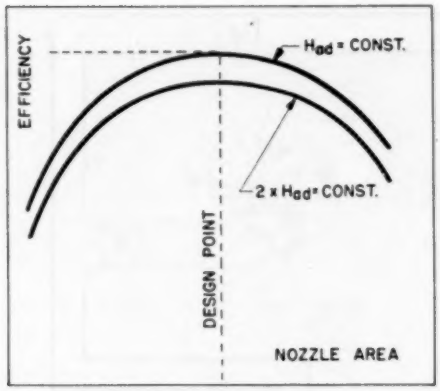

FIG. 21 CHARACTERISTIC DATA FOR SINGLE-STAGE CENTRIPETAL AIR OR GAS TURBINE OF THE 90-DEG TYPE, WITH VARIABLE-AREA NOZZLES

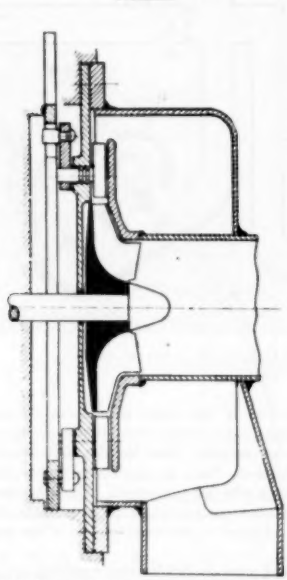

FIG. 22 SMALL EXHAUST TURBOSUPERCHARGER, WHEEL DIAMETER 3 IN., WITH VARIABLE-AREA NOZZLES FOR AUTOMOTIVE APPLICATIONS

obtained. This type of machinery is well suited where conditions require a wide load variation at constant rpm which covers the problem statement, for instance, for a-c generators.

One of the air turbines referred to has also been tested as a compressor (10) in an effort to establish the feasibility of a machine that can be used equally well as a compressor and as turbine. Water-power plants have been built using turbomachinery of the radial type serving as turbines during the times of high loads and as pumps when an excess of energy available permits pumping the water into storage reservoirs.

When testing the first small exhaust turbosupercharger, Fig. 22, mentioned previously, the method used originally to vary the nozzle angle was found not to be as efficient as desired. Satisfactory results were obtained with a system, the basic features of which are shown in Fig. 23. The parts were simple and cheap and caused very little difficulty during the endurance testing,

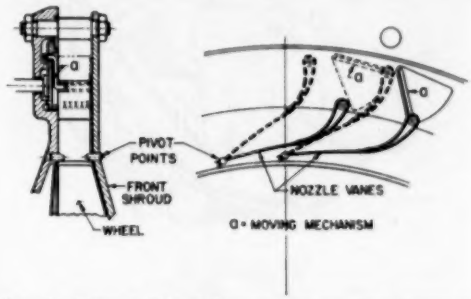

FIG. 23 IMPROVED NOZZLE ARRANGEMENT FOR UNIT SHOWN IN FIG. 22
(Designed and tested in 1944.)

except for lead deposits resulting from operating the reciprocating engine on highly leaded aviation fuel.

INDUSTRIAL RADIAL TURBINES

During their development of small exhaust turbosuperchargers the Swiss Brown-Boveri people also decided to use radial inward-flow turbines, Fig. 10, on some models, whereas in others axial-type turbines are still preferred. However, the blading, shown in Fig. 10, is not of the straight 90-deg type. It is also known that Kapitza used radial-type turbines in his early work, probably on air liquefaction. Meanwhile, several manufacturers have decided to use the radial turbine for compressible fluids when the problem statement calls for low specific speed; other companies are exhibiting an increasing interest. In *Flight Magazine* early this year, the following note, considered to be quite interesting, was found: "Mr. Theed also spoke of the air-cycle-turbine cold air unit, which has recently been modified to employ a radial-flow turbine in place of the axial-flow type previously used. By this means a considerable advantage in performance, size-for-size, has been made possible."

The author is convinced that quite a number of turbines including those for steam now built as axial turbines could be produced much more favorably as radial turbines. There will, of course, be some difficulties and possibly occasional disappointments not now foreseen.

Centripetal turbines have, apparently, established their right of existence for so-called auxiliary power units of a great variety. Some of the units developed have not yet been cleared for publication; illustrations of others were not available at the time of this writing. The turbomachinery equipment manufactured by the author's company uses centrifugal compressors, and most of the turbines are of the centripetal type with 90-deg wheels, Fig. 24. These turbines are being used successfully in five different applications: Gas turbines, air-turbine motors, air-turbine starters, gas-turbine motors, and refrigeration turbines. In all cases the efficiencies are of the magnitude shown in Figs. 6(*a*) and (*b*). In the gas turbines, high wheel-tip speeds and gas temperatures occur simultaneously. Several units have passed hundreds of hours of severe running. Small air turbines for aircraft refrigeration systems have been built, delivered, and used by the thousands

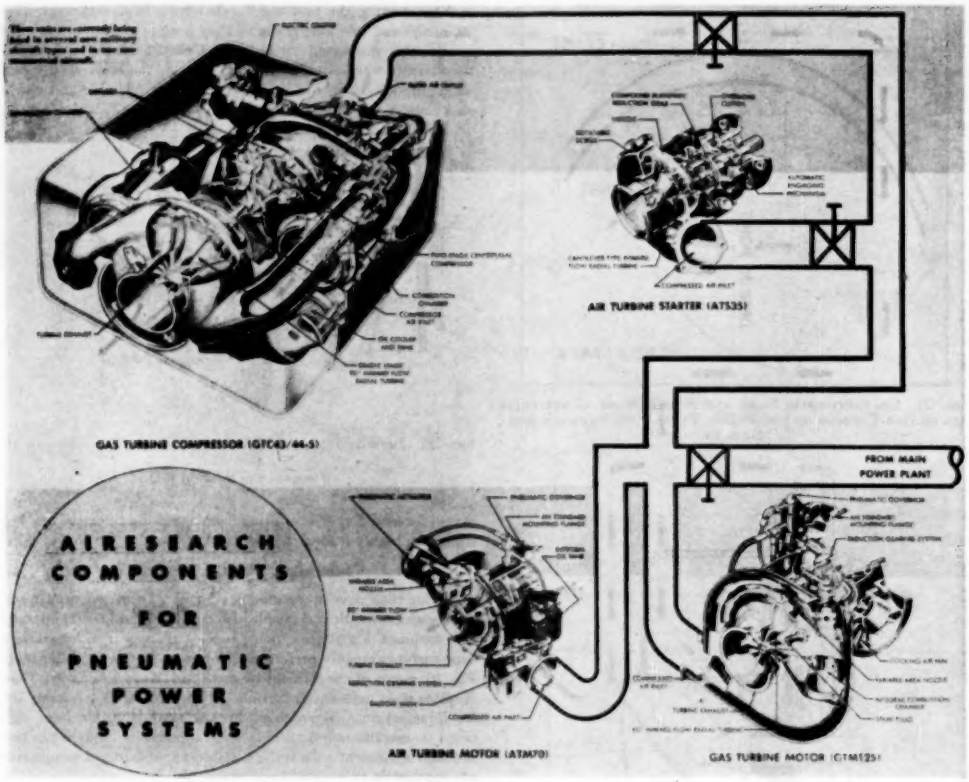

FIG. 24 GAS AND AIR TURBINES OF CENTRIPETAL TYPE FOR AERONAUTICAL APPLICATIONS
(Courtesy AiResearch Manufacturing Company.)

with both the 90-deg wheel and the bucket-type wheel, Fig. 25.

Because of the well-known requirements regarding modern high-speed airplanes, the development of this small turbomachinery had to be done against severe handicaps, such as the many unknowns about this turbine type and extraordinarily critical weight and space limitations. The success obtained in a few years can hardly be denied. Hence, it is not surprising to observe the rapidly disappearing skepticism about its merits, whereas the interest, let alone enthusiasm, for this simple type turbine wheel for gaseous substances was low only a few years ago.

Fig. 24 shows what is called an integrated pneumatic power system the greatest portion of which, incidentally, has undergone ground and flight testing. Arranged in the upper left corner, the gas-turbine unit reveals a typical single-stage 90-deg inward-flow radial wheel driving a two-stage centrifugal compressor. This gas-turbine unit is unusual in that it does not produce shaft power but serves as a source of compressed air. The speed of this unit is 40,000 rpm at rated output, and the efficiencies and the rotating weights are such that neither the automatic starting, the acceleration, nor the thermodynamical performance are objectionable when comparing this very small unit with its big brothers with some 40 to 80 and more times the amount of mass through flow.

The second link in this power plant is an air-turbine starter (for gas turbines), again of the inward-flow type, working on bleed air out of the gas turbine. Semi-impulse buckets are used in this single-stage turbine. Such an air-turbine starter can, of course, also be built with a 90-deg-type wheel. The important feature required from such a pneumatic starter is a torque characteristic, Fig. 26, well adapted to the requirements of the gas turbine to be started.

The third link is an air-turbine motor serving as a generator or pump drive, working on either bleed air from the small gas turbine or bleed air from the propulsion gas turbines of the airplane. Its two elements most interesting here are a simple 90-deg inward-flow turbine wheel again, and a variable-area nozzle-vane system surrounding the wheel in a plane perpendicular to the center line of rotation. The advantages of this type of control system when great load variation and highest economy, even at varying level of energy supply, are required simultaneously have been mentioned before.

Finally, in the lower right corner, a gas-turbine motor is shown. The difference between this unit and the air-turbine motor results from the addition of a combustion chamber, in this case buried in the turbine housing, producing a frequently desired increase in energy available from the bleed-air source. The turbine wheel

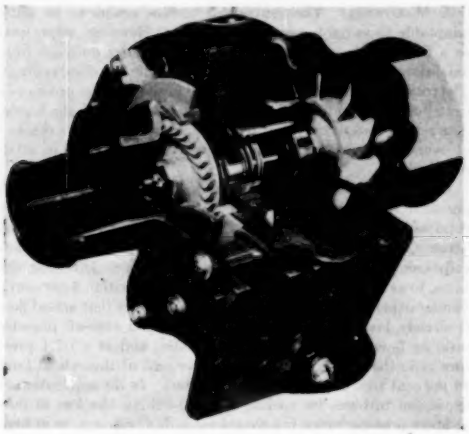

FIG. 25 MINIATURE REFRIGERATION TURBINE OF CENTRIPETAL TYPE
(Courtesy AiResearch Manufacturing Company.)

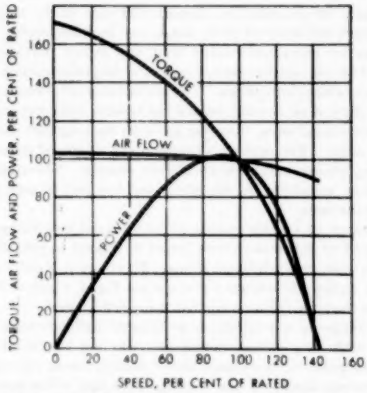

FIG. 26 TORQUE CHARACTERISTICS OF AIR-TURBINE STARTER
(Courtesy AiResearch Manufacturing Company.)

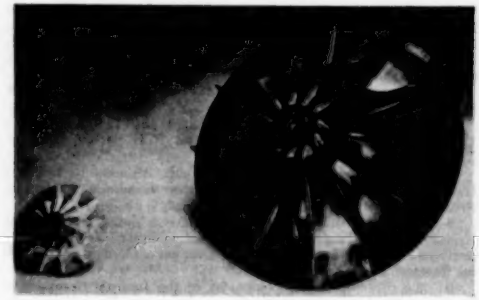

FIG. 27 TURBINE WHEELS
(Courtesy AiResearch Manufacturing Company.)

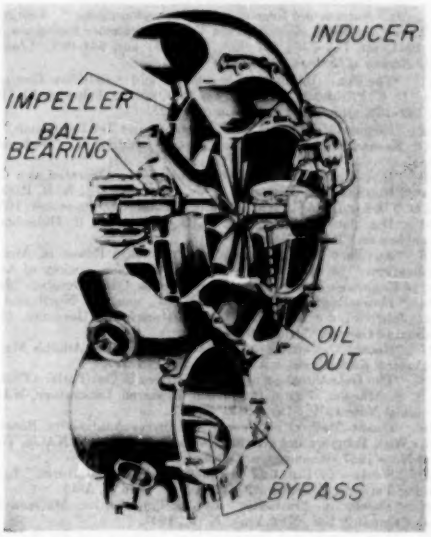

FIG. 28 JUNKERS AIRCRAFT SUPERCHARGER WITH FULLY SHROUDED IMPELLER

again is of the 90-deg type. Fig. 27 shows two turbine wheels which in spite of the difference in size are producing almost equal efficiencies under comparable conditions.

Results from these and similar units seem not to fall in line with opinions expressed in literature regarding the Reynolds-number influence in turbines. Fig. 28 shows a supercharger of a Junkers aircraft engine which is about as compact as such a unit can be built. Being of the vaneless type and having demonstrated very good efficiency, it is shown here as an example for what the author, once closely connected with the development of the unit shown, considers interesting also for the line of radial-turbine development.

CONCLUSION

This paper cannot claim to be more than an accumulation of high lights and side lights. For space and time reasons two subjects of great importance could not be dealt with at all: Control systems and metallurgical problems. Rather extensive publications exist, however, in this field.

As in any other activity, where the work is done in a serious attempt of thoroughness and with an honest willingness to face the facts, one can only confirm wholeheartedly what others have observed before: The longer and the more intensively one studies the problems, the less one knows with certainty.

BIBLIOGRAPHY

1 "Turbinen und Turbinenanlagen," by Viktor Gelpke, Julius Springer, Berlin, Germany, 1906.

2 "Die Gestaltung von Flugmotorenladern," by W. T. von der Nuell, *Luftfahrtforschung* (Aeronautical Research), vol. 14, 1937, pp. 244–253.

3 "Fluid Mechanics of Turbo Machinery," by G. F. Wislicenus, McGraw-Hill Book Company, Inc., New York, N. Y., 1947.

4 "The Radial Turbine," by W. T. von der Nuell, Report No. F-TR-2149-ND, Headquarters Air Materiel Command, Wright Field, Dayton, Ohio, January, 1948. Also, Technical Data Digest, United States Air Force Headquarters, Air Materiel Command, September, 1947.

5 "Steam and Gas Turbines," by A. Stodola, translation by L. S. Loewenstein, Peter Smith, New York, N. Y., 1945.

6 "Efficiency of Radial-Flow Exhaust-Gas Turbine With a 12.75-Inch Tip Diameter," by E. E. Coulter, R. G. Larkin, and D. S. Gabriel, NACA MR E6F03, July, 1946.

7 "Lader," by W. T. von der Nuell, Automobiltechnisches Handbuch (Automotive Handbook), sixteenth edition, Verlag de Gruyter, Germany, 1946.

8 "Die Festigkeit hochbeanspruchter rein radial beschaufelter Kreiselverdichter-Laufrader," by K. J. Muller, Jahrbuch der deutschen Luftfahrtforschung, 1944. (Annual of German Aeronautical Research.)

9 "Lectures on the Development of the Internal Combustion Turbine," The Institution of Mechanical Engineers, Proceedings, vol. 153, 1945. Published by the Institution, Storey's Gate, St. James's Park, London, S.W.1.

10 (a) "Auslegung und Gestaltung der Flugmotoren Lader."
(b) "Abgasturbolader fuer Flugmotoren."
(c) "Ausfuehrungsformen von Flugmotorenladern."
(d) "Antrieb und Regelung der Flugmotorenlader." A series by W. T. von der Nuell, *Zeitschrift des Vereines deutscher Ingenieure*, vol. 85, 1941, pp. 763–773; 847–857; 905–913; and 981–989. (*Journal of the Society of German Engineers.*)

11 "The Sonic Barrier in Centrifugal and Axial-Flow Compressors," by C. Pfleiderer, *Zeitschrift des VDI*, vol. 92, February 21, 1950, pp. 129–133, and June 1, 1950, pp. 406–407.

12 "Elementary Theory of Gasturbines and Jet Propulsion," by J. G. Keenan, Oxford University Press, London, G. Cumberlege, 1946.

13 "Investigation of Centrifugal Compressor Operated as a Centripetal Refrigeration Turbine," by J. J. Rebeske, Jr., R. B. Parisen, and H. J. Schum, NACA RM E50I20, Washington, December, 1950.

14 "Die Dampfturbine," by W. H. Eyermann, R. Oldenbourg, Muenchen und Berlin, 1906.

15 "Auxiliary Gas Turbines for Pneumatic Power in Aircraft Applications," by H. J. Wood and F. Dallenbach, Society of Automotive Engineers, Paper no. 381, Los Angeles, Calif., October, 1949.

16 "Lader-Regelverfahren," by W. T. von der Nuell and H. Pfau, Jahrbuch der deutschen Luftfahrtforschung, Germany, 1941. (Annual of German Aeronautical Research.)

17 "Recent Developments in Gas Turbines," by Adolph Meyer, *Mechanical Engineering*, vol. 69, 1947, pp. 273–277.

18 "The Determination of Elastic Stresses in Gas Turbine Disks," by S. S. Manson, Flight Propulsion Research Laboratory, NACA Technical Note 1279, May, 1947.

19 "Direct Method of Design and Stress Analysis of Rotating Disks With Temperature Gradient," by S. S. Manson, NACA Technical Note 1957, Washington, October, 1949.

20 "Stresses in Rotating Disks at High Temperatures," by A. Stanley Thompson, Trans. ASME, vol. 68, 1946, p. A-45.

21 "Theory of Elasticity," by S. Timoshenko, McGraw-Hill Book Company, Inc., New York, N. Y., 1947.

22 "The Theory and Design of Gas Turbines and Jet Engines," by E. T. Vincent, McGraw-Hill Book Company, Inc., New York, N. Y., 1950.

23 "Thermodynamics," by J. H. Keenan, John Wiley & Sons, Inc., New York, N. Y., 1941.

24 "Discussion to W. D. Downs's 'Starters for Turbojet Engines,'" by W. T. von der Nuell, Society of Automotive Engineers, January, 1951.

Discussion

HEINRICH ADENSTEDT.[8] The intensive heat exchange between gas and turbine wheel, the small hub diameters, the high rpm, and the tendency not to cool such a wheel in the center must produce greater problems for the bearings. Is the author in a position to give any information on these problems? How are overheated bearings avoided? Are insulating and cooling methods used or is the bearing moved some distance away from the rotor, with the turbines running at speeds above the critical frequency of the wheel arrangement?

[8] Dayton, Ohio.

J. MAKOWSKI.[9] The centripetal turbine seems to be quite adaptable to variable nozzle-area design. However, when used as a fixed-nozzle area, it has flow characteristics different from axial-flow turbines, which, in some applications, is a disadvantage. The rotation of air after the nozzles and in the impeller produces a centrifugal gradient affecting pressure at the exit from the nozzle. As a result, the critical pressure ratio across the nozzles is reached at over-all pressure ratios much higher than take place in axial-flow turbines.

In our experience with axial-flow turbines, designed for a high per cent reaction (peak efficiency almost at the same velocity ratio as in similar size centripetal turbines), we have found that actual air flow through the turbine and air flow calculated theoretically using over-all pressure ratio as a reference is almost the same, to as low as 1.7:1 over-all pressure ratio (within 3 per cent). Similar experience with centripetal wheels shows that actual flow is already lower than theoretical (based upon over-all pressure ratio as before) at a 3.5:1 pressure ratio, and at a 1.7:1 pressure ratio the flow is only about 82 per cent of theoretical (and 84 per cent that of the axial-flow turbine). In the application of expansion turbines for cooling airplane cabins, the loss of flow at lower pressure ratios is a considerable disadvantage, as at high altitudes and small pressure ratios across the turbine, smaller flows are passed through the turbine to the cabin with the centripetal turbine than with the axial-flow turbine, even if both turbines have the same flow at sea level (high pressure ratio).

Another peculiarity of centripetal turbines, coming from the centrifugal forces acting in opposite direction of the flow, is its well-known tendency to erode nozzle and impeller blades.

It can be visualized readily that any heavy particle which enters with the air between nozzle and impeller cannot escape until it is broken into pieces. The pieces have to be small enough so that drag of air flowing toward the smaller diameter will overcome centrifugal force, throwing particles back against the nozzle trailing edge. The problem of erosion can be solved successfully by using proper materials and blade shapes. Nevertheless, it diminishes, somehow, the simplicity and low cost of making centripetal turbines.

The range of specific speeds at which axial-flow turbines are as efficient or better than centripetal is difficult to establish and depends upon many different items. Therefore it is quite natural that the author did not put a scale on his Fig. 4, which is the only curve in the paper plotted against the specific speed.

The foregoing comments on centripetal turbines refer to impellers with long blades (compressor running backward type). The centripetal turbines using airfoil profiles are an intermediate step between axial and true centripetal design which have their own problems, not mentioned in this discussion.

HANS SCHWARZ.[10] The writer is interested in radial turbines primarily for Diesel-engine superchargers. The simplicity and ease of manufacturing alone justify their consideration.

Does the author know of any radial inflow turbines being used as a supercharger drive for a Diesel engine operating with divided manifolds?

It appears that the radial turbine has an inherently higher WR^2 value. This would be detrimental to engine acceleration.

Heat dams have been developed to cut down the heat flow to a hot turbine end bearing to a value which is less than the temperature variations obtained in production bearings. Would the author care to comment on the subject of turbine-wheel cooling?

[9] Stratos Division—Fairchild Engine & Airplane Corporation, Farmingdale, L. I., N. Y.

[10] Project Engineer, American Locomotive Company, Schenectady, N. Y. Jun. ASME.

Author's Closure

The author wishes to express to the discussers his appreciation for the interest they have shown in the paper and for their valuable contributions.

Mr. Adenstedt's questions can easily be answered by saying that all of the means he lists have been or are being used to prevent bearing overheating. With AiResearch gas turbines, there have not been major difficulties with the turbine bearings.

With regard to Mr. Makowski's comments the author can only state that, provided that he interprets the observations correctly, they do not coincide with his own experience. No basic discrepancy between observed and properly calculated flow characteristics came to the author's attention. Also, he fails to see why, in this matter, there should be a difference between axial and radial turbines of equal reaction.

Talking about nozzle erosion, Mr. Makowski states very rightfully that this problem can be solved successfully. The author, however, does not happen to agree with the opinion expressed that such solution impairs the simplicity of centripetal turbines.

To answer Mr. Schwartz: A centripetal turbine is being used in the turbocharger of a Diesel engine. Information on the manifolding system is not available. It does not appear necessary for the radial turbine to have an inherently higher WR^2. The author's information about acceleration does not indicate specific difficulties. In regard to wheel cooling, the author is not exactly enthusiastic about it, at present, and is in favor of avoiding it as long as economics will permit.

Research in Exhaust Manifolds

By P. H. SCHWEITZER,[1] STATE COLLEGE, PA.

Over a period of four years, with the aid of the Office of Naval Research, the author has investigated the effect of the exhaust manifold on engine performance, particularly in two-stroke-cycle multicylinder engines. Some aspirator-type manifolds create suction rather than back pressure and result in scavenging-air flows that are greater than obtainable not only with conventional manifolds but even with no manifolds at all.

ALONG the quests to extract more power from every pound of fuel burned in an internal-combustion engine, the important role that the exhaust pipe plays in the engine has been largely overlooked until recently. This is the more remarkable because it has been known that about 40 per cent of the fuel energy escapes through the exhaust pipe and that a fair portion of this can be harnessed. According to Schweitzer and Tsu (1),[2] the convertible exhaust energy of an ideal nonsupercharged Diesel engine is about 9 per cent; of a highly (2 atm) supercharged Diesel engine 17 per cent; of a nonsupercharged spark-ignition engine 15 per cent; and of a similarly supercharged spark-ignition engine 24 per cent of the fuel energy. Some of this energy is being recovered in exhaust turbines in turbocharged engines. In nonsupercharged and in mechanically supercharged engines this energy usually is allowed to go to waste.

The neglect of the exhaust system by engine designers had even more disastrous consequences. Pressure fluctuations in a conventional exhaust manifold generally impair engine performance by interfering with the proper scavenging and charging of the cylinders. Exhaust energy thus becomes a drag on the engine and a spoiler of performance. Two-stroke-cycle engines are particularly sensitive to exhaust-pressure fluctuations because they depend on the pressure gradients rather than on the piston motion for scavenging. The pioneering work of Michael Kadenacy (2) helped to draw attention to the part the exhaust-gas column plays and can play in scavenging the cylinder. While Kadenacy concentrated his attention on the inertia of the gas column that leaves the cylinder, we have investigated the effect of the exhaust manifold on engine performance, *particularly* in multicylinder engines.

The investigation, sponsored by the Office of Naval Research, has been in progress for almost 4 years, and this paper covers the high lights of that phase of the program which was completed by the end of 1950. The experiments were performed on an "air model" and on a "water model" and their main purpose was to study interference between cylinders and develop exhaust manifolds of superior performance characteristics. Before describing the experimental equipment and the results obtained, it may be useful to review briefly the factors that determine the relations between exhaust pipe and the engine performance.

The engine output is limited by its air charge which in turn is a product of the total cylinder charge and its purity (3). The exhaust pipe has a pronounced influence on both of these factors and, therefore, on the engine output. For instance, if the "tuning" of the exhaust pipe is such that a negative pressure wave hits the exhaust opening of the cylinder near the close of the charging period, the cylinder will lose charge during this period, and the power output will suffer. On the other hand, a positive pressure wave may hit the exhaust opening, this pressure wave having been originated from the exhaust blowdown of a neighboring cylinder. Combustion products carried into the cylinder will spoil the purity of the cylinder charge, and power output will again suffer. A good exhaust system is one which helps the cylinder to trap a big charge of little pollution, and the factors to be reckoned with are tuning and interference.

In single-cylinder two-stroke-cycle engines the tuning of the exhaust pipe is of paramount importance. Exhaust-pipe tuning has a considerable literature (4, 5, 6), including analytical and graphical methods for calculating tuning. Pressure fluctuations set up by the exhaust impulses are controlled largely by the geometry of the exhaust system. The pressure waves propagate along the pipe with sonic velocity and are reflected from points of change in cross-sectional area. Pressure waves develop into a certain pattern which repeats itself every engine cycle. A favorable pattern is one which presents at the exhaust port a low or negative pressure during the early part of the charging period and a high pressure during the latter part of the charging period. A low (or negative) pressure during the early part helps to scavenge the cylinder from the residual combustion products and also reduces the parasitic blower horsepower. A high pressure during the latter part of the scavenging period helps to trap more charge in the cylinder. Favorable tuning usually can be accomplished by selecting the proper lengths for the pipes for a given engine speed. The most unfavorable tuning is the case of resonance when the natural frequency of the exhaust pipe happens to coincide with the engine rpm. Then a crest of the exhaust pressure wave closely follows the opening of the exhaust pipe, and the closure is likely to fall in the valley. Such tuning results in poor performance. The difference in output between well-tuned and poorly tuned single-cylinder engines may amount to 30 per cent.

Tuning is much less important in multicylinder engines, but another phenomenon enters the situation, the interference. From four cylinders on, always more than one cylinder is open to the exhaust manifold at any one time, and the exhaust of one cylinder interferes with the other. Interference is more pronounced between cylinders that are close or adjacent to each other and are also near to each other in firing order. Then the exhaust of the cylinder firing later not only will buck the exhaust of the earlier-firing cylinder but exhaust gases are likely to enter and contaminate the other cylinder. Reverse flow in exhaust branch pipes is a common phenomenon in multicylinder engines and results in poor engine performance.

The situation can be understood better by way of a concrete example. An 8-cylinder engine has a firing order of 1-6-5-2-8-3-4-7. The duration of the exhaust is 154 deg. If each cylinder would exhaust through a separate well-tuned exhaust pipe, each would evince exhaust and cylinder-pressure fluctuations as shown by the light lines in Fig. 1, which are satisfactory. But if the cylinders exhaust into a common manifold, all the cylinders will not behave alike. Consider, for instance, cylinder No. 3. Shortly after its

[1] Professor of Engineering, Pennsylvania State College. Mem. ASME.

[2] Numbers in parentheses refer to the Bibliography at the end of the paper.

Contributed by the Oil and Gas Power and Gas Turbine Power Divisions and presented at the Annual Meeting, Atlantic City, N. J., November 25–30, 1951, of THE AMERICAN SOCIETY OF MECHANICAL ENGINEERS.

NOTE: Statements and opinions advanced in papers are to be understood as individual expressions of their authors and not those of the Society. Manuscript received at ASME Headquarters, October 4, 1951. Paper No. 51—A-132.

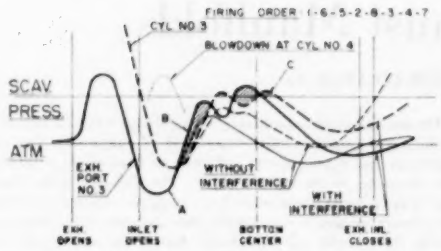

FIG. 1 EXHAUST INTERFERENCE

exhaust blowdown (exactly 45 deg crank angle later) the adjacent cylinder No. 4 blows down. The pressure wave that is generated finds the exhaust and intake ports of cylinder No. 3 largely open for the next 154 — 45 = 109 deg. Naturally the pressure will propagate right into it. In the exhaust duct the pressure gets a sudden kick at A as shown by the heavy line and the cylinder pressure follows suit. In consequence, at B the exhaust-duct pressure will be higher than the cylinder pressure which will force exhaust gas into the cylinder, involving reverse flow in the exhaust branch, indicated by the shaded area. The cylinder pressure is high during most of the scavenging period, and at C it is even higher than the air-box pressure (small shaded area) which results in exhaust gases being forced into the intake manifold. When the inlet port closes the cylinder pressure (dashed line) is way below the scavenge pressure, the cylinder is only partially filled with air and that is contaminated by the combustion products swept in by the reverse flow. Because of its poor scavenging and inadequate charge, No. 3 will be a hot cylinder liable to have ring sticking and cylinder deposits. The shortage of air at full load will cause poor combustion and smoke.

While the theory of exhaust tuning is fairly well developed, little is known about exhaust interference theoretically or experimentally. Since multicylinder engines are of greater practical interest, the emphasis in the research described in this paper was placed upon interference, and tuning has been dealt with only lightly.

AIR MODEL

The mathematical treatment of exhaust-pipe phenomena in a multicylinder engine is complicated, experimental development on full-scale engines expensive, but model testing was found to be both fruitful and relatively inexpensive.

The air model developed at The Pennsylvania State College is shown isometrically in Fig. 2 and photographically in Fig. 3. Any number of cylinders up to eight can be tested. The cylinders have inlet and exhaust ports which are controlled by rotating sleeves driven through a horizontal shaft by an electric motor. The inlet ports are on the lower part of the cylinder and communicate with the air box, the volume of which is so large (2000 times cylinder volume) that it eliminates any pressure fluctuations in the scavenge air. The exhaust ports are in the upper part of the cylinders and communicate through branch pipes to the model manifold to be tested. No combustion takes place in the cylinders but it is simulated by introducing high-pressure air into it after inlet closure and before exhaust opening. This is accomplished by cam-actuated poppet valves. The exhaust manifold is open to the atmosphere but the exhaust back pressure can

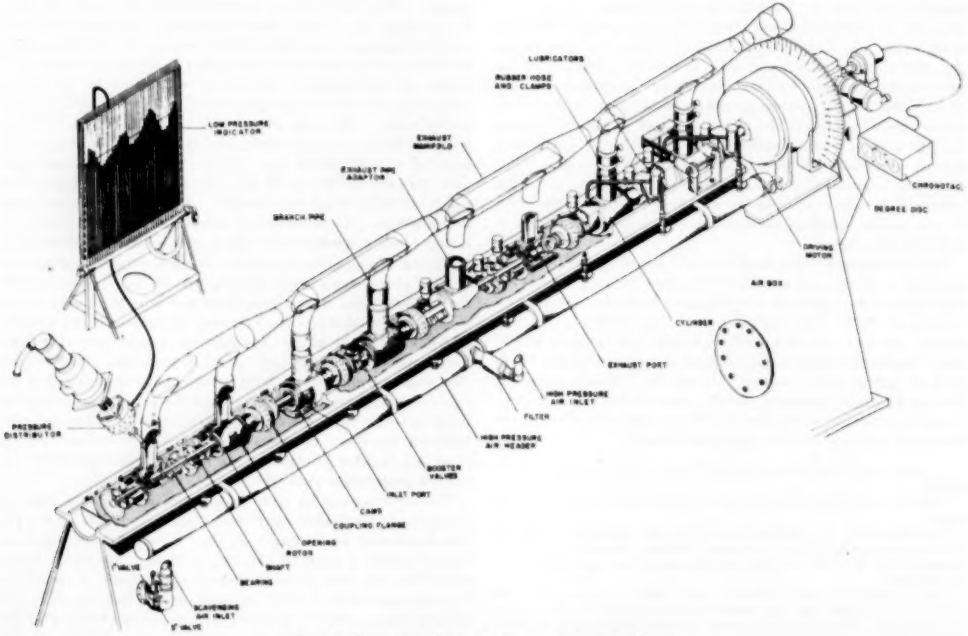

FIG. 2 ISOMETRIC VIEW OF PENN STATE AIR MODEL

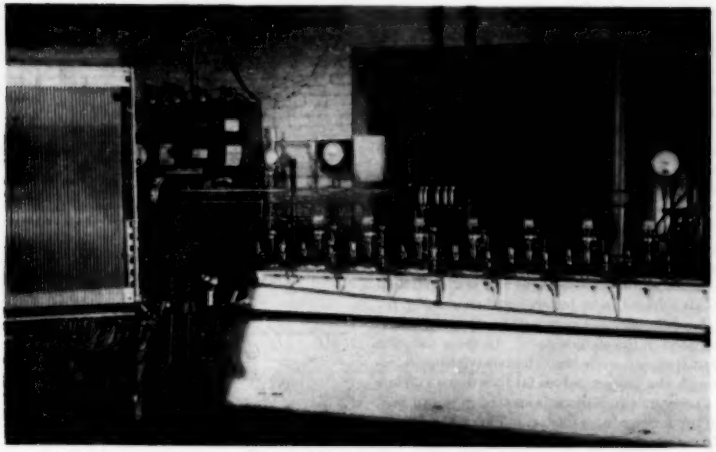

FIG. 3 PENN STATE AIR MODEL
(The base contains the air box. Eight-cylinder, lucite, test manifold mounted.)

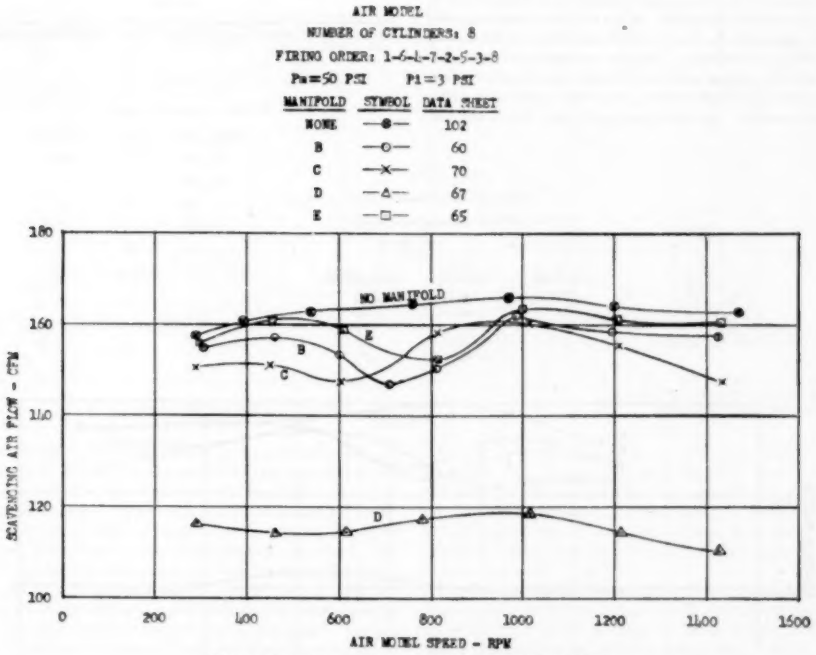

FIG. 4 COMPARISON BETWEEN MANIFOLDS—FLOW TEST

be varied by the number and size of the orifices at the end of the exhaust stack.

The rotating sleeves are coupled to each other by pins in coupling disks with a sufficient number of holes to allow any combination of cylinders and "firing order" to be tested.

Flow Tests. A significant test is the flow test. Keeping the scavenge pressure, boost (exhaust release) pressure, and rpm constant, the scavenge-air flow into the air box is measured by an orifice meter for various exhaust manifolds. The greater the flow the better the manifold, generally speaking.

Fig. 4 shows the results of a series of flow tests with various shapes of manifolds. The scavenge (air-box) pressure was 3 psig and the boost pressure to produce exhaust blowdown 50 psig. In Fig. 5 flow values have been converted into scavenge factors which have the nature of a flow coefficient (3) and are nondimensional. The manifolds referred to by letters are shown in Fig. 6.

Suction Tests. The difference between various types of manifolds is more accentuated in the suction tests. In these tests the air feed to the air box is closed, while the cylinders continue to receive boost air through the poppet valves for blowdown. While the sleeves rotate, a pressure equilibrium is created in the air box, which is measured by a water manometer. The lower the air box pressure the better the manifold, generally speaking.

The suction test is less sensitive to the size of the manifold and, therefore, is particularly suitable to evaluate the merit of certain shapes or design arrangements. According to its response to the suction test, any manifold can be classified in one of three categories. If a manifold produces positive pressure in the air box it is termed a back-pressure manifold. If the air-box pressure remains substantially atmospheric, it is a neutral manifold. If the air-box pressure is below atmospheric, we have an aspirator-type manifold. The air-box pressure produced by a given exhaust manifold usually decreases with engine speed, and at high speed most manifolds produce suction. At moderate speed, however, a conven-

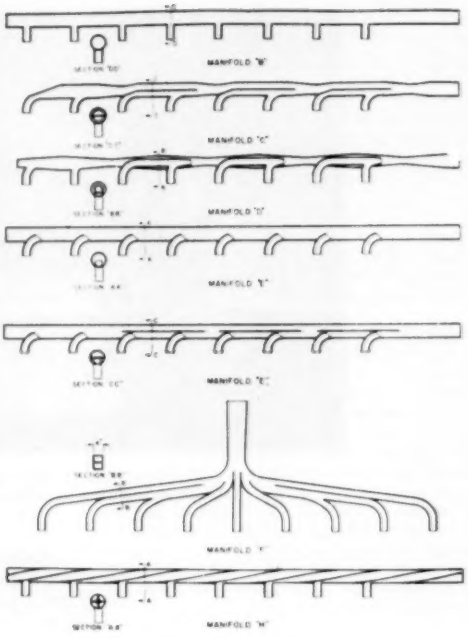

Fig. 6 Exhaust Manifolds

AIR MODEL
NUMBER OF CYLINDERS: 8
FIRING ORDER: 1-6-4-7-2-5-3-8
P_m = 50 psi P_i = 3 psi

MANIFOLD	SYMBOL	DATA SHEET
NONE	—●—	102
B	—●—	60
C	—×—	70
D	—▲—	67
E	—□—	65

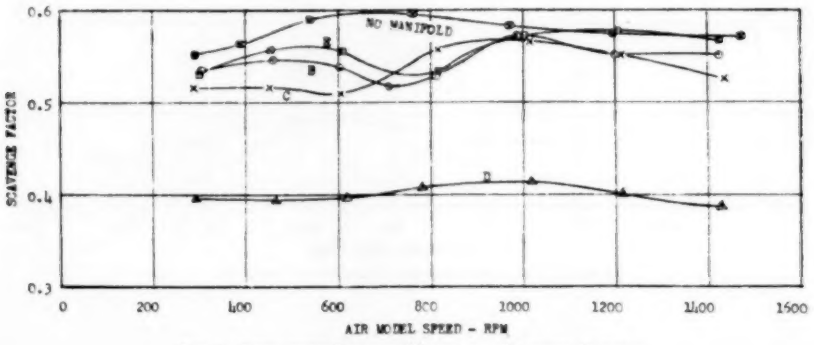

Fig. 5 Comparison Between Manifolds—Scavenge Factors

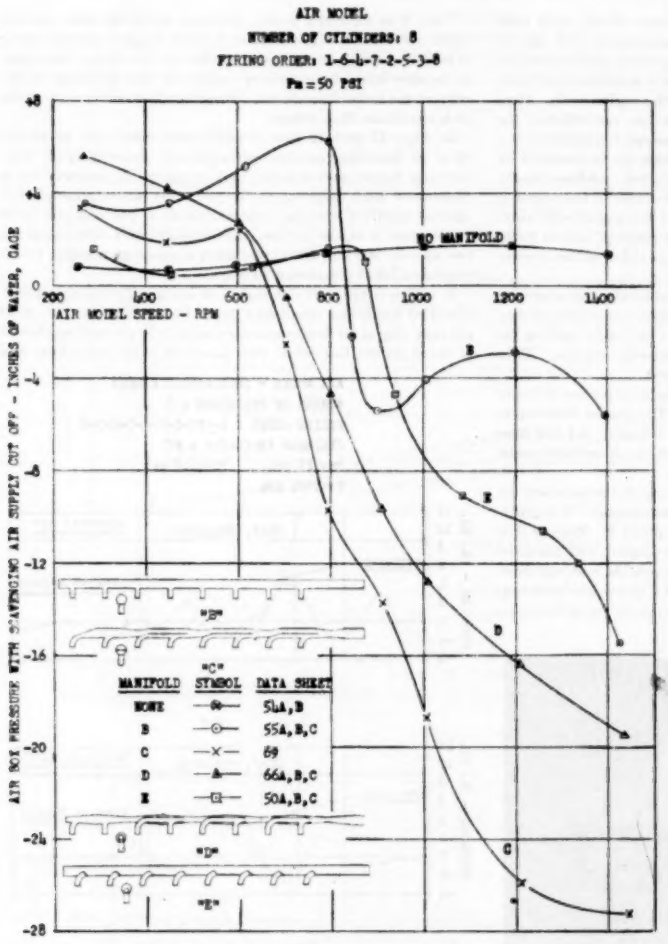

Fig. 7 Comparison Between Manifolds—Suction

tional manifold like manifold B is likely to turn out to be a back-pressure manifold, a manifold like manifold C an aspirator manifold, and no manifold is, of course, a neutral manifold.

Fig. 7 shows a series of suction tests with the same four manifolds, B, C, D, E, and with no manifold at all. It will be noted that no manifold was unable to produce suction at any speed. (In explanation it should be mentioned that because of the horizontal rotating cylinder arrangement the "Kadenacy effect" was insignificant.) The conventional manifold B showed back pressure up to 835 rpm and moderate suction above this speed. The aspirator-type manifold C produced suction above 665 rpm, and at 1400 rpm the suction attained —27 in. of water. The curves obtained by suction tests on various shapes of manifolds are characteristic to their shapes and a change in size changes the curves very little.

Reverse Flow. The suction test serves to establish design principles for exhaust manifolds. Flow tests help to establish the proper dimensions. A manifold which shows up well in both the suction test and the flow test is probably a good manifold. However, to be certain, it is well to subject the model to another series of tests, i.e., check it for reverse flow.

In an ideal exhaust manifold the gases flow always in one direction toward the stack. In a real manifold the gases frequently flow in the reverse direction either in the main header or in the exhaust branches. Reverse flow is caused either by interference between cylinders or by reflected pressure waves. Sometimes only one cylinder is hurt because of its particular location in conjunction with its firing order, yet the engine may suffer seriously from the misbehavior of one or two cylinders.

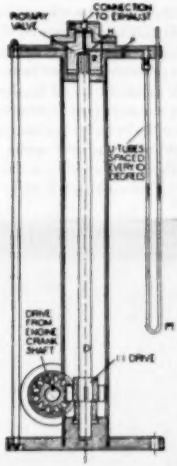

Fig. 8 Schematic Diagram of Penn State Rotary-Valve Low-Pressure Indicator

In the air model tests two methods were used to detect reverse flow. By taking indicator diagrams with the low-pressure indicator, reverse flow can be spotted. It also can be detected by the deflection of a taut thread in the gas stream observed through stroboscope illumination. Direct flow bends the thread upstream, reverse flow downstream. Good manifolds show little or no reverse flow.

Low-Pressure Indicator. The low-pressure indicator as is shown schematically in Fig. 8, consists of a rotor R rotating inside of stator S. The rotor has a single distributor hole H while the stator has 36 equally spaced passages P, one at every 10 deg. The rotor is driven through spline shaft D from the engine crankshaft at 1:1 ratio for two-stroke-cycle engines. The connection to the exhaust (or other space the pressure of which is to be indicated) is through the cover plate C and remains in continuous connection with the distributor hole. Each passage P in the stator is

connected with a manometer tube, and every 10 deg crank rotation brings another manometer tube in connection with the exhaust. Since the leakage between the lap-fitted parts is negligible, the liquid level in the manometer row is stationary and truly represents the pressure fluctuations over the engine cycle. Since the length of the manometer connections does not influence the readings, the manometer tubes can be mounted conveniently at a distance on a board, see Fig. 9, and readings can be recorded by photography. By proper phasing, effected stroboscopically through built-in brush contacts, top dead-center of the engine is brought to the first manometer tube and the second will correspond to 10, the third to 20 deg of crank rotation, and so forth. This indicator is free from calibration errors either of the abscissa or of the ordinate.

The rotor can be driven mechanically but for the sake of greater flexibility an electrical amplidyne-selsyn drive was employed consisting of two synchronous motors, master and slave, locking the two together with an electronically controlled circuit. Thus phase synchronism with ±1 deg was insured.

Fig. 10 shows three indicator diagrams of the same cylinder with three different exhaust manifolds. The dashed lines represent indicator diagrams taken from the cylinder, and full lines those taken from the exhaust branches close to the exhaust ports. The port timing is shown on the bottom.

Exhaust reverse flow is indicated by the shaded areas where the exhaust pressure is higher than the cylinder pressure. It is greatest with manifold E and smallest with manifold F. Reverse flow through the inlet port is detectable on the diagram with manifold E, where the cylinder pressure slightly exceeds the scavenge pressure right after the inlet opens. Manifold F shows good scavenging by displaying a valley in the exhaust-pressure line in the region where the exhaust port is fully open.

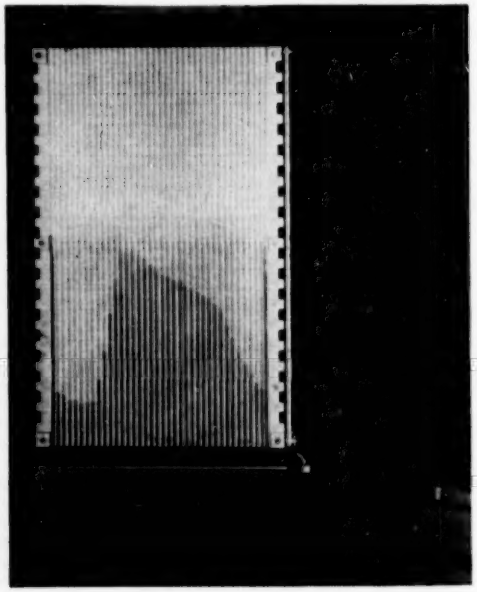

Fig. 9 View of Penn State Rotary-Valve Low-Pressure Indicator
(Manometers are mounted on board.)

Tests With Restricted Outlet. Exhaust manifolds often operate under restricted conditions either because clogging up with soot, or because having an undersize muffler or too long a tail pipe, or because other circumstances restrict the free discharge of the exhaust gas to the atmosphere. Some manifolds suffer more under such conditions than others.

In Figs. 11 and 12 two manifolds are compared as to the effect of throttling on their performance. Scavenging air flow, scavenge factor, and exhaust back pressure, as measured by a manometer next upstream to the restricted outlet, were plotted against manifold opening, expressed both as per cent full cross section and in square inches. All measurements were taken for two speeds, 300 and 1000 rpm, using a scavenge pressure of 4.5 psig and a boost pressure of 70 psig.

It will be noted that although both are good manifolds, under throttled conditions manifold F proved to be far superior. A 10 per cent drop in air flow was occasioned by a 50 per cent restriction of the manifold E-3, while with manifold F the same drop was

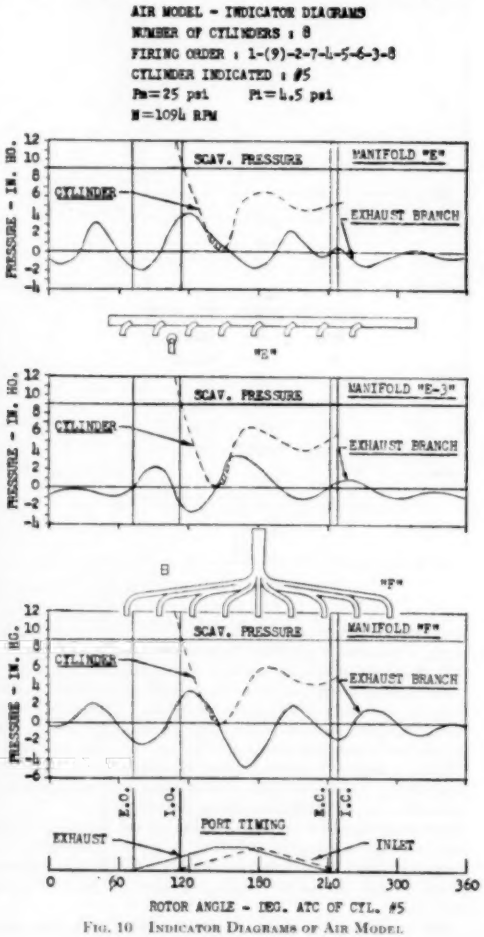

Fig. 10 Indicator Diagrams of Air Model

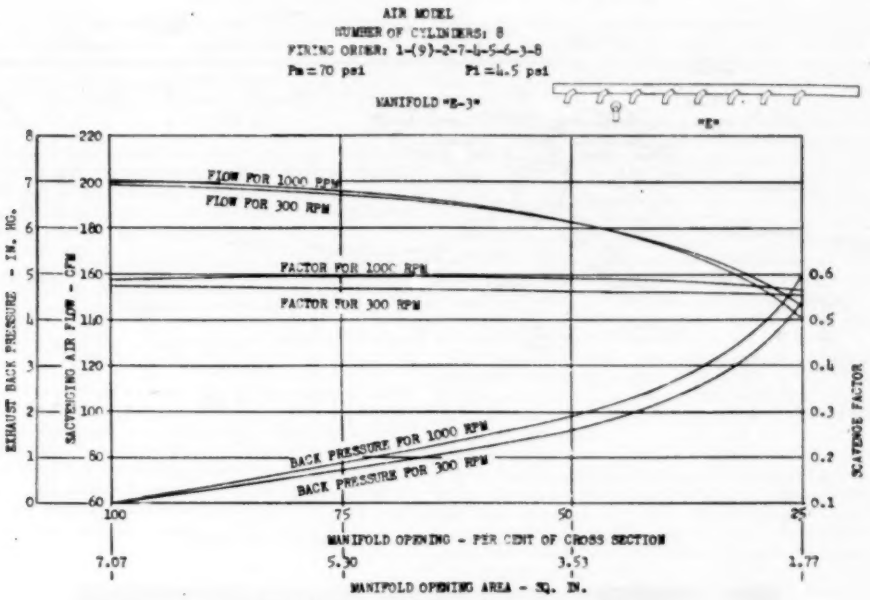

FIG. 11 EFFECT OF THROTTLING OF MANIFOLD E-3

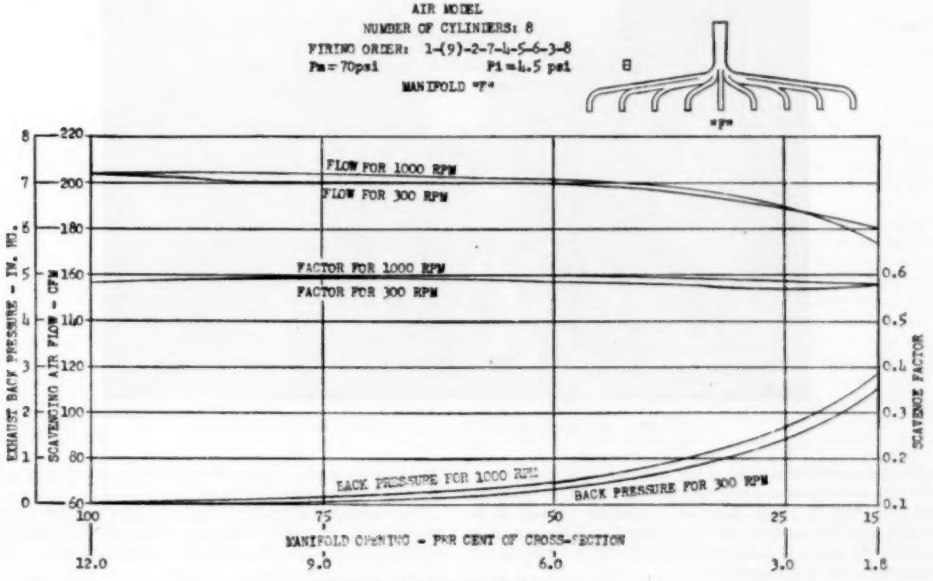

FIG. 12 EFFECT OF THROTTLING OF MANIFOLD F

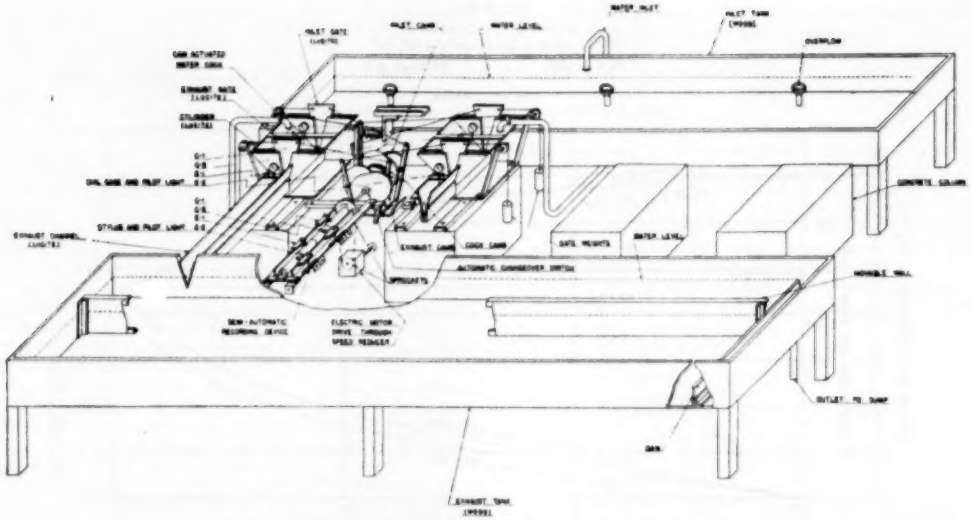

FIG. 13 SCHEMATIC ISOMETRIC VIEW OF PENN STATE WATER MODEL

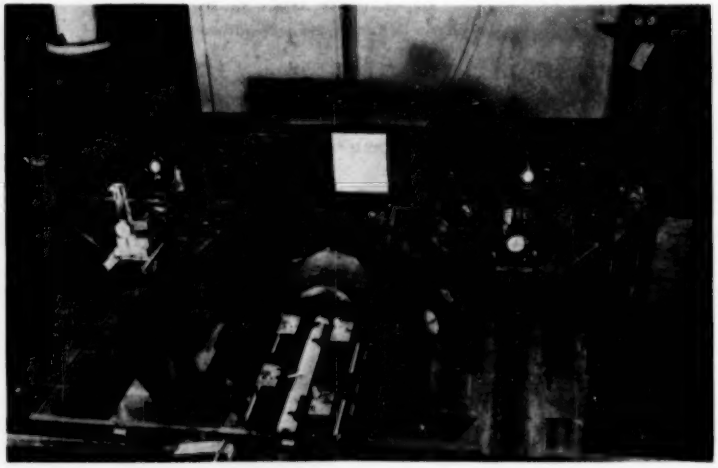

FIG. 14 VIEW OF SEMIAUTOMATIC RECORDING DEVICE FOR WATER MODEL

reached only after 80 per cent of the manifold outlet was covered. The back pressures were roughly 3 times higher with the E-3 manifold than with F. With manifold F operation appears to be feasible when the manifold outlet is reduced to 15 per cent of its original area, while with manifold E-3 and similar manifolds this seems to be out of the question.

WATER MODEL

Based on an analogy between gas flow in a pipe and water flow in an open channel, a water model has been constructed at The Pennsylvania State College, which is shown schematically in Fig. 13 and photographically in Fig. 14.

The mathematical theory of the water model has been derived previously (5, 7). Gas pressures in pipes are represented with water heights in triangular channels by the following relation

$$\frac{p}{p_0} = \left(\frac{h}{h_0}\right)^3$$

where p is the gas pressure in psia, $p_0 = 14.7$ psia, h is the instantaneous water height, and h_0 the equilibrium water height

(chosen 5 in.). The relation of speed between the water model and air model (or engine) is expressed by the following

$$\frac{N_{air}}{N_{water}} = \sqrt[3]{\frac{V_{water}}{V_{air}}} \frac{A_{air}}{\sqrt{\frac{gh_0}{2}}}$$

where N_{air} and N_{water} are the rpm of the air model and water model, respectively, V_{water} and V_{air} are the respective cylinder volumes, A_{air} is the sound velocity in the undisturbed air stream, and $\sqrt{gh_0}/2$ the propagation velocity of waves in the water, corresponding to equilibrium water height.

The channels were made triangular, rather than rectangular, because the hydraulic analogy (7) demands the following relation to exist between the isentropic exponent of the gas k and the equation of the channel profile

$$n = \frac{2 - k}{k - 1} = 1.5$$

With $k = 1.4$ n should be equal 1.5, giving a channel profile shown in Fig. 15 with light lines. For convenience, a straight-walled triangular profile was chosen (heavy line) which would correspond strictly to a cylinder gas with an isentropic exponent of $k = 1.5$, while a rectangular channel would correspond to $k = 2$, a far less realistic assumption. For this reason triangular cylinders and exhaust branch pipes were used, but the inlet and exhaust channels were made rectangular for simplicity.

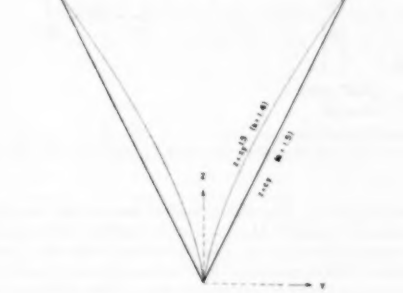

FIG. 15 DEVELOPMENT OF CHANNEL PROFILE

The water admission into and discharge from the "cylinders" were controlled by oscillating gate valves, actuated by cams through steel cables. Combustion was simulated by admitting an extra amount of water into the cylinder while the gates were closed, to bring the water level up to that corresponding to cylinder release pressure.

The cams of the water model were so designed as to give identical port timing with that of the air model. Because for dynamic similitude the speed of the water model must be 1:1345 times the air-model speed, the observations can be made leisurely and, by the use of dyes or powder, reverse flow visually observed. Nevertheless, for the sake of the record several hundred "indicator diagrams" were taken by recording the water heights over the cycle in, and immediately outside of, the cylinder.

The tests were made with a semiautomatic recording device visible in Fig. 14. The styluses were set manually with the dial gages in steps of 0.025 in. to various water heights. At the point of the cycle when the water level reached the stylus, a spark made a mark on the rotating electro-sensitive paper. The spark continued as long as the platinum-pointed stylus was submerged. Thus complete records of water height versus cam angle were obtained.

A typical water-model record is presented in Fig. 16. The inch readings of water height have been converted to pressure readings psi, and the 970 rpm rotative speed also is the converted speed. The actual speed of the water model was 970/1345 = 0.720 rpm.

The record is characteristic of a fairly well-designed exhaust system with the typical blowdown, scavenge, and supercharge period, resulting in filling the cylinder to 3.3 psig, only slightly less than the 4-psig inlet pressure. Due to the large exhaust-channel size there was very little interference from the cylinder firing 45 deg later. Nevertheless, traces of backflow from exhaust pipe into the cylinder and from the cylinder into the inlet tank can be noted in the diagram.

Fig. 17 shows the effect of the exhaust-pipe size. The width of the exhaust channel was reduced from 9 in. to 2.25 in. Two cylinders were tested phased 45 deg from each other, corresponding to an 8-cylinder engine. Cylinder No. 1 was the leading cylinder in firing order.

Comparing the right- and left-hand diagrams, the pronounced effect of the back pressure of the small exhaust will be noted. The cylinder pressure is most of the time above the inlet pressure, so very little scavenging takes place, backflow is considerable both into the cylinder and into the inlet manifold. The relative charge is high but it would be a very polluted charge in the engine.

Comparing the top and bottom-row diagrams, it will be noted that cylinder No. 1 suffers more from interference than cylinder No. 2 even with a 9-in. exhaust channel which corresponds to a large exhaust manifold; cylinder No. 1 shows considerable exhaust backflow and a certain amount of inlet backflow. Cylinder No. 2 shows a negligible amount of exhaust backflow and no inlet backflow except a little at the opening of the inlet port which is normal with well-designed two-stroke-cycle engines.

RESULTS AND CONCLUSIONS

The results and conclusions are based upon a great number of tests, only a few of which have been reproduced in this paper.

The exhaust system of an internal-combustion engine, particularly of the two-stroke-cycle type, has an important influence on its performance.

Exhaust interference between cylinders results in poor scavenging and overheating with loss of power, efficiency, and engine life.

The most important factor in exhaust-manifold design is its geometric configuration. Size and tuning, controlled by the length of tailpipe, have some influence on multicylinder performance and predominant effect on single-cylinder performance.

Exhaust manifolds generally can be classified into three groups, namely, (*a*) back-pressure manifolds, (*b*) aspirator manifolds, and (*c*) neutral manifolds. Back-pressure manifolds create a back pressure in the branch pipes which tends to propagate through the cylinder into the air box, opposing blower delivery and scavenging. Subjected to the "suction test" on the air model, with closed scavenge-air admission but the cylinder being charged with high-pressure air between scavenging periods, the back-pressure manifold shows positive pressure in the air box.

Aspirator manifolds create a vacuum in the branch pipes, which tends to propagate through the cylinder into the air box, reducing counter pressure on the blower and aiding scavenge flow. Subjected to suction test the apirator manifold shows vacuum in the air box.

Neutral manifolds create neither back pressure nor vacuum. Subjected to suction tests the air box shows substantially atmospheric pressure.

	WATER MODEL	CONVERTED TO AIR MODEL
TIMING DIFFERENCE BETWEEN CYL. NO. 1&2	+45°	+45°
EXHAUST SIZE	9"(TANK WIDTH)	" LARGE "
SPEED	0.720 RPM	970 RPM
AMBIENT PRESSURE	5.00 IN. H_2O	14.7 psia
INLET PRESSURE	5.415 IN. H_2O	18.7 psia
EXH. RELEASE PRESSURE	8.20 IN. H_2O	64.7 psia

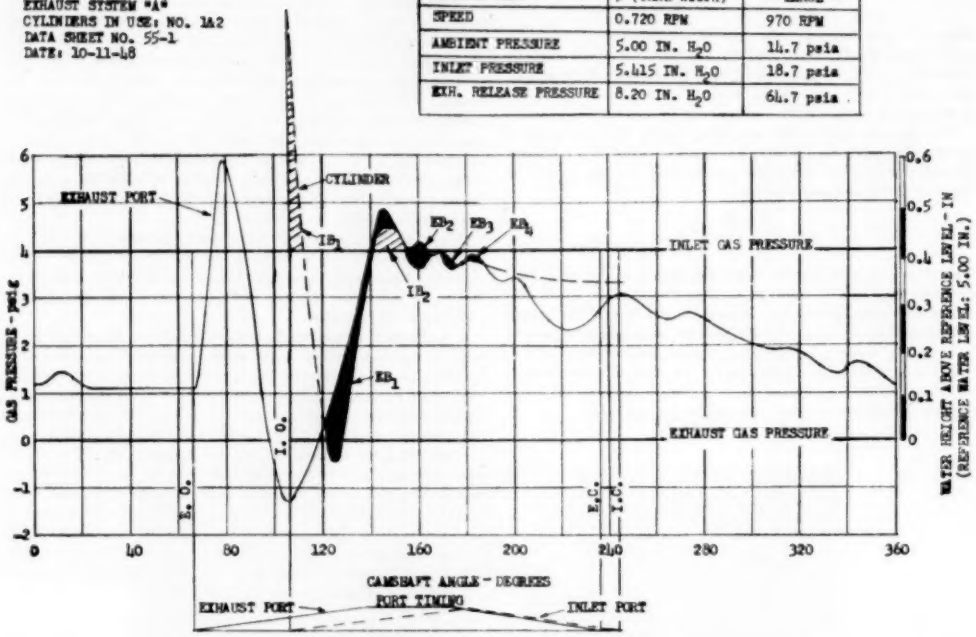

FIG. 16 TYPICAL DIAGRAM FROM WATER MODEL

(Cylinder No. 1 leads cylinder No. 2 by 45 deg. Inlet back flow shown by shaded areas IB_1 and IB_2; exhaust back flow by dark areas EB_1, EB_2, EB_3, and EB_4.)

The classification of a manifold is mostly determined by its geometric shape and the rotative speed. Its size, scavenge pressure, exhaust release pressure, firing order, and other operating conditions have little or no influence on it. A back-pressure manifold at low speed can turn into an aspirator manifold at high speed, especially at favorable firing order. Typical aspirator shapes continue to aspirate (or stay practically neutral) down to very low speeds and are little affected by the firing order.

A typical back-pressure manifold is the conventional manifold, manifold B in Fig. 6, although above 835 rpm air-model speed it showed moderate aspirator effect. Both positive and negative pressures were of greater magnitude with smaller cross-sectional area of the manifold. The Z-shape characteristic with projecting shoulders shown in Fig. 7 for manifold B is typical for this type of manifold. The air flow increases and interference decreases with increased cross-sectional area.

A typical aspirator manifold is manifold C in Fig. 6. It includes quarter-round branch pipes, Venturi throats between cylinders, and separator vanes that keep the exhaust of two cylinders, with close firing order separated to prevent direct interference. The vacuum produced by manifold C is quite pronounced above 700 rpm, but the positive pressures at low speed insignificant. This manifold is not very sensitive to tuning and to the firing order, but the placement of the separator vanes should be determined by the firing order. The air flow is often greater than that of the conventional manifold of similar cross-sectional area, and the interference definitely less. The performance does not improve indefinitely with increased size but reaches a limit at the optimum size and again decreases above that size. Under favorable conditions manifold C produced an air flow that not only was greater than that of conventional manifolds, or divided manifolds, but greater than obtained with no manifold at all!

Manifold D is also an aspirator manifold with similar characteristics as manifold C only with considerably less air flow. That probably is due to the restrictions in many cross-sectional areas.

Manifold E is a conventional manifold with quarter-round branch pipes. It acts as an apirator manifold above 900 rpm but not nearly as pronounced as manifold C. In air flow capacity manifold E is excellent, in reverse flow caused by interference tolerable.

Manifold E_1 is identical with manifold E except for some separator vanes added. The vanes seem to be helpful with certain firing orders but their general merit has not yet been established.

The greatest aspirating effect was observed with manifold F which is a central outlet manifold of slightly tapered rectangular cross section. It also showed up favorably in air-flow capacity and in discouraging reverse flow. The most spectacular feature

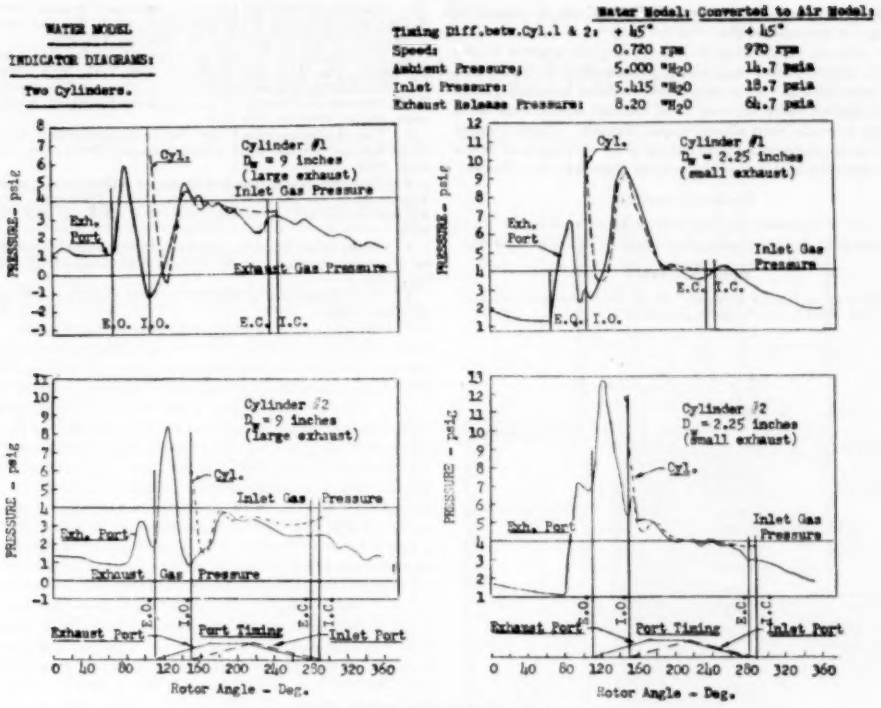

FIG. 17 WATER-MODEL INDICATOR DIAGRAMS

of manifold F, however, is its performance under throttled outlet conditions. It maintained its performance fairly well even when the outlet was reduced to 15 per cent of the original size.

Of the aspirator manifolds, the C manifold works best at high speed, the E manifold works best at low speed, while the F manifold performs equally well at all speeds tested (300 to 1500 rpm).

Manifold H, named by its inventors (8) the "Helixhaust" manifold, is a typical neutral manifold. In performance it is similar to a divided manifold or individual exhaust pipes attached to each cylinder. Interference is absent and so is the aspirating effect. Since most manifolds in practical use are back-pressure manifolds, the Helixhaust manifold represents an improvement. Of course, a conventional manifold like manifold B made with a sufficiently large cross section would also be a neutral manifold, but its weight and its space requirement would make such a manifold unattractive. Manifold H also must be made with sufficiently large cross-sectional areas to prevent excessive throttling and reduction of air-flow capacity.

The extreme in neutral manifolds is represented by no manifold. Again, interference is absent, and flow capacity is also high. No manifold can be approximated with a large exhaust pit connecting to short branch pipes, but such installations are no longer popular because of the excessive space requirements. It seemed improbable that any manifold can exceed the flow capacity of no manifold but manifold C was found to accomplish that under certain circumstances. Other aspirator manifolds probably can be made to equal that record.

How the aspirating or jet effect can increase the air flow through the cylinders was demonstrated spectacularly by bleeding some air from the air box to the closed end of an E manifold. By diverting 4.5 per cent of the air flow from the cylinders, the flow through the cylinders was increased by more than 4.5 per cent. This means that the same amount of blower air by-passing the cylinders did more for charging the cylinders than if it had gone through them.

Most of the test work was conducted on multicylinder arrangements, but numerous tests were made with only one cylinder operating and the rest removed from the air box. The most important results from the single-cylinder tests are the following:

The flow of air through the cylinder can be calculated by the mean inlet-port area and a scavenge factor, the latter being a constant with respect to speed and scavenge pressure and was equal to 0.62 for the air-model cylinder with no pipe.

The frequency of pressure fluctuations in a straight cylindrical exhaust pipe is the same as that in a pipe of double length and both ends closed; it corresponds to the calculated sonic velocity.

An outwardly tapered pipe causes the frequency to increase and the amplitudes to decrease.

A tapered pipe with 4 deg or more included angle usually helps scavenging and is less affected by engine speed than a straight pipe which must be tuned for optimum performance.

Water-model tests brought out the importance of the proper size for an exhaust manifold. Nothing was gained by widening the exhaust channel from 9 to 46 in., but the performance suffered severely by decreasing it below 4.5 in.

A promising way to take advantage of the aspiratory effect in a

moving vehicle is to utilize the ram effect of the air stream for sucking out the exhaust gas.

The exhaust manifolding of four-stroke-cycle engines is also open for improvement, especially if considerable overlap is used in the valve timing. With conventional exhaust manifolds, automobile engines suffer severely from exhaust interference when coasting downhill with almost closed throttle. Power penalty then is of no consequence, but fouling of spark plugs and valves results from the backflow of the exhaust gases into the cylinder.

Acknowledgment

The author acknowledges the assistance rendered by Dr. T. C. Tsu, especially in the experimental phase of this investigation.

BIBLIOGRAPHY

1 "Energy in Engine Exhaust," by P. H. Schweitzer and T. C. Tsu, Trans. ASME, vol. 71, 1949, pp. 665–672.

2 "Taking the Mystery Out of the Kadenacy System of Scavenging Diesel Engines," by P. H. Schweitzer, C. W. Van Overbeke, and L. Manson, Trans. ASME, vol. 68, 1946, pp. 724–729.

3 "Scavenging of Two-Stroke Cycle Diesel Engines," by P.H. Schweitzer, The Macmillan Company, New York, N. Y., 1949.

4 "Improving Engine Performance by Exhaust Pipe Tuning," by P. H. Schweitzer, *Journal of the American Society of Naval Engineers*, vol. 56, 1944, pp. 185–211.

5 "Der Ladungswechsel der Verbrennungskraftmaschine," by Hans List and Gaston Reyl, Julius Springer, Berlin, Germany, 1st part, 1949.

6 "Bewegungsvorgaenge in Gassaeulen insbes. beim Auspuff und Spuelvorgang von Zweitaktmaschinen," by A. Pischinger, *Forschung auf dem Gebiete des Ingenieurwesens*, vol. 6, 1935, pp. 245, 273, and 430.

7 "Study of the Dynamics of the Induction and Exhaust Systems by Hydraulic Analogy," by H. T. Loh, ScD thesis, M.I.T., September, 1946.

8 "U. S. Patent No. 2,390,913," by C. G. Barrett and E. C. Magdeburger, 1945.

Operation and Performance of Modern Reheat Boilers

By P. R. LOUGHIN[1] and H. H. POOR,[2] NEW YORK, N. Y.

This paper illustrates typical designs of reheat boilers and discusses operating procedures for normal start-up, quick start-up, normal operation, and shutdown under normal or emergency conditions.

DURING World War II the price of fuel increased markedly in the United States, outdistancing the less rapidly rising first cost of capital equipment. During the 1930's the straight-condensing regenerative cycle was found to be more economical than the reheat-regenerative-cycle, but the wartime change in price structure made the more efficient reheat cycle economically attractive for many postwar power plants.

Reheat has been applied to a number of different designs. One type of dry-ash-removal unit is illustrated in Fig. 1 which shows the first boiler at the new Tanners Creek Plant of Indiana and Michigan Electric Company. It is designed to deliver 930,000 lb per hr of high-pressure steam at 2080 psi and 1050 F, and 840,000 lb per hr of reheat steam at 390 psi and 1000 F. Constant high-pressure and reheat-steam temperatures are obtained over a considerable range in load by raising the steam temperature at low load by means of flue-gas recirculation or lowering the steam temperature at high load by spray attemperation.

Another design of dry-ash-removal unit is illustrated in Fig. 2 which shows a boiler for the Salem Harbor Station of the New England Power Company. It will deliver 625,000 lb per hr of high-pressure steam at 1500 psi and 1000 F, and 545,000 lb per hr of reheat steam at 410 psi and 1000 F. Steam temperature may be regulated at low loads by selection of burner elevation and at high load by spray attemperation.

Fig. 3 shows the largest boiler we have yet designed, a slag-tap unit for the new Muskingum River Plant of the Ohio Power Company now under construction. It is 56 ft wide center line to center line of side-wall tubes, and will have a heat input of 1,880,000,000 Btu per hr, obtained from the combustion of 89 tons of coal per hr. Maximum continuous rating is 1,335,000 lb per hr of high-pressure steam at 2075 psi and 1050 F, and 1,226,000 lb per hr of reheat steam at 470 psi and 1050 F. Under these conditions the generators will deliver 217 gross megawatts. Steam-temperature control is by flue-gas recirculation at low load and by spray attemperation at high load.

Another type of slag-tap reheat boiler is shown in Fig. 4. This is the fourth unit at the Oswego Steam Station of the Niagara Mohawk Power Company. It will deliver 656,000 lb per hr of high-pressure steam at 1492 psi and 1000 F, and 599,000 lb per hr of reheat steam at 384 psi and 1000 F. Steam temperature control is by spray attemperation.

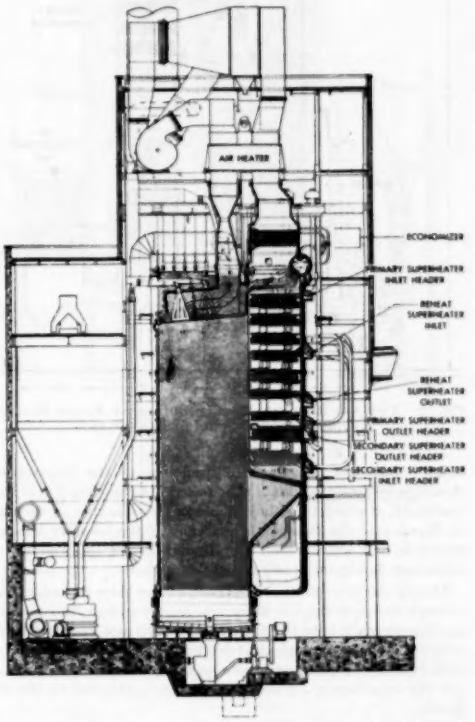

FIG. 1 DRY-ASH-REMOVAL REHEAT BOILER AT TANNERS CREEK PLANT, INDIANA AND MICHIGAN ELECTRIC COMPANY

A cyclone-furnace-fired reheat boiler is illustrated in Fig. 5. It will deliver 830,000 lb per hr of high-pressure steam at 1850 psi and 1010 F, and 733,000 lb per hr of reheat steam at 538 psi and 1010 F. Steam temperature will be controlled by using flue-gas recirculation at low load or spray attemperation at high load.

NORMAL START-UP FROM COLD

There is little difference between the operation of a reheat boiler and a nonreheat boiler during normal start-up from cold. Actually, a reheater is merely an additional superheater which must be drained or boiled out, and protected from overheating, during the pressure-raising period when there is no steam flow through the tubes.

Before the fire is lighted the reheater should be drained as completely as its design will permit. Reheater drains which discharge to the condenser should be left open until a load equivalent to 5 to 10 per cent of full rated steam flow has been put on the

[1] Chief Staff Engineer, The Babcock & Wilcox Company. Mem. ASME.

[2] Staff Engineer, The Babcock & Wilcox Company. Mem. ASME.

Contributed by the Power Division and presented at the Annual Meeting, Atlantic City, N. J., November 25–30, 1951, of THE AMERICAN SOCIETY OF MECHANICAL ENGINEERS.

NOTE: Statements and opinions advanced in papers are to be understood as individual expressions of their authors and not those of the Society. Manuscript received at ASME Headquarters, September 5, 1951. Paper No. 51—A-80.

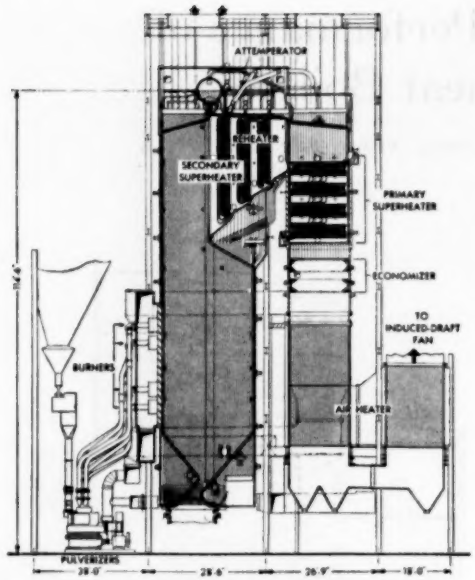

FIG. 2 DRY-ASH-REMOVAL REHEAT BOILER AT SALEM HARBOR STATION, NEW ENGLAND POWER COMPANY

boiler. Reheater drains which discharge to the atmosphere should be left open until it is time to start the hogging jets of the condenser, at which time they should be closed so that air will not be drawn into the condensate system. If the reheater is nondrainable any water which may remain in the tubes must be boiled out during the starting-up firing period.

During the pressure-raising period, before there is steam flow through the reheater, the firing rate must be controlled so that gas temperature entering the reheater will not exceed 900 F before steam flow through the reheater has been established. In most cases the similar restrictions on firing rate necessary to protect the superheater will provide adequate protection for the reheater.

Fig. 6 shows test data obtained during a routine start-up of the Tanners Creek boiler, Fig. 1, which serves a cross-compound reheat turbine. Pertinent operating data are given in Table 1.

TABLE 1 TEST DATA TAKEN DURING START-UP OF TANNERS CREEK BOILER

8:05 pm	High-pressure and low-pressure turbines put on turning gear.
9:20 pm	Induced-draft and forced-draft fans started.
9:45 pm	First lighters put in service (various lighters were put in and taken out of service during the starting-up period).
12:25 am	D pulverizer put in service.
1:50 am	D pulverizer taken out of service.
2:18 am	Steam admitted to turbines to bring them up to speed.
3:00 am	D pulverizer put in service.
3:52 am	Generator synchronized and put on line.
3:55 am	B pulverizer put in service. Electrical load 20 megawatts.

During the pressure-raising period the bottom of the drum is heated by contact with the water and, after the air has been driven out of the drum by the steam, the top of the drum is heated by condensing steam, which is an extremely effective medium of heat transfer. The top and bottom of the drum therefore tend to maintain equal temperatures. Temporary thermocouples monitored the temperature of gas to the secondary superheater so that a temperature of 920 F was not exceeded until after steam flow had been established through the superheater. Since the reheater is situated beyond the secondary superheater it was safe from overheating.

QUICK STARTING FROM HOT BANK

In several papers presented before this Society,[3,4,5] J. C. Falkner and his associates have shown how system load requirements for The Consolidated Edison Company make it necessary to take large high-pressure boilers off the line late in the evening and bring them up to full load quickly the following morning. A high-pressure high-temperature turbine drops about 150 F in temperature during a 6-hr shutdown. To minimize temperature differentials during start-up it is desirable to deliver steam at a temperature close to that of the turbine while the turbine is being brought up to speed, synchronized, and loaded. Since it is not possible to deliver high temperature, high-pressure, and reheat steam at the boiler output (30,000–50,000 lb of steam per hr) required to roll the turbine at no load, it is necessary to apply a temporary

[3] "Quick Starting of High-Pressure Steam-Turbine Units," by J. C. Falkner, R. S. Williams, and R. H. Hare, Trans. ASME, vol. 70, 1948, pp. 201–209.

[4] "Latest Technique for Quick Starts on Large Turbines and Boilers," by J. C. Falkner, D. W. Napier, and C. W. Kellstedt, Trans. ASME, vol. 72, 1950, pp. 1111–1122.

[5] "Supplement" (to preceding paper), Trans. ASME, vol. 72, 1950, pp. 1123–1136.

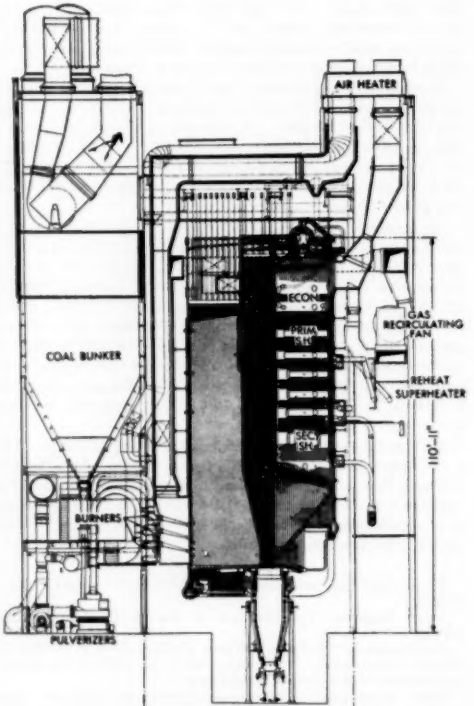

FIG. 3 SLAG-TAP REHEAT BOILER AT MUSKINGUM RIVER PLANT, OHIO POWER COMPANY

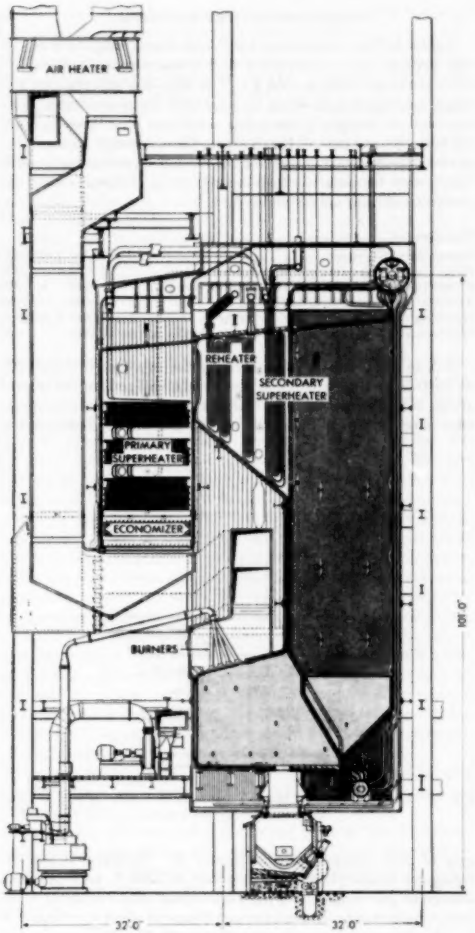

FIG. 4 SLAG-TAP REHEAT BOILER AT OSWEGO STEAM STATION, NIAGARA MOHAWK POWER COMPANY

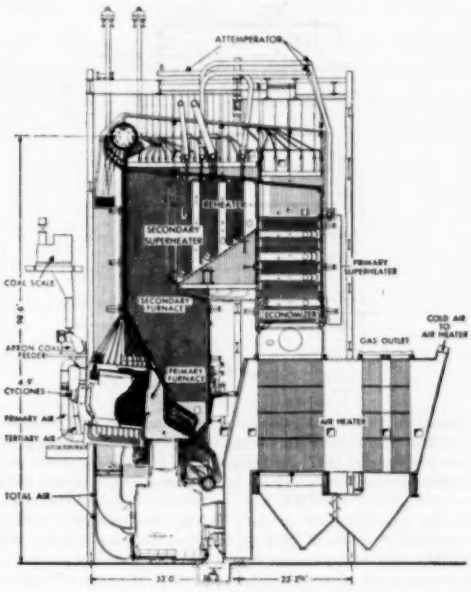

FIG. 5 CYCLONE-FURNACE REHEAT BOILER

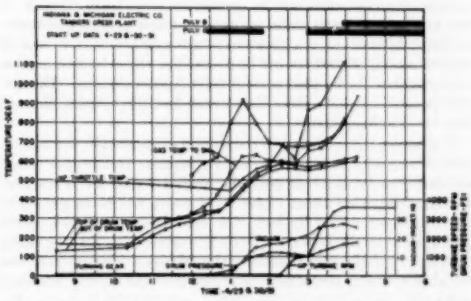

FIG. 6 STARTING-UP DATA FOR HIGH-PRESSURE REHEAT BOILER

artificial load during the 15-min period between putting the boiler on the line and the loading of the turbine.

One arrangement of equipment developed by the Steam Turbine Engineering Division of the General Electric Company in collaboration with the Consolidated Edison Company for applying the artificial load in the case of an 1850-psi, 1000 F high-pressure steam, 1000 F reheat-steam, cross-compound turbine is shown in Fig 7. During normal operation steam from the boiler drum passes through the primary superheater, interstage spray attemperator, and secondary superheater to the high-pressure turbine stop and control valves, through the turbine, through the reheater to the intercept valve of the intermediate-pressure turbine, and then through this turbine and the two double-flow low-pressure turbines to the condenser. A by-pass line around the turbine, serving the same purpose as those developed by the Consolidated Edison Company,[3] is provided so that an artificial load can be applied to the boiler during starting up.

During normal operation shutoff, valves Nos. 1 and 4 are closed; they are opened only during quick start-up. No steam will flow from the superheater during the pressure-raising period. When the pressure reaches 1850 psi the pressure-actuated automatic pressure-reducing valve No. 3 will start to open and an artificial load will be placed on the boiler. Steam flowing through the by-pass line under the control of valve No. 3 will pass through pressure-reducing orifices and a spray attemperator regulated by the temperature of the steam leaving the reheater. After leaving the reheater, by-pass steam passes through another automatic pressure-reducing valve No. 5, which begins to open at 500 psi, and then passes through a spray attemperator and additional pressure-reducing orifices to the condenser. Spray water is

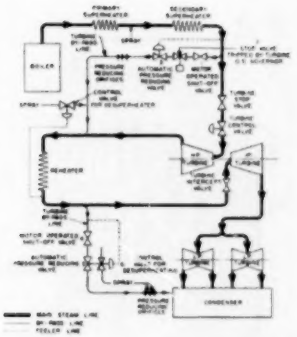

FIG. 7 SCHEMATIC PIPING LAYOUT FOR QUICK-STARTING HOT REHEAT TURBINE

turned onto the condenser inlet attemperator by pressure-actuated control valve No. 6 when the reheater-outlet steam pressure reaches 495 psi. As firing on the boiler is increased the pressure-actuated valves on the by-pass line continue to open until an artificial load of 300,000 lb per hr has been imposed on the boiler. At this time the steam pressure leaving the superheater will be somewhat in excess of 1850 psi and the steam temperature will be 900 F; the steam pressure leaving the reheater will be somewhat in excess of 500 psi and the reheat-steam temperature will also be 900 F.

When this point is reached the steam may be sent to the turbines, and the high-pressure turbine control valve and the turbine intercept valve will be opened to pass steam through all the turbines to bring them up to speed and permit synchronization. As soon as the generators are synchronized a load of approximately 40,000 kw will be picked up; the reduction in pressure will close the by-pass control valves automatically. The motor-operated shutoff valves Nos. 1 and 4 in the by-pass line will then be closed manually.

The automatic operation of the system seems simple, and it is expected that only about 15 min will be required from initial steam admission to the turbines until the load of 40,000 kw is reached. During this period about 75,000 lb of steam will be by-passed to the condenser. The by-pass line should come off the steam piping as near the boiler as possible; connections may be taken directly from the superheater-outlet header. The by-pass line from the reheater outlet may be placed near the turbine intercept valve.

NORMAL OPERATION

During periods of normal operation when steam is flowing through the reheater it will be protected against overheating provided the reheater-outlet steam temperature does not exceed design values. At low loads it usually will be found economical to operate a reheat boiler with high excess air in order to elevate superheated and reheat-steam temperatures, the decreased efficiency of the steam-generating unit being more than compensated by the increased turbine efficiency so that the over-all cycle efficiency is improved. As in all high-efficiency boilers, it is necessary to take steps to protect the air heater from plugging and corrosion at low loads. Methods for doing so have been treated extensively by P. H. Koch.[6]

[6] "Tubular Air Heater Performance and Corrosion Problems," by P. H. Koch. Babcock & Wilcox Bulletin No. 3-509, 1951.

STEAM-TEMPERATURE REGULATION

Reheat boilers are associated with high steam temperatures. At the present time superheated and reheat-steam temperatures lie in the range 1000 to 1050 F. The large-size superheaters and reheaters required for these temperatures are considerably more sensitive to changes in operating conditions than those designed for lower temperature. Fig. 8 shows the schematic arrangement of two hypothetical counterflow convection superheaters A and B which may be used to illustrate this point. Assume that the design conditions are as follows:

Superheater	A	B
Steam flow, lb per hr	1,000,000	1,000,000
Steam pressure leaving superheater, psi	1,400	2,000
Steam temperature leaving superheater, deg F	900	1,050
Feedwater temperature, deg F	400	400
Gas weight over superheater, lb per hr	1,148,000	1,222,000
Gas temperature entering superheater, deg F	2,000	2,000

A drop in gas temperature entering the superheater from 2000 to 1900 F with no change in gas weight will reduce the outlet-steam temperature 22 F in the case of intermediate-temperature superheater A and 30 F or 136 per cent as much, in the

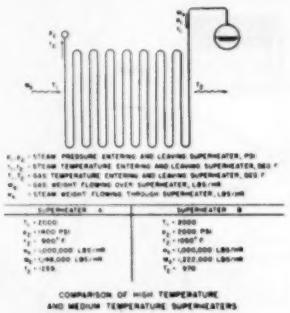

FIG. 8 COMPARISON OF HIGH-TEMPERATURE AND MEDIUM-TEMPERATURE SUPERHEATERS

case of high-temperature superheater B. Similarly, if the entering-gas temperature is held constant at 2000 F, an 8 per cent change in gas weight, causing a heat-absorption change of 5 per cent, would change the outlet-steam temperature of superheater A by 20 F and of superheater B by 30 F. Uncompensated variations in those operating variables which affect steam temperature, such as feedwater temperature, excess air, firing rate, and furnace cleanliness, produce wider steam-temperature fluctuations in modern high-temperature boilers than in earlier intermediate-temperature designs. Reheat-steam temperature is even more sensitive to operating changes than is superheater steam temperature, since reheater heat absorption is affected in the same way as superheater heat absorption, and in addition the superheater outlet temperature changes are passed along with only partial diminution through the high-pressure turbine to the reheater inlet.

These effects, as well as the wide range of steam-temperature control required in many instances, present challenging problems to the boiler designer and the control manufacturer. Furthermore, the American Boiler Manufacturers Association and Affiliated Industries' standard performance form calls for a guarantee of steam temperature within plus or minus 10 F of specified temperature. The increasing accuracy of steam-tem-

perature control required to meet this tolerance as steam temperature increases is illustrated in the following table:

Steam temperature leaving superheater, deg F ...	750	900	1050
Steam pressure leaving superheater, psi.....	650	1400	2000
Permissible variation in superheater heat absorption, per cent.....	3.3	2.6	1.7

Superheat and reheat-steam temperatures may be controlled by using one or more of the following means: spray attemperator, flue-gas recirculation, gas proportioning dampers, or burner-elevation effects. A boiler with a reheater naturally requires more elaborate instrumentation and control equipment than a nonreheat unit because of the need for controlling two separate steam temperatures. Many of these instruments and controls must be duplicated in wide boilers with double-inlet and outlet superheaters and reheaters.

Scheduled Shutdown for Outage

The shutdown of a reheat boiler is the same as that of a nonreheat boiler except for the additional set of drains, which should be opened after the turbine is taken out of service. As in any other high-pressure boiler, rate of cooling is limited by consideration of thermal stresses in the drum. During pressure reduction the bottom of the drum is cooled by contact with the water, whereas the top of the drum is cooled by heat loss through the insulation, conduction of heat circumferentially around the drum plate, and combined radiation and conduction to the stagnant and slightly superheated steam in the upper part of the drum. Since these modes of heat transfer are relatively ineffective, the temperature of the top of the drum lags behind saturation temperature during pressure reduction, and the rate of pressure reduction is limited by temperature differentials between top and bottom of the drum. In many instances it is desired to enter the boiler setting for inspection or repair work as soon as possible after the boiler is taken off the line. The permissible rate of pressure reduction may be increased by raising the water level to the top of the drum after all steam flow from the boiler has been stopped and holding it there so that both top and bottom of the drum will be cooled at nearly the same rate by contact with water.

Fig. 9 shows test data obtained during a routine shutdown of the Tanners Creek boiler, Fig. 1. Pertinent operating data are given in Table 2.

During the load reduction the excess air was raised to quite high values. Superheat and reheat temperatures therefore remained high. Temperature of the top and bottom of the drum came together when the water level was raised to the top of the drum.

Scheduled Shutdown to Hot-Bank Condition

When it is desired to remove the unit from service temporarily, but to resume load at a later time with minimum delay, the available means of steam-temperature control may be used to regulate high-pressure steam and reheat-steam temperatures so as to minimize temperature shock to the turbines when they are returned to service. While the boiler is off the line it may be fired periodically for short periods, if desired, at such a rate that gas temperature entering the superheater or the reheater does not exceed 900 F, to maintain boiler pressure and to prevent the accumulation of condensate in the superheater and reheater. The reheater drains should be open during the periods of outage.

Emergency Boiler Shutdown

If an essential boiler auxiliary is lost or for some other reason the boiler must be taken out of service immediately, the fires should be extinguished and the flow of steam from the boiler stopped as quickly as possible.

TABLE 2 TEST DATA TAKEN DURING SHUTDOWN OF TANNERS CREEK BOILER

7:30 pm—Boiler put on hand control and pressure reduction started, thereby reducing load
8:25 pm—E pulverizer taken out of service, water level put on hand control.
9:00 pm—A pulverizer taken out of service.
9:38 pm—B pulverizer taken out of service.
9:40 pm—D pulverizer taken out of service.
9:48 pm—Steam flow to turbine stopped.
9:50 pm—Opened superheater and reheater drains.
9:55 pm—Water level at top of gage glass.

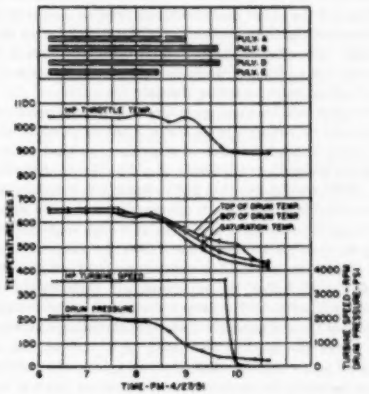

Fig. 9 Shutting-Down Data for High-Pressure Reheat Boiler

Emergency Loss of Electrical Load

Some operating companies wish to shut down the boiler completely on emergency loss of electrical load. Other operating companies wish to keep the boiler on the line, firing at a reduced rating, until it can be decided whether it is possible to regain load immediately or whether a complete shutdown is unavoidable. Automatic control equipment may be provided which will cut back the firing rate to a predetermined minimum load (approximately 20 to 25 per cent of full load) and permit continued firing, exhausting the steam generated through the boiler and superheater safety valves to the atmosphere. Reduction of firing rate for pulverized coal units will involve the tripping out of some of the pulverizers and operation of the remainder at a minimum load. This will reduce the gas temperature entering the reheater to below 1000 F (this temperature is permissible for the short time and rare occurrence of this emergency condition) before the carbon-steel tubes in the reheater have reached this temperature. The superheater will be protected from overheating by the flow of steam through the superheater and out the superheater safety valves. Operation under these unusual conditions must be of short duration in view of the loss of condensate through the safety valves at the rate of 20 to 25 per cent full-load steam flow.

If valves and piping as shown in Fig. 7 have been furnished for quick-starting the turbine they also may be used to protect both reheater and superheater from overheating when electrical load is suddenly lost and it is desired to continue firing the boiler at reduced rating. Steam flowing through the superheater would not be lost to the atmosphere, but would go to the condenser. However, the high cost of valves and piping makes this method of control economically unattractive if quick-starting is not contemplated and the equipment is considered solely for use during infrequent emergency trip-outs.

Discussion

J. C. Falkner.[7] It is of interest to learn that more attention is being given to shortening the time of starting both boilers and turbogenerators. We have been doing this for the past 4½ years, and it is gratifying to know that others now find this advantageous. The writer agrees with the authors that the operation of starting modern reheat boilers in this manner does not cause any more trouble than with the conventional boilers, particularly if the boiler manufacturers provide means of increasing and controlling the temperature of the steam during the start-up period. The Consolidated Edison Company uses a by-pass line around the turbine so that any desired temperature of steam can be obtained before starting the unit.

The belief is held by some operators that the temperature of the steam should be reduced to as low a point as possible while the unit is being unloaded before a shutdown, so that in case of a start-up the steam from the boiler would be the same as the temperature of the turbine in order not to cause a thermal shock to the turbine itself. It is the writer's opinion that where the steam temperature can be controlled and held at a high degree during the starting-up period, it would be better to keep the temperature of the steam up until a point is reached where, owing to low loads on the boiler, the superheat will begin to fall off. At this point the load should be dropped completely and the unit shut down, so that the temperature of the spindle casing will remain the same. When the load is decreased on a turbine, the spindle will cool off more rapidly than the casing, thereby reducing the clearance between the stationary and revolving parts of the unit. Too sudden a decrease might cause a rub. In starting the unit that has been left at the normal operating temperature, it will be much easier and more economical to control the steam temperature to a point 50 to 100 deg above that of the high-pressure casing and bring the machine up to speed in 15 to 30 min.

The Consolidated Edison Company has had 5650 quick starts of from 15 to 20 min duration without one instance of trouble developing during the starting cycle. Furthermore, we have increased the outage time between opening of the turbine from 2 to 6 years, and when opened the machine showed no bad effects from quick starting.

R. L. Reynolds.[8] This discussion will center primarily on the provisions for quick starting, described in the paper and outlined diagrammatically in Fig. 7. Such an arrangement can be justified only in those rare cases where it is planned to shut the unit down for short periods at frequent intervals and, in addition, there is no outlet for the steam other than to by-pass it to the condenser through pressure and temperature-reducing equipment.

It is to be expected that few reheat turbines will be subjected to overnight shutdowns for several years. These units being the most efficient on the system should be kept in almost continuous service, particularly during this period of heavy load demands.

During a normal shutdown on a 1050 F turbine, the temperature of the high-temperature parts of the turbine will have cooled off to about 900 F during the load-reducing and coasting-down periods · During an overnight shutdown of, say, 6 hr the high-temperature turbine parts will cool off another 130 F which will reduce the temperature of these turbine parts to about 770 F.

As pointed out in the paper, it is advantageous after such a short shutdown to have steam temperatures of at least 800 to 850 F available for rolling the turbine during the starting cycle. This

[7] Manager, Electric Production Department, Consolidated Edison Company of New York, Inc., New York, N. Y.

[8] Turbine Engineering, Central Station Section, So. Philadelphia Works, Westinghouse Electric Corporation, Lester, Pa. Mem. ASME.

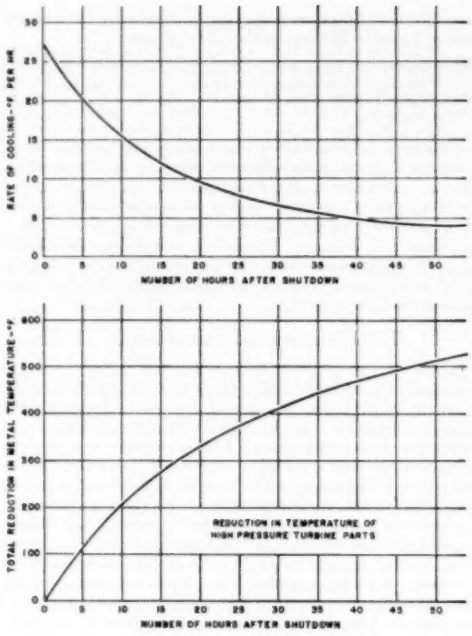

Fig. 10

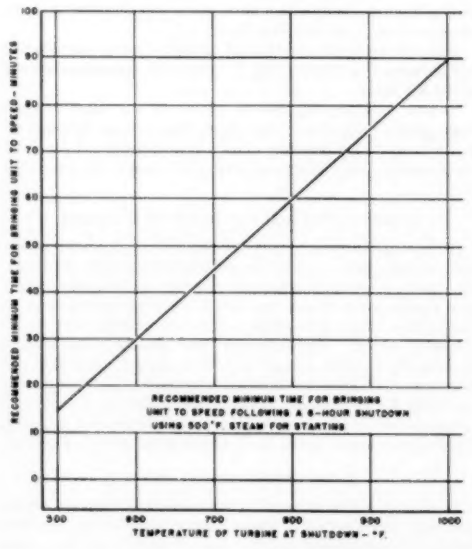

Fig. 11

can be done only by increasing the steam flow artificially through the boiler in a manner similar to that described in the paper.

However, if no increased circulation is provided and the turbine is shut down in its normal manner, the steam available for starting will be at a temperature of about 500 F. With this steam, the recommended starting time will be increased to 75 min, or an extension of about 1 hr in the starting cycle over that required for a controlled quick start under ideal conditions.

While such an extension in starting time is undesirable, such overnight shutdowns will be rather infrequent except on those systems where the night load is only a fraction of the day load.

Starting time, without artificial circulation, can be reduced if means are provided to cool the turbine to a lower temperature at the time the unit is taken out of service. If, for example, the turbine parts can be cooled to 700 F at the time of taking the unit out of service, the rolling time can be reduced to 45 min with the use of 500 F steam for starting. This reduces the additional starting time to only 30 min.

For a week-end shutdown of, say, 36 hr the turbine parts will cool off about 450 F during the shutdown period. If, then, these turbine parts are at 900 F at the time of shutdown, they will cool off to about 450 F when the turbine is started. Under this condition, 500 F steam, which is available with normal circulation, is ideal for quick starting.

For longer shutdowns the turbine will cool off even more, so the use of starting steam at temperatures above 500 F will lengthen rather then shorten the starting cycle and prove undesirable from the standpoint of thermal stresses in the high-temperature turbine parts.

The main advantage of a quick start is the saving of fuel during the starting cycle. However, in the arrangement described in the paper, part of this saving is offset by the heat required to generate the circulated steam, which heat is then rejected to the condenser circulating water. Also, additional pumping power is required by the boiler and condenser auxiliaries and by the boiler feed pump.

Therefore we feel that the additional cost of the artificial circulation arrangement, with its limited application because of the high thermal efficiency of the reheat unit, and with its rather small return from the standpoint of fuel saving, can be justified economically in only a very small number of cases.

Authors' Closure

Both Messrs. Falkner and Reynolds have supplied additional information on the subject of quick-starting hot turbines. Mr. Falkner emphasizes the ease with which this can be done, and cites an impressive record of completely successful experience. Mr. Reynolds points out that it is unusual for an electrical power system to have such a wide range in daily load that it is necessary to take high-efficiency turbines out of service for short periods each night. Both these points are well taken—the situation arises infrequently, but when it does arise, it can be satisfactorily handled.

Some Design Factors Relating to Performance and Operation of Reheat Boilers

By H. H. HEMENWAY,[1] NEW YORK, N. Y.

Reheat boilers designed to operate with low furnace exit-gas temperatures and at the same time to provide control of superheater and reheater-outlet steam temperatures over a wide load range are illustrated and described. Various means for controlling primary and reheat-steam temperatures are discussed as are design provisions for some of the operating and maintenance problems peculiar to reheat units. Some advantages and disadvantages of indirect reheating are given.

Introduction

With increase in steam-pressure and temperature conditions and the addition of reheat to improve cycle efficiency the percentage of heat transferred to steam for superheat and reheat increases. Table 1 gives the heat absorption per pound of primary steam for two nonreheat and two reheat cycles selected by Frisch.[2] The heat-absorpton rates represent conditions when the superheater and reheater absorb only the heat necessary for superheating and reheating.

TABLE 1 HEAT ABSORPTION IN SUPERHEATER AND REHEATER FOR FOUR CYCLES

	Nonreheat		Reheat	
Primary steam temp, deg F	1000	1050	1000	1050
Primary steam press, psi	1500	2050	1500	2050
Reheater steam temp, deg F	....	....	1000	1000
Feedwater temp, deg F	450	450	450	450
Total heat absorbed per lb primary steam, Btu/lb	1062	1076	1207	1221
Heat absorbed in superheater per lb primary steam, Btu/lb	330	387	330	387
Heat absorbed in reheater per lb primary steam, Btu/lb	....	....	145	145
Heat absorbed in superheater and reheater per lb primary steam, Btu/lb	330	387	475	532
Heat absorbed in superheater and reheater, per cent of total	31.0	36.0	39.3	43.6

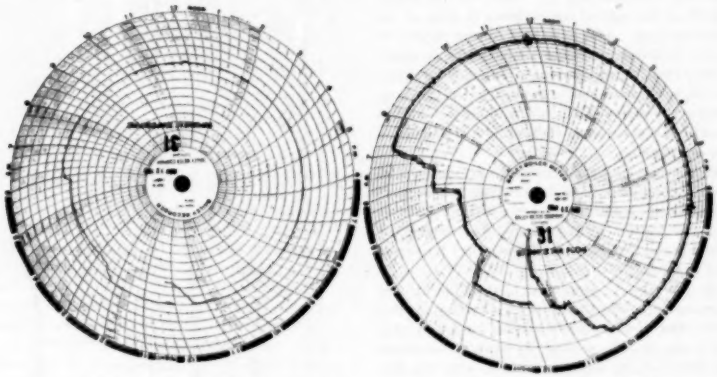

Steam-Temperature Chart — Steam-and-Air-Flow Chart

Fig. 1 Steam-Temperature Control With Condenser in Superheater Inlet Header

In a steam generator designed with no superheat and reheat-temperature control range the heat duties given in Table 1 would obtain. Since a modern plant must be designed for efficient operation at loads below full load it is essential that full steam temperature be provided at partial load. A convection superheater has a temperature characteristic which rises with load and hence with convection superheater and reheater surface the heat absorbed at full load will be greater than indicated in the table, the difference increasing with an increase in the range of temperature control. To absorb this additional heat requires more heating surface than is necessary to produce the control temperature. Increasing surface alone may be insufficient because of the limited heat content of the products of combustion in which case it becomes necessary to increase the furnace exit-gas temperature. The increase in boiler maintenance resulting from slagging at high furnace-exit temperatures and the probability of even greater maintenance in the future as the quality of available coal becomes worse is well known.

In the control range the excess heat to the superheater and reheater must be subject to control. This is done by the use of heat-exchange devices for removing heat from the steam, by spraying water into the steam, by causing some of the gas to bypass heating surface, by differential firing, and so forth. With differential firing the furnace exit-gas temperature at full load may be reduced somewhat below that required for normal firing.

[1] Chief Engineer, Steam Division, Foster Wheeler Corporation. Jun. ASME.

[2] "Steam-Generating Equipment for Resuperheating Cycles," by Martin Frisch, Trans. ASME, vol. 71, 1949, pp. 707–717.

Contributed by the Power Division and presented at the Annual Meeting, Atlantic City, N. J., November 25–30, 1951, of The American Society of Mechanical Engineers.

Note: Statements and opinions advanced in papers are to be understood as individual expressions of their authors and not those of the Society. Manuscript received at ASME Headquarters, November 19, 1951. Paper No. 51—A-142.

With the trend toward more superheat and reheat, including the possibility of several stages of reheat, it would appear that the furnace exit-gas temperatures must be increased in future designs. This would be true were it not for the radiant superheater. A radiant superheater absorbs part of the furnace radiation for raising steam temperature. Therefore, in a steam generator having a radiant superheater it is possible to provide generous furnace heat-absorbing surfaces to reduce furnace exit temperature and improve furnace cleanliness.

At the normal steam velocities and flow rates found in superheaters the cooling effect on the tubes is less than is obtained in a waterwall tube where water is being boiled. For this reason a radiant superheater must be designed so that under all conditions of operation the superheater metal temperatures are within safe limits. That this can and is being done is indicated by the many years of operation of hundreds of radiant superheaters and is particularly well described in a paper by Drewry.[3]

Steam-Temperature Control

A control system must be designed to hold steam temperature reasonably constant during operation in the control range. This may be accomplished with a condenser in the superheater inlet header. A condenser control is one in which the uncontrolled final steam temperature is reduced to the control point by condensing some of the steam in the superheater-inlet header. Control of the flow of feedwater through coils in the header determines the rate of condensation and hence the final steam temperature. Remarkably good results may be obtained with a condenser coupled with a properly designed control system as is shown on the operating charts in Fig. 1. Note how the steam temperature levels off at the control temperature in spite of the rather rapid increase in load. Also note that during periods of load fluctuation, the variation in steam temperature is small. The charts are taken from a unit having a convection superheater only and which was on automatic steam-temperature control at all times during the period shown. The quality of control would be substantially the same for a radiant or a combination radiant-convection superheater.

Another method of controlling temperature is by differential firing. One means of accomplishing this is to provide two or more rows of burners at different elevation which are fired at different rates. By shifting the relative proportions of fuel among the various rows of burners the exit-gas temperature may be varied by as much as 100 F or more.

Differential firing may also be employed in multiple furnace units. Fig. 2 illustrates a nonreheat twin-furnace unit having two furnaces in parallel. One is a completely water-cooled furnace with a boiler bank in series. The second has three water-cooled sides and a fourth that is steam cooled. In series with this furnace is a convection superheater. This unit provides much more flexibility than is normally found with any type of firing since practically any temperature from saturation to maximum temperature can be obtained by the control of the relative fuel fired to the two furnaces. Such a unit may be started up more quickly than a normal unit because the firing rate to the superheater furnace may be small until sufficient steam flow is produced by firing the waterwall furnace. Several modifications of this design are available which include reheat with reheat temperature control.

By-pass control of steam temperature is well known. The degree of maintenance required depends on a number of factors including the temperature of the gases to which the dampers are exposed. Fig. 3 shows a reheat steam generator with a division wall in the furnace, a combination radiant-convection superheater and a convection reheater. Reheat-steam temperature is controlled by dampers below the economizer where the maximum gas temperature is 780 F.

The radiant section of the superheater is in the front wall. Steam passes through alternate tubes of the radiant wall down to the radiant intermediate header in the hopper, then up the remaining tubes across the roof, down behind the screen to the convection inlet header. From there it flows countercurrently to the gas except for the last pass to the superheater outlet. The radiant-superheater tubes are maintained at low metal temperatures by the cooler inlet steam moving at high velocities. The high-velocity steam flow also insures proper steam distribution to the tubes.

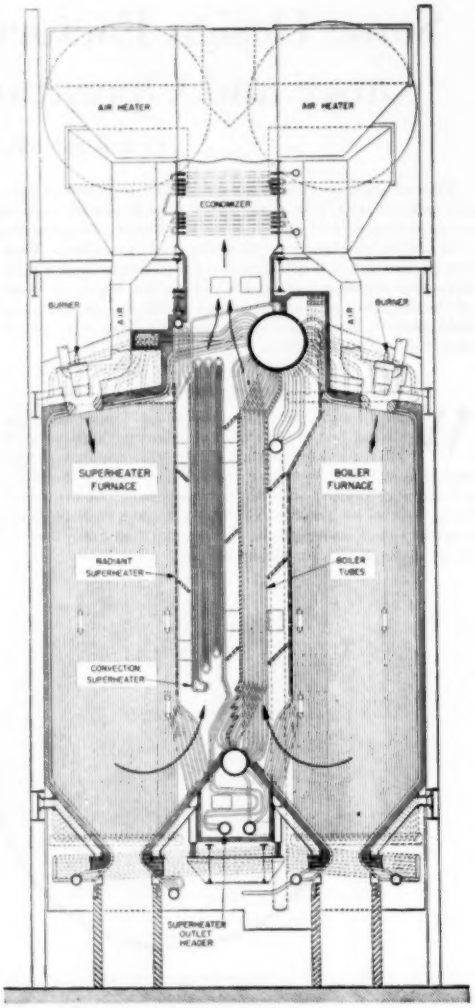

Fig. 2 Twin-Furnace Boiler, Steam Temperature Controlled by Differential Firing

[3] "Reheat Experiences at Port Washington," by M. K. Drewry, published in this issue of the Transactions, pp. 551–556.

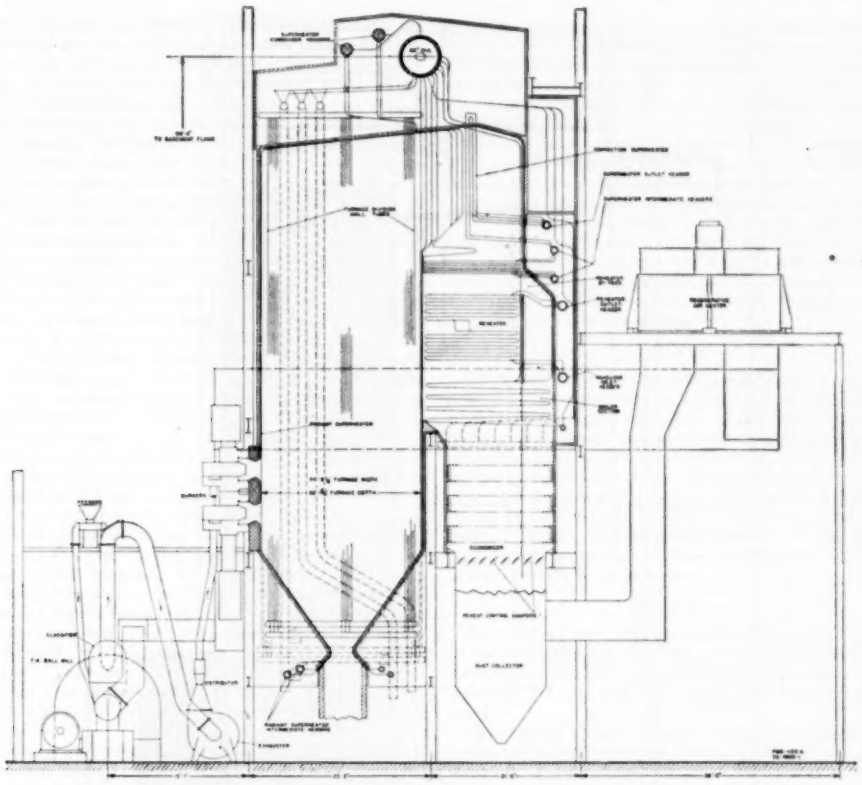

FIG. 3 REHEAT BOILER WITH COMBINATION RADIANT-CONVECTION SUPERHEATER AND CONVECTION REHEATER
(700,000 lb per hr, 1700 psi, 1005 F, 1005 F reheat.)

Positioning the radiant section in the front wall protects it from flame impingement.

Earlier in this paper it was stated that an increase in control range increases superheater duty at full load. An exception to this statement is the combination radiant-convection superheater. The control range of a combination superheater may be from 30 per cent or less to 100 per cent of full load. Fig. 4 shows a typical steam-temperature characteristic curve with load. Note that at 30 per cent load, steam temperature is at the control point. The temperature rises to a maximum at about 55 per cent and then drops to the control point at 100 per cent load. With a convection superheater, steam temperature would continue to rise. As a matter of fact, it would be virtually impossible to design a unit having a convection superheater and reheater for the 30 per cent to full-load superheat-control range particularly with a furnace exit-gas temperature of about 2000 F or less which is common to reheat boilers having combination superheaters.

Steam temperature is controlled by the condenser type of control described previously. Condenser duty is maximum at an intermediate load and is zero at 30 and 100 per cent of load.

An interesting design feature in connection with a combination superheater is that the reheater may be designed with a wide control range in spite of the fact that the furnace exit-gas tempera-

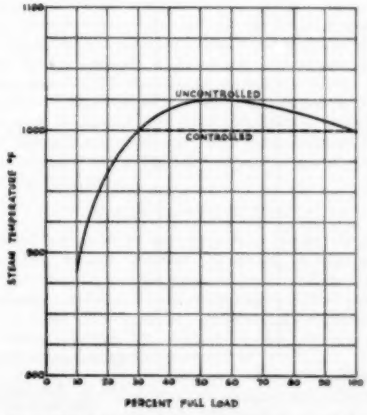

FIG. 4 STEAM-TEMPERATURE COMBINATION RADIANT-CONVECTION SUPERHEATER

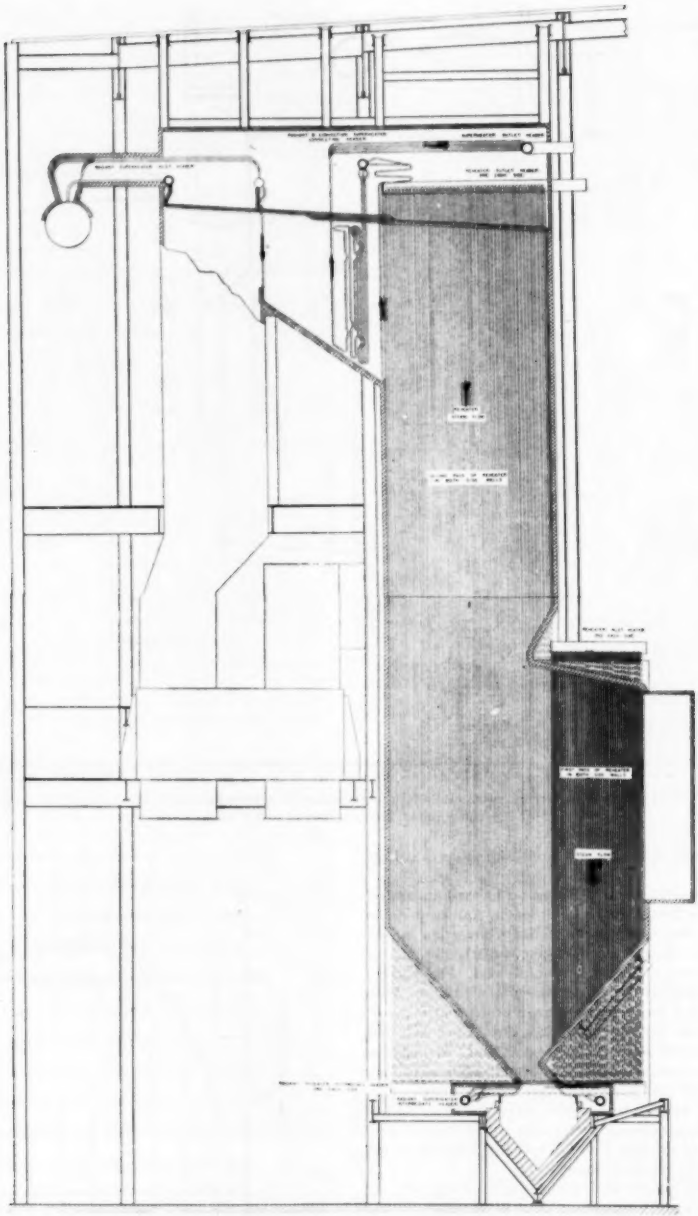

FIG. 5 RADIANT REHEATER ON FURNACE SIDE WALL
(686,000 lb per hr reheater flow, 500 psi, 1000 F.)

ture is held at a relatively low level. This is possible because the heat removed from the gas in the convection superheater of a combination is only a portion of the total heat required for superheating. In addition, the excess heat absorbed in the control range is low and decreases to zero at full load.

Both superheater and reheater shown in Fig. 3 are completely drainable. This fact is an advantage particularly during a start-up when water stored in superheater tubes must be blown out or evaporated before steam may be caused to flow.

A design of reheater having radiant surface only is shown in Fig. 5. This is the design referred to by Drewry[3] in which reheat will be maintained essentially constant by differential firing. The reheater is split into two equal parts, each part occupying all of one side wall. Cold reheat steam will flow downward from the inlet header at the burner arch to the intermediate header at the hopper, then longitudinally along the header and up the outlet tubes lining the main portion of the furnace to the outlet header. Platen waterwalls, having the same area as the first pass of the reheater, divide this section of the furnace. By firing more heavily in the center furnaces at high loads and less at the low loads, constant steam temperature will be maintained. To provide reasonably low metal temperatures in the reheater the inlet is in the hottest portion of the furnace and the outlet is at the furnace exit.

The principle of dual circulation has been adequately described in the literature by Frisch and Lorenzini,[4,5] and others. Briefly, it is based on providing two circulating systems in a steam generator. The primary system comprising all the highly heated waterwall tubes is kept at a relatively low boiler-water concentration. The secondary system comprising boiler surface receiving heat at a low rate has boiler water at the higher concentration normal to a boiler with a single circulating system. Steam from the secondary system is condensed or washed and generally only steam from the primary system, in which the boiler water is purer, is taken from the drum. Steam from a dual-circulation unit is of a higher purity than from a standard boiler, particularly at high pressures where the silica carried over as a vapor is a function of boiler-water concentration.

To design a dual circulation boiler an essential requisite is a low-heat-duty boiler section of sufficient size. With an all-convection superheater and reheater it normally is not possible to provide a boiler section of adequate duty because of the low gas temperature leaving the superheater and reheater. Fig. 6 shows a dual-circulation reheat boiler having a combination superheater with condenser control of steam temperature and a convection reheater with by-pass control. The extended-surface boiler section is located below the reheater in a zone of relatively low gas temperature.

Starting Procedures

Starting up of a reheat boiler is very much like that of a nonreheat unit. Where the reheater is a convection type as shown in Figs. 3 and 6, there is no steam flow through the reheater during start-up. The reheater which is under vacuum is drained to the condenser hot well. The reheater by-pass is kept open. The gas temperature to the reheater with no steam flow must be no greater than that allowed at atmospheric pressure for the materials selected. With a proper boiler design and with the reheater located behind all the superheater surface the gas temperature even during a relatively quick start-up will not reach a dangerous level before the reheater elements are steam cooled.

Radiant-superheater surface is cooled by radiation to the waterwall surfaces of the furnace until steam is generated and steam flow protects the tubes. A study of the effect of quick start-ups on superheater metal temperatures indicates that the unit shown in Fig. 6 may be started up from cold in $3^1/_2$ hours and less with the radiant-superheater tubes at safe temperatures.

Radiant-reheater surface likewise is cooled by radiation to the other furnace surfaces. This is borne out by Drewry's[3] experience on normal start-ups with radiant reheaters.

It is interesting to note that on a quick start-up after an overnight shutdown, with a radiant or a combination superheater the high temperature necessary to protect the turbine is available. With a convection superheater this is not the case. Examination of Fig. 4 shows the steam-temperature characteristic at steady-state conditions. Under starting-up and accelerating conditions these temperatures will be exceeded.

Controls

The control system of a reheat steam generator is only a little more complicated than that for a standard unit. The control of reheat temperature of a convection reheater with by-pass control is relatively simple since damper position affects only slightly the other components of the control system. For air-flow indication the draft loss across any of the components of the reheater, boiler, or economizer having a by-pass section in parallel should not be used in an index because of variation in draft loss with damper position. Where a radiant reheater is used as in Fig. 5, reheat temperature is controlled by differential firing between the wing furnaces and the center furnaces.

Protection

Safety valves having 100 per cent of reheater capacity should be installed between the reheater and the turbine. An average installation would have valves for 75 to 80 per cent of capacity before the reheater and 20 to 25 per cent of capacity after the reheater.

Means should be provided for protecting the reheater during a sudden loss of load, when it is located in a zone of high gas temperatures. Placing the reheater after the superheater, as shown in Figs. 3 and 6, reduces the possibility of damage under such conditions, and adequate protection is provided by the combustion control which reduces the firing rate and hence reduces the gas temperature to the reheater to a safe value. Steam by-pass lines for providing steam flow through the reheater under emergency conditions will offer protection for some time, the period of time varying inversely with the gas temperatures and heat-transfer rates to which the reheater surface is exposed.

More care must be taken in a reheat installation in the layout of the plant because of the added complication caused by the introduction of a reheat system. With a proper design, however, there is no reason why a reheat unit should be less safe to operate than a nonreheat unit.

Preliminary Procedures

Most of the problems associated with reheat are relatively minor. For instance, consider the setting of reheater safety valves. Among the various means for accomplishing this are (*a*) the provision of steam from another source; (*b*) by-pass steam from the drum to the reheater; (*c*) the raising of reheater pressure during operation by pinching on the interceptor valves where these are provided.

Blowing out of reheat lines requires large steam-flow rates. Normally these flow rates cannot be attained without rather sizable auxiliary steam connections. When these are not available perhaps the best solution is to exercise particular care in keeping parts clean and free of sand during construction.

[4] "The Problem of Generating Pure Steam at High Pressures," by Martin Frisch and R. A. Lorenzini, Proceedings of the Tenth Annual Water Conference of the Engineers Society of Western Pennsylvania, 1949, pp. 17–33.

[5] "The Dual Circulation Boiler, Its Design and Operation," by R. A. Lorenzini, Proceedings of the Midwest Power Conference, vol. 12, 1950, pp. 23–33.

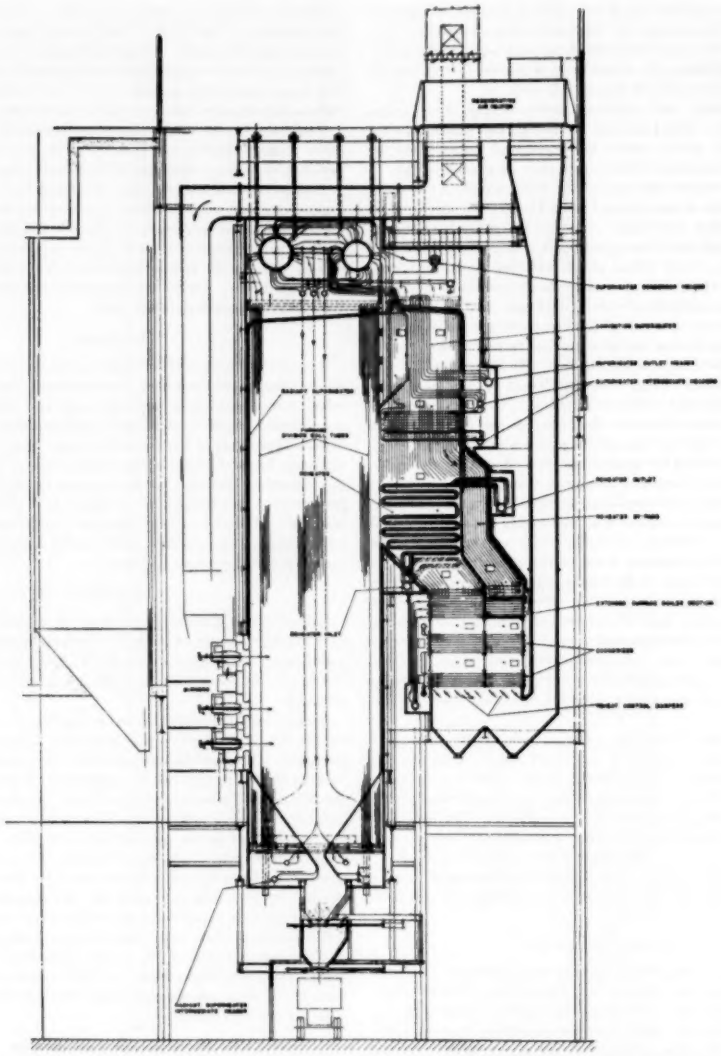

FIG. 6 DUAL-CIRCULATION REHEAT BOILER WITH COMBINATION RADIANT-CONVECTION SUPERHEATER AND CONVECTION REHEATER (1,450,000 lb per hr, 2075 psi, 1000 F, 1000 F reheat.)

Where acid-cleaning of a reheater is contemplated the necessary fill, drain, and vent connections should be provided. With a completely drainable reheater the problem is greatly simplified.

Hydrostatic testing of a reheater after the initial test is readily possible where isolating valves are installed. Where these are not provided and the breaking of connections for blanking off is awkward, other means such as that proposed by one operator of using compressed air through the turbine, utilizing Freon or other gas which may be detected at leaking joints, will be effective.

INDIRECT REHEATERS

Reheaters for heating secondary fluids, which in turn reheat steam between stages at the turbine, may be of approximately the same design as the reheaters previously described. The advantages of indirect reheaters are impressive: (1) The large and expensive piping between the turbine and boiler is eliminated and

relatively short piping between the turbine and secondary reheater substituted. The additional piping for carrying the secondary fluid will be much smaller and less costly. (2) Reheat pressure drop is reduced, thus increasing cycle efficiency. (3) More reheat stages may be provided because of the short connections. (4) The secondary-fluid system may be designed for low pressure, i.e., the pressure necessary for pumping the fluid. (5) Reheat temperature may be controlled over wider limits by varying the flow rate of the secondary fluid.

The disadvantages at present are great: (1) Development of means for safe handling of the secondary-fluid which may be a molten salt or liquid metal has not yet reached the commercial stage. (2) Two sets of heating surfaces must be used to replace one. (3) The mean temperature difference is reduced between the products of combustion and reheater thus increasing surface, except for a radiant unit.

Conclusions

With increased primary-steam pressures and temperatures and reheat temperatures the furnace exit-gas temperatures must be increased with increase in slagging difficulties unless radiant superheater surface is used. With combination radiant and convection superheater surface the steam-temperature-control range may be increased to extend from 30 to 100 per cent.

Starting up, control, and protection of reheat boilers offer no particular problems. From the design standpoint there are no deterrents to the construction and operation of steam generators for more efficient reheat installations.

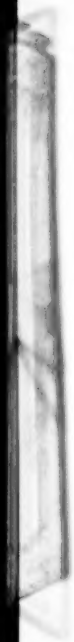

A Progress Report of Reheat Boiler Design and Operation

By W. J. VOGEL[1] and E. M. POWELL,[2] NEW YORK, N. Y.

A complete symposium on the reheat cycle was presented to the Society at the Annual Meeting in 1948. At that time, representatives of the various manufacturers of boilers and turbines reviewed the history of reheat and described in some detail the designs then being offered. A considerable number of these units have been placed in operation since then. The object of this paper is to discuss the performance of several of these new units and to describe some of the special features of operation.

OF the eighty-seven reheat units of postwar design by the authors' company, thirteen either have been placed in commercial operation or are expected to be shortly. The design capacities, steam conditions, and approximate starting dates are given in Table 1. All of these units were put in service without any abnormal difficulties, indicating that the addition of reheat equipment has not complicated the design or operation or reduced the reliability of the steam-generating unit.

TABLE 1 REHEAT UNITS PLACED IN OPERATION SINCE AUGUST, 1949, BY AUTHORS' COMPANY

Name	Station	No. of unit	Throttle pressure, psi	Primary temperature, deg F	Reheat temperature, deg F	Maximum capability, kw	Starting date
Boston Edison Company	Edgar	9	1450	1000	1000	81250	Aug. 1949
Niagara Mohawk Power Company	Dunkirk	1	1450	1000	1000	100000	Oct. 1950
Niagara Mohawk Power Company	Dunkirk	2	1450	1000	1000	100000	Nov. 1950
Rochester Gas & Electric Company	Russell	2	1450	1000	1000	62500	Nov. 1950
Dayton Power & Light Company	Hutchings	1	1450	1000	1000	62500	Dec. 1950
Dayton Power & Light Company	Hutchings	2	1450	1000	1000	62500	Apr. 1951
Metropolitan Edison Company	Titus	1	1450	1000	1000	75000	Feb. 1951
Metropolitan Edison Company	Titus	2	1450	1000	1000	75000	May 1951
Duke Power Company	Lee	1	1250	950	950	100000	Apr. 1951
Duke Power Company	Lee	2	1250	950	950	100000	June 1951
New York State Gas & Electric Co.	Goudey	1	1450	1000	1000	75000	Dec. 1951[a]
Public Service Electric & Gas Co.	Sewaren	4	1550	1050	1000	125000	July 1951
Central Hudson Gas & Electric Co.	Danskammer	1	1700	1000	1000	62500	Dec. 1951[a]

[a] Estimated.

Principles of Design

All but one of these units have been designed from certain basic principles and, therefore, are very nearly standardized. Fundamentally the reheat steam temperature is controlled by vertical adjustment of the burners which are arranged for tangential firing. Since the primary superheater does not have the same temperature characteristic as the reheater it is necessary to provide supplementary control which usually has taken the form of a spray-type desuperheater to limit the temperature of the high-pressure steam at reduced loads.

This control system was chosen instead of regulating the high-pressure steam with the burners to avoid the necessity of adding spray water to the reheat steam. Water added at that point would reduce the steam flow through the high-pressure turbine and sacrifice some over-all cycle efficiency.

In order to appreciate more fully the significance of these principles it may be necessary to review briefly the heat-transfer requirements of each of the superheaters involved. Saturated steam is supplied to the superheater at all loads. To maintain a constant steam temperature at the turbine throttle the heat added per pound of steam flow through the superheater must be held constant. As the load on the turbine varies the feedwater temperature also will vary, thereby changing the ratio of heat input to the unit and gas flow over the superheater per pound of steam generated. Therefore, to regulate the steam-temperature rise in the superheater it is necessary to vary the entering-gas temperature correspondingly. That temperature characteristic is indicated as curve A in Fig. 1.

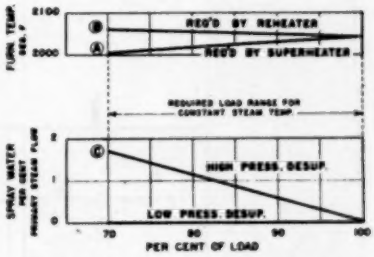

FIG. 1 TEMPERATURE CHARACTERISTIC CURVES

The problem in the reheater is quite different in that the temperature and pressure of the steam leaving the high-pressure turbine decrease with a reduction of load which increases the heat per pound of steam to be added in the reheater. The gas

[1] Chief Engineer, Combustion Engineering—Superheater, Inc. Mem. ASME.

[2] Assistant Chief Engineer, Combustion Engineering—Superheater, Inc. Mem. ASME.

Contributed by the Power Division and presented at the Annual Meeting, Atlantic City, N. J., November 25–30, 1951, of THE AMERICAN SOCIETY OF MECHANICAL ENGINEERS.

NOTE: Statements and opinions advanced in papers are to be understood as individual expressions of their authors and not those of the Society. Manuscript received at ASME Headquarters, November 8, 1951. Paper No. 51—A-114.

temperature leaving the furnace which will be required to satisfy the needs of the reheater is indicated as curve B. Obviously, no single furnace temperature characteristic can satisfy the needs of both superheaters. In order to minimize the quantity of water to be used for desuperheating and to obtain the maximum cycle efficiency over the widest possible load range the heating surfaces have been proportioned to require the same furnace temperature at full load. At reduced load the burners are regulated to follow curve B. Obviously, this will exceed the needs of the superheater, requiring the addition of spray water to limit the steam temperature. The quantity of water to be added for this example is shown as curve C and reaches a maximum at the design point (70 per cent full load) equivalent to 1.7 per cent of the primary steam flow. How this theory actually works in practice will be shown later in the paper.

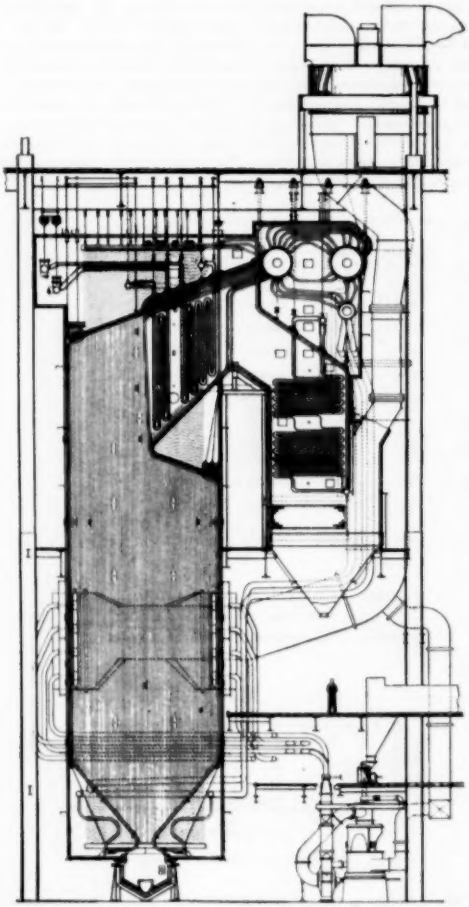

FIG. 2 STEAM-GENERATING UNITS NOS. 1 AND 2, DUNKIRK STEAM STATION

(Maximum continuous capacity 670,000 lb per hr at 1492 psi and 1000 F initial steam temperature, reheat to 1000 F steam temperature.)

INSTALLATION AT DUNKIRK STEAM STATION

One of our first postwar reheat units was placed in service in October, 1950, at the Dunkirk Steam Station of Niagara Mohawk Power Company. This unit serves an 80,000-kw turbine having a maximum capability of 100,000 kw and supplies steam to the throttle at 1450 psi and 1000 F reheated to 1000 F. The boiler unit is illustrated in Fig. 2. Constant primary and reheat steam temperatures were guaranteed from full load to 70 per cent load.

Two series of tests were conducted on this unit in January, 1951. The first series was run primarily to determine the performance characteristics of the turbine over a wide range of ratings. However, since each of these tests was to be of 6 to 8 hr duration with constant steam conditions we welcomed the opportunity it presented to run the numerous gas-temperature traverses required to study the detailed performance of each individual section of the superheater and reheater. The furnace was cleaned by normal operation of the soot blowers prior to most of the tests, particularly at high loads. The desuperheater valves were set in such a manner as to avoid the necessity for changing their position for the duration. In this way furnace temperatures and steam temperatures were held constant by adjusting the burners alone, permitting us to collect sufficient data to study all of the component parts of the unit with constant operating conditions. Pertinent data are summarized in Fig. 3.

The furnace outlet was traversed with thermocouples to obtain representative average gas temperatures leaving the furnace. These are plotted as curve A, and show the gas temperature required leaving the furnace to maintain constant primary and reheat steam temperatures. The steam-temperature control range was considerably greater than guaranteed with full temperature of primary and reheat steam being maintained from full load to 36 per cent load. It will be noted that the gas temperature required

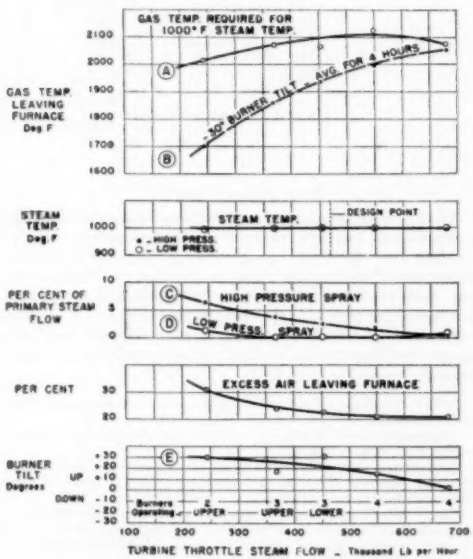

FIG. 3 TEST DATA ON DUNKIRK INSTALLATION

to accomplish this is relatively constant over the entire range, dropping off somewhat at the minimum load because of a slight increase in excess air permitted by the automatic combustion control.

During the second phase of this test program, furnace temperatures were measured while the burners were positioned at various degrees of tilt. Curve B has been plotted from these data to show the normal furnace temperature characteristic with stationary burners tilted downward 30 deg. This performance represents average conditions over a 4-hr test period following wall blowing and illustrates the degree of control available on this unit for steam-temperature regulation.

Curves C and D show the quantity of water delivered to the high- and low-pressure desuperheaters during the first series of tests plotted on curve A. It will be noted that there was an insignificant amount at full load indicating a perfect balance of heating surface between the primary superheater and reheater for the excess air corresponding to these tests. During normal operation a small percentage of desuperheating water may be used at times, depending on the frequency with which the furnace is cleaned and the degree of cleanliness.

The burner tilt at the start of each test is plotted on curve E. As the test progressed the burners were lowered to compensate for the ash accumulation on the walls. Four coal nozzles are provided in each corner of the furnace. The number and location of those in service during each test are indicated. Following the normal operating practice of taking the lower burners out of service as the load was reduced, was of some assistance in maintaining high steam temperatures with a minimum change in excess air as indicated.

Steam-temperature and flowmeter charts representing a typical daily load at this plant are shown in Fig. 4. The minimum load carried during this period was approximately 65 per cent of maximum.

Reheat at Russell Station

Unit No. 2 at Russell Station of the Rochester Gas and Electric Corporation was placed in operation during November, 1950. This unit has a rated capability of 62,500 kw with the same steam conditions as Dunkirk. The arrangement of the steam-generating equipment is shown in Fig. 5 and is also similar to Dunkirk except for size and the location of the air heater and fans. A set of charts showing steam flow and temperatures is presented in Fig. 6. It will be noted that a load of 475,000 lb of steam per hr was carried for a substantial portion of the day which corresponds to 69,000 kw or about 10 per cent above the rated capability of the turbine.

During the early morning hours the load was reduced to 9000 kw and at that time the steam temperatures were somewhat low (970 F primary and 825 F reheat). As the load was increased these temperatures rose and reached the design conditions at 27,000 kw or 39 per cent of full load at 6:30 a.m. Other load changes throughout the day were accomplished without any abnormal variations of primary-steam or reheat temperature.

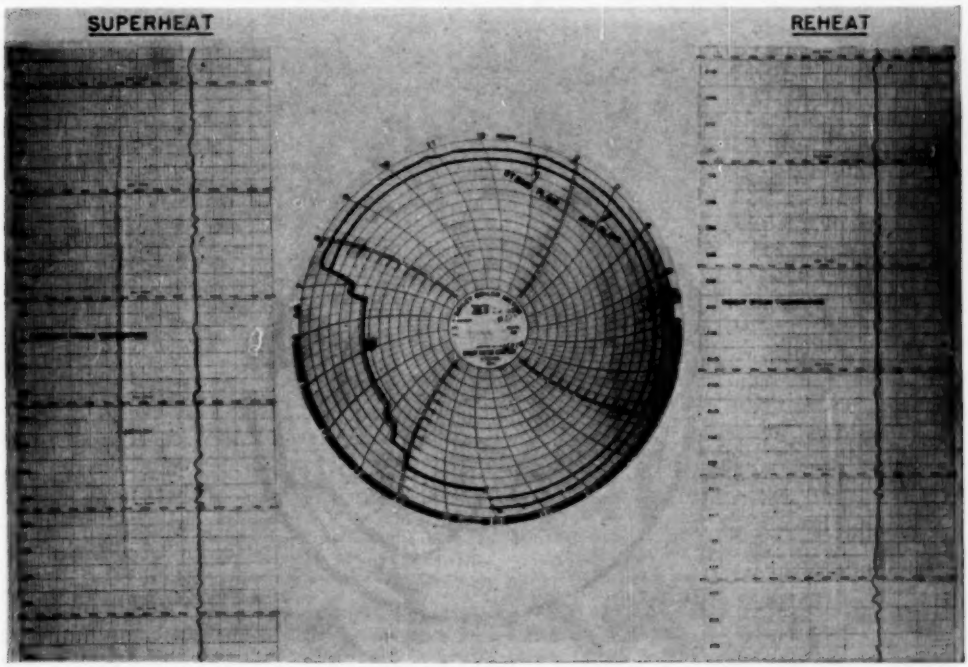

Fig. 4 Steam-Temperature and Flowmeter Charts Taken at Dunkirk Station

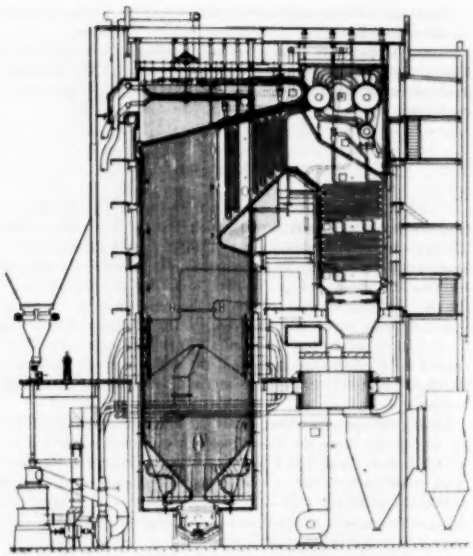

FIG. 5 REHEAT STEAM GENERATOR AT RUSSELL STATION
(Maximum continuous capacity 430,000 lb per hr at 1500 psi and 1000 F initial steam temperature, reheat to 1000 F steam temperature.)

DAYTON POWER & LIGHT COMPANY ADOPTS REHEAT

Two reheat units have been installed at the Hutchings Station of Dayton Power & Light Company which are substantially duplicates of Russell. The first of these was placed in operation in December, 1950. In February, after 3 months of operation, performance data were collected continuously at half-hour intervals for a 2-day period to show the action of the burners and desuperheaters as affected by changes in load and furnace cleanliness. These data are shown in Fig. 7. This unit carried full load about 16 hr per day. During that time the primary-steam temperature was controlled by admitting from 1 to 3 per cent desuperheating water. The reheat-steam temperature was controlled by burner tilt supplemented occasionally by desuperheating up to a maximum equivalent to 1 per cent of the primary-steam flow depending on the load carried and furnace cleanliness. Wall blowers were operated twice a day, once in the afternoon and again in the evening, at which time the burners would move upward and the low-pressure spray valves would close.

The load was reduced to 45 and 38 per cent for about 3 hr during the two nights reported. The design temperature of the primary steam was maintained through both of these periods while the temperature of the reheat steam was reduced only 35 and 45 deg, respectively.

POSTWAR TRENDS

During the postwar period there has been a notable tendency toward greater conservatism in furnace sizing and the complete elimination of exposed refractory. This, coupled with the use of burner regulation for the control of gas temperature has changed completely the nature of ash accumulations on the furnace walls as they were known in the past. This has permitted the develop-

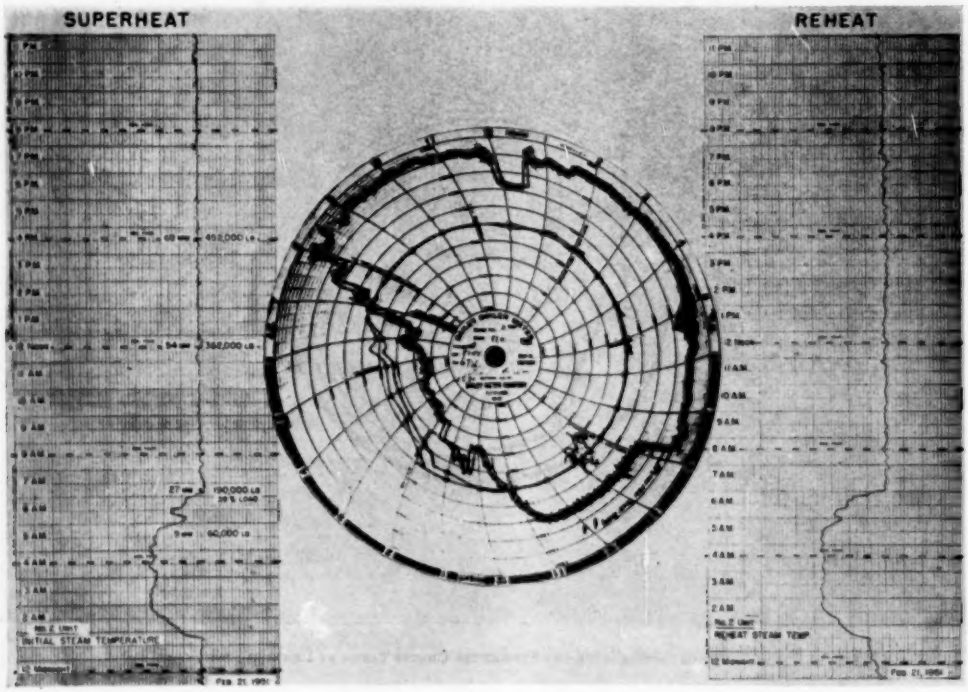

FIG. 6 CHARTS SHOWING STEAM FLOW AND TEMPERATURE AT RUSSELL STATION

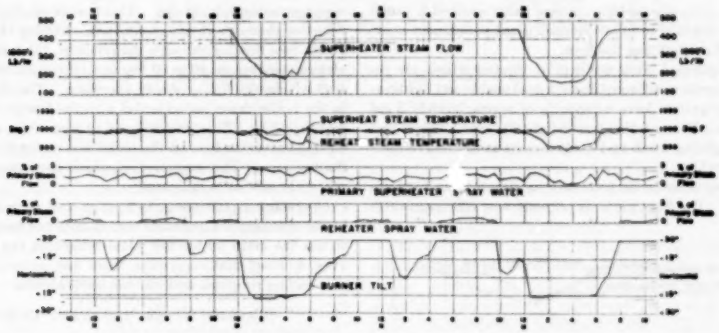

FIG. 7 PERFORMANCE DATA OF REHEAT UNIT AT HUTCHINGS STATION

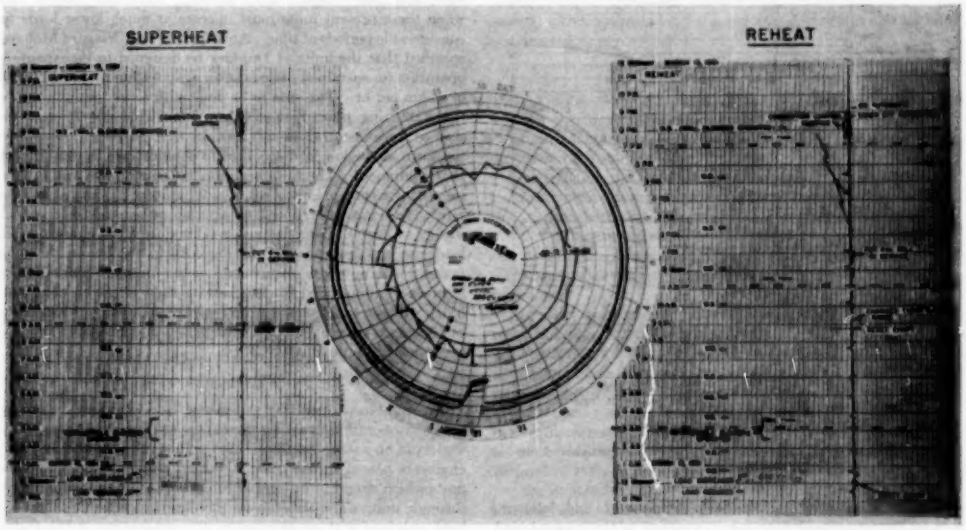

FIG. 8 TYPICAL OPERATING DATA AT TITUS STATION

ment of wall blowers as a supplementary steam-temperature control device rather than slag-removal equipment.

A number of plants have established the practice of operating one or two blowers at a time spaced at intervals as required to regulate steam temperature. The particular blowers to be operated at any one time are, of course, determined by observation of the furnace depending on the area of ash accumulation. Such practice not only lessens the burden of the control equipment but increases the equivalent capacity of the compressor and air-storage tanks with an air system. Although it would appear that this results in frequent blowing, actually it may correspond to less than one complete cycle per shift.

An example of this type of operation is shown in Fig. 8. These are instrument charts taken from one day's operation of boiler No. 1 at the Titus Station of the Metropolitan Edison Company. The center chart shows that one or two wall blowers at a time were operated at intervals to keep the burners between slightly below horizontal and tilted 15 deg upward, while the boiler operated at maximum continuous capacity throughout the entire 24-hr day.

EFFECT OF SUDDEN LOSS OF ELECTRICAL LOAD

During the development of the modern reheat boiler, many engineers expressed concern with possible complications to operating procedures resulting from the addition of reheat. One of the more important considerations was the protection of the reheater heating surface in the event of the sudden loss of electrical load, at which time the steam flow to the reheater might be interrupted. In order to study this problem and establish standard operating procedures, the Niagara Mohawk Power Company arranged to conduct a series of tests on unit No. 1 at Dunkirk. This program involved tripping the electrical load with the exception of station auxiliaries at three different loads from 25 to 100 megawatts. This unit is equipped with automatic relays to trip the firing

equipment 3 sec after the turbine control valve reached a closed position. It was decided to follow normal plant procedures existing at that time for relighting the fires.

This unit is equipped with small pilot torches which are referred to as side igniters adjacent to each coal nozzle and lighting-off torch. These igniters have a capacity of approximately 5 gal of light oil per hr. The practice was to light the side igniters and from them the lighting torch and coal streams as successive mills were placed in service.

Data pertaining to boiler performance for one of these tests are shown in Fig. 9. The load prior to trip-out was 100 megawatts

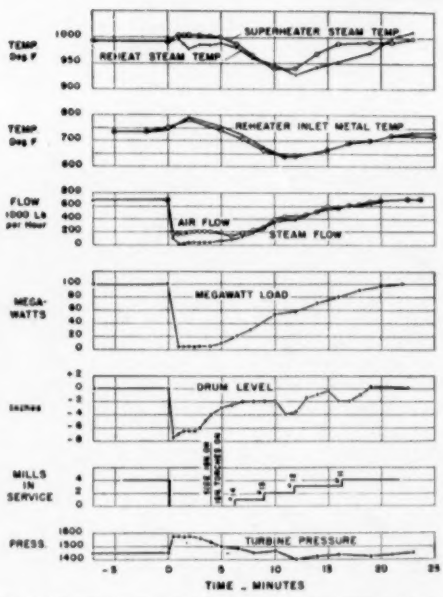

FIG. 9 BOILER PERFORMANCE DATA UNDER SUDDEN LOSS OF ELECTRICAL LOAD

which was dropped to approximately 3 megawatts and, following a short predetermined time delay, restored to the original load. It will be noted that there was very little change in steam temperature until steam was taken from the boiler during the restoration of load. The maximum temperature change during this test was approximately 60 deg. Thermocouples were installed on the reheater elements in the gas stream. During the period when no steam was flowing through the reheater, the temperature of these elements increased 40 or 50 deg to a maximum of 790 F which was well within the limits of safe operation. The drop in water level in the boiler drum coincidental with the loss of fire in the furnace was only 7 in. This was restored to normal by automatic control equipment as the load on the boiler was restored with no abnormal fluctuations. The sequence in which the various burners were placed in service is indicated.

Operating experience gained since that time with the stability of the side igniters indicates that it may not have been necessary to use the main oil torches when relighting the coal fires. However, without that experience there was no reason to complicate this testing program with further experiments.

PLANNING FUTURE OPERATION AT DUNKIRK

At the present time all of the modern reheat units operate at a high load factor. As more obsolete equipment is replaced, however, and more efficient units develop, there will come a time when these present units must operate at much lower loads for considerable periods of time. Anticipating this, Niagara Mohawk specified that the units at Dunkirk be designed to be capable of operation for sustained periods at an evaporation rate of 50,000 lb of steam per hr. This was to be done with a minimum use of oil for stabilizing pulverized-coal burners. The side igniters described were installed on this unit for that purpose. Tests have been run at the low load specified to demonstrate the stability of that equipment. The tests were conducted with one mill in service with its corresponding set of side igniters. Coal feed to the pulverizers was interrupted to simulate stoppages in the coal-supply system and the fire was reignited from the igniters. The load also was transferred from one mill to another in the same manner with no undue disturbance in the furnace. Furnace-wall blowers were operated to demonstrate their effect on flame stability. These experiments were repeated many times with complete success covering an extended period of continuous low-load operation of approximately 24 hr.

CONCLUSION

The combined operating experience from the many units already in operation covering numerous start-ups, trip-outs, and a variety of operating conditions has justified fully the faith so many engineers placed in the manufacturers' ability to design reheat units which would be at least as reliable as the standard straight-through unit. The substantial increase in cycle efficiency has been obtained with no sacrifice in the availability of the equipment. There is little doubt that we can anticipate an almost complete shift to reheat in utility stations located in high-fuel-cost areas in the future.

Reheat Experiences at Port Washington

By M. K. DREWRY,[1] MILWAUKEE, WIS.

The following are treated: (a) Starting schedules after shutdowns of various durations, (b) reheat economics based on experiences, (c) conversion to centralized control of auxiliaries, (d) reheat steam-temperature control, (e) turbine overspeed control as affected by reheat, and (f) reliability data. That reheat has been desirable in all respects is indicated.

Starting Procedures

THIRTY-minute starting after shutdowns of less than 30 hr, and 7½ to 15 hr to rated load when starting from cold, have been used successfully since 1940. Uniform moderate heating rates characterize normal startings.

Turbine-metal temperature, related to outage duration, indirectly determines starting and loading times. Axial expansion of the turbine cylinder is used as the primary guide in turbine starting rate. Table 1 shows how 0.060 in. per hr axial expansion is maintained, uniformly, when heating normally; 0.120 in. per hr is permissible when infrequently desirable.

Upon synchronizing after starting from cold, the axial-expansion rate becomes very high unless load is limited to unusually low outputs, as shown in Table 1, last column, wherein 1, 2, and 5 mw are recorded at the start of each hour after synchronizing. Before synchronizing, the flow, temperature, and pressure of steam are all too low to accomplish much heating. Upon synchronizing and loading, all advance sharply. By relating heating to axial expansion, not to load, thermal stresses of turbine components apparently are controlled better.

That axial-expansion rate is not a perfect index of thermal stresses is well realized, but extensive experience proves quite well that the method affords a practical control.

Carrying a load of 1000 kw for the first hour after synchronizing following a long shutdown probably will raise questions about high exhaust temperature. Pressure in the exhaust must be low, especially for units with high blade-tip speeds, in order that an adequate pressure drop occurs past the last stage to limit heating. A Port Washington unit (No. 2) was operated initially for electrical tests at approximately 1000 kw, for 24 hr without superheat in the exhaust. Never has exhaust temperature become excessive when following the starting procedure of Table 1.

Full vacuum has been obtained on turbines 3, 4, and 5 on many occasions while at a turning-gear speed of 25 rpm, because steam seals are effective, independent of speed. The ability to confirm at low speed that full vacuum can be obtained is valuable in limiting exhaust temperature when synchronizing. Condenser troubles can be corrected before they result in excessive turbine-exhaust temperatures.

The turbine cylinders have not become permanently distorted to oval shape when using the starting procedure of Table 1, nor have there been any difficult horizontal-joint tightness problems. Joint faces have remained parallel, unlike those of other smaller units that are heated more rapidly, and they have remained steam-tight for at least 4-year periods between dismantlings, though stopping and starting are infrequent. Turbine efficiency has been maintained closely, as proved both by weighed-water-rate tests and by monthly heat rates of each unit continuing closely the same year after year.

These reheat turbines are now started essentially like straight-condensing ones. There are no by-passes for pipe-warming purposes. Piping and turbine are warmed together. Operating simplicity and overspeed safety are aided appreciably. Reheat piping, under vacuum, is drained to the condenser hot well (not to atmosphere, requiring throttling the downstream intercept valve). The normal starting rate indicated in Table 1 does not heat radiant reheater surfaces above 600 F before they are well steam-cooled, which suggests why the contingency rate, twice as high, can be used safely.

Economics of Reheat

That 5.22 per cent[2] theoretical reheat thermal gains have actually been realized is suggested by Table 2, which summarizes all of Port Washington heat-rate experience. Further summarizing based on Table 2 follows in Table 3.

Boiler efficiency of later units has improved during the 1935–1950 installation period, and other refinements have aided reduction of the heat rate although the basic design continued unchanged.

No comparable experience without reheat has been obtained, but the foregoing, actual, long-time, heat-rate data represent close attainment of theoretical reheat rates, 5.22 per cent below non-reheat rates.

Reheater maintenance has been negligible. Including 6 per cent replacement of boiler No. 1 radiant reheater 18-8 tube surface in 1946, the first appreciable repair, when 10 years old, the annual reheater maintenance cost for units 1 to 4 during 1946 to 1950, inclusive, has averaged $553 per unit per year, or only ½ per cent of the annual coal saving creditable to reheat.

Considering the amount of heat absorbed and the added electrical output creditable to the reheater, this $553 per year per boiler-unit maintenance cost undoubtedly is at a lesser rate than for the remainder of the boiler unit. All other parts of the reheating process have been of similarly low maintenance, justifying the conclusion that the reheat cycle has certainly not added to maintenance costs.

Judgment indicates that if credit is taken for the lesser coal burned, and therefore less maintenance of all coal-handling and burning equipment, less ash handling, and less other boiler-room costs proportional to lesser coal burned, reheat maintenance costs have proved substantially less than without reheat. Apparatus for reheating has required less maintenance than other boiler-plant equipment, thus causing reheat to decrease total maintenance costs.

Because the author's company has employed reheat consistently in every electric generating station since 1926, comparative maintenance experience without reheat is unavailable. The 1950 experience given in Table 4 shows that total maintenance is only 4.3 per cent of fuel cost.

The fairest maintenance cost difference seemingly is derived by multiplying the 0.010 cent per kwhr boiler-room maintenance by

---

[1] Chief Engineer of Power Plants, Wisconsin Electric Power Company. Mem. ASME.

Contributed by the Power Division and presented at the Annual Meeting, Atlantic City, N. J., November 25–30, 1951, of The American Society of Mechanical Engineers.

Note: Statements and opinions advanced in papers are to be understood as individual expressions of their authors and not those of the Society. Manuscript received at ASME Headquarters, August 15, 1951. Paper No. 51—A-45.

[2] C. W. Bloedorn's complete cycle calculations for Port Washington conditions.

TABLE 1 PORT WASHINGTON UNITS NOS. 1 AND 2 NORMAL STARTING SCHEDULES

Based upon following uniform heating rates:
Boiler and piping: 100 deg F per hr (except as noted after 3rd hour)
Turbine: 0.060 in. axial expansion per hr

Boiler					Turbine						
Time, hours	Remarks	Max water temp, deg F	Press, psig	Superheated steam, deg F	Remarks	Total axial expansion, in.	Rpm	Vacuum, in. Hg	Exhaust temp, deg F	1st inlet, psig (approx.)	Mw (approx.)
0	Start burners	100	0	100							
1		200	0	100	Put on turn gear[a]		25	0	100		
1 1/2		250	15	250	Start heating	0	25	0	100		
2		300	50	300		0.030	25	0	100		
3	Rate: 50 deg F per hr[b]	400	230	400		0.090	25	0	100		
4	Rate: 25 deg F per hr[b]	450	400	500	Start accelerating[c]	0.150	800	18	180		
5		475	525	600	Synchronize	0.210	1800	26	175	50	1
6		500	680	700		0.270		29.5	30	75	2
7		525	830	800		0.330				100	5
8		550	1030	840		0.390				200	9
9		575	1260			0.450					15
10		581	1335			0.510					22
11						0.570					30
12						0.630					40
13						0.690					52
14						0.750					65
15[d]						0.810					80
					Total expansion	0.870					

[a] Keep turbine shaft 0.001 in. true for starting, by turning gear.
[b] To limit superheat and reheat temperature.
[c] Start vacuum and accelerating in any case before exhaust temperature exceeds 180 F. For turbines Nos. 1 and 2 increase rpm to water-gland-sealing speed (about 800 rpm) in about 5 min. Take about 45 min to increase uniformly to 1200 rpm; then 10 min to 1800 when vacuum is high enough (25 in.) to keep exhaust temperature below 210 F.
[d] If desirable, for unusual circumstances, the 15-hr period can be halved to 7 1/2 hr, by using 0.120 in. per hr axial expansion rate.

NOTE: When starting with turbine warm (turbine shortens upon "heating" when half warm, or warmer)

Axial expansion	
0.100 in.	2 hr heating on turning gear; 45 min to synchronize if vacuum is adequate (25 in.)
0.200 in.	1 hr heating on turning gear; 40 min to synchronize if vacuum is adequate (25 in.)
0.300 in.	1/2 hr heating on turning gear; 35 min to synchronize if vacuum is adequate (25 in.)
0.400 in.	1/4 hr heating on turning gear; 30 min to synchronize if vacuum is adequate (25 in.)
0.500 in.	0 hr heating on turning gear; 30 min to synchronize if vacuum is adequate (25 in.)

Short starting time when warm or hot assists in keeping No. 2 gland clearances within limit set by manufacturer. However, vacuum must be adequate to prevent high exhaust temperature. High steam temperature is desirable after short shutdowns.

TABLE 2 HEAT RATES, BTU PER NET KWHR

Unit no.	1	2	3	4	5	Plant
Period I, inclusive (since starting)	1935[a]–1950	1943[a]–1950	1948[a]–1950	1949[a]–1950	1950[a]–1951[b]	1935–1950
Heat rate	10862	10609	10074	10007	11818[a]	10656
Period II (recent year)	1950	1950	1950	1950	1951[b]	1950
Heat rate	11024	10651	10057	10027	9615	10407

[a] Starting dates, units Nos. 1–5, respectively, Nov. 22, Oct. 27, Oct. 5, Aug. 25, and Dec. 15 of the year indicated.
[b] Jan.–May, inclusive

TABLE 3 TYPICAL ANNUAL HEAT RATES

(To nearest 100 Btu per kwhr)

Units	1 and 2	3 and 4	5	Plant
Throttle and reheat maximum temperatures, deg F	850–850	900–900	950–950	
Throttle pressure, psig	1230	1255	1480	
Approximate annual heat rate, Btu per net kwhr	10700	10100	9600	10200

TABLE 4 MAINTENANCE VERSUS COAL COSTS

Maintenance:	¢ Per kwhr	Percentage of Total cost	Percentage of Fuel cost
Boiler room	0.010	2.7	
Turbine room	0.0036	0.9	
Total	0.0136	3.6	4.3
Other costs:			
Fuel	0.3128	83.7	100
All others	0.0477	12.7	
Total generating cost	0.3741	100	

TABLE 5 NET GAIN DUE TO REHEAT

	Per cent of fuel cost
Lesser fuel	5.22
Lesser maintenance (0.0005¢ per kwhr)	+0.02
Greater investment ($1.30 per kw, at 10 per cent FC, 60 per cent LF)	−1.19
Net saving	4.05

the lesser amount of fuel burned with reheat (5.22 per cent), or 0.0005 cent per kwhr.

Table 5 attempts to derive the net gain due to reheat, by correcting the fuel saving for this 0.0005 cent per kwhr lesser maintenance, and for an estimated $1.30 per kw greater net investment cost.

The $1.30 per kw greater investment cost was derived by adding all extra net costs due to reheating (reheater, piping, turbine changes, and so forth) and subtracting lesser coal and ash-handling, boiler-plant apparatus and condensing system costs, and the like, occasioned by the 5.22 per cent less fuel burned. Operating labor was assumed the same, due to compensating influences.

Reliability has not been impaired by reheat, as availability data presented later will indicate. The lesser maintenance costs derived in the foregoing support this conclusion. The net gain due to reheat in per cent of fuel cost is given in Table 5.

Thus net dollar savings due to reheating have proved to be 4.05 per cent of annual coal cost. The minor extra investment for reheat ($1.30 per kw) is repaid by reduced operating costs, at 60 per cent load factor, in 1 3/4 years.

The five Port Washington reheat units are currently netting an annual over-all saving (in operating expenses minus fixed charges) of $360,000. This quite well indicates the high economic value of reheat.

Centralized Control of Auxiliaries

Each of the five Port Washington units has in the past employed a boiler feed pump operator, a condenser-auxiliaries operator, and a mill operator (see Table 6). By current installation of

centralized controls at the boiler feed pump position, one operator will function for all three positions of each unit. For employment at 40 hr per week (4.2 men per position), this will release 42 operators. Retention of one per shift for lubrication and inspection of all mills once daily, and addition of another to assist supervision of all units, will cause a net reduction of 34 men, while manpower shortage is acute.

Reheat has permitted this change readily, because its operating requirements are low. The boilers and turbines always have been centrally controlled, at least enough to preclude any manpower releases in their cases without impairing reliability in emergencies.

Plant organization before and after centralized auxiliaries controls is listed in Table 6. With these centralized controls, total on-the-site year-round personnel averages 0.57 employee per 1000 kw of rated capacity. Newer stations (PW1 was designed in 1930) probably have fewer, but in no way is Port Washington's requirement increased because of reheat.

TABLE 6 OPERATING ORGANIZATION

	Centralized auxiliaries controls	
	Before	After
Per unit (each of five) per shift:		
Boiler operator	1	1
Boiler-operator helper	1	1
Mill operator	1	0.2
Feed-pump operator	1	1
Auxiliaries operator helper and ashman	1.2	1.2
Turbine operator	1	1
Turbine auxiliaries	1	0
Training, relief, vacations	0.3	0.3
Leading boiler and turbine operator	0	0.2
Totals	7.5	5.9
Totals, all shifts, including relief men:		
Engineer in charge	1	1
His assistants	3	3
Watch engineers	4	4
Boiler-room watch engineers	4	4
Boiler room and turbine room (above)	158	124
Yard crew (coal and ash)	12	12
Janitor and grounds service crews	8	8
Office	4	4
Technical	7	7
Maintenance (equivalent 40-hr employees)	43	43
Electrical organization	26	26
Total on plant payrolls	262	228
Total employees per 1000 kw rated capacity	0.63	0.57

Temperature-Control Problems

Radiant superheating and reheating have a profound effect on steam-temperature control. All Port Washington units employ the following: Combination radiant-convection superheaters; all-radiant reheaters.

Essentially constant superheated-steam temperature throughout the load range is assured by the combination superheater.

Reheater temperature rise at low loads needs be substantially higher than at high loads because modern high-temperature turbines with multivalve regulation and relatively "flat" heat-rate curves cause approximately 200 F drop in reheater-inlet temperature from full load to quarter load. Convection reheaters have similar drops, thus adding to the 200 F turbine drop.

Radiant reheaters are at least partly compensatory, decreasing the 200 F reheater-inlet drop to about 150 F at the reheater outlet. Fig. 1 shows typical Port Washington unit No. 4 practice in this regard, indicating that multivalves and higher steam temperatures suggest the need of still further increasing reheater temperature rise at low loads.

Flat superheat and reheat steam-temperature curves are reasonably expected at a new station in which Port Washington's reheater and radiant superheater positions will be exchanged in order that differential firing (less heat transfer to water-tubes and more to radiant-reheater tubes) will transfer more heat at low loads into the reheater and less into the waterwalls. Port Washington experience and that of the manufacturers agree in the conclusion that both stages of steam temperatures will be maintained

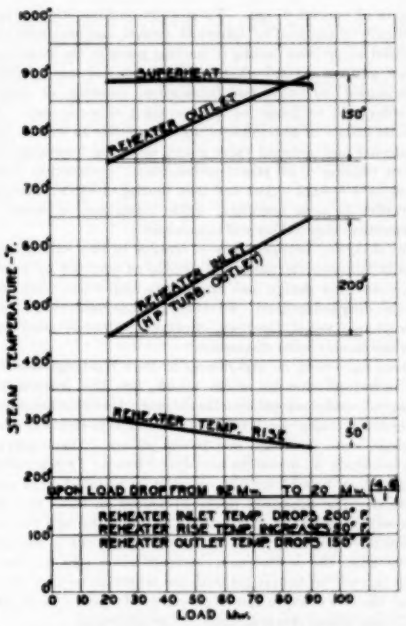

Fig. 1 Steam Temperatures Versus Load

(As load decreases from 100 to 22 per cent, the high-pressure turbine-outlet temperature drops 200 F, in spite of practically constant superheat temperature. The radiant reheater regains 50 F of this drop, thus limiting the decrease in reheated-steam temperature to 150 F.)

essentially constant, regardless of load and without any desuperheating, in this newer installation.

High reliability of the radiant-convection superheater plan is indicated by the following relatively low average annual maintenance costs per superheater section for the past 5 years: radiant, $222; convection, $460. Port Washington experience indicates that employment of radiant superheating and reheating surfaces to regulate steam temperatures contributes to station reliability.

Turbine Overspeed Control in Emergencies

The 750 lb of steam in the reheater and piping of each unit, upon sudden loss of full load, will accelerate units Nos. 1 and 2 by 33 per cent, and units, Nos. 3, 4, and 5 by 22 per cent if intercept or dump valves do not intervene. Larger exhaust-blade wheels of the later three units are principally creditable with the safer uncontrolled speed.

Reheat valving practice varies as follows:

Turbine no.	1	2	3	4	5
Intercept valves	2	2	1	1	0
Dump valves	1*	1*	1	1	2

* On hand, for installation this year.

Whether a single intercept valve, or more in parallel, are adequately safe for reheat units of relatively low inertia seems to deserve careful study.

When failure of control valves to operate causes dangerous overspeed, a "second line of defense" seems desirable because experience indicates that no valve is of adequately high reliability

in spite of careful design. Valve-stem-packing friction can be practically eliminated by labyrinth design, and strainers can be provided to prevent fouling of moving parts in the steam and oil spaces, and the several other possible causes of unreliability can be attended carefully, but fabrication, erection, or operating variables tend to make for nonoperation in some cases. Some possible causes of unreliability are: Materials in steam; failure of internal and external valve parts, including loosening; corrosion or binding of oil power-piston parts; destruction of steam screen by a foreign object and then fouling of valve; inadequate clearances in stem bushings; oxide formation on stems; and interferences due to thermal expansions.

The diversity between time of trouble in two valves, and especially between the nature of trouble as afforded by valves of widely different design and function, is important when serious overspeeding is involved. For these reasons dual reheat valving, as previously noted, has been employed. More detailed reasons are cited in an earlier discussion.[3]

There have been no experiences at Port Washington of excessive overspeed due to reheat steam, but the possibility has prompted careful attention to the subject. Downstream intercept valves are partially closed manually each shift to insure freedom of packings, stem bushings, and power pistons. Dismantling has been necessary on occasions to reduce friction. Dump valves for turbines Nos. 1 and 2 are now on hand for installation as soon as practical. The upstream intercept valves on these two initial units were installed to stop leakage of steam through the reheat labyrinth, which can cause overspeed, though not in the second or two when the downstream intercept valve fails to close. A dump valve is protective for both the labyrinth leakage and failure of the downstream intercept valve. It passes 75 to 80 per cent of the reheat steam directly to the condenser.

Upon dump-valve operation, condenser vacuum decreases for a second or two, thus causing a substantial braking effect by the longer blading through which there is little pressure drop. Experience with dump valves has not been unfavorable in any regard.

Availability

Experience amounting to 25.7 unit years with the Port Washington apparatus shows quite well that reheat does not impair availability. In fact, the maintenance experiences described previously suggest that it has helped availability.

Reheat at Port Washington undoubtedly assisted in escaping graphitization troubles, for the two stages of moderate steam temperatures permitted good economy without employment of the then-current high temperatures. This virtue was circumstantial and purely fortuitous, and may apply in the future only if nonreheat plants use advanced steam temperatures. Reheat problems appear less destructive to high reliability than do high-temperature metallurgical problems.

Only one experience wherein reheat impaired availability and reliability seriously can be recalled. A 2-month forced outage resulted when 8 rows of blading required replacement due to uneven heating when starting. Sticking of the intercept-valve relay valve kept the intercept valve closed until about 1200 rpm, preventing the normal distribution of steam flow through the reheat system and introduced nonuniform heating. Upon release of the relay valve, sudden normal flow through the blading downstream of reheat caused further distortion and resulted in heavy rubbing. Thus the extra apparatus required with reheat (the intercept valve and its relay) impaired reliability.

During the 25.7 unit-years treated in Table 7, availabilities were as follows: Boilers, 95.2 per cent; turbines, 93.8 per cent; boiler-turbine units, 92.3 per cent. During the 4 years of 1947–1950 availability of the boiler-turbine units has averaged 94.6 per cent, and their forced outages have been 0.7 per cent. This recent experience reflects better the effect of reheat, for it omits earlier boiler-tube corrosion, turbine-blade, and generator trouble, all unrelated to reheat. Generator trouble is responsible for over 50 per cent of Lakeside and Port Washington forced-outage time. These data quite well prove that reheat is not antagonistic to reliability.

Acknowledgments

For association with a company that encourages free interchange of experience and information, and to those individuals who afforded helpful criticism, the author is grateful.

BIBLIOGRAPHY

1 "Design Features of the Port Washington Power Plant," by G. G. Post, AIEE, June 26–30, 1933.

2 "The Port Washington Plant—Unique Design Features and Operating Experiences," by F. L. Dornbrook, *Mechanical Engineering*, vol. 58, 1936, pp. 697–704 and 728.

3 "Port Washington's Second Year," by M. K. Drewry, *Combustion*, vol. 9, February, 1938, pp. 18–24.

4 "Port Washington's Third Year," *Combustion*, vol. 10, January, 1939, pp. 16–19.

5 "Port Washington Sustains Its Economy," *Combustion*, vol. 11, January, 1940, pp. 33–34.

6 "Port Washington 1941 Operation," *Combustion*, vol. 13, January, 1942, p. 37.

7 "Port Washington 1942 Experience," *Combustion*, vol. 14, January, 1943, pp. 36–37.

8 "Port Washington Second Unit in Operation," *Combustion* vol. 15, January, 1944, pp. 30–34.

9 "Port Washington Performance for 1944," *Combustion*, vol. 16, January, 1945, pp. 32–34.

10 "1945–1946 Performance at Port Washington," *Combustion*, vol. 18, January, 1947, pp. 31–34.

11 "Development of a Major Principle in Pulverized-Coal Firing," by F. L. Dornbrook, Trans. ASME, vol. 63, 1941, pp. 261–266.

12 "Fuels Performance at Port Washington Station," by W. A. Pollock, Trans. ASME, vol. 71, 1949, pp. 97–104.

[3] Discussion, "Reheat Symposium," Trans. ASME, vol. 71, 1949, p. 738.

TABLE 7 OUTAGE TIME IN PER CENT OF ELAPSED TIME

	Single-boiler-turbine units[a]											
	1935[b]–1939	1940	1941	1942	1943	1944	1945	1946	1947	1948	1949	1950	Average
Total outages:													
Unit no. 1	12.3	10.6	3.4	7.5	12.5	11.9	12.8	16.7	5.0	4.2	5.1	6.0	9.7
Unit no. 2	..	..	..	..	12.0[b]	9.7	10.4	6.4	3.8	3.5	5.2	3.2	6.2
Unit no. 3	..	..	..	..	..	..	..	..	..	9.6[b]	5.1	6.0	5.9
Unit no. 4	..	..	..	..	..	..	..	..	..	..	4.9[b]	4.5	4.6
Unit no. 5	..	..	..	..	..	..	..	..	..	..	..	0.5[b]	0.5
All units (25.7 unit years)	12.3	10.6	3.4	7.5	12.4	10.8	11.6	11.6	4.4	4.9	5.1	4.9	8.1
Forced outages:													
Unit no. 1	1.7[b]	1.4	0	0	11.5	0.3	0	14.4	0.7	2.2	0	1.3	2.6
Unit no. 2	..	..	..	..	1.0[b]	0.1	0.1	0	0.3	0.4	0.2	0	0.2
Unit no. 3	..	..	..	..	..	..	..	..	..	3.5[b]	1.2	0	0.9
Unit no. 4	..	..	..	..	..	..	..	..	..	..	1.2[b]	0.8	0.9
Unit no. 5	..	..	..	..	..	..	..	..	..	..	..	0[b]	0
All units (25.7 unit years)	1.7	1.4	0	0	10.7	0.2	0.05	7.2	0.3	1.6	0.5	0.5	1..

[a] No main steam nor feedwater interconnections. Demand time was practically 100 per cent of elapsed time.
[b] Nov. 22, Oct. 27, Oct. 5, Aug. 25, and Dec. 15 startings, respectively, Units Nos. 1–5.

13 "Port Washington No. 3 Goes on the Line," *Power Generation*, vol. 53, March, 1949, pp. 66–69 and 129–130.
14 "Port Washington 1948 Performance," *Combustion*, vol. 20, January, 1949, pp. 45–46.
15 "1949 Port Washington Experiences," *Combustion*, vol. 21, January, 1950, pp. 45–48.
16 "1950 Experiences at Port Washington Station" *Combustion*, vol. 22, January, 1951, pp. 39–40.

Discussion

E. H. KRIEG.[4] It is well to recall how the outstanding plants, turbines, and boilers discussed in the current series of papers, have evolved. We have them because of meetings of this Society, those of the Prime Movers Committee of the Edison Electric Institute and other committees, together with our technical journals, all of which provide a forum where manufacturers and users alike literally vie with each other as to how they can best tell their competitors in what ways and how they have advanced, so that others not only can catch up, but go further. This is competition of the most progressive type; the product of our free-enterprise system; a distinct contrast to the stifling of stimulation to human achievement that occurs when governmental agencies take over, as in the USSR. Let no American retreat from the invigorating freedom that is now ours.

The present paper is a really valuable addition to a series that makes Port Washington one of the best, if not the best, documented plants.

The primary purpose of a power plant is to produce electrical energy as economically as possible, and to do this, the combination of investment, fuel, labor, and maintenance costs should be a minimum and availability a maximum. Port Washington meets these criteria to an unusual degree, and so we are grateful both to the author and the Wisconsin Electric Power Company for presenting their costs and operating experiences so frankly.

Seldom is there an opportunity to install a prototype unit and then follow its basic design with four well-timed extensions in which design refinements can be introduced to meet conditions that developed in actual operation. This makes for optimum economy both in investment and operating cost, and one wonders why the advantages of such a program are not more generally exploited.

Starting Procedures. Although axial expansion of 0.060 in. per hr of the turbine cylinder is used as the primary guide in turbine starting rate, the author states that it is not the perfect index of thermal stresses in turbine components. At least it is simpler than having numerous thermocouples scattered about. However, the General Electric Company developed a differential-expansion recorder for Twin Branch Unit 3 in 1941, an instrument which the writer has often used to indicate relative movement (really, relative average temperature) of the rotor and cylinder. This guide has been most satisfactory for indicating the possibility of a rub during starting or operating conditions.

It would be of interest to know whether in Table 1 of the paper the 0.300-in. axial movement between the 22 and 80 mw loads imposes any limitation on the speed of loading or unloading while the turbine is in normal operation, or whether axial expansion is thus limited only during the starting cycle.

If full vacuum can often be obtained while units Nos. 3, 4, or 5 are on turning gear, might it not be desirable to start rolling the turbine at 150 psi or even lower steam pressure instead of 400 psi? The amount of air leakage experienced, as well as the type of shaft seals and air-removal equipment used, would be of real interest.

Attention is called to the omission of intercept valves in Port Washington unit No. 5 reheat line, using dump valves only to prevent overspeeding. It is possible that this is the first time such design has been used.

Economics. It is time to stop using the expression "trend to reheat." That there is little question about reheat being here to stay, is expressed by the author in such statements as the following:

"That 5.22 per cent theoretical reheat thermal gains have actually been realized.

"The reheat cycle has certainly not added to maintenance costs.

"Reliability has not been impaired by reheat and this is confirmed by low maintenance.

"In no way is Port Washington's personnel requirement increased because of reheat."

That reheat need not impair availability appears well substantiated by the 1.7 per cent of elapsed time in forced outages and 92.3 per cent of availability in 25.7 unit years. This is an excellent record.

The present resurgence of the reheat cycle confirms the judgment used by the Wisconsin Electric Power Company in employing reheat so consistently since 1926.

C. A. ROBERTSON.[5] Mr. Drewry's paper on reheat experiences at Port Washington is a definite contribution particularly because of its factual nature. It covers many aspects of the problem of reheat operation extending over a long period of reheat turbine experience. The first 825 F reheat steam turbine-generator unit was installed in 1935 at the Port Washington Station of the Wisconsin Electric Power Company. It is an 80,000-kw unit, and it now operates with steam conditions of 1230 psig 850 F, reheat to 850 F, and $^1/_2$ in. Hg abs exhaust pressure. This tandem-compound turbine with reheat between stages in the high-pressure cylinder was the first installation to use the now almost universally accepted one-boiler per turbine arrangement in which the reheater is an integral part of the boiler, simplifying reheat temperature control.

This paper is important because it recounts operating experiences with a succession of five similar 80,000-kw tandem-compound 1800-rpm reheat turbines and unit boilers, each one being an improvement over the preceding one. The period of this carefully recorded operating experience is 1935 to 1951.

The steam flow in all five Port Washington turbines is basically the same; that is, steam flow is unidirectional through the high-pressure turbine to the double-flow exhaust turbine. A reheat diaphragm is used in the high-pressure turbine. The first two units are of the straight reaction type, the others are impulse-reaction. The last three units are practically identical except that the initial steam conditions have been increased successively. Fundamentally, the reheat operating experiences for the five units show a comparable progression of improvement. This comparability provides data of particular value.

The author's discussion of starting procedures is noteworthy. The idea presented that starting is related to turbine expansion, especially starting from cold, is important. In this way the turbine itself is used as a self-inclusive, sturdy, and reliable instrument indicating clearly and directly to the operators a means whereby the thermal stresses may be controlled.

The author states, "Upon synchronizing after starting from cold the axial expansion rate becomes very high unless the load is limited to unusually low outputs." This is the critical point in the starting cycle during which there is a tendency to apply too high a rate of loading. Here is where the correlation between

[4] Consulting Engineer, Stone & Webster Engineering Corporation, Boston, Mass. Fellow ASME.

[5] Engineer in Charge, Test and Engineering Calculations Groups, Steam Turbine Section, Power Department, Allis-Chalmers Manufacturing Company, Milwaukee, Wis. Mem. ASME.

rate of loading and expansion rate becomes valuable. This fundamental idea relative to initial application of loading will tend to lengthen the time usually considered fufficient for loading.

Author's Closure

Messrs. Krieg's and Robertson's discussions are valued additions to the paper.

Concerning Mr. Krieg's question whether the 0.300-in. expansion between 22 and 80 Mw of a previously cold unit imposes any limitation on the speed of loading or unloading while the turbine is in normal operation, reporting that the normal change in axial expansion in this load range after equilibrium is 0.180 in., seems significant. Normally, 90 minutes are taken to make this load increase, for system load changes do not require faster change, but occasionally the change has been made safely in 45 minutes. Expansion lags behind load change, of course.

Mr. Krieg is right that rolling can be started with low steam pressure when steam seals permit full vacuum at low speed. A new plant will employ water ejectors in order that approximately an hour can be gained by starting the turbine rolling at lower steam pressure. Air leakage averaged during 30 unit-years is 3.4 cfm. Steam-jet air pumps and single-stage starting ejectors are used at Port Washington. The shaft seals of Units 1 and 2 are water glands, and those of the last three units are steam seals.

Mr. Robertson rightly emphasizes the need of reasonable heating rates when starting from cold, especially during the early loading period. With higher pressures and temperatures, increased attention to careful heating seems increasingly worthwhile, for higher efficiency and better reliability.

The First Year's Operation of the Dunkirk Steam Station

By J. N. EWART,[1] BUFFALO, N. Y.

The Dunkirk Steam Station went into commercial service on November 19, 1950, when the first unit was placed in regular operation. The second unit went into commercial operation on December 28 of the same year. The first year's operation has not been without troubles which are likely to occur in breaking in a plant incorporating several new and untried developments. Nevertheless, its performance has been generally satisfactory. Operation of the reheat units has introduced no new limitation in flexibility nor increase in operating personnel over the nonreheat units, and the improved economy has more than justified its adoption.

THE Dunkirk Steam Station comprises two single-boiler single-turbine reheat units. The turbines are rated at 80,000 kw, 0.8 power factor, 100,000 kva at 0.5 psi hydrogen with a capability of 100,000 kw, 120,000 kva at 25 psi hydrogen. Steam conditions are 1450 psi, 1000/1000 F at the turbine control valves. The turbine generators are tandem-compound, reverse-flow, double-flow, 3600-rpm manufactured by the General Electric Company. The reheat boilers are of the bent-tube, radiant-reheat, single-pass type with water-cooled furnaces, two-stage superheaters, interstage reheaters, fin-tube economizers, and Ljungström air heaters, furnished and installed by Combustion-Engineering Superheater, Inc. They are fired by tilting tangential burners which are positioned automatically to maintain reheat temperature of 1000 F from 70 per cent to full load of the units. Each boiler generates 670,000 lb per hr of primary steam for the maximum continuous output of 100,000 kw.

The two units are controlled from a central control room located between the boilers and the turbines on the operating floor. This control room contains all of the controls for the two main units with the exception of the turbine supervisory instruments and the hydrogen control panels.

A further description of the station and its auxiliaries has been published previously (1).[2]

Summary of First Year of Operation

Table 1 lists the pertinent data concerning the first year of operation. The table starts with the month of January, since that is the first complete month that both units were in commercial service.

Column 7 indicates the percentage of total time that the units actually were in service and carrying load. The outage time indicated in this column would reflect both forced and scheduled outages. The total unscheduled outages for the two units during this period amounted to 6, and were divided equally, 3 being caused by the boilers and 3 by the turbines. These troubles are described elsewhere in this paper.

Column 8 shows the average gross load carried by the two units during their actual in-service hours. These units were operated mainly in the upper region of their capability curve as can be seen from this column. This fact is significant and contributes to the favorable heat rates shown in column 9. There is an apparent anomaly shown with column 9 and column 10 wherein the station heat rate improves with increasing circulating-water temperatures. About the only explanation for this is that the heat rate is reflecting the tune-up of the station and is improving in spite of the higher temperatures. If this is so, the heat rate should show further improvement as the water becomes cooler.

Station service, column 3, is running between 4.7 and 4.8 per cent of gross generation. This compares with 5.5 to 6.0 per cent for comparable nonreheat machines on our system. The operation and maintenance expense for the station to date is shown in columns 11 and 12. These values are shown in cents per kilowatt of rated capacity rather than the coventional units of mils per kilowatthour, because both operating and maintenance costs are affected more by over-all design, age of the station, and local labor conditions than they are to station output. In the instance of this station, it can be expected that there will be some further increase in the maintenance expense as the station takes on its normal cycle of inspection and replacements.

TABLE 1 OPERATION AND PERFORMANCE DATA, YEAR 1951

	Gross gen mw hr	Net station output, mw hr	Station service, per cent	Avg net gen, mw	Unit hr in period	Unit hr in service	In service factor per cent	Avg in service gross gen, mw	Net station heat rate, Btu/kwhr	CW temp, deg F	Operating costs exclusive of fuel cents per kw rated cap. Oper	Maint
1951	Col. 1	Col. 2	Col. 3	Col. 4	Col. 5	Col. 6	Col. 7	Col. 8	Col. 9	Col. 10	Col. 11	Col. 12
Jan.	95686	90911	4.92	122.19	1488	1243	83.7	155	9650	40.0	18.5	9.7
Feb.	117921	112334	4.73	167.16	1344	1330	99.0	178	9880	40.0	22.4	9.6
Mar.	136348	130048	4.64	174.80	1488	1474	99.1	185	9690	40.0	21.0	7.1
Apr.	115663	110165	4.77	153.22	1438	1299	90.2	197	9650	45.8	18.9	11.0
May	118349	112716	4.76	151.80	1488	1255	86.4	189	9440	52.4	21.2	15.2
June	114025	108453	4.88	150.63	1440	1239	87.4	181	9530	63.5	22.5	12.3
July	112430	106918	4.95	147.71	1488	1310	88.0	175	9480	72.0	18.8	9.9
Aug	144720	138027	4.6	185.52	1488	1488	100.0	195	9450	74.1	17.8	8.1
Sept.	127693	121683	4.7	168.77	1442	1333	92.3	191	9470	67.4	17.7	9.4
Oct.	104743	99564	4.95	133.82	1488	1109	74.5	189	9440	59.0	17.7	18.8

Station Personnel

An organization chart comprising the station personnel for the two units is shown herewith. Three control-room operators per

---

[1] Chief Mechanical Engineer, Niagara Mohawk Power Corporation. Mem. ASME.

Contributed by the Power Division and presented at the Annual Meeting, Atlantic City, N. J., November 26–30, 1951, of The American Society of Mechanical Engineers.

Note: Statements and opinions advanced in papers are to be understood as individual expressions of their authors and not those of the Society. Manuscript received at ASME Headquarters, November 12, 1951. Paper No.51—A-138.

[2] Numbers in parentheses refer to the Bibliography at the end of the paper.

DUNKIRK STEAM STATION ORGANIZATION CHART, NOVEMBER 1, 1951

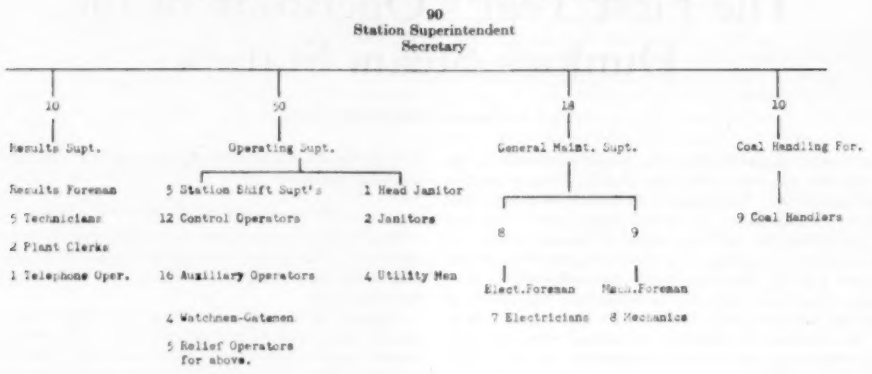

shift are stationed in the central control room. These men are equally qualified to take over control of either the boilers, turbines, or electrical switchboard located in this room. There have been a number of instances when this arrangement has proved very helpful. For example, there have been some instances of a run of excessively wet coal which has caused sticking in the hoppers and mill feeders. In these cases the operator assigned to the electrical switchboard, or the operator assigned to the other boiler immediately would assist to whatever extent necessary and still be able to give general attention to his own equipment.

The mechanical and electrical maintenance department cares for the routine maintenance only. The major boiler or turbine inspections or repairs are handled by bringing in the required number of personnel from the Huntley Station located at Buffalo.

Operation and Maintenance Problems

In spite of the circumstances that Dunkirk is the first reheat installation on the Niagara Mohawk Power Corporation system and that a new type of reheat turbine was being placed in service, the preliminary operation of this station was quite successful, and there have been no more than might be considered the normal starting troubles during the first year of service.

The first forced shutdown occurred on December 17, 1950, when unit No. 1 became rough at a load of 2 mw during a routine unloading of the unit prior to taking it off load. The cause was a failure of the bucket covers on the 18th-stage wheel of the turbine. The buckets were not damaged. No definite cause for this failure has been found, and it can only be presumed that a foreign object inadvertently must have been left in the machine during assembly and subsequently became dislodged in such a manner as to cause interference. The manufacturer has examined the design of these covers carefully for stresses, resonance, and so forth, and can find nothing wrong with the design. The unit was back in service on January 3, 1951, and was forced out again the same day on account of a furnace explosion in No. 1 boiler. The damage in this case was confined principally to the insulation and casing at the top of the boiler. The cause is attributed to exceeding the minimum coal-air velocity to the burners, especially when bringing in a cold boiler. The unit was out for 3 days on account of this trouble.

Unit No. 2 was forced out for 2 days on January 15, because of a leak in a field weld at the economizer-inlet header.

Unit No. 2 was forced out for two days in May, because of an iron-oxide deposit resulting in sticking of the turbine control valves. Subsequent to this, all of the control valves for both units were dismantled, inspected, and cleaned up on prearranged outages of the units. None of the remaining valves was stuck but deposits of from 0.002 to 0.0025 in. were found on the stems with a somewhat lesser amount on the bushings. The last of these valves was cleaned in June, and there has been no further indication of sticking.

Unit No. 1 was forced out the latter part of June on account of a failure of the liners in the desuperheaters for the boiler reheater. These liners, made of stainless steel, failed at the welds. They were removed at the time and since have been replaced by a 4 to 6 per cent chrome material and an improved method of support.

The intercept valve, unit No. 2, failed to close the final $^3/_4$ in. of its travel on a scheduled shutdown of this unit the first of September. It was necessary to dismantle this valve to find the cause of this sticking, which was found to be iron oxide. Previously, it had been the practice to operate this valve once per shift to check freedom of stem movement, but the valve is not closed completely during these tests. It is now our practice to reduce load to 40 per cent and completely close this valve once each week in addition to exercising it through part of its travel once per shift. The manufacturer is furnishing a test device for this valve which will permit closing and reopening fast enough so that the test can be made with a load reduction to 60 per cent of maximum load. The disadvantage of having to reduce load for 15 min once per week for this purpose is not considered serious in our case.

During the month of October, unit No. 1 was taken off load for a prearranged shutdown to install the new liner assemblies in the boiler desuperheaters. During this shutdown, scheduled for a a week, the turbine was inspected partially, and it was found that the welds were broken at one end of all seven struts in the upper half of the exhaust hood. The failure of these welds is attributed to improper workmanship. The design is considered satisfactory and no changes are considered necessary. The welds which failed are all rather inaccessible and therefore difficult to make, but similarly difficult welds in the lower half of the casing on this machine were found to be entirely adequate and sound.

Turbine and Generator Trip-Out Tests

During the month of June, in co-operation with the General Electric Company and Combustion-Engineering Superheater, Inc., tests were made to determine the ability of these units to trip out when carrying full load and to study the effects of such an operation on pressure of reheat steam, reheat-metal temperature changes, superheat and reheat steam temperatures,

action of the control and intercept valves, safety valves, and so forth. Load was first dropped from 25 mw, then 60 mw, then three times from 100 mw. In each case the load was dumped by hand-tripping of the main generator breaker, leaving the auxiliary load of approximately 2 mw on the unit. The pulverizers are arranged to trip automatically when the turbine control valves go closed and remain closed for a period of 3 sec. With the exception of the first test at 25 mw, automatic combustion control was in service at the time of each trip-out. Immediately upon tripping of the pulverizers, all major control equipment was moved to hand control. No attempt will be made to give the details of these tests in this paper, but merely to point out a few significant conclusions.

The controls for both the boiler and the turbine are considered adequate and satisfactory in the event of an accidental loss of any or all of the load on the unit. The maximum speed reached by the turbine was 3840 rpm, or 106.7 per cent. The reheater-inlet metal temperature increased approximately 30 F during a 2-min period for the 100-mw test and then fell off at a rate of 7 to 8 F per min. The water in the gage glass fell out of sight almost immediately, as was expected, but was restored after 2 min. In all probability the time required to determine the cause of an accidental tripping of the unit will determine how quickly it can be restored to service. However, tests have substantiated that for least disturbance to either the boiler or the turbine it is desirable to restore load as quickly as possible.

Starting and Loading Procedure

At the outset of the design of the reheat units at Dunkirk it was believed that boiler pressure could not exceed 50 to 100 psig until the turbine had started to take steam in order not to exceed the allowable reheater-metal temperature. This belief has proved unfounded, and there is no limitation on boiler starting pressure from the standpoint of reheat temperature. It has been found that pressure can be brought to 1500 psig for safety-valve testing with no reheat flow without exceeding 800 F on the reheater thermocouples.

The starting procedure is not appreciably different at Dunkirk than for a high-pressure nonreheat condensing unit of the same size. There is no difference in starting time for the boiler, the limitation being the rate of rise of saturation temperature, which has been established as 100 F per hr. The boiler is fired initially with oil, the first mill being put in when the unit is synchronized and put on load. The turbine is rolled at a pressure of 400 psig, about 4 hr after the start of firing. Approximately 1 hr is required to bring the unit to speed. By the time the turbine is at speed, the boiler pressure has reached a value of 1250 psig. Little or no time is required after the unit is at speed to cool off the exhaust hood because the crossover spray water is applied at 1800 rpm, and this cooling maintains the exhaust hood temperature lower than 125 F. The turbine is then synchronized, at which time the first mill is put in operation and a load of 10 mw is applied immediately. The load of 10 mw is held for approximately 30 min or until the shaft eccentricity and exhaust temperature have reached a minimum value. Then load may be applied to the turbine at a rate of 1 mw per min. The total elapsed time from lighting off until full load is 7 hr.

Load-Change Tests

Studies are now in process to determine the maximum rate, consistent with safe rate of temperature change, at which load on the turbine can be applied. A total of 21 thermocouples have been installed at various locations on the high-pressure, intermediate-pressure, and low-pressure turbine shells for this purpose.

Five tests have been made to date, in which the load was changed from one steady-state level to another steady-state level at different rates of load change. For the first three of these tests the load was decreased and increased between 100 and 20 mw at rates of load change of 1.0, 1.9, and 5.0 mw per min. The maximum change of steam temperatures due to boiler characteristics amounted to 250 F at the throttle and 320 F at the intercept valve. These tests served to give information under the condition of a load change accompanied by a change in inlet-steam temperatures.

The fourth and fifth tests of this group were made to study the effect on the turbine of an instantaneous load change equal to 25 per cent of rating with constant inlet-steam temperatures. The load was dropped rapidly from 100 mw to 80 mw and, after the turbine-shell temperatures leveled out, the load was returned rapidly to 100 mw. A similar test was conducted between 40 and 20 mw. The time required for these 20 mw changes was about 20 sec.

During these tests there was no change in vibration or eccentricity. The maximum change in differential was only 20 mils. Shell temperatures showed that no excessive thermal stresses were present.

Starting and Loading Tests

Two of these tests were made, each after the turbine had been out of service for about 40 hr. Before the turbine was taken off the line it had undergone cooling because of a low load of 20 mw which was carried at least 2 hr before the unit was shut down. This was not done purposely for the starting tests but was a part of the load-change tests. Therefore the week-end shutdowns in these tests are really equivalent to a longer period of time.

For the first test the turbine was rolled, brought to speed, and synchronized in 43 min; then it was loaded to 80 mw at an average rate of 0.9 mw per min. In a second test the turbine was rolled, brought to speed, and synchronized in 31 min; then it was loaded to 80 mw at an average rate of 2.4 mw per min.

It was found during both of these tests that with the exception of the steam chest the turbine shell heated very little during the starting period and that the heating began when load was applied to the machine. Vibration and eccentricity during these starting and loading tests were normal. No excessive thermal stresses were indicated by the shell temperatures. The differential expansion again was very little, the maximum change being in the order of 10 mils.

No definite conclusions can be reached until this series of tests have been completed and the data analyzed, but it is believed that load changes can be made at a somewhat faster rate than is our present practice.

BIBLIOGRAPHY

1 "Features of Dunkirk Steam Station," by R. P. Moore, *Combustion*, vol. 22, 1950, pp. 40–48.

2 "Dunkirk Station Departures Based on Prototype Experience," by J. N. Ewart and J. M. Geiger, *Electrical World*, vol. 134, December 4, 1950, pp. 97–101.

3 "Centralized Control Desirable for Single Boiler-Turbine-Generator Units," by J. A. Lind and J. M. Geiger, Trans. AIEE, vol. 69, 1950, part 2, pp. 1176–1179.

4 "Selective Tripping of Low Voltage Air Circuit Breakers for Power Station Auxiliaries," by J. M. Geiger and L. L. Fountain, Conference Paper, AIEE, 1949 Summer Convention, Swampscott, Mass.

5 "Relay Inverse Time Characteristic Doubles," by George Steeb, *Electrical World*, vol. 118, 1942, pp. 1484 and 1486.

6 "Bus Protection Independent of Current Transformer Characteristics," by George Steeb, Trans. AIEE, vol. 60, 1941, pp. 859–862.

7 "Electrical Features of the Dunkirk Steam Station," by J. M. Geiger, AIEE North Eastern District Meeting, Syracuse, N. Y., May 3, 1951.

8 "Design Features and Initial Operating Experience of the Dunkirk Steam Station," by R. P. Moore, AIEE North Eastern District Meeting, Syracuse, N. Y., May 3, 1951.

Twenty-Five Years of Reheat Operating Experience on the American Gas and Electric System

By S. N. FIALA,[1] NEW YORK, N. Y.

Interest in the reheat regenerative cycle, as manifested in boiler and turbine sales data, has been intensified greatly in the postwar years. The intent in submitting this paper is to contribute to the general historical record of reheat development by citing some of the experiences of the American Gas and Electric Company during the past 25 years. Operating features of some of the older units on the system are described but the emphasis has been placed on the characteristics of the modern units. Starting and stopping procedures, emergency shutdowns, temperature control, and performance are some of the topics discussed.

The Earliest Reheat Units

IN the fall of 1924 the first of a long series of reheat units was placed in operation at the Philo Plant of The Ohio Power Company, a constituent of the American Gas and Electric System. This unit consisted of a 40,000-kw bleeder-type 1800-rpm turbogenerator, supplied with steam from four chain-grate stoker-fired boilers (1).[2] Primary-steam conditions were 600 psi and 710 F. Steam exhausted from the 7th stage of the turbine at 155 psi under full-load conditions was reheated to 710 F in the reheat section of one of the four boilers and readmitted to the turbine at the 8th stage. This first reheat unit was followed by five additional units of similar characteristics, a second at Philo Plant, two at Twin Branch Plant of the Indiana & Michigan Electric Company, and two at the Stanton Plant of the Scranton Electric Company. The only departure from the Philo No. 1 design was an increase in reheat-steam temperature to 734 F.

The proving-out of these early reheat units, from the points of view of economy, flexibility, and reliability paved the way for further exploitation of the reheat cycle. Accordingly, in 1929, when further system expansion became necessary, a triple-compound 165,000-kw reheat unit was placed in service at the Philo Plant. Steam for this unit was supplied by eight boilers, six of which delivered 600 psi 725 F primary steam exclusively. Two boilers in addition to generating primary steam, reheated the exhaust steam from the high-pressure turbine to 725 F at 155 psi. It is interesting to note in passing that two of the standard boilers were arranged for unit-system pulverized-coal firing.

In all the reheat installations described to this point, the exhaust steam was reheated in one or more special units of the steam-generating battery. These special boilers were designed to produce primary steam and reheat exhaust steam. Firing rate of these reheat boilers was controlled by reheat steam temperature. The primary-steam output of these units fluctuated according to reheat temperature requirements.

To protect the reheat sections of the boilers from damage due to interruption of steam flow, provision was made to admit cold air to the gas side of the reheaters under such circumstances. Large motor-operated doors, located in the boiler settings and interlocked with the turbine trip mechanisms for automatic opening upon loss of load, served this purpose. Provisions also were made for manual operation of the doors to assist in the starting cycle. By-pass piping was installed around the reheat boilers so that the turbines were operable on a nonreheat cycle in the event of outage of the reheat boiler(s).

There has been no difficulty in operating these reheat units and they have been treated over the many years as standard equipment. Such problems as were first encountered in placing the equipment in service were largely due to lack of centralized controls and the resultant inefficiency in synchronizing the activities of a large group of operators. Because of their excellent performance, these units became the backbone of energy supply of the American Gas and Electric System. The first Philo unit gave a net heat rate of 13,800 Btu per kwhr and the 165,000-kw triple-compound unit, largely due to size factor, improved this performance to a net heat rate of 12,500 Btu per kwhr at full load under similar boiler-efficiency and back-pressure conditions.

During the 25 years of operation of Units 1 and 2 at Philo Plant, there were no alterations of the original design. The reheaters on both Units 1 and 2 were replaced about 2 years ago because of external gas-side corrosion which was the result of low output operation, more frequent shutdowns during postwar years, and more extensive consumption of high-sulphur coal. Turbine maintenance also has been very low. At the present time, these units are operated at full load each day and are taken off the line every evening after peak. Some work has been done on introducing quick starting and now the total time from standstill to full load averages 52 min. This is still subject to further improvement over the original allowance of 127 min.

The Second Phase

In the years between the installation of Philo 1 and Philo 3, progress was reflected principally in size development of both turbines and boilers. The departure from the multiboiler battery, the extension of the pressure and temperature limits, and the unqualified acceptance of the use of pulverized coal came in the second phase.

In 1930 the new Deepwater Plant in New Jersey, which was built jointly for the Atlantic City and Philadelphia Electric Companies, was placed in service. The two 53,000-kw cross-compound reheat units installed at Deepwater not only reflected the considerable progress made in the 6 years following the original Philo installation, but represented new advancements in the application of the reheat cycle (2). The number of boilers was reduced to two per unit, one standard type and one reheat type, both fired with pulverized fuel and both of the fluid-bottom type. The control of reheat-steam temperature had become

[1] Head, Mechanical Engineering Division, American Gas and Electric Service Corporation. Mem. ASME.

[2] Numbers in parentheses refer to the Bibliography at the end of the paper.

Contributed by the Power Division and presented at the Annual Meeting, Atlantic City, N. J., November 25–30, 1951, of The American Society of Mechanical Engineers.

 Manuscript received at ASME Headquarters, August 29, 1951. Paper No. 51—A-70.

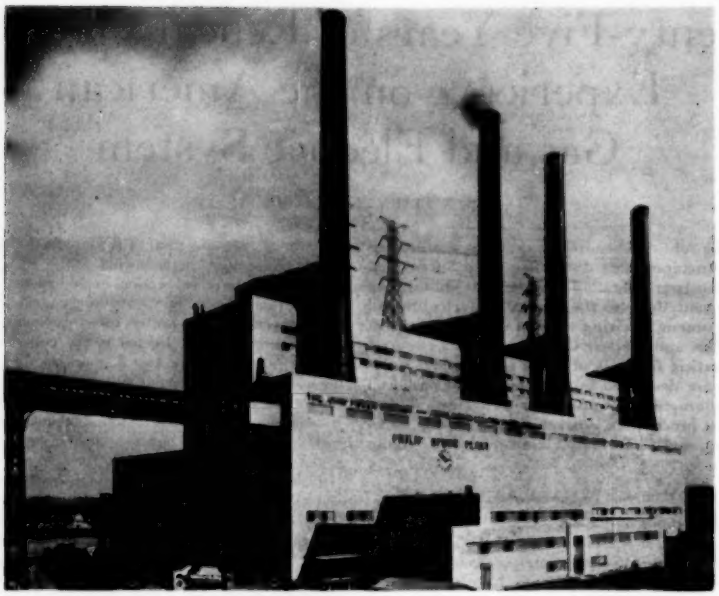

FIG. 1 THE PHILIP SPORN PLANT

a simpler problem with pulverized-coal-firing. One standard boiler, operating at 1200 psi and 725 F, was controlled for steam pressure and unit output; the reheat boiler was controlled for reheat-steam temperature of 750 F only. The method of protecting the reheater tubing from overheating was the same as that adopted on the Philo installations.

By-pass piping was provided so that the low-pressure turbine could be operated with primary steam with the reheater boiler and high-pressure turbine out of service.

There were many problems during the initial start-up of the Deepwater Plant but none had any direct relation to the reheat cycle. It is interesting to note that after the period of shakedown, the greatest problem was that of control of ash in its various stages of plasticity as it flowed through the generating unit, and this was precisely the same problem causing the greatest concern in 1951.

The experience, confidence, and satisfactory operation resulting from this reheat pioneering on the AG&E System led to the 2300-psi reheat unit at the Twin Branch Plant (3). This 76,500-kw single boiler-turbine unit, placed in service in 1941, was a natural development of experience gained at Philo, Twin Branch, Stanton, and Deepwater. Only the economic illness of the 1930's prevented its earlier realization.

BACKGROUND FOR MODERN REHEAT UNITS

The systematic progress made in the 23 years following the installation of the first Philo reheat unit, the lessons learned in those years, and the confidence gained were directly responsible for the large modern units on the AG&E System today.

In 1924 four boilers were required to supply primary steam at 600 psi and 710 F to one 40,000-kw unit. Reheat-steam temperature was controlled at 710 F by firing-rate adjustment of a special boiler. The relation between kilowatts and number of boilers was roughly 10,000 kw per boiler. In 1929 the 165,000-kw triple-compound unit at Philo Plant operated under similar steam conditions but each of the eight boilers produced 20,000 kw. In 1930, at Deepwater Plant, progress was represented by an increase of primary pressure to 1200 psi, complete adoption of pulverized fuel, reduction in number of boiler units, and an increase to roughly 27,000 kw per boiler. In 1940 a single boiler unit was designed to develop primary steam at 2300 psi and 940 F, and within the same unit, reheat the exhaust steam from the high-pressure turbine to 900 F, the process developing a total of 76,500 kw for the single boiler. When this development work was completed, a new phase in the history of reheat units on the AG&E System was entered.

THE MODERN REHEAT UNITS

In 1947 the fundamentals learned in the past, particularly in connection with the 2300-psi Twin Branch unit, were used to design a single boiler-turbine unit developing a gross generation of 150,000 kw. Primary-steam conditions were 2000 psi, 1050 F. Reheat was to 1000 F (4). Five such units are now in operation; one at Twin Branch Plant, one at the Tanners Creek Plant, of the Indiana & Michigan Electric Company located at Lawrenceburg, Ind., and three at the Philip Sporn Plant, jointly owned by the Appalachian Electric Power Company and The Ohio Power Company, and located at Graham Station, West Va. (see Fig. 1). Two additional units are still under construction, one each for the last two plants.

Now, in 1951, four still larger units are under construction. Two of these are for the Kanawha River Plant of the Appalachian Electric Power Company, located near Charleston, W. Va. The others are for the Muskingum River Plant of The Ohio Power Company, at Beverly, Ohio (5). Each unit of this group of four will be of the single boiler-turbine type and will generate 217,000

kw at 2000 psi, 1050 F primary and 1050 F reheat steam temperatures. At full load this will require a heat input to the boiler of 1.86×10^9 Btu per hr. The net heat rate is expected to be just over 9000 Btu per net kwhr. At the completion of the present construction program, the total net capability of all reheat units on the AG&E System will amount to 2,250,000 kw.

In recent years the technical and economic soundness of power production by means of the reheat cycle and the reliability of reheat equipment finally have received wide acceptance. This trend over the past 14 years is illustrated in Fig. 2 which shows the relationship between the new capacity added by electric utilities and that portion of the new capacity which was of the reheat type. In this plot the discontinuity caused by restricted construction during the war years has been eliminated.

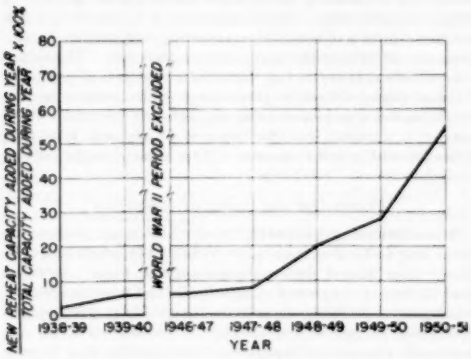

FIG. 2 RELATIONSHIP BETWEEN REHEAT CAPACITY INSTALLED EACH YEAR AND TOTAL CAPACITY INSTALLED EACH YEAR BY PUBLIC UTILITIES, 1938–1951

Load growth of the AG&E System during the past 3 years has been so rapid that it has been impossible to devote the effort and manpower necessary to develop complete operating characteristics of one of the modern large generating units now in service. It is hoped that a paper on this subject will be presented within the next few years.

INITIAL START-UP

Except for one relatively minor operation, the number of tasks to be performed prior to initial start-up of a reheat unit is the same as required for starting a standard unit. Present AG&E practice for starting large reheat units requires thorough blowing out of the reheater tubing using compressed air one element at a time. The connected reheat piping is cleaned out manually.

Of the five 150,000-kw reheat units now in operation there has been only one opportunity to examine the blading of a reheat turbine. The first-stage buckets were found to be well battered on the inlet side owing to small steel chips that must have passed through the fine steam strainer at the turbine inlet. Although the degree of damage will not affect the performance of that wheel, serious consideration is being given to special arrangements for a thorough steam blowout of reheat tubing and piping before future units are placed in service.

ACCELERATED START-UP AND SHUTDOWN PROCEDURE

Although peak-period availability of the modern units has been satisfactory, it was apparent that reductions in starting and stopping time requirements would provide a more comfortable margin for off-peak and holiday maintenance. Consequently considerable thought and effort have been directed toward the development of faster start-up and shutdown procedures.

The original start-up schedule developed for the Twin Branch 2300-psi reheat unit required 18 hr, the limits being set principally by manufacturers' recommendations on rate of pressure and temperature changes. By the time the first unit at the Philip Sporn Plant was ready for service, a start-up schedule allowing 10 hr from a cold furnace to full load had been developed. Later, by increasing the steam-drum temperature limits on the ends of the drum, a considerable gain in speed of allowable pressure rise was obtained and the period required to bring the units from cold start to full load of 150,000 kw was reduced to 7 ½ hr. An abbreviated log for a start-up of this type is shown in Table 1. Work is in progress now to reduce the time of 7½ hr by improvement in vacuum-producing equipment.

TABLE 1 LOG OF FEBRUARY 18–19, 1951, START-UP OF UNIT 1, PHILIP SPORN PLANT

Feb. 18:	7:30 pm	With 6 oil lighters in service started coal firing using one pulverizer and two burners.
	8:00 pm	Steam blowing from vents. Closed drum and superheater attemperator vents and all superheater header drains. Main inlet drain open.
	9:00 pm	Drum pressure 250 psi. Throttled main inlet drain to one turn.
	9:20 pm	Opened turbine stop valve above-seat drain.
	9:25 pm	Started hogging jet for vacuum. Drum pressure 600 psi.
	9:35 pm	Stopped coal firing to wait for vacuum. Drum pressure 950 psi.
	9:50 pm	Resumed coal firing.
	10:00 pm	Started turbines. Coal firing reduced to one burner awaiting turbine coming up to speed.
	11:30 pm	Turbines on governor. Drum pressure 1750 psi.
	11:45 pm	Generators synchronized. Drum pressure 2000 psi.
Feb. 19:	3:00 am	Up to rating—150,000 kw Total elapsed time: 7½ hr.

Shutdown procedures likewise have received considerable attention. The period of cooling has been reduced from an average of 16 hr to 6 hr. In speeding up the rate of cooling, the same analysis was established as in the case of starting up, namely, observing the drum temperature differential at the mid-point. An abbrevinted log for a typical shutdown is shown in Table 2.

TABLE 2 LOG OF FEBRUARY 16–17, 1951 SHUTDOWN OF UNIT 1, PHILIP SPORN PLANT

Feb. 16,	11:30 pm	Unit tripped out after dropping load by decreasing pressure. Pressure at trip-out 900 psi.
	11:40 pm	All superheater drains and steam main inlet drain opened wide.
	11:50 pm	Water level raised to within 5 in. of top of drum. (Maintained at that level by feeding water from time to time during following 3½ hr.)
Feb. 17,	12:10 am	Forced-draft fans tripped out. FD fan-inlet vanes and air-heater by-pass dampers wide open, outlet dampers closed. Setting, ash-pit, and secondary-air duct doors open.
	12:30 am	Induced-draft fans loaded up as much as possible without exceeding 3 in. water gage suction in furnace.
	1:40 am	Gas temperature entering air heaters 350 F. Air heaters shut down. All doors except lowest three in convection pass were closed. FD fan outlet dampers were opened and FD fans started. Both FD fans run at maximum load possible without putting a positive pressure in furnace. (ID fans were fully loaded, FD fans approximately ½ loaded at this stage.)
	3:00 am	Drum pressure 50 psi. Drum vents opened.
	3:30 am	Drum pressure 0 psi. Feeding of water discontinued because wide-range drum-level-column thermocouples became ineffective owing to absence of steam above water level.
	4:30 am	South ID fan shut down and released to Maintenance Department. (Note: Shutting down fan decreased cooling rate.)
	5:30 am	Engineers entered convertion-pass inlet cavity for inspection.
	6:00 am	All fans shut down. Inspectors entered dust collector. Total elapsed time: 6½ hr.

REHEAT-TEMPERATURE CONTROL

In the reheat installations of some 20 years ago, reheat temperatures were maintained by controlling the firing rate of the reheat-type boiler. As first costs mounted over the years, such an arrangement became economically unattractive. As a result,

considerable effort by the boiler manufacturer and by AG&E was directed toward the development of a commercially workable steam-generating unit with superheater and reheater surfaces arranged to give a simple, direct, and wide range of steam-temperature control. The 2300-psi Twin Branch unit was the outcome of these efforts. This unit employs a radiant-convection combination reheater with control of steam temperature accomplished by throttling of gas flowing over the convection reheat surface. Operating and maintenance experience with this unit demonstrated the advisability of employing an all-convection-type reheater. Numerous complications and high costs of gas-flow control provisions made it quite evident that control of reheat temperature above the design point could be accomplished more economically, and with greater ease, by spray desuperheating at the reheater inlet in spite of some loss in cycle efficiency due to the degradation of energy.

Experience on about a dozen large boilers has established the validity, from an operating viewpoint, of the practice of controlling primary-steam temperature by means of attemperation with boiler feedwater. No superheater tubes have been lost, nor has there been any increase in turbine-blade deposit rate as a result of this method of steam-temperature control.

In order to develop best average cycle efficiency over normal range of operation, there are two opposing reheat-control requirements. (*a*) At high load, it is desirable to maintain attemperation at the lowest possible point; and (*b*) to maintain high reheat temperature with decreasing load. These aims are accomplished by flue-gas recirculation. All of the 150,000-kw boilers now operating are equipped with a single-width single-inlet centrifugal fan arranged to extract a portion of the flue gas from the economizer outlet and return it to the secondary-air ducts immediately ahead of the burners, furnace, and convection pass. By recirculating this flue gas at rates varying from zero at full load to 15 per cent at two-thirds load, a substantial betterment in cycle efficiency is obtained at lower loads. Improvement in net heat rate as a result of gas recirculation compared with zero recirculation is as high as 2 per cent. The results of this type of operation on the characteristics of reheat- and primary-steam temperatures are shown in Fig. 3.

In large steam-generating units the effects on steam temperatures of unbalanced firing resulting from pulverizer interruptions and outages are pronounced. These transient conditions require wide control range and quick response. Spray attemperation fulfills these requirements at low cost. The application of spray attemperation carries with it some potential hazard. With this type of control, wide fluctuations in steam temperature are possible and this may have an adverse effect on the life of turbines. Attemperators must be engineered properly with full consideration of all possibilities, and their instrumentation and interlocking must be foolproof.

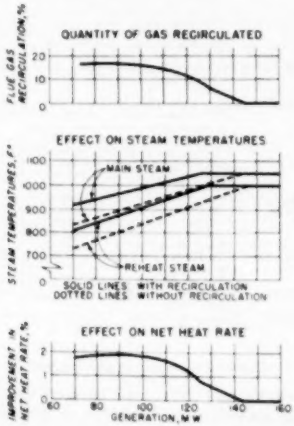

FIG. 3 FLUE-GAS RECIRCULATION CHARACTERISTICS 2000 PSI, 1050/1000 F BOILER

Because the superheaters and reheaters absorb a large proportion of total heat, the amplitude of steam-temperature variations is increased considerably by fluctuations in furnace excess air. Even with skillful application of fan controls and air-flow measurement, the problem of maintaining accurate flows when controlling a battery of fans in series and in parallel is at best a rough approximation. AG&E experience has been that better air-flow control is obtained when operating with positive furnace pressure and without the use of induced-draft fans. The steam-temperature controls do less work under this type of operation. Various minor difficulties encountered with pressure furnace operation are in process of being eliminated at this time. However, it is expected that the bogey of 95 per cent total time operation with positive pressure will be attained in the not too distant future.

FLEXIBILITY AND RANGE OF OPERATION

The additional problem of control of reheat-steam temperature is the only factor that may cause flexibility of a reheat unit to be poorer than that of similar straight-through units. Assuming that the basic arrangement of superheater and reheater is sound, the degree of flexibility depends on the quality of selection and application of control equipment. For smooth operation and eventually longer life of equipment, it is necessary that the controls maintain the heat input to the furnace in step with the heat output to the turbine. The boiler unit with its expensive alloy-steel superheaters and reheaters should not be used under any except the most unusual circumstances as a heat accumulator to iron out the insensitivities and malfunctionings of boiler controls. Instrumentation must be of the highest quality, must be complete, and control equipment must be centralized. Beyond that necessary requirement, provision of supplementary equipment in the control rooms to permit complete remote operation is considered essential to modern power plants. With these provisions it is possible to handle a complete unit trip-out from the control room. This of course includes relighting of coal burners.

All the reheaters on the postwar AG&E units are of the convection type, and there are no special provisions for cooling in the event of steam-flow stoppage. On the first units of this series, an interlock arrangement was provided so that a number of pulverizers would be tripped out, retaining such number in service as would not produce excessive gas temperatures at the reheater inlet. Experience has shown that except under very unusual conditions the time required to restart the turbines is appreciable and that with remote-burner-ignition system, tripping out of all pulverizers is more desirable. Once the shakedown period has passed, trip-outs may be expected to become rare occurrences. However, in a plant with additional units under construction and with new personnel, some trip-outs are bound to take place. There have been several of these at the Philip Sporn Plant and considerable delay in returning the unit to service was experienced because of excessive vibration of turbines when bringing them up to speed. Analysis of operating procedures indicated the cause to be badly deteriorated temperature of primary and reheat steam.

In order to solve this problem, a full-load trip-out and restarting cycle was conducted under close observation of engineering specialists. With all equipment in service at 150,000 kw and the

boiler operating under positive furnace pressure, the generator breaker was tripped. This automatically took the excitation and all boiler auxiliaries except forced-draft fans, air preheaters, and pulverizer-seal air blowers out of service. The motor-operated relief valve blew for 3 min, one superheater safety valve blew for 30 sec. After relief valves closed, there was another pop of the motor-operated relief valve a few minutes later for about 15 sec. Following this pressure-relieving period, the drum pressure remained constant at 2060 psi for about 15 min and then began to drop slowly. The drum water level dropped momentarily to the bottom of the gage glass and then came back rapidly to about 2 in. above normal, when the safety valve opened, as had been expected.

Immediately after the trip-out, the boiler was "bottled" by shutting down forced-draft fans and closing all air-supply dampers. This was done to conserve the heat stored in the 500 tons of metal in the superheater, reheater, and connected headers and piping. When these cross-compound machines are disconnected from the system and at the same time excitation circuits are interrupted, the speeds break apart. It is inadvisable to throw on excitation until the units are near synchronism. As a practical limit, turning-gear speed has been established as the point for re-establishing excitation. A procedure to make synchronism possible at higher speeds is being developed. In view of that limitation, the field current was applied 41 min after trip-out. A number of delays, totaling 26 min in lost time, were experienced in producing the required vacuum. The rolling of the machines was started 67 min after trip-out. This included the time lost in re-establishing vacuum. The machines were brought up to speed and synchronized in 15 min. Just before the generators were synchronized, boiler auxiliaries were started and pulverizers were placed in service with considerable overfiring, while load was being restored to 100,000 kw in the next 15 min. At this point conditions were considered practically normal and the test was terminated. During the entire test, the superheater- and reheater-temperature variations did not exceed 200 F.

There is room for improvement in this time schedule. However, the key to proper restarting after a quick shutdown and a short outage was confirmed to be the conservation of the stored heat in superheater and reheater metal by the "bottling" procedure and the elimination of draining of the superheater, reheater, and piping during the nonfiring period. There is considerable range of temperature control to be obtained by overfiring, and, with intelligent handling, high metal temperatures can be tolerated profitably without impairing the life of the boiler and at the same time produce a favorable restarting condition for turbines.

The use of the reheat cycle has no effect on range of operation of the unit. The load on the 150,000 kw reheat Unit 5 at Twin Branch Plant is frequently reduced during the night hours to 60,000 kw. This low limit is set entirely by flue-gas temperature. At lower gas temperature there is excessive plugging of air heater and dust collector.

Chemical Control

Experience has indicated that reheat has no known effect upon the chemical control of steam condensate, feedwater, and boiler water, as compared to that required for straight condensing units. The control problems in each instance appear to be the same. Although there are many factors which influence the rate of build-up of deposits in turbines receiving steam from boilers of 2000 psi and above, and these factors rarely are identical for two units, it is believed that reheat assists in reducing water-insoluble deposits in the low-temperature stages. AG&E experience to date is that such deposits, as have been encountered in reheat units, have been water-soluble in the high-temperature stages and are removable under load by reduction in steam temperature to the lowest point possible. With spray attemperation, it has been possible to lower steam temperature sufficiently so as to permit washing the unit, in rare cases, at almost full load.

Availability and Maintenance

The availability of a pioneering power-generating installation, whether extremely high or relatively poor, when measured by its performance during the first few years of operation may be misleading. It is beyond the scope of this paper to discuss problems in connection with high-temperature high-pressure operation, and the effect on the availability, maintenance, and economics of operation but some general remarks would appear to be in order.

The employment of the reheat cycle has a negligible effect on the over-all availability and maintenance cost of a power-generating unit when compared with a straight-through unit having similar design and operating functions except for reheat. In so far as the turbine is concerned, the reduced maintenance because of much lower moisture content in the exhaust steam is balanced by the increase in attention required by steam shutoff valves at the reheat-turbine inlet. Problems brought about by high reheat-steam temperature have been compensated for by the profits in efficiency gained.

There has been only one mishap in AG&E's long experience with the reheat cycle directly chargeable to that cycle. On May 8, 1951, Unit 1 at Philip Sporn Plant carrying 43,000 kw on the high-pressure machine and 107,000 kw on the low-pressure machine, was tripped out by the opening of the generator breaker resulting from an error by a maintenance man checking control circuits. Normally, such an interruption would cause the two high-pressure emergency stop valves and high-pressure control valves to close within $^1/_2$ sec, while the intercept valves on the lower-pressure reheat-turbine element would maintain turbine speed at less than 5 per cent overspeed until steam stored in the boiler reheater and connected piping was released to the condenser. The time normally required for emptying the reheater is 4 min. The intercept valves, however, stuck in almost wide-open position and the energy stored in the reheater was released through the turbine to the condenser. The turbine rotor consequently was accelerated from its normal speed of 1800 rpm to 2700 rpm. A portion of this overspeed was due to the energy supplied by the flashing of condensate lying in the two high-pressure feedwater heaters as the bleed lines to these heaters were without check valves. The rotational stresses reached approximately $2^1/_4$ times normal operating values. While the machine was rotating at high speed, an operator opened the vacuum breaking valve and this assisted in arresting the speed and bringing the turbine to a standstill.

All rotating elements of the machine, including the generator, were inspected following this experience. The only damage directly attributable to the overspeed was a loss of several sections in the shroud band on one wheel of the last (22nd) stage of the double-flow section, and some cracks in the shroud band of one of the 21st-stage wheels. The 30-in. last-stage buckets were undamaged. There was no injury to the generator field. A slight run-out in the commutator of the direct-connected exciter was found and corrected.

The cause for the sticking of the intercept valves was found to be a deposit of iron oxide, 3 mils in thickness, which collected on the surface of the valve stems and their bushings, and closed the clearance between the two causing a seizure. This machine has four intercept valves, two in the top and two in the bottom shell, with a camshaft arrangement for gang operation. Temporary measures have been taken to prevent a recurrence of this accident by increase in clearances and establishment of routine inspection and full closure tests periodically. On all the units awaiting correction, the load is reduced once a week to 120,000 kw,

and at that load pressure is applied to the governor beam to obtain a full closure. The time required for this operation is so short that build-up in pressure in the reheater does not reach the safety-valve setting. In addition, the practice of making a partial movement check every shift is being continued. While this check was found to be inadequate to show that the valves are free to move over the entire travel, it is considered worth while continuing as a general indicator. New intercept valves which will have stem-sealing provisions and arrangements for remote testing over full stroke from the control room are now in process of manufacture. Check valves also have been installed in the bleed lines to the high-pressure heaters.

Efforts to find a method of preventing iron-oxide carry-over from the steam-generating unit have been accelerated greatly. Iron-oxide deposits associated with high-temperature units are not a new experience on high-pressure steam generators. However, in the past they have been limited on the AG&E system to the emergency stop valves and control valves on high-pressure turbines. Experience to date has indicated that the iron-oxide carry-over is not a continuous process and that it seems to be limited to the initial period of operation. This fact has not been established firmly, however. Study and consultation with the manufacturer have led to the conclusion that the intercept valves of corrected design, augmented by testing provisions, will give all the security required to avoid similar overspeeding troubles in the future.

Experience on recent units has not revealed any signs of required maintenance on reheaters with the exception of one installation in which part of the reheater consisted of radiant surface. In this installation part of this radiant surface had to be replaced with alloy-steel tubing because of oxidation of the original carbon-steel tubes after about 6 years of service. The life of the replaced sections has not yet been established but on the basis of such limited experience as we have had with radiant superheaters, it seems probable that all-convection-type reheaters are preferable.

Performance and Production Costs

Fig 4 shows the industry-wide best plant-heat-rate trend from 1938 to 1949. Data are from the literature published by the national utility regulating bodies. The trend curve has been extended to 1950, using the heat rate calculated from the Philip Sporn Plant operating records as a value for that year. The decrease in heat rate from 10,350 Btu per kwhr, which was the best plant heat rate ever recorded previously, to 9482 Btu per net kwhr, clearly indicates the high-grade performance of modern reheat units.

It is noteworthy that this plant heat rate was established in spite of the hampering effects of two initial start-ups, and a number of outages for design changes. It is estimated that the Philip Sporn Plant heat-rate figure for 1951 will be well under 9300 Btu per net kwhr.

A number of figures for the most recent 12 months of operation available are given in Table 3.

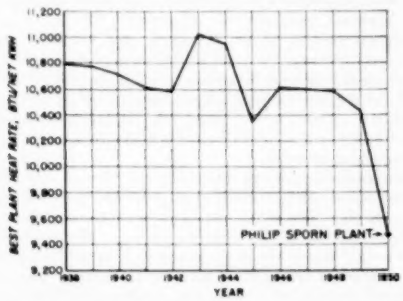

Fig. 4 Best Plant-Heat-Rate Trend Curve, 1938–1949, Extended to 1950 Using Philip Sporn Plant Heat Rate for That Year

TABLE 3 PERFORMANCE DATA OF PHILIP SPORN PLANT, MAY 1950—APRIL 1951

Months of operation, unit No. 1	12
unit No. 2	10
Total gross generation, kwhr	1,993,079,000
Total net generation, kwhr	1,874,044,000
Average net heat rate, Btu per kwhr	9270
Average gross load, kw per unit	143000

Conclusions

The technical and economic soundness of the application of reheat units to the regenerative cycle, operating at the highest commercially acceptable pressure and temperature levels, has been established clearly. The 25 years of successful and satisfactory operation of this type of unit on the American Gas and Electric Company System verifies past decisions and attests to the desirability of making future expansions in terms of reheat units.

BIBLIOGRAPHY

1 "Philo Station Sets Record, General Conditions and Mechanical Features—I," by M. L. Sindeband and Philip Sporn, *Electrical World*, vol. 86, August 22, 1925, pp. 355–359.

"Philo Station Sets Record, Electrical Features and Control—II," by M. L. Sindeband and Philip Sporn, *Electrical World*, vol. 86, August 29, 1925, pp. 403–408.

2 "Deepwater—A New Idea in Central Stations," Anon., *Power Plant Engineering*, vol. 33, November 15, 1929, pp. 1204–1214.

"Deepwater—A Double Purpose Station," Anon., *Electrical World*, vol. 93, May 11, 1929, pp. 919–923.

3 "Twin Branch Plant of Indiana & Michigan Electric Company (b) Twin Branch Extends High-Pressure Economies," by Philip Sporn, *Electrical World*, vol. 116, October 18, 1941, p. 80.

"Twin Branch Plant of Indiana & Michigan Electric Company (i) Technically Sound and Commercially Workable," by Philip Sporn, *Electrical World*, vol. 116, October 18, 1941, p. 80.

"The 2500-Psi Twin Branch Plant of Indiana & Michigan Electric Company (a) Operating History of the 2500-Psi Twin Branch Plant," by Philip Sporn and E. G. Bailey, Trans. ASME, vol. 66, 1944, pp. 1–16. (Furnace Performance Factors, special pamphlet.)

4 "The 2000-Psi, 1050F, and 1000 F Reheat Cycle at the Philip Sporn and Twin Branch Steam-Electric Stations," by Philip Sporn, Trans. ASME, vol. 69, 1948, pp. 287–294.

5 "The Development and Implementation of a Generation Program on the American Gas and Electric Company System—I. System Fundamentals," by Philip Sporn; presented at the Annual Meeting, Atlantic City, N. J., November 25–30, 1951, of The American Society of Mechanical Engineers. Paper No. 51—A-115.

"The Development and Implementation of a Generation Program on the American Gas and Electric Company System II—Fuel Supply," by Philip Sporn and H. A. Kammer, presented at the Annual Meeting, Atlantic City, N. J., November 25–30, 1951, of The American Society of Mechanical Engineers. Paper No. 51—A-11

"The Development and Implementation of a Generation Program on the American Gas and Electric Company System III.—200,000 Kw, 2000 Psi, 1050 F—1050 F—An Advance in the Economics of Integrated Power System Generation," by Philip Sporn and S. N. Fiala, presented at the Annual Meeting, Atlantic City, N. J., November 25–30, 1951, of The American Society of Mechanical Engineers. Paper No. 51—A-117.

Discussion

I. E. Moultrop[3] and G. A. Orrok.[4] Technically, there are many features of the American Gas Company reheat designs, incorporated in their early installations and carried through to the

[3] Consulting Engineer, Belmont, Mass. Fellow ASME.

[4] Acting Superintendent of Engineering, Boston Edison Company, Boston, Mass. Mem. ASME.

modern designs, which differ from our Boston practice. American Gas used cross-compound units, that is, low-pressure units without governors and without separate low-pressure headers and boilers. This failed to give the flexibility and stability attained in our Edgar Station, where high-pressure and low-pressure machines were separate independent machines, and the loss of one did not necessarily result in the loss of both. This, however, entailed more piping.

Again, reheat and superheat control at Edgar were much simpler and more flexible since each boiler had both reheater and superheater, and there were three complete header systems—one for superheated high-pressure steam, one for high-pressure turbine exhaust, and one for reheated steam. Thus control could be obtained by varying the flow through reheater, superhenter, and by changing firing rates in the various boilers, independently of machine loads, and steam was always available from the headers for cooling reheaters during start-up and trip-out conditions.

In our modern reheat units, which are single-boiler single tandem-compound turbine installations, although we shall be faced with some of the author's trip-out problems, we shall not have to struggle with loss of synchronism between high-pressure and low-pressure elements.

In reviewing the whole historical development of the use of reheat and of improving the heat performance of the units, stress should be laid on the fact that this was not a one-man or one-company development. In the economic field, Professor Slichter believes one of our great advantages over Russia lies in the fact that in America business decisions are made by hundreds of thousands of executives under the stress of competition and cumulatively reach a much higher level of accuracy than when made by a single govermental organization. Similarly, developments and decisions in the economical generation of power were made by hundreds of engineers in hundreds of companies of the industry, representing the users, the manufacturers, and the research men, both here and abroad. The writers have searched their files of early days and found a long list of engineers, experiments tried, patents obtained, records of successes and of failures.

In the early days, the industry consisted of a group of vigorous men who kept in touch with progress through the societies. In the 1920's there was tremendous pressure to improve performance. New York pioneered with large size; Milwaukee pioneered with pulverized coal, Boston pioneered with high pressure. Reheat, used in England in the North Tees Station in 1920, was incorporated in many of these units at American Gas, Boston, Chicago, and others. Even the regenerative-feed heating cycle was new, and its full utilization made an important contribution at this time.

The results of industry-wide friendly rivalry, co-operation, and effort are shown not only by best plant curves so long dominated by Hartford's mercury vapor and Milwaukee's sound design and superb operation at Port Washington, but by the actual result of the cost per kilowatt to the customer, which shows for the whole United States its unsurpassed record of continually lowered prices since the inception of the industry. All of us, from Jimmy Watt to our youngest member, can feel proud of this record.

W. H. Rowand.[5] Evidently from the figures mentioned in the paper, more than 40 per cent of the present AG&E System capability is in reheat units and by 1954 this will increase to more than 65 per cent.

The author mentions the smoothness of operation and control when the boilers are operating with positive furnace pressure and without the induced-draft fans in service. This same experience has been confirmed by the other companies operating boilers in a similar manner.

In connection with restoring load following an emergency trip-out, the author mentions abandoning the interlock arrangement for firing coal at reduced rate during this period because of the appreciable time lapse. In an effort to reduce the temperature shock to the turbine still further, it may prove worth while to relight the oil or gas lighters during the outage period to keep all of the several hundred tons of superheater and reheater metal near a 1000 F level. Even though this might require a vent line direct from the drum to the condenser to maintain the pressure within a suitable range, the quantity of saturated steam condensed would be negligible because of the short time involved.

[5] Chief Engineer, The Babcock & Wilcox Company, New York, N.Y. Mem. ASME.

Author's Closure

The author does not find himself in agreement on all points with Messrs. Moultrop and Orrok, but in the matter of recognizing that many have contributed to the development of the reheat principle, we are in absolute accord. The purpose of this paper as indicated in the abstract was to make contribution to the general historical record by reviewing experience on the AG&E System.

It would be a tremendous undertaking, beyond the scope of an ASME paper, to attempt to describe the work of all associated with the development of the reheat cycle. It would, indeed, be presumptuous for an engineer associated with one organization to attempt, unsolicited, to describe the underlying philosophy of another organization's designs. Comparisons with the designs of other organizations are omitted until such comparisons are invited or suggested by the discussers of the paper. Public comparisons, under these latter circumstances, are most proper.

Messrs. Moultrop and Orrok have described the manner in which reheat installations were incorporated into the Edgar Station. The author found their comments very interesting and is in agreement that a maximum of flexibility and stability is obtained under circumstances where the low-pressure reheated steam can be supplied to an existing low-pressure header which is also supplied, if necessary, by existing low-pressure boilers.

In the case of the first AG&E reheat installations at Philo and Twin Branch, both new plants, there were no existing low-pressure headers or low-pressure boilers to which connection could be made. In these circumstances, the economic justification of any plan to build low-pressure boilers to provide flexibility for a high-pressure reheat installation would have been impossible. Studies and discussions with the boiler and turbine manufacturers indicated that all that was required for reasonable reliability was a tying together of the primary steam headers (in instances where two similar units were being installed) and provision for operating the turbines with the reheat boilers out of service. These provisions, economically justifiable, were made. The reliability record of these early units stands as testimony to the correctness of the decisions made some twenty-eight years ago.

Regarding the control of steam temperatures, it was our practice in the early designs to control superheat and reheat temperature in separate boilers. As indicated in the paper, three boilers were provided for primary steam generation with a fourth boiler functioning as a reheater for all. This arrangement required a minimum investment in boiler plant and piping. Apart from cost considerations, this arrangement eliminated the need for a fine balance of superheat and reheat temperatures in the same unit. This fine balance would be particularly difficult to maintain during periods of operation with wet coal or under conditions in which slag deposits were changing.

These are some of the reasons for the technical differences between AG&E installations and those of the Boston Edison Com-

pany. Each must be viewed in the light of: Plant existing before the reheat installation was made, fuel cost, the degree of reliability needed, and the economic weight given to the added complexity of one plan over another.

Operating Experience With Reheat at Edgar Station

By H. E. STICKLE,[1] BOSTON, MASS.

Operating experience with the new 81,250-kw 1450-psi 1000 F/1000 F reheat unit at Edgar Station is compared with operation of earlier reheat units. No operating difficulties have been experienced with reheat at this station during a 25-year period. Availability of earlier units was lower than that of the new unit. Increased reliability is a large contributing factor toward renewed interest in reheat.

Introduction

THE reheat cycle has been in use at Edgar Station since the year 1925. The first installation was a single boiler with high-pressure topping turbine which exhausted into existing 350-psi condensing turbines. The exhaust from the high-pressure turbine was at a temperature of only a few degrees above the saturation and, therefore, had to be reheated before it could be used in the existing 350-psi turbines. This reheating was accomplished by means of reheater surface located in the second and third passes of the high-pressure boiler. The second addition was completed in 1929, and consisted of one more 350-psi 725 F condensing machine, two 1200-psi 700 F topping turbines and four 1400-psi 750 F/750 F reheat boilers. This so-called second addition was a departure from the unit system and was cross-connected at the 1200-psi level, the high-pressure-turbine exhaust level, and at the 350-psi main steam header which supplied all of the 350-psi turbines. The steam flow through the individual reheaters was regulated by means of motor-operated regulating valves on the outlet of each reheater. The temperature regulation was accomplished manually by the boiler-room personnel as required to maintain optimum steam temperatures. The third addition to this station returned again to the unit system and was started up in August, 1949. This paper will describe operating experience with this new 81,250-kw, 1450-psi, 1000 F/1000 F reheat unit and will refer only to the older units for comparison.

A comparison of the older part of this station with the new should serve to point out some of the advances that have been made in power generation with steam, especially as to the reliability of new designs. The progress that has been made and is still being made bespeaks the confidence that has been and is being placed in the engineer. Quoting from the fourth James Clayton Lecture that was given by one of the Past Presidents of the Society: "When any new engineering project is now proposed, its validity and eventual success is seldom questioned. Faith in the engineer has been established because of his recognition of known facts."[2] Facts as well as ideas and opinions become better known through the activities of the Society. The recent Symposium on the Reheat Cycle[3] most certainly brought a number of interesting matters to the attention of the engineers who design our new units.

Brief Description of Unit 4

The new unit, hereinafter called Unit 4, was designed on the unit system with a single boiler arranged to supply only its accompanying turbine. The turbine is a three-cylinder tandem-compound, double-flow exhaust, 3600-rpm turbine with a guaranteed maximum output of 81,250 kw. The 1450-psi 1000 F steam is supplied through six governor-controlled valves. The steam goes back to the reheater section of the steam generator after passing through the 18th-stage blading and is reheated to 1000 F before returning to the intermediate-pressure cylinder of the turbine. There are five stages of regenerative feedwater heating which raise the feed to a final temperature of 435 F. The steam-generating unit is of the two-drum radiant-furnace type, equipped with primary and secondary superheaters, a reheater, an economizer, and two regenerative-type air preheaters. The boiler unit can be fired with either pulverized coal or oil. Further details of the unit will be discussed later in the paper.

Starting and Stopping Procedures

The starting up of a reheat boiler is no different from the starting up of a nonreheat boiler. From the operating engineer's standpoint, the inclusion of a reheater in the unit results in only one more temperature to watch and to do something about when and if required. If the design engineer has provided suitable indication of this temperature and suitable means for controlling it the incremental complexity due to reheat is practically nil. The inclusion of a reheater adds far less to the anxiety of the operating engineer than the inclusion of a number of new or untried gadgets that so often find their way into the design of a power plant.

A typical starting and stopping cycle for Unit 4 has been included in the Appendix so that the reader may draw his own conclusions concerning the additional complication resulting from reheat.

Comparison of Early Reheat Units With Unit 4

In order to realize the savings in the heat rate of 4 to 6 per cent which has been attributed to the reheat cycle,[3] the unit must have a high load factor. In other words, in order to pay the fixed charges on the added investment, the unit must be available to run during a high percentage of the load-hours of the year. The availability of the earlier reheat units at this station was not as high as that of Unit 4. The type of fuel-burning equipment used was the largest single factor responsible for the lower availability. A brief description and a few comments concerning this fuel-burning equipment will help to clarify the meaning of availability although it does not have any direct bearing on the reheat cycle.

The fuel-burning equipment consisted of underfeed stokers that were 45 tuyères long and 16 retorts wide having a projected grate area of 540 sq ft. The combustion air was supplied through tubular air preheaters that brought the temperature of the air up to 400 F. The main cause of outage was to repair the grates and

---

[1] Assistant Chief Engineer of Steam Stations, Boston Edison Company. Mem. ASME.

[2] "Invention and Sifting Out Engineering Facts," by E. G. Bailey, Proceedings of The Institution of Mechanical Engineers, vol. 160, 1949, pp. 196–207.

Contributed by the Power Division and presented at the Annual Meeting, Atlantic City, N. J., November 25–30, 1951, of The American Society of Mechanical Engineers.

Note: Statements and opinions advanced in papers are to be understood as individual expressions of their authors and not those of the Society. Manuscript received at ASME Headquarters, October 17, 1951. Paper No. 51—A-135.

[3] "Symposium on the Reheat Cycle," Trans. ASME, vol. 71, 1949, pp. 673–749.

supporting ironwork under the grates. The grates or tuyères would fuse together during the operation of the boiler which would block off the air supply to the fuel bed and make it necessary to take the boiler out of service. The 400 F air was the only cooling provided for these tuyères and when the clinker formed over the tuyère in one section of the fuel bed, the cooling air would be directed to other sections thus robbing the clinkered section of all cooling. The heat from the fuel bed above would then soak down into the iron and fuse it together. It was found to be practically impossible to maintain the fuel bed in a uniform thickness at all times so that clinkers would not form. The 400 F air together with the large projected grate area were major factors contributing to the formation of the clinkers.

It was because of the low availability of these boilers that full advantage of the reheat cycle was not obtained at Edgar Station until the system load had increased enough to make it necessary to add more capacity to the system. This increase in capacity was added to Edgar Station in 1938, by rebuilding the four high-pressure boilers. The capacity of each boiler was increased to some extent by adding larger fans and higher-capacity fuel-burning equipment but the major increase of capacity was the increase in dependability.

Prior to rebuilding, the operating records were searched to determine all of the causes of outages and every known improvement that was possible to include was incorporated in the rebuilt units. The results of this rebuilding have been entirely satisfactory in that these boilers have been available to carry load during a large percentage of the total load-hours of the past 12 years.

Through the combined efforts of the manufacturers' engineers and the engineers of operating companies, the availability of all power-plant equipment has been improved considerably during the past 25 years.

The Reheat Symposium chairman pointed out in his discussion[4] two or three reasons for the revived interest in the reheat cycle. The author would like to suggest that the increased reliability that is being built into present-day power-plant equipment is in no small way responsible for the increased interest in the more efficient power-plant cycles. This is based on the proposition stated earlier in the paper that in order to realize the savings inherent in the reheat cycle, the unit must have a high availability.

Performance of Unit 4

This unit is rated at 81 250 maximum and has demonstrated that the temperature of both the 1450-psi steam and the low-pressure reheated steam can be maintained at the design value of 1000 F at full load with oil being burned with a minimum of excess air. In order to maintain the reheat-steam temperature, the burners are operated in the maximum tilt upward position part of the time and well above the horizontal position at all times. The superheaters are of such a design that when the reheat temperature is at 1000 F, the superheated steam must be desuperheated. This desuperheating is done in a vertical chamber located outside of the boiler casing at a point in the flow stream between the primary and secondary superheaters. The desuperheating is accomplished by spraying water into the steam within this vertical chamber. In view of the fact that the feedwater chemicals are added in the deaerator storage tank, the desuperheating water is taken from the deaerating section of the heater above the storage tank and is pumped to the spray nozzles by special steam-driven reciprocating pumps that were installed for this purpose. These pumps have been a source of considerable annoyance. They have required packing frequently and at times of low load when very little water is required their control has been unsatisfactory. Changes are being made to obtain the desuperheating water from the boiler-feed line. These changes should cure the difficulties with these pumps permanently because after these changes have been made, the pumps will be used for emergency supply only.

The required outages of Unit 4 have been of such a nature that almost all could be scheduled in periods of low load. The main cause of outage was the fouling of the air-preheater elements caused by the low exit-gas temperatures and the high dew point of the combustion gases. Up to early in 1951, it was necessary to take the unit out of service at intervals of 5 to 6 weeks to wash the air-preheater elements. Since then this has been unnecessary because of better methods for cleaning the elements periodically. The new method of cleaning consists of burning coal for 1 hr each week, and immediately thereafter blowing the air preheaters with steam through a blower furnished by the heater manufacturer. This blower oscillates in an arc across the top of the air-preheater elements. The blower had been used before, but the weekly 1-hr period of coal firing prior to the use of the blower apparently furnished enough ash to give the blowing operation a scouring action that was necessary to keep the heater clean for extended periods.

Only a few of the performance figures have much significance owing to the short time the unit has been operating. These are listed in the following table for the year 1950:

Btu per net kwhr	10250
Capacity factor, per cent	88.87
Load factor, per cent	88.87
Availability factor, per cent	92.08
Per cent make-up estimated	3.00

The heat rate is the total heat fired to the furnace plus heat in the auxiliary steam taken from the older part of the station, divided by the total net output for the year. No accounting was made of small amounts of heat added or subtracted from the cycle resulting from changes in the make-up water temperature and changes in the combustion-air temperature.

The capacity factor is the total gross generation in kilowatt-hours divided by the product of the number of hours and the capacity.

The load factor is the average load carried during the year divided by the peak load.

The high percentage of make-up is made up of about $\frac{1}{2}$ per cent blowdown and $2\frac{1}{2}$ per cent unrecoverable condensate from steam used for soot blowing, steam-jet air ejectors, desuperheating water pumps, and for heating and atomizing fuel oil. The contemplated changes in the supply of desuperheating water should reduce this figure materially.

The availability factor is the ratio of the hours of operation to the total hours in the year 1950. An outage of 269 hr occurred during the summer when the boiler was taken out for annual inspection (a requirement in Massachusetts).

Less than a month after the unit first started, a forced outage occurred that lasted for 757 hr. This outage was in the year 1949 and is not included in the foregoing figures but is worthy of mention. The outage was initiated by the tripping of the main solenoid-operated fuel-oil valve. This valve is actuated normally by loss of the fans or by a drop in fuel-oil pressure to a value below that for safe ignition conditions. Neither condition is believed to have existed at the time. Inadvertent tripping of this valve is the probable cause, workmen having been in the vicinity of the pressure switch at the time.

The coal-burning equipment was not in service, and about 9 minutes after the solenoid valve tripped, the turbine throttle was tripped. The fires were relighted and the turbine turned again under steam in 23 minutes previously having been on the turning gear. The unit was not returned to service because excessive vibration developed after the turbine had been turning with steam for a short period. It was found that the turbine shaft was

[4] See footnote 3, discussion by Philip Sporn, p. 735.

bent. The total runout, at the test point between No. 2 bearing and the low-pressure packing of the high-pressure spindle was about 10 mils. The turbine was kept turning with the turning gear for a period of about 30 hr in an effort to straighten the shaft. Since this turning did not help the runout, the high-pressure spindle was sent back to the factory to be straightened.

The cause of the inadvertent tripping was determined and suitable guards and braces were installed around the pressure switch to prevent recurrence but the true cause of the bent shaft is still undetermined. Several theories have been advanced but none provides too satisfactory an explanation. All of the theories are based on incidents that are assumed to have happened at the same time for which no definite proof is available. It seems safe to assume that the reheat cycle was not responsible because the bent shaft was confined to the high-pressure spindle.

Conclusion

Reheat has been in use at Edgar Station for over 25 years and no operating difficulties have been experienced that can be attributed to the reheat cycle. With the increased reliability being built into power-plant equipment today, analyses of the economics of various cycles may be approached with confidence that the expected return on the additional investment will be obtained.

Appendix

Starting Procedure for Unit 4

For the purpose of describing the starting as well as the stopping procedures the valves will be numbered as follows:

1 Throttle valves.

2 Interceptor valves: These valves act as emergency stop valves for the intermediate- and low-pressure end of the turbine and are necessary because of the large volume of steam in the reheater and connecting piping. These valves serve the same purpose as the throttle valves on the low-pressure machines of cross-compound units.

3 By-pass valves: There are two of these in parallel. One is automatic and will be designated 3a and the other is manually operated and will be designated 3m. They are located in a starting line which by-passes the superheater and the high-pressure turbine and carries steam from the boiler drum direct to the reheater inlet.

4 Nonreturn valve: This valve is located in the exhaust line from the high-pressure cylinder and is held closed by air pressure when valve 3a is open. This prevents the admission of steam to the high-pressure cylinder via the exhaust connection.

5 Dump valve: There are two of these valves also and the automatic one will be designated 5a and the manually operated one as 5m. These valves are in parallel and located on the reheater outlet for the purpose of venting it to the atmosphere. There are also safety valves on this line that accomplish the same purpose but at a slightly higher pressure.

Before lighting the fire in the boiler, the throttle valves (1) are closed, the superheater and reheater drains are opened, the valve (3m) is opened slightly, and the valves (2) are open.

One or two oil torches are lighted as required to bring the drum pressure gradually to 400 psi over a period of 3 hr. During this 3-hr period the superheater and reheater tube temperatures are observed frequently to keep them below 1000 F. Two selectors with indicating instruments are provided on the boiler gage board. Each selector switch is connected to 12 thermocouples

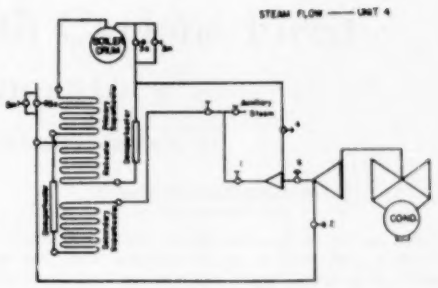

Fig. 1

evenly spaced across the superheater and reheater elements. One selector is connected to the twelve thermocouples on the superheater and the other is connected to the 12 thermocouples on the reheater. The superheater-tube temperatures are controlled by adjusting the drain valve, and the reheater-tube temperatures are controlled by adjusting the reheater drain and the valve (3m).

When the pressure is at 400 psi, the throttle valve (1) is opened enough to speed the turbine off the turning gear. When the turbine is turning, the rate of firing is increased gradually at a rate sufficient to bring the turbine to speed in $2^1/_2$ hr. As soon as sufficient flow is established through the cycle to maintain the tube temperatures below 1000 F, the superheater and reheater drains and valve (3m) may be closed.

Stopping Procedure

When all of the load has been removed and the generator tripped off the bus, the unit may be shut down quickly by tripping the throttle with the overspeed device manually. This closes the throttle valve (1) and the interceptor valves (2). The closing of the interceptor valves (2), opens by-pass valve (3a) and dump valve (5a) and closes nonreturn valve (4). Open valves (3m) and (5m) and close valves (3a) and (5a). Open the superheater and reheater drains and proceed with the normal routine of shutting down the air ejectors, pumps, opening the casing drains, and so forth.

Emergency Stopping Procedure

A by-pass valve is provided that allows steam to flow from the exhaust of the high-pressure cylinder to the intermediate-pressure cylinder. This valve is opened manually and is closed automatically by the overspeed device of the emergency governor. For the purpose of this discussion this valve will be designated as valve (6).

In the event that the unit should drop all or most of its load the following procedure should be used:

Since the main governor speed changer is in such a position that no-load speed is higher than 3600 rpm, the speed of the unit will rise suddenly and at some speed between 3600 and 3700 rpm control of the unit will be taken over by the auxiliary governor which will act to close the governor valves. Should the speed continue to increase to 3700 rpm the interceptor valve (2) will start to close and at 3725 rpm the valve (2) will be closed and valves (3) and (5) will open and valve (4) will close. From this point the normal procedure for shutting down should be followed.

Station Design With Cyclone-Fired Steam Generators

By H. C. SCHROEDER[1] and R. J. STRASSER,[1] CHICAGO, ILL.

The need for finding better methods of burning Central Illinois coal led to the cyclone-furnace development. Sufficient operating experience has been gained since the first cyclone-fired steam generator was installed, as well as with numerous installations of recent years. Station design for cyclone-fired steam generators is treated in this paper as well as engineering design features of the installations now in operation. Consideration is also given to units in process of design and construction.

THE development and early operating experience with a cyclone-fired steam generator were described in a paper by A. E. Grunert, L. Skog, and L. S. Wilcoxson,[2] before the ASME in 1946. This paper listed the aims, advantages, and savings that might be achieved with this type of furnace. It described the fundamental principles involved and the experiences to that date by tests on two pilot-plant models (one 3-ft-diam cyclone and one 5-ft-diam cyclone), and following these experimental units, the installation of a development unit at the Calumet Station of the Commonwealth Edison Company.

Since that paper was presented, a number of installations have been made and much valuable experience has been gained with this type of furnace.

Two current papers continue the story of the engineering designs of the various installations, the operating experiences, and the results attained. One of these is by V. L. Stone of the Commonwealth Edison Company and I. L. Wade[3] of the Public Service Company of Northern Illinois.

This paper deals with station design where cyclone-fired steam generators are used, and it will describe the engineering design features of the installations that are in operation, and also those in the process of construction or design.

The principal factor that led to the development of the cyclone-type furnace was the need for finding better methods for burning Central Illinois coal. This coal is high in ash and sulphur and has a low ash-fusion temperature. Its burning characteristics are such that research for improved methods of burning was a necessity, and, therefore, led to the cyclone-furnace development. Previous methods of firing permitted a much larger percentage of ash to pass through the heat-absorbing surfaces.

[1] Partners, Sargent & Lundy. Mems. ASME.

[2] "The Horizontal Cyclone Burner," by A. E. Grunert, L. Skog, and L. S. Wilcoxson, Trans. ASME, vol. 69, 1947, pp. 613–627. (Presented at the 1946 Annual Meeting of the ASME.)

[3] "Operating Experiences With Cyclone-Fired Steam Generators," by V. L. Stone and I. L. Wade, MECHANICAL ENGINEERING, vol. 74, 1952, pp. 359–368.

Contributed by the Fuels and Power Divisions and presented at the Annual Meeting, Atlantic City, N. J., November 25–30, 1951, of THE AMERICAN SOCIETY OF MECHANICAL ENGINEERS.

NOTE: Statements and opinions advanced in papers are to be understood as individual expressions of their authors and not those of the Society. Manuscript received at ASME Headquarters, October 6, 1951. Paper No. 51—A-118.

COMMONWEALTH EDISON COMPANY
CALUMET STATION

The theory and early developments of the cyclone, including the first steam generator, known as Boiler 20A, at Calumet Station of the Commonwealth Edison Company, in Chicago, were covered in detail in the 1946 paper.[2] It might be mentioned here that Boiler 20A is still giving very satisfactory service today. The success of the horizontal cyclone warranted the installation of a vertical cyclone on Boiler 22 at Calumet Station. This boiler has a capacity of 300,000 lb of steam per hr at 350 psi and 650 F. The final design had a vertical cyclone 6 ft diam on one side and pulverized-coal and gas firing on the other side.

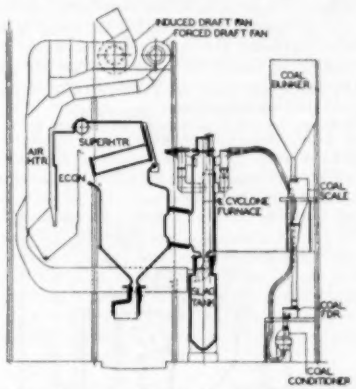

FIG. 1 CROSS SECTION OF BOILER NO. 22 AT CALUMET STATION

The vertical cyclone was fired tangentially at the top, the molten slag being removed continuously from a tap hole in the bottom of the cyclone and with the gases passing in a horizontal direction from the bottom portion through a water-cooled vestibule into the existing furnace of the unit. The original installation did not give the coal the same cyclonic action as in the horizontal cyclone. Also, the slag did not stick to the side walls to help the combustion of the coal. Various changes were made in the shape and location of the inlet scroll, but after 4 years of experimenting, without too much success, it was decided to reinstall the pulverized-fuel-burning equipment. We are in hopes that The Babcock & Wilcox Company will continue working on the vertical cyclone in its laboratories, as we feel that it could be adapted to existing boilers where objectionable atmospheric pollution is a problem, without rebuilding the whole boiler room.

PUBLIC SERVICE COMPANY OF NORTHERN ILLINOIS
WAUKEGAN STATION—BOILER NO. 13

Boiler No. 13 in the Waukegan Power Station of the Public Service Company of Northern Illinois is one of three boilers that were installed in 1929 with turbine-generator unit No. 4, which is a 65,000-kw reheat unit. Boiler No. 11

is a reheat type and boilers Nos. 12 and 13 are standard steam-generating units, each having a capacity of 300,000 lb of steam per hr at 675 psig steam pressure and 760 F total temperature. Boilers Nos. 11 and 12 are equipped with Fuller (B&W) coal pulverizers and the third boiler (No. 13) had three Bethlehem mills. These mills were in regular operation from 1929 until 1948, and had reached a state that required heavy maintenance. Therefore this boiler was chosen for the installation of cyclones for the purpose of studying this method of firing, and in particular, the reduction of fly ash in the flue gases.

It was originally intended that this boiler be equipped with two vertical cyclones, but as the early experience with this type of cyclone on boiler No. 22, Calumet, did not come up to expectations, it was decided that the installation for boiler No. 13, Waukegan, should not be delayed, and to proceed with the horizontal type.

This was the first commercial installation of multicyclones on an existing boiler furnace, and since there has been much interest displayed in the possibilities of modernizing existing boilers by fitting them with cyclones, this paper gives a rather complete description of the problems and changes that were involved.

The boiler is a Babcock & Wilcox cross-drum type with economizer and air heater, quite typical of the design used at that time. The conversion from pulverized-coal firing to cyclone firing required, of course, the removal of the old equipment, such as the pulverizers and their feeders, the exhausters, burners, piping, and the forced-draft fan.

Fig. 2 shows the boiler as it looks after being fitted with cyclones.

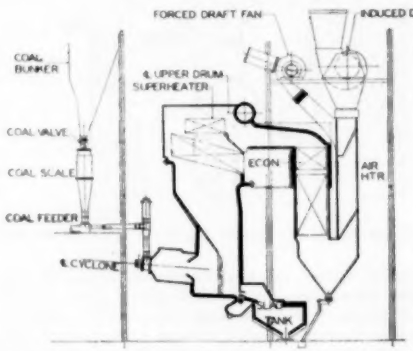

FIG. 2 CROSS SECTION OF BOILER NO. 13 AT WAUKEGAN STATION

The new equipment purchased for the cyclone installation consisted principally of the following:

One coal crusher for preparing coal to cyclone size.

Two screw-type feeders.

Two 8-ft cyclones.

Two blowers for supplying combustion air and creating the turbulence required for cyclone firing.

One slag tank.

In addition to the installation of this equipment, many parts of the boiler unit were rebuilt, and some building structural changes were also required. A list of these item is as follows:

1 Conveyer and building changes for installation of the coal crusher in the breaker building. This location was chosen for the coal crusher because there was space available, and also for the purpose of confining coal preparation in this one building.

2 The original coal bunker was arranged with three spouts for the three pulverizers and was changed for two feeds (one for each cyclone), in order to eliminate a dead pocket.

3 Furnace waterwalls were rebuilt. A new front wall was required for the installation of the two cyclones and for the slag screen, and the other walls were rebuilt to conform to present-day construction, in order to make them more reliable. The rebuilding of these walls also involved the installation of new insulation and a casing for the furnace areas. The original two slag-tap openings were rebuilt in the rear wall.

4 A new furnace floor was installed to convert the method of removing molten slag from intermittent tapping to a continuous system. The slag tank, which was installed for receiving the slag, presented a difficult problem because of the limited headroom under the boiler-steel supports. It was necessary to locate the tank at the rear of the boiler, which did not lend itself to the best design for the flow of slag from the furnace to the tank.

5 The water-circulating system of the boiler was rebuilt, and extensive additions were made because the existing low head was not sufficient for the rapid circulation required by a cyclone furnace.

6 On account of additional heat absorption in the cyclones and in the lower part of the furnace, a row of steam-generating tubes was removed, in order to maintain steam temperature.

7 The air-heater casing was reinforced with stiffeners and tie bars to withstand the 50-in. pressure developed by the two new blowers. The air-heater tubes were rolled in both tube sheets, in order to minimize air leakage, and this required the installation of an expansion joint in the casing.

8 Air ducts were reinforced for the higher air pressures.

9 New galleries were installed to suit the new levels required for the cyclones and the slag tank.

10 Complete new control wiring, a new combustion-control system, and a new gage board with new instruments to suit the new draft conditions, and so forth, were installed.

11 The electrical system required fewer metal-clad switches because of bus equipment, but it was necessary to change the current transformers for the higher requirements of the blowers.

12 In connection with all of the foregoing items, there were many alterations to building steel and concrete floors.

The same slag and soot-blower equipment which was used with pulverized-coal firing proved to be adequate for keeping the boiler clean after conversion to cyclone firing.

The installation of the cyclones in this boiler served its purpose for obtaining experience with this method of firing, and it is also available for trying out new features. At the present time a new design of screw-type feeder is being installed, which, if successful, will have some advantages over the apron-type feeder.

This installation was experimental and cost was not the principal consideration. It was unfortunate that the installation could not have been made with vertical cyclones as originally intended, as this undoubtedly would have resulted in a much lower cost. However, the conclusion from this installation shows that, for the modernization of existing boilers, a careful study should be made beforehand of the costs involved, not only for the new equipment but for the changes that might be required because of existing conditions.

COMMONWEALTH EDISON COMPANY
FISK STATION—UNIT NO. 18

The next installation was unit No. 18 at Fisk Station of the Commonwealth Edison Company. This was in the spring of 1949. The installation consisted of two 750,000 lb per hour, 1250 psi, 935 F steam generators. Each generator is fired by

four 8-ft-diam horizontal cyclones. The principal auxiliary equipment for each boiler consists of the following:

Two motor-driven blowers with vane control.
Two motor-driven induced-draft fans with vane control.

Fig 3 shows how the coal handling had to be adapted to the existing bunker installation. Vertical coal conveyers, transfer hoppers, and coal crushers had to be installed for each cyclone. One of the most perplexing problems of this installation was the design of a satisfactory gallery system to take care of the initial

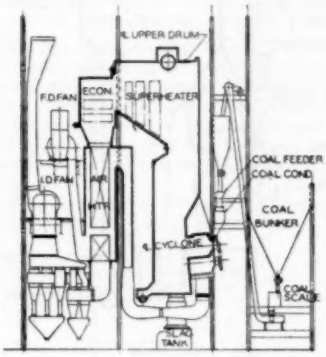

Fig. 3 Cross Section of Boiler No. 18 at Fisk Station

soot blowers, as well as the additional blowers installed after going into service. Mechanical dust collectors were installed on these units which fitted very well into the design, but owing to the greater proportion of finer fly ash than was expected, the performance was not up to expectations.

Public Service Company of Northern Illinois
Joliet Station—Unit No. 5

In January, 1950, two cyclone-fired boilers were placed in operation by the Public Service Company of Northern Illinois, in connection with the installation of unit No. 5, a 107,000-kw turbine generator, for the Joliet Power Station. Each boiler has a rating of 600,000 lb of steam per hr at 1325 psig, total temperature of 1010 F at the superheater outlet, and feedwater temperature to the economizer of 450 F. The three 8-ft cyclones on each boiler are arranged for natural-gas firing, as well as for coal. Joliet boilers Nos. 3 and 4 are shown in cross section in Fig. 4.

The principal auxiliary equipment for each boiler consists of the following:

Two motor-driven blowers with vane control.
Two motor-driven induced-draft fans equipped with hydraulic couplings for variable-speed operation.

The boilers were installed in an extension to the present building, but the shape of the property limited the size of the extension on one side to such an extent that the cyclone-fired-type boilers fitted into the space available better than pulverized-coal-fired units.

No dust precipitators were installed with these boilers, because of the lower quantity of fly ash, and because of the fact that the power station is located well outside the city. The present pulverized-coal-fired boilers in this station have no dust precipitators.

Northern Indiana Public Service Company
Michigan City Generating Station

The Michigan City installation includes three 375,000 lb per hr boiler units, each with two 8-ft-diam cyclones, which, in so far as design is concerned, are duplicates of the cyclones installed at Fisk and Ridgeland. The boiler design is for 1325 psi, 960 F superheater-outlet conditions, with 395 F feed and 325 F exit-gas temperature. These three boiler units will supply steam to two 70,000-kw, 1250-psi, 950 F turbine generators.

The first of these turbine units has been in operation since October, 1950, and the second unit was due to be completed late in 1951.

The unit operated for 2½ months on one boiler before the second was completed. During this time the steaming capacity ranged between 375,000 and 425,000 lb per hr for 14 hr per day.

The coal burned at this station is 80 per cent Indiana fifth vein mixed with 20 per cent Central Illinois coal, and this has given no trouble from plugging or slag deposits. The blowers in the superheater section are operated twice a day and others only once a day.

In February, 1951, the second boiler was put into operation, and the third boiler was completed in May, 1951. Since that time, two boilers have been on the line with the one turbine unit, and the steam load on each does not exceed 280,000 lb per hr. Operation at these lighter loads has also been satisfactory.

Wisconsin Power and Light Company
Edgewater Power Station

This installation is a 600,000-lb per hr unit, which was put into operation during the summer of 1951. It is fired with three 8-ft-diam cyclones, similar to the installation at Joliet. The steam conditions at the superheater outlet are 1325 psig and 960 F. The turbine is a 60,000-kw unit, with final feedwater temperature of 405 F at rated load.

Coal burned at this power station comes principally from southern Illinois. Crushing for cyclone burning is done in a coal-handling building extension exterior to the power station.

At the time of writing this paper, the boiler had been in service only a few weeks and therefore there has been insufficient experience to report on operations.

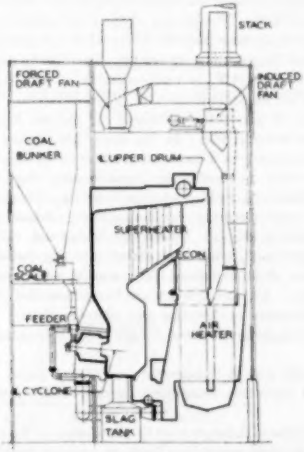

Fig. 4 Cross Section of Boilers Nos. 3 and 4 at Joliet Station

Commonwealth Edison Company
Ridgeland Station—Units No. 1 and 2

The design for units Nos. 1 and 2 at Ridgeland Station was very interesting, as we could start from scratch and not worry about fitting a unit into an existing area or an extension to a station. Two cyclone-fired generators, each with a capacity of 730,000 lb per hr, 1800 psi, and 1050 F steam were installed for each of the two 150,000-kw turbines. These boilers are all cross-connected. The first two boilers went into service during the fall of 1950, and the second two in the spring of 1951. The principal auxiliary equipment for each boiler consists of the following:

Two motor-driven blowers with vane control.

Two motor-driven induced-draft fans with vane control. These units are shown in cross section in Fig. 5.

The new-type slag screen and a full complement of blowers were installed on these generating units. It was felt that the slagging of the superheaters could be eliminated by blowers, and to avoid possible points of air leakage, no provisions were incorporated for hand-lancing of the superheater sections. As shown in Fig. 5, a bin system is used for storing the crushed coal. The coal scales and feeders are located between the bunker outlets and the cyclones. There are four 8-ft cyclones per generating unit. These units are equipped with electrostatic precipitators, which are much more efficient with fine fly ash than the mechanical type.

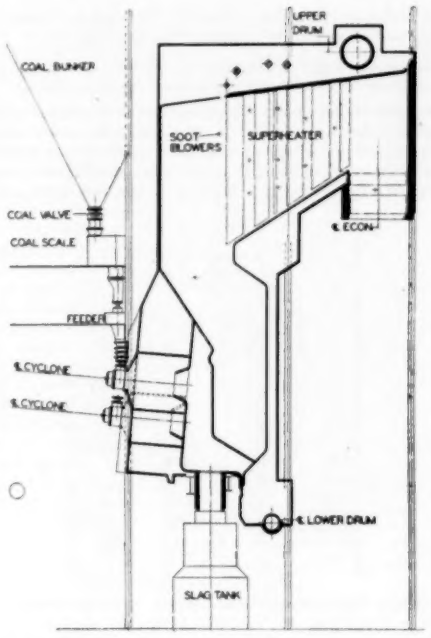

Fig. 5 Cross Section of Boilers Nos. 1 and 2 at Ridgeland Station

Commonwealth Edison Company
Ridgeland Station—Units 3 and 4

The design for units Nos. 3 and 4 at Ridgeland Station incorporates single boiler, single reheat-turbine units, with no cross-connections. Each of the steam generators has a capacity of 1,100,000 lb per hr, 1800 psi, 1050 F at the superheater outlet, and 1000 F reheat steam. Each generating unit is equipped with six 8-ft cyclones and a coal-handling system similar to units Nos. 1 and 2, except that the coal scales have been eliminated. Fig. 6 shows a cross section of the boiler.

These generating units have pressurized casings, but induced-draft fans are included in the design. The expected increase in boiler efficiency with the tight casing should more than offset the increased cost. The design of the draft system is such that the induced-draft fans may be removed if operating experience indicates that they are not necessary. In order to get the reheat temperature of 1000 F, it was necessary to put the secondary superheater in the radiant section of the furnace. This section is made up of the tubes arranged in platens hanging down through the furnace roof. In the upper section the platens are spaced 18 in. apart, and the lower section on 3-ft centers. Adequate provision is made for hand-lancing the superheater platens. This is a radical change from the previous designs, and to get some operating experience, three platen sections have been installed in the No. 1 boiler at Ridgeland. After several months' experience, it has been found that slag builds up on the lower section of each platen. The slag is easily removed with a hand lance. Air soot blowers are being installed to determine their effectiveness in keeping the platens clean. The reheat and primary superheater elements are in the convection section of the boiler.

To keep the reheat temperature up at low loads, gas will be recirculated from the economizer outlet back to the primary furnace.

Another feature incorporated in the design is the use of tempering gas at high generating loads to prevent build-up of slag in the superheater sections by lowering the gas temperature entering the secondary superheater. The same fans used for recirculating gas for reheat control at low loads are used for

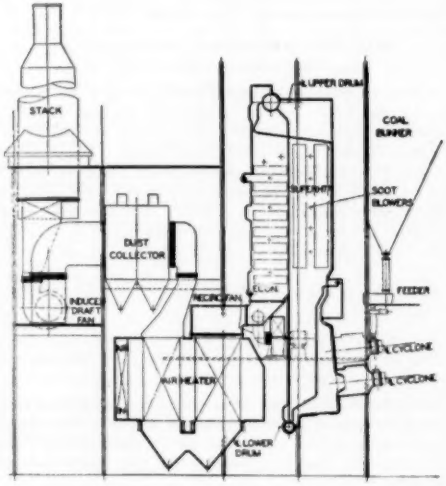

Fig. 6 Cross Section of Boilers Nos. 3 and 4 at Ridgeland Station

supplying tempering gas at high loads. This tempering gas is admitted all across the front of the secondary furnace just below the superheater platens. To obtain operating experience with this tempering gas, a similar duct system has been installed on one of the Fiak boilers. At the time of this writing the fans have not been delivered, but a temporary connection to the hot-air outlet has been made, and experiments with air are being conducted until the fans are installed. After several weeks of operation, the results, while still of a preliminary nature, are encouraging.

Public Service Company of Northern Illinois
Waukegan Station—Unit No. 6

The installation of turbine unit No. 6, a 110,000-kw turbine generator of the reheat type, and a steam generator with four 9-ft-diam cyclones, having a capacity of 830,000 lb per hr, are now nearing completion in the Waukegan Power Station for the Public Service Company of Northern Illinois. This will be the first installation of a reheat-type boiler with cyclone firing. A cross section of the boiler room and steam-generating unit is shown in Fig. 7.

Steam-operating conditions and the main features of the installation are as follows:

Pressure at superheater outlet	1850 psig
Steam temperature at superheater outlet	1010 F
Steam temperature at reheater outlet	1010 F

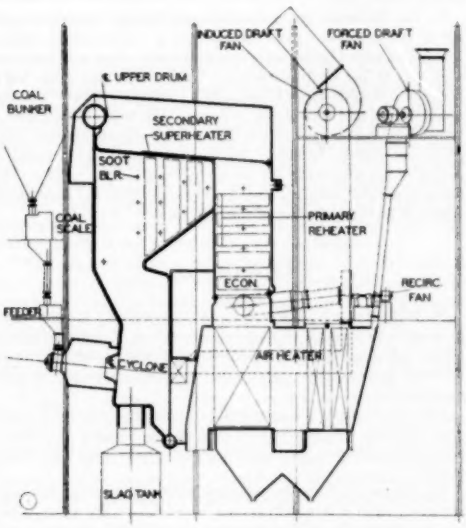

Fig. 7 Cross Section of Boiler No. 6 at Waukegan Station

Recirculation of boiler gases is used to maintain steam temperatures at lower boiler ratings. There are two fans for this recirculation which take gases from the exit side of the economizer and discharge them back to the furnace.

Size of cyclones is increased from 8 ft diam as in previous installations to 9 ft diam. Auxiliary equipment includes the following:

Three motor-driven blowers with vane control.

Two motor-driven induced-draft fans with hydraulic couplings for variable-speed operation.

Public Service Company of Northern Illinois
Will County—Units Nos. 1 and 2

Units Nos. 1 and 2 in the new Will County Station for the Public Service Company of Northern Illinois are in the early stages of design. Two 150,000-kw turbine units and two steam-generating units of the reheat type, each having a capacity of 1,200,000 lb of steam per hr have been purchased for supplying steam to the turbines at 1850 psig, 1050 F total temperature, and steam return to the turbine from the reheater at 1000 F.

Each boiler will have five 9-ft-diam cyclones, and the furnace will be similar in design to those for Ridgeland Nos. 3 and 4, with all walls practically vertical to eliminate footings for slag accumulation and for better removal of slag by wall blowers.

The design and location of the secondary superheater are also similar to Ridgeland Nos. 3 and 4.

Typical Coal-Handling System

Fig. 8 shows the general design of a coal-handling system such as is being used in new stations with cyclone-fired steam generators.

The coal comes from barges, car dumper, or storage on conveyer belts to the breaker building. Breakers reduce the coal to about $1^1/_2$-in size, and this coal then drops into the crushers and is reduced to a maximum size of $^1/_4$ in. Coal is conveyed then to the boiler bunkers, and thence to the cyclone furnaces.

As a result of an explosion that occurred at Ridgeland Station, we have made, or are making, the following changes:

1 All conveyer belts handling $^1/_4$-in. or finer coal will be of the conducting type which has a high-carbon-content rubber coating in order to eliminate static electricity.

2 All bunkers where $^1/_4$-in. or finer coal is stored will have continuous flow of fresh air through them.

Conclusions

We will review the conclusions of the 1946 paper,[3] and show how they apply to the larger-capacity, higher pressure and temperature, cyclone-fired steam generators.

1 The ash-handling systems are no more complicated for cyclone than pulverized-coal-fired units.

2 With less fly ash in the discharge gases, smaller dust collectors are required. Fig. 9 shows that for the same fly-ash concentration in the stack gases, the pulverized-fuel-fired boiler requires a much larger dust collector, and that more dust is passing through the heat-absorbing surfaces.

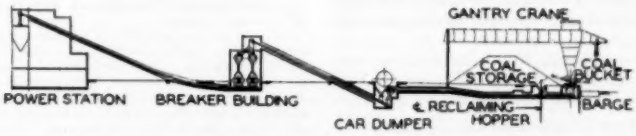

Fig. 8 Cross Section of Coal-Handling System at Ridgeland Station

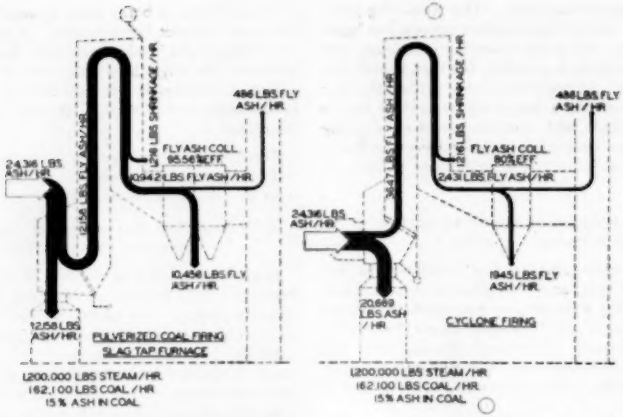

FIG. 9 ASH AND FLY-ASH DISTRIBUTION—PULVERIZED-COAL VERSUS CYCLONE-FIRED BOILERS

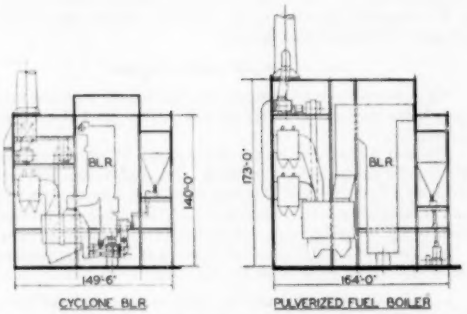

FIG. 10 COMPARISON OF SPACE REQUIREMENTS—CYCLONE BOILER VERSUS PULVERIZED-FUEL-FIRED BOILER

3 The gases passing through the boiler sections contain less dust, but the dust with Central Illinois coal is of such composition, high in alkalies, that it sticks to the surfaces. To date there has been no reduction in equipment and labor for cleaning the absorbing surfaces when burning Central Illinois coal. It is hoped that the use of tempering gas and other methods of cleaning will be successful and permit a reduction.

4 The cyclone-fired steam generator permits the use of a smaller unit for the same capacity, compared with other methods of combustion.

5 The cost of preparing coal for burning, both from the power and maintenance standpoints, is considerably less than for pulverizing coal. All of the troubles with coal conditioners outlined in the 1946[2] paper have been eliminated, and they are now considered very reliable and give long service between overhauls.

6 The elimination of induced-draft fans on the large generating units has not been made, but it is hoped that this will become a possibility in the not too distant future. Smaller industrial boilers with cyclone furnaces are now operating successfully without induced-draft fans.

7 Fig. 10 shows a comparison between the size of the boiler room for a pulverized-coal-fired boiler and a cyclone-fired boiler. The cyclone-fired boiler takes approximately 10 per cent less floor area and 25 per cent less volume. This study was made for a boiler of 1,200,000 lb per hr capacity at 1800 psig, 1050 F throttle temperature, and 1000 F reheat steam. The boiler is used with a 150,000-kw turbine-generator unit. Our estimate for the complete installation, including building and equipment, shows a saving of approximately $3 per kw in favor of the cyclone-fired steam generator, which is considerably lower than the anticipated figures of $6 to $6.50 given in the 1946 paper.[2]

Discussion

W. H. ROWAND.[4] The authors have presented a fair and comprehensive evaluation of where the operation of cyclone-furnace boilers burning Kincaid coal stands today and of the differences in design between them and the new cyclone-furnace reheat units now on order.

It is evident from this presentation that when burning Kincaid coal we have not yet reached one of our original objectives, namely, to minimize the required cleaning of heat-absorbing surfaces.

We will continue our development until this objective has been attained, so that rightfully it can be added to the many other benefits which the cyclone furnace already offers for the more economical generation of power.

[4] Chief Engineer, The Babcock & Wilcox Company, New York, N. Y. Mem. ASME.

Effect of Velocity on Tensile Impact Properties of Polymethyl Methacrylate[1]

By BRYCE MAXWELL[2] and J. P. HARRINGTON[3]

The history of impact testing of plastics is reviewed and the current theories of impact resistance are discussed. The effect of velocity on the energy absorbed by polymethyl methacrylate at various temperatures has been studied with the aid of two new testing machines. The results are interpreted in terms of the classical theories of mechanics of materials and the current theories of the rheology of high polymers. It is concluded that there are two distinct critical velocities of straining in this material—the lower one corresponding to the relaxation of the bonds restraining chain-chain slipping and the higher one corresponding to the relaxation of the secondary bonds involved in chain uncoiling. Both of these relaxations are temperature dependent—the lower one to a slight extent and the upper one to a marked extent. Above the two critical velocities the response of the material is purely elastic. A method of calculating the energy to break at rates of straining above the second critical velocity from the slow-rate stress-strain curves is demonstrated.

Introduction

IT HAS long been realized by engineers that some materials which exhibit great strength or toughness under static or low-rate tests will fracture easily when hit with a sharp blow. Some types of steels can withstand high loads and large elongations in slow-speed tests but will fracture with a brittle or glass-like break when hit with a hammer blow. Perhaps the most striking example of this phenomenon can be demonstrated with ordinary pitch at room temperature. When pulled between the fingers at a slow steady rate it will flow like a liquid but when pulled rapidly it will snap with little or no elongation.

These phenomena have led to the common belief that there is a fundamental difference between the behavior of materials at slow rates of straining and at impact rates; or, to put it another way, there is no correlation between impact testing and "static" or slow-rate testing. It will be shown later that the results of high and low rates of loading are related and that the impact test is really only a special case of the slow rate or static test.

Techniques of impact testing for plastics have been taken over from the metals industries where the Izod and Charpy type tests have been firmly established for many years. Although these tests have been useful in some cases to rate the relative shock resistance of materials, they are subject to certain limitations and do not give quantitative data suitable for design calculations. The broken-end error (1)[4] or "toss factor" is also inherent in these tests. For many years workers in the plastics field have studied these problems and many attempts have been made to devise testing machines which would shed some new light on the subject of impact resistance.

Telfair and Nason (1) have investigated the factors which contribute to the energy measured by the Izod machine and have devised a method of testing which measures only the energy required to initiate fracture. In a later paper (2) the same authors have considered such factors as specimen shape, temperature, and rate of stressing. Liander, Schaub, and Asplund (3) have shown that a falling-weight test from various heights can give data that do not include the "broken-end error"; but the question of the fatigue effect is brought up by this method and this factor was further studied by Lubin and Winans (4). Stock (5), and Bailey and Ward (6) have devised ingenious machines of the ski-ball type with which it is possible to find the energy required to just break a specimen. Quackenbos (7) et al., have studied the notched and unnotched Charpy tests at various velocities by the use of resistance strain gages.

All of the foregoing workers used some form of beam-type specimens, either cantilevers or simple beams with or without notches. These types of specimens are of course difficult to analyze because of stress concentrations, and because too many parameters of the material enter into the result. The effects of velocity and quantity of energy available have not been studied independently, so it is difficult to obtain a true conception of the velocity effect. For the ideal test the amount of energy available in the striking member should be very large compared to the energy required to fracture so that very little decrease in velocity of straining takes place during the break.

Myers (8) devised a test in which the velocity of straining remained essentially constant during the test. The decrease in impact resistance corresponding to a decrease in temperature was demonstrated. Unfortunately, this method did not permit measurement of the energy to break. Workers (9, 10) in the field of metals have devised many ingenious devices for obtaining the complete stress-strain curve in tension at various rates of straining. These machines are usually costly and rather complicated. Many depend on some sort of electronic device to transpose the stress and strain to an oscilloscope. Although these studies with metals have been encouraging they have not as yet been applied to plastics.

Basic Theory

When a plastic component is subjected to a sudden shock, the failure usually occurs in tension. Referring to Fig. 1, if a force is suddenly applied in the direction of arrow 1 to the typical housing section shown, the failure would take place at A or B. If the force is applied by arrow 2, the failure would be initiated at C. In either case the failure starts in that part of the component which is subjected to the highest tensile stress by the suddenly applied force. Obviously, proper design of sections and fillets can help to prevent breakage, but unless the direction of the blow

[1] The research reported here was sponsored jointly by the Army, Navy, and Air Force under Signal Corps Contract No. DA-36-039-sc-133.

[2] Research Associate, Plastics Laboratory, Princeton University. Jun. ASME.

[3] E. I. du Pont de Nemours and Co., Wilmington Del.

Contributed by the Rubber and Plastics Division and presented at the Annual Meeting, Atlantic City, N. J., November 25–30, 1951, of The American Society of Mechanical Engineers.

Note: Statements and opinions advanced in papers are to be understood as individual expressions of their authors and not those of the Society. Manuscript received at ASME Headquarters, August 15, 1951. Paper No. 51—A-65.

[4] Numbers in parentheses refer to the Bibliography at the end of the paper.

can be anticipated, it is impossible to design the component so that some section will not be put in tension if a shock is applied to the unit.

For this reason it was decided that if the test specimen were

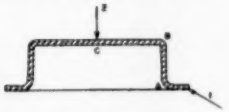

FIG. 1

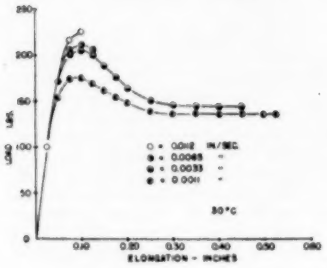

FIG. 2(a)

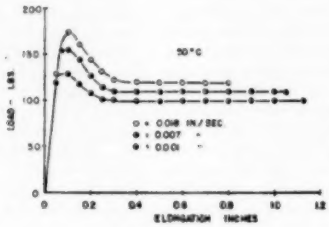

FIG. 2(b)

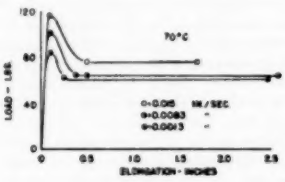

FIG. 2(c)

subjected to a simple tensile stress rather than flexure, results would be obtained which would be more directly applicable to practical problems and also more easily subject to theoretical analysis.

Early studies of the stress-strain curves for plastics showed that the rate of testing has a marked effect on the shape of the curve. In general, the yield stress and ultimate stress increase and the ultimate elongation decreases with an increase in testing speed, as shown in Fig. 2. A more striking demonstration of the effect of rate of straining on the shape of the stress-strain curve is shown in Fig. 3. The initial part of this curve was made at 0.001 ips. At a strain of 0.1 in. per in. the rate of straining was increased to 0.05 ips, which resulted in a sudden increase in the slope of the curve as shown; that is, at the increased rate of straining, a higher stress-energy level must be reached to permit the bond mechanism of flow to relax. Similarly, it has been found that the testing temperature is equally important, an increase in temperature acting like a decrease in straining rate.

The common unit of impact-strength measurements is the energy to break, that is, the integral of the force times the elongation or the area under the force-elongation curve

$$I = \int F d\epsilon \quad \ldots\ldots [1]$$

where

I = energy to break
F = force
ϵ = elongation

If the force is directly related to the rate of straining and the elongation is inversely related to the rate of straining, it becomes apparent that the energy to break as a function of the rate of straining will be a rather complex expression depending on the relative rate of change of the two variables, force and elongation, with change in rate of straining.

The mechanism of deformation of linear amorphous polymers is considered to be made up of three or more systems (11). The first of these is the truly elastic deformation of the bond angles; another is the uncoiling of the chain segments; and the last is the slipping of the chain segments past each other. The first of these deformations takes place instantaneously and is also instantaneously recoverable. The next deformation is time-dependent, that is, it depends on the relaxation times of the bonds involved (the secondary or van der Waals forces between chain segments and substituent groups on the chain segments). These relaxation times are in turn dependent on the activation energy of the bonds and the local temperature and the stress energy applied. The last deformation is similar to the second in that it also depends on the relaxation of secondary bonds (true only for linear amorphous polymers) but differs in that it is an irrecoverable deformation.

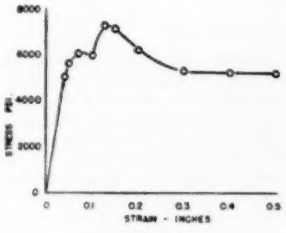

FIG. 3

FIG. 4

Each of the foregoing deformations can be represented by a series of mechanical elements. (This method of representation has been used by many authors and is repeated here only for reasons of completeness.) Referring to Fig. 4, the first mechanism of deformation D_1 may be represented by a spring. The second D_2 by a spring and dashpot in parallel, and the third D_3 by a dashpot. In the case of materials obeying Hooke's law in the initial part of the stress-strain curve, the spring of D_1 is linear. The dashpot D_3 may have a shear pin so that it will not start to flow until a specific stress has been reached.

Each of the three elements of the model, Fig. 4, will respond in a different way to an applied load. The spring D_1 is considered to be Hookean and the resulting strain ϵ will have a linear relation to the stress S

$$\epsilon = \frac{S}{E} \quad \ldots\ldots [2]$$

where E = modulus of spring.

The spring and dashpot in parallel making up the element D_2 is known as a Voigt model. It will respond to an applied stress according to

$$\epsilon = \frac{S}{E}(1 - e^{-t/\lambda}) \quad \ldots\ldots [3]$$

where

t = time of load application
E = modulus of spring
λ = relaxation time of dashpot

that is, when the time of loading is very short, practically no deformation will take place; but as time approaches infinity the strain approaches that which corresponds to the elastic response of the spring.

The third element D_3 is considered to be a dashpot containing a Newtonian liquid. It will respond according to

$$\epsilon = \frac{S}{\eta} t \quad \ldots\ldots [4]$$

where η = coefficient of viscosity for dashpot.

The elements D_1 and D_2, when taken together in series without the element D_3, is called a Maxwell model. Such a model will respond to an applied load according to the equation

$$\frac{dS}{dt} = E\frac{d\epsilon}{dt} - \frac{S}{\lambda} \quad \ldots\ldots [5]$$

where λ = relaxation time of dashpot D_2. Integrating Equation [5] for constant stress

$$\epsilon = \frac{S}{E\lambda} t + \frac{S}{E} \quad \ldots\ldots [6]$$

The total deformation of the model Fig. 4 when some stress S is applied will be given by the sum of Equations [3] and [6]

$$\epsilon = \frac{S}{E_1} + \frac{S}{E_2}\left(1 - e^{-\frac{t}{\lambda_2}}\right) + \frac{S}{E_3}\frac{t}{\lambda_3} \quad \ldots\ldots [7]$$

that is, the elongation of the model is made up of the elastic response of D_1 plus the viscous flow of D_3 plus the retarded flow of D_2. We can see from Equation [7] that the strain of a specimen is dependent upon the rate of load application and the two relaxation times λ_2 and λ_3. In most materials, the relaxation time of the retarded element D_2 is usually much shorter than that of the element D_3. In actual mechanical relaxation tests of high-polymeric materials, difficulties of experimental techniques prevent the observation of the relaxation of D_2 as it takes place so rapidly, but theoretically the complete relaxation curve should have the general shape of Fig. 5. Andrews (12) has shown the

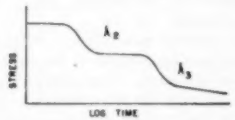

FIG. 5

shape of a nearly complete relaxation curve for polyisobutylene by shifting the curves at various temperatures along the time scale.

With reference to the stress-strain curves of polymethyl methacrylate shown in Fig. 2, we may say that the initial straight portion of the curve is due to the elastic response of D_1. The deviation from linearity from the proportional limit to the yield point is due to the response of D_3, and the flow from the yield point to failure is due to D_2.

The process of chain uncoiling and the process of chain-chain slipping depend on the rate at which the secondary bonds break and reform. This rate is dependent on temperature. The higher the temperature, the more often any given bond will acquire the energy necessary to break the bond permitting it to reform in another position. The average time required for this process is the average time required for the type of bond involved to attain the activation energy u. This time should be proportional to $e^{u/RT}$ where R is the molar gas constant, and T is the absolute temperature. Therefore the limiting flow velocity should be given by

$$V_s = Cle^{-u/RT} \quad \ldots\ldots [8]$$

where l = average distance the two structural units move between the breaking of the bond and the forming of a new bond. Since C is also a constant, we may rewrite the equation

$$V_s = Ke^{-k/T} \quad \ldots\ldots [9]$$

where K and k are constants. Two of these limiting velocities should be found—one corresponding to the maximum velocity at which D_2 can be strained, the other corresponding to D_3 maximum velocity.

Let us now consider at what velocity a strain wave will propagate through a specimen. Consider the section of specimen shown in Fig. 6. Let point a be moved with a velocity V_0 as

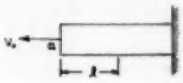

FIG. 6

shown by the arrow. If this is a purely elastic material, the strain will move through the specimen with the velocity of sound, which can be determined from

$$V_s = \sqrt{\frac{E}{\rho}} \quad \ldots\ldots [10]$$

where

V_s = velocity of sound in specimen
ρ = mass density

Therefore, in any given length of time t after the start of straining

$$V_0 t = \epsilon l = \epsilon V_s t \quad \ldots\ldots [11]$$

where V_0 = some velocity below V_s and from which the unit tensile strain ϵ equals

$$\epsilon = \frac{V_0}{V_s} \quad \ldots\ldots [12]$$

From Hooke's law the stress equals

$$\sigma = E\frac{V_0}{V_s} \quad \ldots\ldots [13]$$

From Equation [13] we can see that when V_0 is greater than V_s the tensile strength of the material is exceeded, and the specimen is broken. Such a break would take place without any strain, and therefore from Equation [1] we can say that the break would take place with theoretically no energy being expended; that is, if we attempt to stretch a specimen at a velocity faster than strain can be propagated through the material, a low-energy break will occur.

For cases where a material can exhibit plastic deformation, the foregoing equations must be modified.

Von Kármán (13) has extended the theory for the plastic case as follows. Since the slope of the stress-strain curve is not constant in the plastic case he has suggested the replacing of E by $\frac{\partial \sigma}{\partial \epsilon}$ or rewriting Equation [13]

$$\sigma = \frac{\partial \sigma}{\partial \epsilon} \frac{V_0}{\sqrt{\frac{\partial \sigma}{\partial \epsilon}/\rho}} \quad [14]$$

or in the integral form with proper limits

$$V = \int_0^{\epsilon_m} V(\epsilon) d\epsilon \quad [15]$$

that is, the maximum velocity of propagation of a plastic wave may be found from this equation. The value of the integral can be calculated from the static stress-strain curve for the material. This has been done by Hoppmann (10) for the case of cold-drawn copper where fairly good agreement was found between the calculated value and the measured value. The actual discrepancy may be attributed to the difference between the static and dynamic stress-strain curves. These calculations for polymethyl methacrylate are demonstrated in the Appendix.

To summarize the basic theory we may say that the energy to break a specimen depends on the integral of the product of the force and deformation as given by Equation [1]. The deformation is a function of the form of Equation [7] and the extent of deformation is dependent on time. Two critical velocities of straining should be found corresponding to the maximum velocities of deformation of the retarded elastic and viscous elements. These should vary with temperature according to Equation [9].

Apparatus

The standard impact testing machines for plastics are of the excess-energy pendulum type with the following inherent errors and limitations. The energy to toss the broken end is included as part of the impact strength, the velocity is limited to one specific value (11 fps), the specimen is of the cantilever type usually with a notch on the tension side with the result that analysis of the stress distribution is impossible. A testing machine which overcomes most of these limitations has been described by the author (14) in an earlier paper. This principle of operation has been used in a new machine designed to test specimens in tension.

Referring to the schematic drawing in Fig. 7, one of the specimen grips A is attached to the periphery of a flywheel B. The rotor or flywheel is brought up to the desired testing speed by a friction clutch and electric-motor drive. When the desired velocity is reached, the clutch is disengaged and the flywheel allowed to rotate freely. At the proper time a trip C is placed in the path of a pair of projections D on the trailing grip and the specimen is broken. The energy required to break is taken from the kinetic energy of the flywheel and causes a reduction in angular velocity. A record of the angular velocity both before and after the break is traced by means of a vibrating pointer on a smoked disk attached to the flywheel. Knowing the moment of inertia of the rotor and the change in angular velocity during the break, the energy to fracture the specimen can be found. With the addition of weights to the rotor, tests at slow velocities can be performed without a prohibitively large change in straining rate taking place during the test. This machine can be used in the range of from 20 ips to 80 fps straining rates.

The specimen used for all the tensile impact tests is shown in Fig. 8. A $^1/_8$-in. $\times$ $^1/_8$-in. $\times$ $2^1/_2$-in. blank is used, from which the specimen is machined. In order to prevent slipping in the grips, the specimen is held by the $^1/_8$-in-radius shoulders.

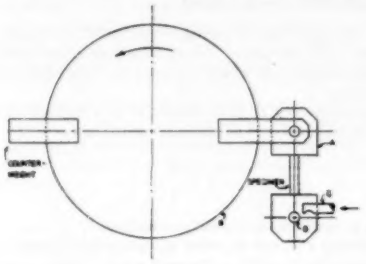

Fig. 7

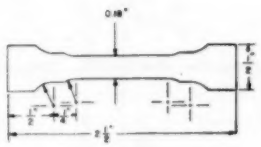

Fig. 8

This gives a positive grip and does not permit slipping as would take place in wedge-type grips. Since the energy absorbed by the entire specimen is the quantity measured, any slipping would introduce a serious error. The smaller set of shoulders is milled in to produce the reduced part of constant cross section. This reduction is necessary to prevent the specimens failing in the grips.

For the tests in the medium range of velocities (0.0045 ips to 17.9 ips), a second machine has been developed. A direct spring-operated load-weighing device is coupled with a mechanical elongation-measuring system to give the complete load-elongation curve. Refering to the schematic drawing Fig. 9, the specimen A is held in the same grip B as used in the high-speed machine. The upper grip is attached to the load-weighing spring C, while the lower grip has a hooking device to catch projections on the drive chain D. The chain is driven by a constant-speed motor through the gearbox E. By shifting gears, twelve different straining rates can be used.

The method of operation is as follows: After the specimen is placed in the grips and brought up to the desired testing temperature, the motor is started. After constant speed is reached, the lower grip is caught by the drive chain D. The force on the specimen contracts the weighing spring C actuating the pointer F, through the 5:1 mechanical magnification linkage G. Concurrently, the recording drum H is being rotated through a mechanical magnification linkage at a rate of 4 times the linear velocity of the chain. The resulting plot on the drum, when the elongation is corrected for the spring deflection, is a chart of the load versus elongation. From this chart the energy to break can be found by measuring the area under this curve with a planimeter.

For very low rates of straining a universal Baldwin testing machine has been used. Adapting a recording extensometer so that it measures the elongation of the entire specimen (the same measurement as the machine just described), a plot of the load

versus elongation can be obtained. From this the same properties can be found.

Results

Specimens of polymethyl methacrylate cut from $^1/_8$-in-thick sheet stock have been tested at velocities from 0.001 ips to 185

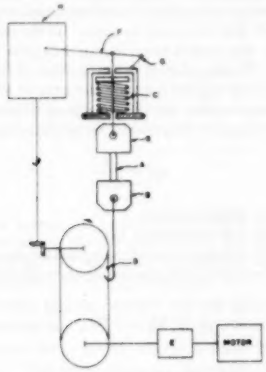

Fig. 9

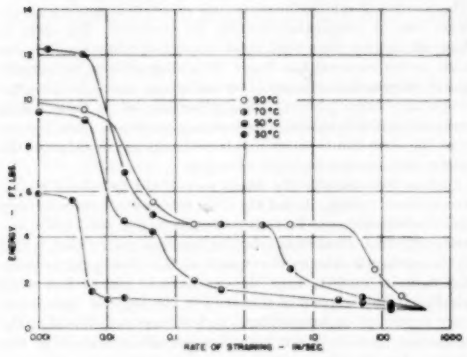

Fig. 10

ips at 30, 50, 70, and 90 C. The energy to break the specimens at these conditions is plotted in Fig. 10 as a function of the logarithm of the rate of straining. In the 30 C curve a distinct drop in the energy to break takes place at 0.0045 ips. In the 50, 70, and 90 C curves, this same drop appears in addition to another energy drop further out on the velocity scale. Each point is the average of three tests. Considerable scatter in the points at any one condition was found in the regions where the slope of the curve is high. In the other regions very little scatter was found.

In order better to envision the interdependence of the three variables, energy, temperature, and rate of straining, the data in Fig. 10 are replotted as a three-dimensional solid in Fig. 11. From this we can see immediately that there are two energy drops and three energy plateaus or planes. The complexity of the figure shows that impact data at one specific velocity and one testing temperature give us very little information about the material. Even the measurement of impact strength at various temperatures but at only one velocity is of little value. The complete three-dimensional plot is needed to really understand the rheological properties of any material.

In addition to the energy to break, the elongation of the specimens at each condition except at the very high velocities was also measured. Fig. 12 shows these data at various temperatures versus the log of the rate of straining. It should be noted that there is an increase in the slope of these curves in the velocity range corresponding to the first energy drops in Fig. 9.

The ultimate yield stress as a function of the log of the rate of straining at the various temperatures is shown in Fig. 13. In the cases where the material did not yield, the ultimate stress was used; in the other cases the yield stress was used. Since these curves turn out to be straight lines, we may assume that an exponential-type equation will express the relationship between stress and rate of straining with an appropriate constant to account for their shift along the rate scale due to temperature changes; that is, an increase in temperature moves the line further up on the velocity scale to a higher rate.

Some of the specimens tested at low rates and high temperatures necked down after reaching the yield point, and then, after reaching some constant cross section, the necked-down portion continued to grow until failure took place. After the constant cross section was reached, the load required to continue the elongation remained constant, as shown in Fig. 2. At the very high temperatures, this necked-down region grew until it reached the shoulders of the specimen. The necked-down cross section was found to be dependent on both the temperature and the rate of straining.

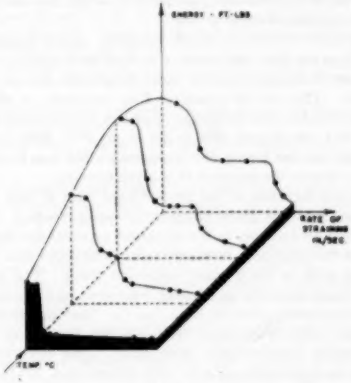

Fig. 11

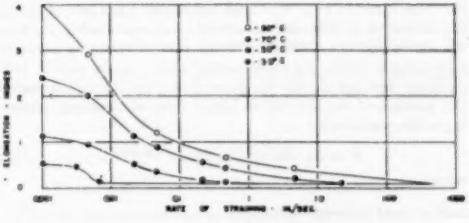

Fig. 12

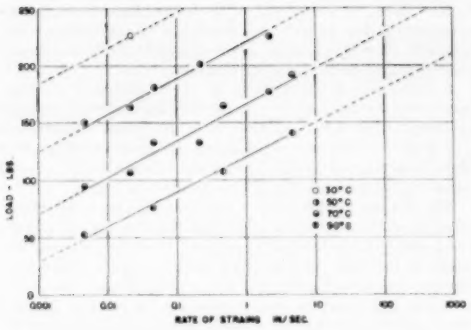

FIG. 13

DISCUSSION

The amount of energy absorbed by the material during the tensile test is proportional to the area under the load-deformation curve. The general shape of this curve is affected by the rate of loading and the testing temperature. Several important criteria of the material can be determined from the load-deformation curve, namely, the elastic modulus, the proportional limit, the yield strength or maximum strength, and the ultimate strength, or ultimate elongation. All of these are affected by the two variables, temperature and rate of straining, and of course are the ultimate factors which determine the energy absorbed by the material. Therefore it becomes necessary to study the effect of the variables on each of these factors.

Let us first consider the elastic modulus. From an inspection of Fig. 2 we see that the initial portion of each curve is straight. The slope of this part of the curve determines the modulus of elasticity. The rate of straining does not seem to affect this slope appreciably, but the temperature has a pronounced effect on it. At 30 C the slope is 3880 lb per in., at 50 C, 2600, and 70 C, 2160—that is, the higher the temperature the less the load required to deform the spring of D_1, a given amount.

The exact location of the proportional limit is very hard to determine. At any given temperature an increase in straining rate causes an increase in the apparent proportional limit. As shown in the Appendix, there are some indications that the proportional limit is not a truly significant point. The deviation from linearity seems to be entirely dependent on time, according to the relationship given in Equation [3]; that is, the strain for any given stress is increased from Hooke's law by an amount which varies exponentially with time. This deviation from linearity is apparently due to the deformation of D_2, and if tested at an infinitely rapid rate of straining the material would exhibit a strictly linear relationship of stress to strain.

The yield stress or ultimate stress, if no yielding takes place, has been found to vary with both temperature and rate of straining as shown in Fig. 13. A straight-line relationship between the stress and the logarithm of the rate of straining seems to approximate closely the experimental data. An increase in temperature does not change the slope of the line but rather moves the position of the line out to higher rates of straining, according to the relationship

$$F = 14.5 \ln (1.3 \times 10^{11} R e^{-0.192T}) \quad [16]$$

where

F = yield or breaking force
R = rate of straining, ips

This shows that irrecoverable flow will take place at lower stress if the rate of straining is slow or the temperature is high; that is, it takes time to initiate plastic flow.

The elongation at break has been found to be dependent on both rate of straining and temperature as shown in Fig. 12. At the lower rates or the higher temperatures the material yields and then deforms plastically. This plastic deformation appears as a necking down at one point in the specimen after which this necked-down section continues to grow. If the rate of straining is slow enough the necked-down section will grow to the ends of the specimen. This is believed to be the cause of the nonlinearity of the curves in the regions for very low rates of loading. From the data we may express the relationship of ultimate elongation to rate of straining and temperature by the following

$$\epsilon_{ult} = \frac{1}{CR^n} \quad [17]$$

ϵ_{ult} = ultimate strain
R = rate of straining, ips
C = constant dependent upon temperature
n = constant dependent upon temperature

In the Appendix the von Kármán critical velocities for polymethyl methacrylate at 30, 50, and 70 C are calculated with the following results:

30 C, 136.8 fps critical velocity
50 C, 108.2 fps critical velocity
70 C, 87.5 fps critical velocity

These values should be the maximum velocities at which a plastic wave can be propagated through the material. The data in Figs. 10 and 11 show that these calculated values must be too high as the material has begun to exhibit nothing but purely elastic deformation at much lower velocities; that is, both energy drops have taken place at lower velocities. Since these values were calculated from static stress-strain curves, we must assume that the error comes about due to a change in the shape of the curves with increased velocity of testing.

Let us now consider the significance of the two sharp energy drops shown in Figs. 10 and 11. The first or lower velocity drop may be considered to be that corresponding to the highest velocity at which chain-chain slipping can take place; that is, this is the maximum velocity of response of D_3. Below this velocity the material exhibits very high amounts of plastic flow after yielding. The location of this drop on the velocity scale is not very dependent on temperature, and we may conclude that the relaxation time λ_3 is not very temperature-dependent in this range. The maximum velocity at which plastic deformation can take place depends on the ratio of t/λ in Equation [7], the ratio of the time of load application to the time of relaxation. This critical velocity varies slightly with temperature from approximately 0.0045 ips at 30 C to 0.02 ips at 90 C for the size specimens used.

The second energy drop on the velocity scale which appears in the 50, 70, and 90 C curves is that corresponding to the maximum strain rate for the response of D_2, that is, the retarded elastic response. This energy drop manifests itself in a distinct change in the shape of the stress-strain curve. At velocities lower than this critical velocity, curves such as A in Fig. 14 are obtained. At velocities above this critical value, the stress-strain curve has the shape of B. From this we may conclude that this energy drop corresponds to the maximum velocity of straining at which deviation from Hooke's law can appear. This critical velocity is very temperature-dependent, varying from 45 ips at 90 C to 0.06 ips at 50 C. This critical velocity is indistinguishable from the lower one at 30 C.

In the velocity range between the higher and lower critical rates of straining, the energy to break remains constant. This does not mean that the stress-strain curve remains the same over this velocity range, but rather that the strain at break is decreasing and the maximum load is increasing at such rates that the area under the curve remains constant.

After the upper critical velocity is exceeded, the material can respond only by purely elastic deformation D_1. A method of

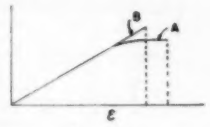

FIG. 14

predicting the energy for a completely elastic break from the slow-rate stress-strain curves is shown in the Appendix. The results obtained by this calculation correspond very nicely with the energy measured at very high velocities.

CONCLUSIONS

The conclusions to be drawn from this study may be divided into two parts. One is the theoretical interpretation in terms of the rheological properties and the structure of the material. The other is the practical application of the results.

From the theoretical point of view we may conclude that the rate of straining has a marked effect on the rheological properties:

1 The elongation at break decreases with increased straining rate according to Equation [17].

2 The ultimate strength or yield strength increases with the rate of loading according to Equation [16].

3 An increase in temperature acts similarly to a decrease in the rate of straining.

4 Two distinct energy drops can be found in the velocity scale.

5 These velocity drops are both at lower rates of straining than would be predicted by the von Kármán theory.

6 The lower critical velocity is the maximum straining rate at which plastic flow can take place; that is, above this velocity chain-chain slipping cannot take place. Above this rate of straining, the relaxation time of these bonds λ_2 is exceeded, and plastic flow cannot take place. The relaxation times of these bonds do not seem to be extremely temperature-dependent.

7 The second critical velocity is the maximum straining rate at which retarded elastic deformation can take place. This is the maximum rate of straining at which chain uncoiling can take place. Above this velocity the secondary bonds do not relax fast enough to permit changes in the configuration of the molecules. This relaxation time λ_3 is very temperature-sensitive—an increase in temperature causing a marked decrease in the relaxation times of the bonds involved.

8 Above the second critical velocity, only elastic deformation can take place. The energy to break at this velocity can be calculated from the slow-speed stress-strain curves.

9 The two critical velocities correspond to two relaxations in the material which are not usually observed in conventional relaxation tests since they occur too rapidly.

As for the practical application of the results the following conclusions can be reached:

10 Single velocity impact tests (such as the Izod) are not adequate for determining the shock-resistant properties.

11 Tension-type tests are of more value than flexural tests since the results can be more easily interpreted.

12 Quantitative design data can be obtained which may be used by engineers in planning plastic components provided the direction and velocity of impact blows can be predetermined.

In general, we may say that for a material to have a high impact strength it must have the ability to give with the blow. This may be accomplished in several ways. One is by a high truly elastic response, by requiring a large amount of energy to break above the second critical velocity. The second is by having either a very rapid retarded elastic response (this is a high second critical velocity), or by a high energy of retarded elastic response. The third is by a rapid plastic response.

The locations of the two critical velocities depend on the relaxation times λ_2 and λ_3 of the bonds involved, the sharpness of the energy drops being dependent on whether or not λ_2 and λ_3 are distinct relaxation times or broad spectra of relaxation times, the broad spectra of relaxation times causing the energy drops to be more gradual.

It is planned to continue this study with a similar investigation of other materials, such as rigid vinyl-chloride-acetate copolymer, to determine the relaxations involved in this material. It is also planned to study the effects of plasticizers on cellulose materials. It should prove interesting to see if the addition of plasticizers causes a shift in the critical velocities or a rise in the energy levels between the critical velocities.

BIBLIOGRAPHY

1 "Impact Testing of Plastics—I: Energy Considerations," by D. Telfair and H. K. Nason, *Modern Plastics*, vol. 20, 1943, pp. 85–88.

2 "Impact Testing of Plastics—II: Factors Which Influence the Energy Absorbed by the Specimen," by D. Telfair and H. K. Nason, *Modern Plastics*, vol. 22, 1945, pp. 145–149 and 186.

3 "Investigation of the Resistance to Impact Loading of Plastics," by H. Liander, C. Schaub, and A. Asplund, ASTM Bulletin No. 148, October, 1947, pp. 88–94.

4 "Preliminary Studies on a Drop Ball Impact Machine," by G. Lubin and R. R. Winans, ASTM Bulletin No. 128, May, 1944, pp. 13–18.

5 "A Ball Impact Tester for Plastics," by C. R. Stock, ASTM Bulletin No. 130, October, 1944, pp. 21–24.

6 "Laboratory Testing of Plastics—Small-Scale Impact Tester," by A. Bailey and O. W. Ward, ASTM Bulletin No. 140, May, 1946, pp. 50–54.

7 "The Significance of the Charpy and Flexure Tests in Evaluating the Impact Resistance of Plastics," by H. M. Quackenbos, Jr., J. M. Hill, Jr., and C. E. Staff, ASTM Bulletin No. 159, July, 1949, pp. 56–62.

8 "Impact Strength of Plastic Sheet," by C. S. Myers, *Modern Plastics*, vol. 20, October, 1942, pp. 81–87, 116, and 118.

9 "High-Speed Tension Tests at Elevated Temperatures," by M. Manjoine and A. Nadai, Proceedings of the ASTM, vol. 40, 1940, pp. 822–837.

10 "The Velocity Aspect of Tension—Impact Testing," by W. H. Hoppmann, II, Proceedings of the ASTM, vol. 47, 1947, pp. 533–544.

11 For a more detailed description see—"Essays in Rheology," British Rheologists' Club, Pitman Publishing Corporation, New York, N. Y., 1947.

12 "Calculation of Bulk Viscosity of Polyisobutylene From Relaxation of Stress Data," by R. D. Andrews and A. V. Tobolsky, Princeton University, Princeton, N. J., Plastics Laboratory Technical Report No. 16A, December, 1949.

13 "On the Propagation of Plastic Deformation in Solids," by Th. von Kármán, National Defense Research Council Report No. A-29, 1943.

14 "Impact Testing of Plastics: Elimination of the Toss Factor," by B. Maxwell and L. F. Rahm, ASTM Bulletin No. 161, October, 1949, pp. 44–47.

Appendix

CALCULATIONS FOR POLYMETHYL METHACRYLATE

The von Kármán method of calculating the maximum velocity of a plastic wave has been outlined in the section on basic theory.

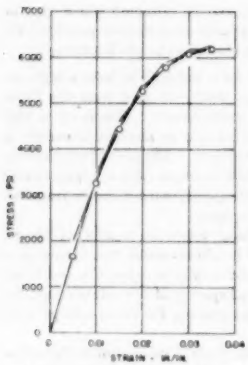

FIG. 15

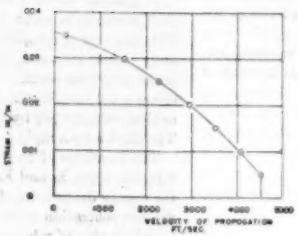

FIG. 16

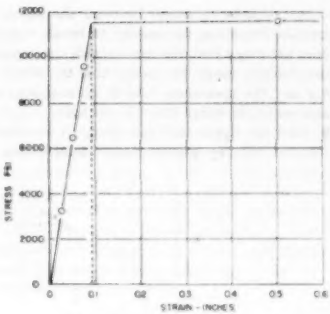

FIG. 18

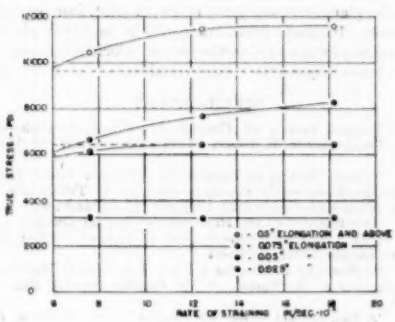

FIG. 17

The solution of Equation [15] may be found graphically as follows: The slope of the stress-strain curve for various values of strain is determined as shown in Fig. 15. The velocity of propagation corresponding to these slopes is then determined by dividing the slope by the mass density and taking the square root. These velocities of propagation are then plotted versus the strains at which they were determined as shown in Fig. 16. The area under this curve is the velocity of propagation of a plastic wave.

This calculation has been made for polymethyl methacrylate at 30, 50, and 70 C with the following results:

30 C, 136.8 fps
50 C, 108.2 fps
70 C, 87.5 fps

All of these rates are in the region beyond the second energy drop in Fig. 10; that is, at these rates of straining, only elastic deformation seems to be taking place. The theory assumes that the shape of the stress-strain curve does not change with rate of straining. Since Fig. 2 shows us that this is not a valid assumption, we may assume that the results obtained by this method are in error for this reason.

Calculation of Energy to Break Above Second Energy Drop

The following is a method of calculating the energy to break at velocities above the second energy drop, that is, when only elastic deformation takes place: Using the data in Fig. 2(*b*), the true stress for various values of strain at each velocity was calculated. Plotting these values as shown in Fig. 17, we see that the stress for any given strain varies with the rate of straining according to the relation

$$S = E\epsilon(1 - me^{-nR}) \quad [18]$$

that is, as the rate of straining is increased, the value of stress for any given strain asymptotically approaches the value of $E\epsilon$. Similarly, the true stress after yielding approaches some constant value as the rate of straining is increased.

A plot of these asymptotes versus the strain, as shown in Fig. 18, gives the maximum strain for elastic deformation, and the area under this line up to the yield point gives the energy to break elastically. The value calculated from these data at 50 C is 0.92 ft-lb.

This compares quite favorably with the energy to break after the second critical velocity in Fig. 10, approximately 0.9 ft-lb.

Discussion

I. L. Hopkins.[1] This paper presents a promising method of analysis, and it is quite possible that the ultimate description of physical properties at all rates of stress will be on some such basis.

In the treatment of the tensile test at constant rates, according to the model in Fig. 4, the expression for force as a function of test rate and time might be more revealing than Equation [7]. The expression is of the form

$$S = E_1 V [(e^{-at} - e^{-bt}) + b\lambda_2(1 - e^{-at}) - a\lambda_2(1 - e^{-bt})]/(b - a)$$

where V is the test rate and a and b are functions of E and λ only. This shows quite clearly that if the model in Fig. 4 is valid then

(*a*) The stress S at any time is proportional to the velocity.

(*b*) When t is very small $S = E_1 Vt = E\epsilon$, which is observed in the early straight-line parts of the plots in Fig. 2.

(*c*) When t is very large $S = E_1 V \lambda_1$ which again is proportional to V, but certainly does not show up in the later parts of the curves in Fig. 2. Such a function also fails to account for the maxima observed in the actual tests. In fact, any linear structure must fail in these respects.

The comment after Equation [13] is difficult to understand. The equation indicates that the stress is equal to Young's modulus when $V_0 = V_s$. Since the tensile strength is ordinarily only a

[1] Bell Telephone Laboratories, Inc., Murray Hill, N. J.

fraction of the modulus, it would seem that the rupture would occur at a much lower velocity than V_r. This may account for some of the discrepancy between the observed critical velocities and those calculated by the von Kármán theory.

It is especially interesting and important that the authors have available the means for testing over such a wide continuous range of strain rates. It is to be hoped that further data on other materials will be made available and that this may lead to the development of more satisfactory models.

Author's Closure

Mr. Hopkins proposes that the expression for stress as a function of rate of loading is preferable to the expression for strain, Equation [7]. Since the energy to break is a function of both the stress and the strain any interpretation of the results of our tests should include a consideration of both equations.

The comments on the interpretation of Equation [13] seem valid and the author would like to thank Mr. Hopkins for his assistance in clarifying this point.

An Investigation of Electromagnetic Flowmeters[1]

By H. G. ELROD, JR.,[2] AND R. R. FOUSE,[3] ALLIANCE, OHIO

The measurement of the flow of molten corrosive metals in small sizes of conduit presents a number of difficulties. Of the devices and methods for accomplishing such a measurement, electromagnetic (EM) flowmeters appear to possess the greatest number of advantages. Accordingly, the work described in this paper was undertaken to acquire further knowledge of the characteristics of these instruments and some experience in their operation.

A Working Formula and a Design of EM Flowmeter

FIG. 1 shows two schematic views of an EM flowmeter. Flowmeters of similar type have been described and analyzed in the literature (see the Bibliography of this paper). A conducting fluid passes through a uniform magnetic field in a tube made of nonmagnetic material. An electromotive force (emf) is thereby generated normal to both the fluid motion and the direction of the magnetic field. This emf is directly proportional to the volumetric-mean fluid velocity, and can be used as an indication of the magnitude of the flow. In Fig. 1 a permanent magnet is shown, although a 60-cycle electromagnet also might be used.

In terms of pertinent physical variables, the flowmeter emf is given by

$$E = (BVd)10^{-8}\left[\frac{2\,\frac{d}{D}}{1+\left(\frac{d}{D}\right)^2+\frac{\rho_f}{\rho_w}\left\{1-\left(\frac{d}{D}\right)^2\right\}}\right] \quad [1]$$

where

E = generated emf across contact points shown in Fig. 1, mv
B = magnetic induction between magnetic poles, gausses
d, D = tube ID and OD, respectively, cm
V = volumetric-mean fluid velocity, cm per sec
ρ_f, ρ_w = electrical resistivities of fluid and wall material, respectively, any consistent dimensions

A detailed derivation of this flowmeter formula is given in the Appendix of this paper. The wall-correction term in square brackets is a result of the present research, the remainder of the formula having been derived previously (1, 2).[4] Obviously, this term is of importance in cases where metal tube walls must be used. In the derivation of Equation [1] it is assumed that the interface resistance between the fluid and the tube wall is negligible, that the fluid velocity distribution is axially symmetric [$v = f(r)$], and that the magnetic field is uniform and infinite in the axial direction. Subject to these assumptions, Equation [1] represents an exact solution of Maxwell's field equations.

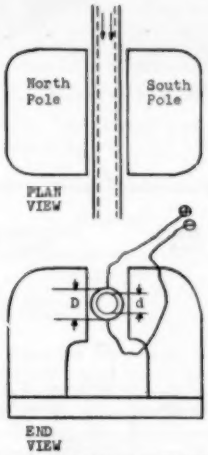

FIG. 1 SCHEMATIC DIAGRAM OF EM FLOWMETER

The predictions of Equation [1] are compared with experiment later in the paper, Fig. 5. In view of the variety of physical measurements needed to effect these comparisons, the agreement may be considered quite satisfactory. It will be observed that with practically no exceptions, all experimental emf's lie in the range of 92–100 per cent of the theoretical emf's. (In Fig. 5 Equation [1] is tested on a basis of emf, rather than on velocity.)

Recommended Flowmeter

The flowmeter described in this section is recommended, not because it is necessarily the best that might be devised, but because of the simplicity and reliability of its operation. Fig. 2 shows its main components, which are as follows: Two permanent magnets to provide an intense magnetic field, two soft-iron slabs to spread this field and make it uniform, a brass disk which rotates in the magnetic field with two brass wires to contact its hub and periphery, a stainless-steel housing for the fiber bearings which support the disk shaft, and a synchronous motor.

---

[1] The work described in this paper was performed at The Babcock & Wilcox Company, Research and Development Department, under subcontract with the NEPA Division, Fairchild Engine and Airplane Corporation, Oak Ridge, Tenn.

[2] Research Engineer, The Babcock & Wilcox Research and Development Department.

[3] Test Engineer, The Babcock & Wilcox Research and Development Department.

Contributed by the Fluid Meters Research Committee and Industrial Instruments and Regulators Division and presented at the Annual Meeting, Atlantic City, N. J., November 25–30, 1951, of THE AMERICAN SOCIETY OF MECHANICAL ENGINEERS.

NOTE: Statements and opinions advanced in papers are to be understood as individual expressions of their authors, and not those of the Society. Manuscript received at ASME Headquarters, September 27, 1951. Paper No. 51—A-79.

[4] Numbers in parentheses refer to the Bibliography at the end of the paper.

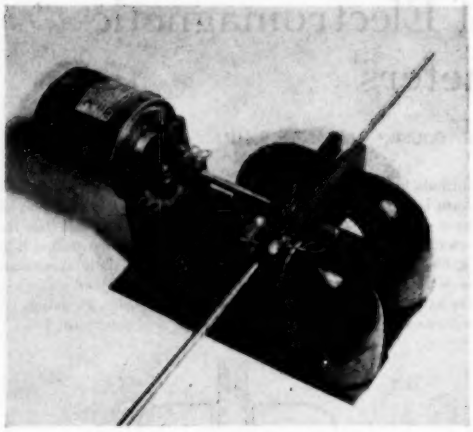

FIG. 2 VIEW OF FLOWMETER

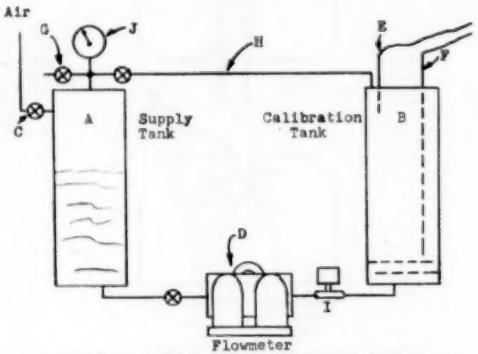

FIG. 3 SCHEMATIC SKETCH OF EXPERIMENTAL APPARATUS

The emf connections to the flow tubing should be located carefully at opposite ends of a diameter normal to the magnetic field and centrally located with respect to the rotating disk. In order to make these contacts, fine wires may be soldered or spot-welded to the metal tubing, but all excess solder should be filed from the tube surface.

To eliminate the possibility of undetected changes of magnetic-field strength, an emf is measured across a radius of the rotating disk (known as a homopolar generator, reference 3). If the emf leads for this generator, or gaussmeter, are of the same composition as the disk and shaft, no important thermoelectric effect will be observed. In the case of the flowmeter under test the brasses for the disk and the wire brushes were not of the same origin, yet a temperature difference of 600 F between contacts altered the gaussmeter emf by less than 1 per cent.

The emf's of both the flow circuit and the gaussmeter may be read on a standard potentiometer designed for use with thermocouples. The flow-circuit emf appears directly in Equation [1]. The gaussmeter emf, on the other hand, is used to compute the induction of the magnetic field by means of the following equation

$$B = \frac{2E \times 10^8}{\omega(R^2 - r^2)} \quad \ldots\ldots\ldots\ldots\ldots\ldots\ldots\ldots [2]$$

where

E = generated emf between disk hub and periphery, mv
B = magnetic induction between magnetic poles, gausses
r, R = hub radius and disk radius, respectively, cm
ω = angular velocity of disk, radians per sec

EXPERIMENTAL CONFIRMATION OF FLOWMETER FORMULA

Experimental Procedure. The apparatus used to check experimentally flowmeter Equation [1] is shown in the schematic diagram of Fig. 3. During a run, mercury was pushed from tank A to tank B by means of compressed air supplied through line C. The flow velocity at the flowmeter section D was calculated from the time taken to effect a known volumetric displacement in tank B between electrodes E and F, and from a knowledge of the inside diameter of the tube at D. During the transfer process, the system was stabilized by bleeding considerable air out to atmosphere through valve G. Return of the mercury to tank A could be accomplished by applying a back pressure through line H. The solenoid valve I was inserted in the mercury flow circuit to guard against blowout. The pressures recorded by gage J served to set the conditions of operation.

Both alternating and direct current and flowmeters were tested on the foregoing circuit. In both cases Equation [1] was checked by experimental evaluation of each term contained in it. The details of these evaluations will now be grouped according to the physical quantity concerned.

Flow-Circuit Emf (E). Positioning of the contacts for determining the flow-circuit emf has been partly discussed already. Two types of tubing were employed in the present tests. The first type was made of polystyrene, and in this case small brass rods of 0.025 in. OD were brought in on opposite sides of the tube until they were approximately flush with the inner surface. The second type of tubing was made of an alloy called "Advance," similar in composition to constantan. In this case the contacts were made as described earlier. Both the brass and the Advance alloy were chosen because mercury alloys slowly with each of them, and it was believed that, consequently, the fluid-solid interface resistance would be very small. Moreover, both materials are nonmagnetic.

When the a-c flowmeter tests were made, considerable effort was spent in reducing the "base pickup." Even without any flow in the tubing, the changing magnetic field of the a-c electromagnet generated an emf in the leads to the flow-circuit contacts. This pickup was reduced considerably by the use of twisted and shielded leads, but it could not be reduced to a negligible magnitude.

The d-c flow-circuit emf's were read with a Leeds and Northrup precision potentiometer, No. 8662, with a range of 0–80 millivolts. The a-c emf's were measured with a Ballantine electronic voltmeter, Mod. 300, in conjunction with a Ballantine decade amplifier, Mod. 220. This combination provides a range of 0.00001 to 100 volts. Both the d-c and a-c instruments give a precision of better than 0.01 mv. Their accuracy was not checked against standards, but since they were used both for the determination of the flow emf and the magnetic-field strength, it is clear from Equation [1] that any constant percentage errors, at least, would not affect verification of the flowmeter formula.

During an experimental run the flow velocity would decrease slightly due to a changing static head of mercury. To correct approximately for this effect, the initial and final flow emf's were averaged arithmetically.

Magnetic-Field Induction (B). The procedure and formula for finding the field strength between the permanent magnets of the d-c flowmeter have been given already. Pertinent physical values for the gaussmeter are as follows:

Diameter of brass disk, 2.098 in.
Diameter of disk hub, 0.127 in.
Rpm of disk, 1800 (synchronous speed)

The entire field contained between the soft-iron slabs of the d-c flowmeter was explored with a General Electric gaussmeter, Mod. 409X59, No. 2053678, and was found to be surprisingly uniform. The results obtained for the particular portion covered by the rotating disk are given in Table 1.

TABLE 1 RESULTS WITH ROTATING DISK

Distance from hub, in.	Angle in plane of disk, deg	Magnetic induction, gausses
0	...	1940
1/2	0	1980
1	0	2000
1/2	90	1995
1	90	1900
1/2	180	1970
1	180	1970
1/2	270	1980
1	270	1950

The area-mean field strength for the measurements in Table 1 is 1972 gausses. At the same time the rotating disk generated 13.44 mv, for which the corresponding magnetic induction is 2016 gausses. The discrepancy was approximately 2 per cent. The *magnetic induction of 2016* was assumed to be correct.

The field strength for the a-c electromagnet was determined in quite a different manner. An isometric sketch of the jaws of this magnet is shown in Fig. 4. For a winding current of 15

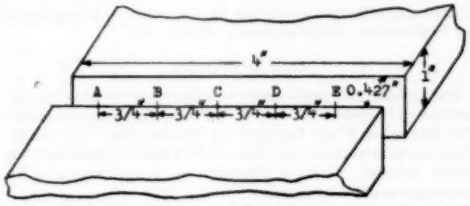

FIG. 4 LOCATIONS OF MAGNETIC-FIELD DETERMINATIONS ON A-C MAGNET

amp (which was maintained constant during all subsequent a-c experiments), millivolt readings were obtained from a 10-turn coil of 0.493 in. diam at the locations indicated. The leads to this coil were twisted closely to minimize extraneous pickup. The results are as follows:

Location	A	B	C	D	E
Millivolts	8.55	8.80	8.80	8.75	8.30

The corresponding area-mean induction for the section from B to D is 1892 gausses and this value was used in subsequent calculations.

Fluid Velocity (V). As stated before, the fluid velocity was deduced from the time required to pass a known volume of mercury through a known size of tubing. The measurements of the displacement volume were as follows:

Inside diameter, in.	2.070
Spacing between electrodes, in.	5
Weight of Hg held between electrodes, g (at 20 C)	3752.5

From the displacement-volume geometry a volume of 16.83 cu in. is calculated, whereas the volume corresponding to the weighed mercury is 16.90 cu in. A volume of 16.87 cu in. was used in subsequent calculations.

The displacement time was read on several different stop watches. These watches were not calibrated, but no discrepancies attributable to their use were observed.

The methods used for finding flow-tube ID's are described in the next section.

Tube Diameters (d) *and* (D). The ID of the polystyrene tubing was determined by measuring the axial extension of a known volume of mercury. Two measurements of this diameter gave the dimensions of 0.1923 in. and 0.1936 in., respectively. An ID of 0.193 in. was used in subsequent calculations. The brass electrodes for obtaining the flow emf were brought snugly to bear on a 0.180-in-OD rod inserted through the flow section. Thus the emf contacts were not quite flush with the inner tube surface. The external diameter of the polystyrene tube was of no importance.

The ID of the Advance alloy tubing was determined by four independent methods: (a) By the insertion of various drills into the tubing it was ascertained that the ID exceeded 0.1935 in. (b) A microscope traverse gave a value of 0.1953 in. (c) A filling with mercury, as in the case of the polystyrene tubing, yielded 0.1958 in. (d) A known length of tubing was weighed. From a knowledge of its weight, its external dimensions, and the density of the Advance alloy, the ID of the tubing was calculated to be 0.1973 in. An ID of 0.196 in. was used in subsequent calculations. The OD measurements of the flow section were averaged with respect to length and polar angle to give an external diameter of 0.335 in.

Physical Properties. The physical properties employed in computations are given in Table 2.

TABLE 2 PHYSICAL PROPERTIES EMPLOYED IN COMPUTATIONS

MERCURY	
Specific gravity at 20 C	13.548
Electrical resistivity at 20 C, microhm-cm	95.78
ADVANCE ALLOY (2)	
Nominal composition	55 Cu, 45 Ni
Density at 20 C, grams per cc	8.83
Resistivity at 20 C microhm-cm	49

Comparison of Theory and Experiment. In Fig. 5 the experimentally determined emf's from two a-c and two d-c runs are plotted as percentage deviations from the theoretical flowmeter formula, Equation [1]. The same data are listed in Table 3.

The discrepancy between theory and experiment as illustrated in this figure is so small, and the number of measurements entering into the comparisons is so large, that it is difficult to assign

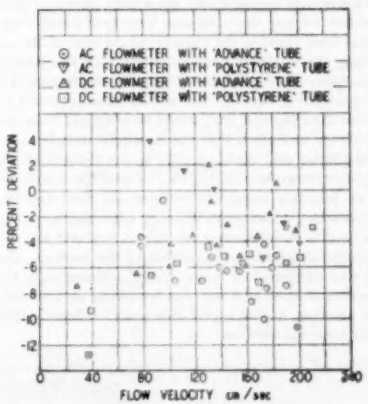

FIG. 5 PERCENTAGE DEVIATION OF EXPERIMENTAL RESULTS FROM THEORETICAL FORMULA

TABLE 3 EXPERIMENTAL DATA FOR FLOWMETERS

Time to fill displacement tank, min	Millivolts at no flow (180 deg phase)	Millivolts with flow (0 deg phase)	Total millivolts (0 deg phase)	Flow velocity cm per sec
A-C Flowmeter With Advance Tube				
0.250	0.160	0.235	0.395	94.7
0.179	0.157	0.370	0.527	132.2
0.165	0.157	0.408	0.565	143.5
0.145	0.159	0.466	0.625	163.2
0.135	0.158	0.522	0.680	175.3
0.130	0.158	0.570	0.728	182.1
0.124	0.158	0.620	0.778	190.9
0.302	0.174	0.143	0.317	78.4
0.302	0.174	0.141	0.315	78.4
0.229	0.170	0.235	0.405	103.4
0.190	0.174	0.313	0.487	124.6
0.171	0.175	0.372	0.547	138.4
0.154	0.173	0.432	0.605	153.7
0.137	0.172	0.480	0.652	172.8
0.125	0.178	0.558	0.736	189.4
0.120	0.175	0.564	0.739	197.3
A-C Flowmeter With Polystyrene Tube				
0.287	0.070	0.755	0.825	85.1
0.217	0.083	0.975	1.058	112.5
0.180	0.081	1.185	1.266	135.6
0.142	0.085	1.420	1.505	171.9
0.130	0.085	1.625	1.710	187.8
0.122	0.075	1.700	1.775	200.1
Time to fill displacement tank, min	**Gaussmeter, mv**	**Flowmeter, mv**		**Flow velocity, cm per sec**
D-C Flowmeter With Advance Tube				
0.814	13.407	0.120		29.1
0.320	...	0.308		74.0
0.236	...	0.420		100.3
0.235	...	0.430		100.7
0.200	13.377	0.509		118.4
0.181	...	0.593		130.8
0.150	...	0.663		157.8
0.141	...	0.720		167.9
0.133	...	0.780		177.9
0.129	...	0.824		183.5
0.120	13.361	0.850		197.2
0.173	13.403	0.584		136.8
0.180	...	0.580		131.5
0.163	...	0.628		145.2
0.154	...	0.650		153.7
D-C Flowmeter With Polystyrene Tube				
39.6 secs.	13.435	0.320		37.0
37.5	...	0.352		39.1
18.2	13.530	0.748		80.5
13.9	...	0.982		105.4
11.4	...	1.213		128.5
10.3	...	1.336		142.2
9.1	...	1.515		161.0
8.2	...	1.650		178.7
7.7	...	1.781		190.3
7.3	...	1.898		200.7
6.9	13.448	2.025		212.3
9.4	13.471	1.452		155.9
8.7	...	1.550		168.4

causes for the differences that do exist. The location and finite size of the flow-emf contacts may have been sources of error. On the Advance tubing the contacts were positioned "by eye," and, as has been pointed out already, in the case of the polystyrene tubing, the contacts were not flush with the internal surface of the tube. It can be shown that the emf measured by two contacts protruding slightly into a fluid stream should be only slightly less than the emf that would be obtained from the same contacts if they were flush with the stream boundaries. It is this last full-diameter emf which is used as the theoretical standard for the polystyrene runs in Fig. 5. A possible source of error may be an interface resistance between the fluid and the tube wall or contacts. In some preliminary experiments, where mercury was used in stainless-steel tubing, no flow emf was obtained from contacts attached to the outside of the tubing. The phenomenon was attributed to "nonwetting." However, in the present experiments slow alloying was occurring at the surface of electrical junction, and it is probable that the liquid-solid interfacial resistance was very low.

The agreement between flowmeter theory and experiment, as found in the present series of experiments, compares favorably with that obtainable with flow nozzles. Certainly the flowmeter formula should be tested with fluids other than mercury, and with additional wall materials, but it may be assumed tentatively that EM flowmeters can provide, without special calibration, sufficient accuracy for many purposes.

Summary and Conclusions

1 The theory of EM flowmeters has been generalized to account for the short circuiting by a conducting tube wall of the electromotive force (emf) generated by the internal flow.

2 The theory has been confirmed, in the case of mercury, by tests with alternating-current and direct-current flowmeters, and with both conducting and nonconducting tube walls.

3 An EM flowmeter has been developed to conform with the theory, and sufficient information is given in the paper to permit this flowmeter to be reproduced.

4 On the basis of the experiments performed with mercury, and the physical assumptions required for the theoretical analysis, the following empirical relation may be employed tentatively:

$$\begin{pmatrix}\text{Actual volumetric-}\\\text{mean velocity}\end{pmatrix} = (1.04 \pm 0.04)\begin{pmatrix}\text{Theoretical velocity}\\\text{based on experimental emf}\end{pmatrix}$$

provided (*a*) the fluid wets the tube wall or emf contacts; (*b*) the applied magnetic field is adjusted to a low value. Distortion of the fluid-velocity profile is thereby minimized.[8]

Acknowledgment

The authors wish particularly to acknowledge the helpful suggestions and assistance of Mr. W. T. Hage, Electronics Engineer, The Babcock & Wilcox Research and Development Department. They also wish to thank The Babcock & Wilcox Company and the NEPA Division, Fairchild Engine & Airplane Corporation for permission to publish this paper.

BIBLIOGRAPHY

1 "An Alternating Field Induction Flowmeter of High Sensitivity," by A. Kolin, *Review of Scientific Instruments*, vol. 16, 1945, p. 109.

2 "Methode für electrischen Geschwindigkeitsmessung von Flüssigkeiten," by B. Thürlemann, *Helvetica Physica Acta*, vol. 14, pp. 383–419.

3 "Principles of Electricity and Electromagnetism," by G. P. Harnwell, McGraw-Hill Book Company, Inc., New York, N. Y., 1949, p. 429.

4 "A Variable Phase Transformer and Its Use as an A.C. Interference Eliminator," by A. Kolin, *Review of Scientific Instruments*, vol. 12, 1941, p. 555.

5 "Metals Reference Book," by C. J. Smithells, Interscience Publishers, Inc., New York, N. Y., 1949, p. 553.

6 "An Electromagnetic Blood Flow Meter," by J. W. Clark and J. E. Randall, *Review of Scientific Instruments*, vol. 20, 1949, pp. 951–954.

7 "Fluid Velocity—Measurement and Control," by E. M. Bennett, *Radio and Television News*, vol. 43, February, 1949, p. 10.

8 "Experimental Investigations of Magneto—Hydrodynamic Waves," by J. Lundquist, *Physical Review*, vol. 76, December 15, 1949, p. 1805.

[8] Further study is being given to this aspect of the EM flowmeter problem.

Appendix

Derivation of Flowmeter Formula

Maxwell's equations for a fluid conductor are given by Lundquist (8) in the following form

$$\nabla \times \frac{\vec{B}}{\mu\mu_0} = \vec{i} \quad [3]$$

$$\nabla \times \vec{E} = -\frac{\partial \vec{B}}{\partial t} \quad [4]$$

$$\nabla \cdot \vec{B} = 0 \quad [5]$$

$$\vec{i} = \sigma(\vec{E} + \vec{V} \times \vec{B}) \quad [6]$$

In addition, the following two equations involving the flow and its acceleration are applicable

$$\nabla \cdot \vec{V} = 0 \quad [7]$$

and

$$\rho \left\{ \frac{\partial \vec{V}}{\partial t} + (\vec{V}\nabla)\vec{V} \right\} = -\nabla p + \vec{i} \times \vec{B} + \vec{F} \quad [8]$$

In the foregoing equations the MKS system has been used; thus

$\vec{B}$ = magnetic flux density, webers per sq m
μ = magnetic permeability of material, dimensionless
μ_0 = magnetic permeability of free space, 1.257×10^{-6}, henries per m
$\vec{i}$ = current density, amp per sq m
$\vec{E}$ = electric field vector, volts per m
t = time, sec
σ = electrical conductivity, mho per m
$\vec{V}$ = fluid velocity, mps
ρ = fluid density, kg per cu m
p = pressure, newtons per sq m
$\vec{F}$ = frictional shear, newtons per sq m

We shall apply Equations [3] to [8] to the physical situation shown in Fig. 1.

To find a useful solution to the foregoing equations, we take as starting point the following assumptions:

1 Steady conditions so that

$$\frac{\partial}{\partial t} = 0 \quad [9]$$

Thus the flowmeter magnets are assumed to be permanent.

2 The magnet, which is of uniform construction, extends an infinite distance along the tube. Then

$$\frac{\partial^n}{\partial z^n} = 0, \; n = 1,2 \quad [10]$$

3 All fluid velocities are parallel to the tube axis, that is

$$\vec{V} = \hat{\kappa} V(x, y) \quad [11]$$

According to Equations [4] and [9]

$$\nabla \times \vec{E} = 0, \text{ or } \vec{E} \equiv -\nabla U \quad [12]$$

If, then, we eliminate $\vec{i}$ between Equations [3] and [6] by taking the curl of each, we obtain

$$\nabla^2 \vec{B} = -\sigma\mu_0[(\vec{B}\nabla)\vec{V} - (\vec{V}\nabla)\vec{B}] \quad [13]$$

(Note: Equations [5] and [7] were used to reduce Equation [13].)

The following components of $\vec{B}$ are consistent with both Equation [13] and Equation [5]

$$B_z = \text{const}; \; B_y = 0; \; B_x = B_x(x, y) \quad [14]$$

Physically, it seems simpler to work with the electric potential U. Therefore we take the divergence of Equation [6] and obtain

$$\Delta^2 U = \nabla \cdot \hat{j} \, VB_x \quad [15]$$

Equation [15] is valid for any axially directed velocity distribution.

Now, in fully developed turbulent flow the velocity distribution is axially symmetric, and this distribution we shall now assume.

If $\hat{r}$ and $\hat{\theta}$ are used to denote unit vectors in the r and θ-directions, respectively, we have

$$\hat{j} = \hat{r} \sin\theta + \hat{\theta} \cos\theta \quad [16]$$

and

$$\nabla \cdot \hat{j} \, vB_x = \frac{B_z}{r}\left[\frac{\partial}{\partial r} rV(r) \sin\theta + \frac{\partial}{\partial\theta} V(r) \cos\theta\right] \quad [17]$$

$$= B_z V'(r) \sin\theta \quad [18]$$

$$\therefore \frac{\partial^2 U}{\partial r^2} + \frac{1}{r}\frac{\partial U}{\partial r} + \frac{1}{r^2}\frac{\partial^2 U}{\partial\theta^2} = B_z V'(r) \sin\theta \quad [19]$$

As a particular solution for the potential field within the fluid we try

$$U_f = F(r) \sin\theta \quad [20]$$

First we insert this solution in Equation [19] and then perform the integrations indicated

$$F''(r) + \frac{1}{r}F'(r) - \frac{F(r)}{r^2} = B_z V'(r) \quad [21]$$

$$F'(r) + \left(\frac{F(r)}{r}\right)' = B_z V'(r) \quad [22]$$

$$F'(r) + \frac{F(r)}{r} = B_z V(r) + K \quad [23]$$

$$[rF(r)]' = B_z V(r) r + Kr \quad [24]$$

$$rF(r) = B_z \int_0^r V(r) \, r dr + K\frac{r^2}{2} \quad [25]$$

At $r = a = d/2$ the fluid velocity is necessarily zero. Thus from Equation [23] we have

$$F'(a) + \frac{F(a)}{a} = K \quad [26]$$

Also, Equation [25] may be rewritten in terms of the volumetric-mean velocity $\overline{V}$, to give

$$\frac{F(a)}{a} = \frac{B_z \overline{V}}{2} + \frac{K}{2} \quad [27]$$

The integration constant K can now be eliminated from Equations [26] and [27] to give

$$F(a) = B_z \bar{V} a + aF'(a) \quad [28]$$

The boundary conditions to be applied at the interface between the fluid and the wall material are as follows:

(*a*) The continuity of the normal component of the current

$$\sigma_f (E_r)_f = \sigma_w (E_r)_w \quad [29]$$

(*b*) The continuity of the transverse component of the electric-field vector

$$(E_\theta)_f = (E_\theta)_w \quad [30]$$

Turning now to the electric potential within the tube wall, we try the particular solution

$$U_w = G(r) \sin \theta \quad [31]$$

Since this potential must satisfy Equation [21] with $V'(r) = 0$, we have

$$G''(r) + \frac{G'(r)}{r} - \frac{G(r)}{r^2} = 0 \quad [32]$$

Now at $r = b = D/2$, the radial component of the electric field vector must vanish. By manipulations similar to those performed earlier we easily deduce that

$$G(r) = \frac{G(b)}{2} \left(\frac{r}{b} + \frac{b}{r} \right) \quad [33]$$

We proceed next to match the fluid and wall solutions at the interface according to Equations [29] and [30]. Equation [28] will be satisfied if

$$\sigma_f F'(a) = \sigma_w G'(a) \quad [34]$$

Equation [29] will be satisfied if

$$F(a) = G(a) \quad [35]$$

Putting $F(a)$ and $F'(a)$ in terms of $G(a)$ and $G'(a)$ in Equation [28], we obtain

$$\frac{G(b)}{2} \left(\frac{a}{b} + \frac{b}{a} \right) = B_z \bar{V} a + \frac{\sigma_w}{\sigma_f} \frac{G(b)}{2} \left(\frac{1}{b} - \frac{b}{a^2} \right) \quad [36]$$

This last equation can be rearranged to give

$$G(b) = B_z \bar{V} d \frac{\frac{d}{D}}{1 + \left(\frac{d}{D} \right)^2 + \frac{\sigma_w}{\sigma_f} \left[1 - \left(\frac{d}{D} \right)^2 \right]} \quad [37]$$

According to Equation [31] the maximum potential difference at the outside of the tube will be $U_w (b, \pi/2) - U_w (b, -\pi/2)$. Therefore

$$E = B_z \bar{V} d \left[\frac{2 \frac{d}{D}}{1 + \left(\frac{d}{D} \right)^2 + \frac{\sigma_w}{\sigma_f} \left\{ 1 - \left(\frac{d}{D} \right)^2 \right\}} \right] \quad [38]$$

This result, in slightly more convenient units, is given as Equation [1] of the paper.

Discussion

L. Grossman[6] and A. Charwat.[7] The authors of the paper have made a significant contribution to the technique of electromagnetic flow measurement by deriving a relation permitting the calculation of the induced emf in the case of an axisymmetric flow bounded by a "conducting" wall.

In the derivation of this equation, however, the authors were required to assume that the magnetic field is infinite and uniform in the axial direction. This is a rather restrictive assumption and limits the applicability of the derived correction for wall conductivity. The agreement of the authors' measured results with those derived from theory is indeed excellent, but may be due to the geometry of the experimental setup and the fluid used. It is felt, for example, that the large length-of-field to diameter ratio used in the experiment strongly reduced the influence of the short-circuiting resulting from axial conduction but that this favorable ratio might be difficult to achieve in many practical cases. It would be interesting to see the effect of increasing the tube diameter and carrying out experiments on fluids of varying conductivity.

As the authors point out, the induction equation for flow-rate measurements in the case of nonconducting walls has been well confirmed by previous investigators. Probably the most accurate measurements were reported in a paper by Thürlemann (8) of the authors' Bibliography.

At the University of California we have been engaged in the development of an apparatus using the same principle as that employed by the authors for studying the details of turbulent velocity fluctuations in liquid flow in a circular pipe. We have found good agreement with the theoretical relation for average velocity traverses and have obtained reliable data relating to the microstructure of turbulent fluctuations in a liquid flow.

Authors' Closure

The authors appreciate the comments of Messrs. Grossman and Charwat and are in essential agreement with them. For the work reported in the present paper, time requirements indicated the choice of a magnetic field long enough to eliminate field length as an important variable. This choice yielded an EM flowmeter for which there is a simple theory. It is true, however, that the geometry of our recommended flowmeter can become awkward for larger sizes of fluid conduit. At the Case Institute of Technology a research program has been drawn up to determine the effects of length and strength of magnetic field, fluid properties (especially electrical conductivity and mass density), surface wetting, etc.

It is to be hoped that this work together with the considerable research being undertaken by the discussers and others, will eventually make the EM flowmeter as well understood and predictable as more conventional fluid meters.

---

[6] Assistant Professor, Department of Mechanical Engineering, University of California, Berkeley, Calif.

[7] Instructor, Department of Mechanical Engineering, University of California. Jun. ASME.

Analysis of Some Hydraulic Components Used in Regulators and Servomechanisms

By S. Z. DUSHKES[1] and S. L. CAHN[2]

Hydraulic servomechanisms have come into wide use in recent years as a result of the low inertia of hydraulic servomotors compared to electric servomotors of the same power rating. This paper discusses the theory of operation, static characteristics, and dynamic characteristics of some hydraulic components that have been used for many years in regulator applications. Previously, the dynamics of these components were not of great importance because of the slowness of the processes controlled. The important considerations were static gain and static accuracy. The dynamic characteristics have been investigated more recently as a result of the high dynamic-performance demands of servomechanism applications. Dynamics are considered from the frequency-response approach.

THE hydraulic components that will be investigated in this paper are the jet pipe, distributor block, and auxiliary piston. The jet pipe and distributor block constitute a hydraulic integrator and may be used directly with a cylinder where neither high static gain nor a high maximum cylinder speed is required. In applications requiring high static gain and high maximum cylinder speed, a pilot valve is used as the integrator and is stroked by an auxiliary piston operating from a jet pipe. The jet pipe and auxiliary piston constitute a positional servomechanism utilizing unity feedback.

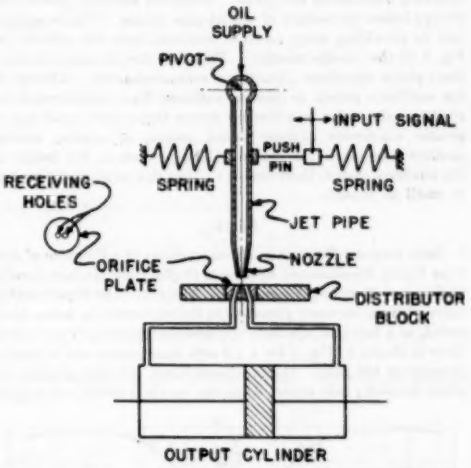

FIG. 1 SCHEMATIC DIAGRAM OF JET PIPE, DISTRIBUTOR BLOCK, AND CYLINDER

THEORY OF OPERATION

Jet Pipe, Distributor Block, and Cylinder (Fig. 1). The jet pipe is a tube pivoted at one end and terminating in a small-diameter nozzle at the other end. It is connected to a constant-pressure oil supply at the pivoted end. The oil flow through the jet pipe is constant and depends upon the supply pressure and nozzle diameter. The input signal to the jet pipe is a torque (or force) from a low-power impulse system and is applied to the jet pipe through the push pin. The jet pipe is spring-loaded by opposing compression springs so that the nozzle displacement is proportional to the applied torque about the jet-pipe pivot. Displacement-error signals could be used to deflect the jet pipe directly but seldom are available. Most physical quantities to be controlled can be converted easily to torque or force. Small electric torque motors are especially useful where electrical-data transmission systems must be used. The oil jet from the nozzle impinges on an orifice plate (in a distributor block) which has two closely spaced receiving holes drilled in it. These holes are connected to opposite ends of a cylinder. When the jet-pipe nozzle is centered over the receiving holes, equal static recovery pressures will exist in the receiving holes and the output cylinder will not move. When the jet pipe is displaced from its centered position, more oil will impinge on one receiving hole than on the other, resulting in different static recovery pressures in the two receiving holes. The cylinder will then move with a speed proportional to the nozzle displacement from the centered position, with the cylinder flow being taken from the jet-pipe flow. Since the jet pipe supplies the oil flow to the cylinder, the maximum

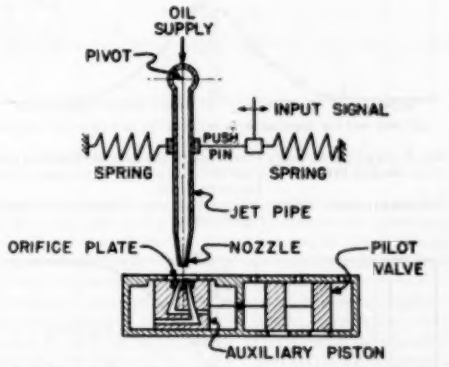

FIG. 2 SCHEMATIC DIAGRAM OF JET PIPE AND AUXILIARY PISTON

[1] Special Devices Division, Askania Regulator Company, Chicago, Ill. Now, Hydraulic Controls Division, Mare Island Naval Shipyard, Vallejo, Calif.

[2] North American Aviation, Downey, Calif.

Contributed by the Industrial Instrument and Regulators Division and presented at the Annual Meeting, Atlantic City, N. J., Nov. 25–30, 1951, of THE AMERICAN SOCIETY OF MECHANICAL ENGINEERS.

NOTE: Statements and opinions advanced in papers are to be understood as individual expressions of their authors and not those of the Society. Manuscript received at ASME Headquarters, July 13, 1951. Paper No. 51—A-22.

cylinder speed will depend upon the jet-pipe flow and will occur when the nozzle is directly over one receiving hole.

Jet Pipe and Auxiliary Piston (Fig. 2). In Fig. 2 the auxiliary piston is shown as it is used with the jet pipe. The orifice plate is in the auxiliary piston and the receiving holes connect with passages leading to opposite ends of the piston. Whenever the nozzle is displaced from the centered position over the receiving holes, the piston will move in such a direction as to recenter the receiving holes under the nozzle. Thus the auxiliary piston will always follow the motion of the jet-pipe nozzle. This is equivalent to providing unity position feedback from the cylinder in Fig. 1 to the jet-pipe nozzle. Therefore the jet pipe and auxiliary piston constitute a positional servomechanism. The use of the auxiliary piston to provide sufficient force amplification to stroke a pilot valve and thereby obtain higher static gain and a greater maximum cylinder speed means, of course, adding another time lag to the system. The problem in the design of the auxiliary piston, therefore, is to keep this additional time lag as small as possible.

Statics

Static Recovery Pressure in Receiving Holes as a Function of Jet-Pipe Nozzle Displacement Relative to Orifice Plate (Infinite Load); Stiffness of Auxiliary Piston (Figs. 3 and 4). An experimental curve of static recovery pressures in the two receiving holes, dead ended, as a function of nozzle displacement relative to the orifice plate is shown in Fig. 3 for a 1.2-mm diam nozzle and a supply pressure of 100 psig. The maximum static recovery pressure in either receiving hole occurs when the nozzle is directly over that hole. The recovery falls off for larger jet-pipe displacements. For maximum recovery pressures, an optimum ratio of receiving-hole size to nozzle diameter has been established. The differential pressures across the two receiving holes, dead ended, are the difference ordinates between the two curves in Fig. 3. Differential pressure across the receiving holes as a function of jet-pipe nozzle displacement relative to the orifice plate is plotted in Fig. 4. These experimental data were not taken for other nozzle sizes (1.6 mm, 2.0 mm, and 2.5 mm), primarily because it was felt that Figs. 3 and 4 can be nondimensionalized by dividing the recovery pressures by the supply pressure and jet-pipe nozzle displacements by the nozzle diameter.

The slope of the differential-pressure curve in Fig. 4 around zero displacement is one of the important characteristics of the auxiliary piston. For a 1-in. diam auxiliary piston used with a 1.2-mm jet pipe operating from a 100-psig supply, the "stiffness" is 4.1 lb/10^{-3} in. The term stiffness is used to describe the differential force gradient because it is a measure of the ability of the auxiliary piston to hold its position against load disturbances such as coercive reaction upon the pilot valve being stroked. This large stiffness value makes the auxiliary piston well suited to stroking pilot valves operating at supply pressures of the order of 400 psig and maximum flows of the order of 10 gpm.

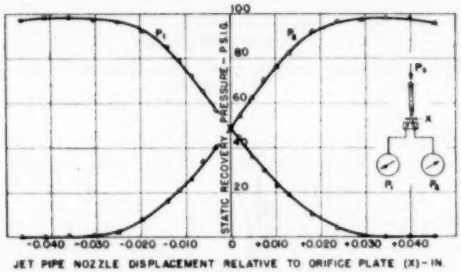

Fig. 3 Static Recovery Pressure in Receiving Holes as Function of Jet-Pipe Displacement Relative to Orifice Plate; Infinite Load

(Conditions of test: Supply pressure to jet pipe = 100 psig; 1.2-mm jet-pipe nozzle.)

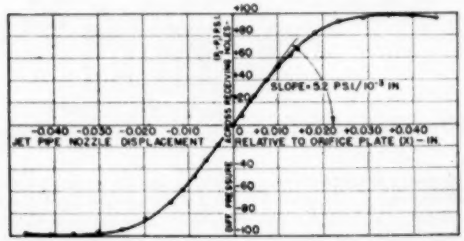

Fig. 4 Differential Pressure Across Receiving Holes as Function of Jet-Pipe Displacement Relative to Orifice Plate; Infinite Load

(Conditions of test: Supply pressure to jet pipe = 100 psig; 1.2-mm jet-pipe nozzle.)

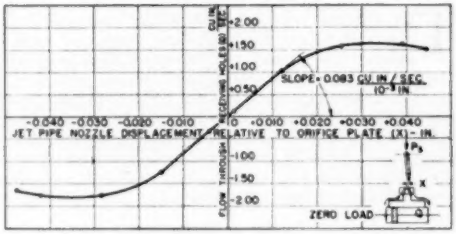

Fig. 5 Flow Through Receiving Holes as Function of Jet-Pipe Displacement Relative to Orifice Plate; Zero Load

(Conditions of test: Supply pressure to jet pipe = 100 psig; 1.2-mm jet-pipe nozzle; jet-pipe flow = 2.04 cu in/sec.)

Zero Load Flow Through Receiving Holes as a Function of Jet-Pipe Nozzle Displacement Relative to Orifice Plate (Fig. 5). An experimental curve of flow through the receiving holes for zero external load as a function of jet-pipe nozzle displacement relative to the orifice plate is shown in Fig. 5 for a 1.2-mm diam nozzle and a supply pressure of 100 psig. The maximum flow in either direction occurs when the nozzle is directly over one receiving hole and falls off for larger jet-pipe displacements. Again it was felt that the data could be nondimensionalized by dividing the flows by the jet-pipe flow and the displacements by the nozzle diameter. The slope of the flow curve around zero displacement is an important factor in the dynamic response of the auxiliary piston and a cylinder operating directly from a jet pipe and distributor block, and is considered further in the sections on the dynamics of these components.

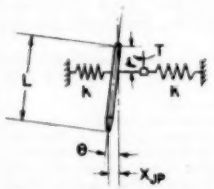

Fig. 6 Line Diagram of Jet Pipe

Static Gain of Jet Pipe (Fig. 6). The static gain of the jet pipe for torque input signals is the ratio of nozzle displacement to applied torque. It is given by the following relation

$$\frac{X_{jp}}{T} = \frac{L}{k_\theta} \quad \ldots\ldots [1]$$

where

X_{jp} = nozzle displacement
T = torque applied to jet pipe about pivot
L = length of jet pipe from pivot to nozzle
k_θ = rotational spring stiffness (torque per radian) = Σkr^2, where k is linear spring stiffness and r is distance from jet-pipe pivot to axis of spring

The static gain is considered in conjunction with jet-pipe bandwidth under the section dealing with jet-pipe dynamics, but is introduced here to facilitate the consideration of jet-pipe "noise."

Sticking Friction and Jet-Pipe Noise. The reaction of the oil jet against the jet pipe is along the jet-pipe axis and, therefore, has no component in the signal direction. This reaction is taken up by the jet-pipe bearings and contributes to the bearing sticking friction.

The jet-pipe oil splashing away from the orifice plate, however, produces a small random force disturbance at the nozzle in the signal direction with predominantly high-frequency components. This disturbance is referred to as noise because of the analogy with thermal noise in vacuum tubes. It is of sufficient magnitude to keep the jet pipe broken loose against the bearing sticking friction and, therefore, serves the same purpose as a deliberately introduced dither. For a particular physical arrangement there will be an average noise force which will apply a torque to the jet pipe in the signal direction. This noise torque is given by the following relation

$$T_n = F_n L \quad \ldots\ldots [2]$$

where

T_n = average torque about pivot due to noise
F_n = average noise force at jet-pipe nozzle in signal direction

The displacement of the nozzle due to the noise will depend upon the static gain of the jet pipe and is given in Equation [3], using the results of Equations [1] and [2]

$$X_{jp(n)} = \frac{T_n L}{k_\theta} = \frac{F_n L^2}{k_\theta} \quad \ldots\ldots [3]$$

where

$X_{jp(n)}$ = average nozzle displacement due to noise

In applications using a jet-pipe supply pressure of 100 psig and a 1.2 or 1.6-mm nozzle, $X_{jp(n)}$ is usually of the order of magnitude of ±0.001 in.—±0.002 in. F_n increases with increased jet-pipe oil flow and increased oil temperatures, although the analytical relations here are not known.

The sticking friction of the auxiliary piston and the pilot valve it strokes will depend upon the diametral clearances and the pressures used. It is usually of the order of magnitude of 1 lb or less for a 1-in. diam auxiliary piston. From Fig. 4 (1.2-mm nozzle; supply pressure = 100 psig), it can be seen that a jet-pipe noise disturbance of ±0.001 in.—±0.002 in. would keep the auxiliary piston broken loose. The noise can be kept from feeding through the pilot valve to the cylinder by overlapping the drain sides of the pilot-valve spools. The effective dead zone of the pilot valve will be the difference between the overlap and the average noise displacement of the auxiliary piston. For the case of the jet pipe, distributor block, and cylinder, the sticking friction of the particular cylinder used, its net area, and the nature of the load will determine whether the jet pipe will keep the cylinder broken loose.

Dynamics

Analysis of Jet Pipe (Fig. 6). The jet pipe is a second-order mechanical system since it possesses some inertia, has some damping due to the movement of the nozzle through a pool of oil, and is spring-loaded. The differential equation of this system is

$$T = J\frac{d^2\theta}{dt^2} + f\frac{d\theta}{dt} + k_\theta\theta \quad \ldots\ldots [4]$$

where

J = inertia of jet-pipe system referred to pivot
f = viscous damping
θ = angular displacement of jet pipe

since

$$\theta = \frac{X_{jp}}{L} \quad \ldots\ldots [5]$$

Equation [4] may be rewritten as

$$T = \frac{1}{L}\left(J\frac{d^2x_{jp}}{dt^2} + f\frac{dx_{jp}}{dt} + k_\theta X_{jp}\right) \quad \ldots\ldots [6]$$

This equation transformed is

$$T(s) = \frac{X_{jp}(s)}{L}(Js^2 + fs + k_\theta) \quad \ldots\ldots [7]$$

where s represents the operator $d/(dt)$. The transfer function then is

$$KG(s) = \frac{X_{jp}(s)}{T(s)} = \frac{\frac{L}{k_\theta}}{\frac{J}{k_\theta}s^2 + \frac{f}{k_\theta}s + 1} = \frac{K}{\frac{1}{\omega_n^2}s^2 + \frac{2\zeta}{\omega_n}s + 1} \quad \ldots\ldots [8]$$

from which

K(static gain) = $\frac{L}{k_\theta}$ (as previously defined in Equation [1]). [9a]

ω_n(undamped natural frequency) = $\sqrt{\frac{k_\theta}{J}}$ [9b]

ζ(damping ratio) = $\frac{\text{actual damping}}{\text{critical damping}} = \frac{f}{2\sqrt{k_\theta J}}$ [9c]

For a given jet pipe, J and f are fixed, and only k_θ can be varied. As the rotational spring stiffness is increased, the undamped natural frequency will increase but both the static gain and damping ratio will decrease. The latter two considerations will limit the maximum bandwidth that can be attained.

The experimental frequency-response characteristic (amplitude and phase responses for sinusoidal inputs) of an $8^{19}/_{32}$-in-long jet pipe for two different values of k_θ (3000 oz-in/rad and 6120 oz-in/rad) are presented in Fig. 7. The amplitude response is based on a zero frequency value of unity and is plotted in decibels. A torque input to the jet pipe corresponding to a zero frequency stroke of 75 per cent maximum was employed. The jet pipe was operated with oil flow at a supply pressure of 100 psig.

The frequency at the —90-deg phase point was taken as the undamped natural frequency in each case and the amplitude response at this frequency was used to calculate the damping ratio. The values of ω_n and ζ thus obtained were used to fit second-order curves to the experimental curves. The agreement between the experimental and calculated response curves is good. The two response equations obtained are

$$G(s) = \frac{1}{(4.32)10^{-4}s^3 + (2.63)10^{-3}s + 1} \quad \ldots\ldots [10]$$

for $k_\theta = 3000$ oz-in/rad

$$G(s) = \frac{1}{(1.87)10^{-4}s^3 + (1.37)10^{-3}s + 1} \quad \ldots\ldots [11]$$

for $k_\theta = 6120$ oz-in/rad

The undamped natural frequency could be calculated from Equation [9b] since the inertia of the jet-pipe system was known. The theoretical values of ω_n are compared with the values extracted from the experimental results in Table 1.

TABLE 1 THEORETICAL AND EXPERIMENTAL VALUES OF UNDAMPED NATURAL FREQUENCY

k_θ oz-in/rad	Theoretical ω_n (cps)	Experimental value ω_n (cps)	Per cent error in theoretical ω_n
3000	23.5	24.2	2.9
6120	33.6	36.7	8.5

The jet-pipe damping (f) was calculated from Equation [9c] using the experimental values of ζ. The results are given in Table 2.

TABLE 2 EXPERIMENTAL VALUES OF DAMPING

k_θ oz-in/rad	ζ	f oz-in rad/sec
3000	0.20	8.1
6120	0.16	9.3

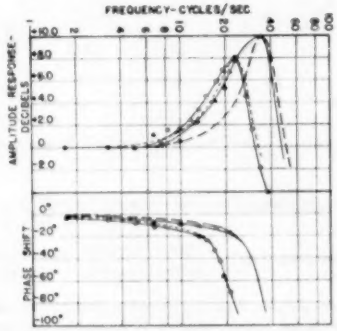

FIG. 7 EXPERIMENTAL FREQUENCY-RESPONSE CHARACTERISTIC OF STANDARD $8^{10}/_{32}$ IN. JET PIPE WITH OIL FLOW

Curve Code:

$k_\theta = 3000$ oz-in/rad
—⊙—⊙—⊙—Experimental curve
$\omega_n = 24.2$ cps
$\zeta = 0.20$
– – – – Second-order approximation

$$= G(j\omega) = \frac{1}{(4.32)10^{-4}(j\omega)^3 + (2.63)10^{-3}(j\omega) + 1}$$

$k_\theta = 6120$ oz-in/rad
—△—△—△—Experimental curve
$\omega_n = 36.7$ cps
$\zeta = 0.16$
—— —— —— Second-order approximation

$$= G(j\omega) = \frac{1}{(1.87)10^{-4}(j\omega)^3 + (1.37)10^{-3}(j\omega) + 1}$$

The jet-pipe inertia will vary very nearly as the cube of the length, and the damping will vary as the square of the length with only the nozzle immersed in oil. If the jet-pipe length is changed and the spring stiffness is changed proportionately to hold the static gain (L/k_θ) const (Equation [9a]), ω_n will vary as $1/L$ (from Equation [9b]) and ζ will remain constant (from Equation [9c]). Therefore the jet-pipe bandwidth may be increased without sacrificing static gain or altering the damping ratio by decreasing the length of the jet pipe.

Analysis of Cylinder Operating From Jet Pipe and Orifice Plate in Distributor Block (Figs. 8 and 9). A jet pipe, orifice plate in a distributor block, and cylinder are shown schematically in Fig. 8. The characteristic curves of pressure drop across the output cylinder versus flow with jet-pipe displacement relative to the orifice plate as parameter are represented in Fig. 9. The

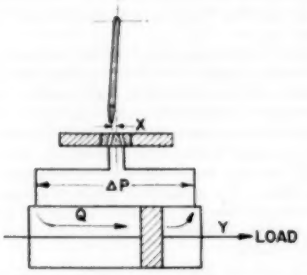

FIG. 8 LINE DIAGRAM OF JET PIPE, DISTRIBUTOR BLOCK, AND CYLINDER

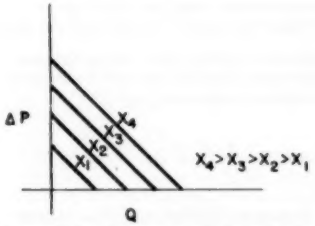

FIG. 9 PRESSURE DROP VERSUS FLOW CURVES FOR JET PIPE, DISTRIBUTOR BLOCK, AND CYLINDER

curves are approximated by straight lines. The vertical axis intercepts are points on the curve of differential pressure across the receiving holes versus jet-pipe nozzle displacement relative to the orifice plate for infinite load, Fig. 4. The horizontal axis intercepts are points on the curve of flow through the receiving holes versus jet-pipe nozzle displacement relative to the orifice plate for zero load, Fig. 5. The equation of any curve is

$$\Delta P = \frac{d\Delta P}{dQ} Q + \frac{d\Delta P}{dX} X \quad \ldots\ldots [12]$$

where

ΔP = differential pressure across receiving holes (= pressure drop across cylinder)
Q = flow through receiving holes (= cylinder flow)
X = jet-pipe nozzle displacement relative to orifice plate

Multiplying the equation by the cylinder area to obtain the

force across the piston, and equating this force to the accelerating and damping forces gives

$$\Delta P\, A_{cyl} = \Delta F = \frac{d\Delta P}{dQ} Q\, A_{cyl} + \frac{d\Delta P}{dX} X\, A_{cyl} = M \frac{d^2Y}{dt^2} + f \frac{dY}{dt} \quad \ldots\ldots [13]$$

where

ΔF = force due to differential pressure across cylinder
A_{cyl} = net cylinder area
M = mass of piston, oil, and load
f = viscous damping of cylinder and load
Y = cylinder position

Since

$$Q = A_{cyl} \frac{dY}{dt} \quad \ldots\ldots [14]$$

Equation [13] may be written as

$$\Delta P\, A_{cyl} = \frac{d\Delta P}{dQ} A^2_{cyl} \frac{dY}{dt} + \frac{d\Delta P}{dX} X\, A_{cyl} = M \frac{d^2Y}{dt^2} + f \frac{dY}{dt} \quad [15]$$

Rearranging Equation [15] gives

$$M \frac{d^2Y}{dt^2} + \left(f - \frac{d\Delta P}{dQ} A^2_{cyl} \right) \frac{dY}{dt} = \frac{d\Delta P}{dX} A_{cyl}\, X \quad [16]$$

This equation transformed is

$$M s^2 Y(s) + \left(f - \frac{d\Delta P}{dQ} A^2_{cyl} \right) s\, Y(s) = \frac{d\Delta P}{dX} A_{cyl}\, X(s) \quad [17]$$

The transfer function then is

$$K_v G(s) = \frac{Y(s)}{X(s)} = \frac{\dfrac{d\Delta P}{dX} A_{cyl}}{M s^2 + \left(f - \dfrac{d\Delta P}{dQ} A^2_{cyl} \right) s} \quad \ldots\ldots [18]$$

Neglecting the damping of the cylinder and load and recognizing that $(d\Delta P)/(dQ)$ is negative gives

$$K_v G(s) = \frac{\dfrac{d\Delta P}{dX} A_{cyl}}{s \left(M s + \left| \dfrac{d\Delta P}{dQ} \right| A^2_{cyl} \right)} \quad \ldots\ldots [19]$$

Simplifying

$$K_v G(s) = \frac{\dfrac{dQ}{dX} \dfrac{1}{A_{cyl}}}{s \left(\dfrac{M}{\left| \dfrac{d\Delta P}{dQ} \right| A^2_{cyl}} s + 1 \right)} = \frac{K_v}{s(\tau s + 1)} \quad \ldots\ldots [20]$$

from which

$$K_v \text{ (velocity constant or static gain)} = \frac{dQ}{dX} \frac{1}{A_{cyl}} \quad [21a]$$

$$\tau \text{ (time constant)} = \frac{M}{\left| \dfrac{d\Delta P}{dQ} \right| A^2_{cyl}} \quad \ldots\ldots [21b]$$

A cylinder operating from a jet pipe and distributor block may then be represented as an integrator with a single first-order lag.

An examination of Equation [21b] shows that the bandwidth of a cylinder with a specified load operating from a jet pipe and distributor block can be increased by using the following:

(*a*) A large cylinder area.
(*b*) A small-diameter nozzle.
(*c*) A high supply pressure to the jet pipe.

By Equation [21*a*] a large cylinder area and a small-diameter nozzle, however, will reduce the static gain (velocity constant) and the maximum cylinder speed. Increasing the supply pressure will improve the static gain as well as the bandwidth but will also increase jet-pipe noise. The load is the greatest contributing factor to the total mass if the length of oil lines (and, therefore, the mass of oil that must be moved) is kept reasonably small. Thus static gain and jet-pipe noise considerations limit the maximum bandwidth that can be attained. Where very much greater static gains are necessary without too great a decrease in over-all dynamics, it is necessary to go to a pilot valve as the integrating element and add an auxiliary piston to provide the force amplification necessary to stroke the pilot valve. No experimental frequency responses have been taken of a cylinder operating from a jet pipe. The order of magnitude of the cylinder time constant encountered is illustrated by the following hypothetical example:

Weight of load, piston, and oil	100 lb
Supply pressure to jet pipe	100 psig
Jet-pipe nozzle diameter	1.2 mm
Cylinder dimensions: 4-in. bore, 1-in. rod;	double-ended

Using Figs. 4 and 5 and Equations [21*a*] and [21*b*]

$$K_v = 7.0 \text{ sec}^{-1}$$
$$\tau = (29.6)10^{-6} \text{ sec.}$$
$$\text{Break frequency} = \frac{1}{\tau} = 5380 \text{ cps}$$

Analysis of Auxiliary Piston (Fig. 10). The jet pipe and auxiliary piston are shown schematically in Fig. 10. Since the orifice plate is in the auxiliary piston, the loop is closed with unity position feedback from the auxiliary piston to the jet-pipe nozzle. The open-loop transfer function of the auxiliary piston is the same as the transfer function of the cylinder operating directly from the jet pipe and orifice plate in a distributor block. The closed-loop transfer function $h(s)$, may be derived from the open loop transfer function $K_v G(s)$, from the following equation

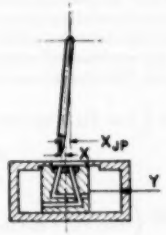

FIG. 10 LINE DIAGRAM OF JET PIPE AND AUXILIARY PISTON

$$h(s) = \frac{Y(s)}{X_{JP}(s)} = \frac{K_v G(s)}{1 + K_v G(s)} \quad \ldots\ldots [22]$$

where

$$K_v G(s) = \frac{Y(s)}{X(s)}$$

Using the expression for $K_sG(s)$ given in Equation [20]

$$h(s) = \frac{1}{\frac{1}{K_sG(s)} + 1} = \frac{1}{s\frac{\left(\frac{M}{\left|\frac{d\Delta P}{dQ}\right|}s + 1\right)}{\frac{dQ}{dX}\frac{1}{A_{sp}}} + 1} \quad \ldots [23]$$

where

A_{sp} = area of auxiliary piston

Simplifying Equation [23] gives

$$h(s) = \frac{1}{\frac{M}{\frac{d\Delta P}{dX}A_{sp}}s^2 + \frac{A_{sp}}{\frac{dQ}{dX}}s + 1} = \frac{1}{\frac{1}{\omega_n^2}s^2 + \frac{2\zeta}{\omega_n}s + 1} \quad \ldots [24]$$

from which

$$\omega_n \text{ (undamped natural frequency)} = \sqrt{\frac{\frac{d\Delta P}{dX}A_{sp}}{M}} \quad [25a]$$

$$\zeta \text{ (damping ratio)} = \frac{A_{sp}\sqrt{\frac{\frac{d\Delta P}{dX}A_{sp}}{M}}}{2\frac{dQ}{dX}} \quad \ldots [25b]$$

The experimental frequency-response characteristic of a 1-in. diam auxiliary piston is given in Fig. 11. A jet pipe with a 1.6-mm nozzle was used with the auxiliary piston and was operated from a 100-psig supply. The jet pipe was displaced by a mechanical sine drive through 30 per cent of its maximum stroke. The theoretical frequency-response characteristic of this auxiliary piston was obtained from Equation [24] by using its experimentally determined static characteristics and was plotted for comparison with the experimental response curve. ω_n and ζ were calculated from the following information

$\frac{d\Delta P}{dX}$ = 3890 psi/in. (from Fig. 4 and the relation $\frac{d\Delta P}{dX} \propto \frac{1}{\text{nozzle diam}}$)

$\frac{dQ}{dX}$ = 110 cu-in/sec / in. (from Fig. 5 and the relation $\frac{dQ}{dX} \propto$ nozzle diam)

A_{sp} = 0.785 sq in.

$M = (7.9)10^{-4}$ lb / in/sec^2

The values of ω_n and ζ obtained are

ω_n = 1970 rad/sec = 313 cps

ζ = 7.04

The theoretical closed-loop transfer function by Equation [24] is

$$h(s) = \frac{1}{(2.58)10^{-7}s^2 + (7.15)10^{-4}s + 1} = \frac{1}{[(3.63)10^{-4}s + 1][(7.11)10^{-3}s + 1]} \quad \ldots [26]$$

The transfer function can be factored into two first-order lag terms because it is overdamped. The smaller time constant can be neglected for frequencies below 200 cps, and the transfer function reduces to a single first-order lag term

$$h(s) = \frac{1}{(7.11)10^{-3}s + 1} \quad \ldots [27]$$

The time constant of this auxiliary piston is then 0.007 sec. This result could have been obtained by neglecting the squared term in Equation [24] and using as the closed-loop transfer function

$$h(s) = \frac{1}{\frac{A_{sp}}{\frac{dQ}{dX}}s + 1} \quad \ldots [28]$$

Equation [27] is plotted in Fig. 11 and the agreement with the experimental response curve is very good.

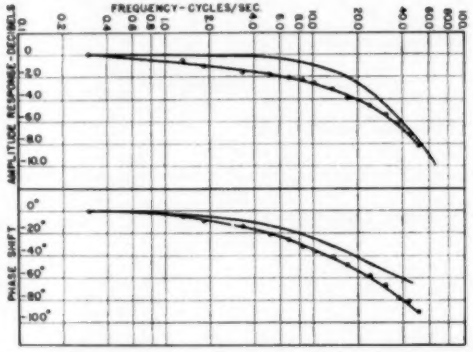

FIG. 11 EXPERIMENTAL AND THEORETICAL FREQUENCY-RESPONSE CHARACTERISTIC OF STANDARD AUXILIARY PISTON

(Conditions of test: Supply pressure to jet pipe = 100 psig; 1.6-mm jet-pipe nozzle and corresponding receiving-hole size in auxiliary piston orifice plate.)

Curve Code:

—⊙—⊙—⊙—Experimental curve

————Theoretical curve using $h(j\omega) = \frac{1}{j\omega(7.11)10^{-3} + 1}$

From Equation [28] it can be seen that the effect of mass can be neglected and nothing can be gained by reducing the mass of the auxiliary piston from its present value. The dominant time constant can be reduced by using the following:

(*a*) A smaller diameter auxiliary piston.

(*b*) A larger jet-pipe nozzle diameter.

(*c*) A higher jet-pipe supply pressure.

A smaller area, however, will decrease the stiffness of the auxiliary piston, and larger nozzle sizes and higher oil pressures will increase the jet-pipe noise. Also, it is important to note that using smaller auxiliary piston areas and larger nozzle sizes will increase the second time constant.

CONCLUSIONS

Analytical expressions have been developed for the transfer functions of the jet pipe, distributor block and cylinder, and

auxiliary piston. The jet-pipe response could not be predicted in advance of the experimental tests because of the difficulty of predicting the magnitude of the viscous damping. The experimental frequency-response tests show that the jet pipe is a second-order mechanical system, lightly damped, with a high resonant frequency. It should be possible to predict the dynamic response for any other values of spring stiffness. Theoretical considerations indicate that the natural frequency can be increased without sacrificing static gain or making the response more oscillatory by reducing the jet-pipe length and decreasing the spring stiffness proportionately. This offers the most promising means of extending the bandwidth.

A cylinder operating from a distributor block may be represented as an integrator with a single first-order lag. The bandwidth can best be extended by using higher jet-pipe supply pressures. The resultant increase in noise will limit the results that can be achieved in this direction.

The auxiliary piston has a heavily overdamped second-order response. The transfer function may be factored into two first-order lag terms and the smaller of the two time constants neglected. This means that the mass of the auxiliary piston does not enter significantly into its response. The stiffness of the auxiliary piston may be much more than is needed in present applications and a reduction in area would decrease the larger time constant. At the same time, this would increase the second time constant. Very close agreement exists between the predicted and experimental response curves.

Sufficient experimental work has been conducted to yield the order of magnitude of the dynamic responses of the components discussed and to indicate possible ways of extending the bandwidths.

Acknowledgment

This work was done at the Askania Regulator Company with facilities and funds of the Bureau of Ships, U. S. Navy Department, under Contract No. NObs-46483.

AN ASME PAPER

Its Preparation, Submission and Publication, and Presentation

To a large degree the papers prepared and presented under the ASME sponsorship are evidence by which its professional standing and leadership are judged. It follows, therefore, that to qualify for ASME sponsorship, a paper must not only present suitable subject matter, but it must be well written and conform to recognized standards of good English and literary style.

The pamphlet on "AN ASME PAPER" is designed to aid authors in meeting these requirements and to acquaint them with rules of the Society relating to the preparation and submission of manuscripts and accompanying illustrations. It also includes suggestions for the presentation of papers before Society meetings.

CONTENTS

PREPARATION OF A PAPER—

General Information—Style, Preferred Spelling, Length Limitation, Approvals and Clearances.

Contents of the Paper—Title, Author's Name, Abstract, Body of Paper, Appendixes, Acknowledgments, Bibliographies, Tables, Captions, Photographs, Other Illustrations.

Writing the Paper—Outline Tabulations, Tables, Graphs, Charts for Computation, Drawings, Mathematics, Accuracy, Headings and Numbering, Lantern Slides, Motion Pictures, Typing, Number of Copies.

SUBMISSION AND PUBLICATION OF A PAPER—

Intention to Submit Paper Required in Advance, Meeting Dates, Due Dates for Manuscript, Discussers, Review and Acceptance, Proofs, Advance Copies and Reprints, Discussion and Closure, Publication by Others.

PRESENTATION OF A PAPER—

Time Limit, Addressing Your Audience, Public Address Systems, Use of Slides.

REFERENCES—

References on Writing and Speaking, Engineering Standards.

Price 40¢. No discount allowed. *A remittance must accompany all orders for $5.00 or less. U. S. Postage Stamps are acceptable.*

THE AMERICAN SOCIETY OF MECHANICAL ENGINEERS

29 West 39th Street, New York 18, N. Y.